

THIS COPY NASA # 1008  
SINGLE COPY ONLY

REPORT

NO. LED-500-3

DATE: 30 Sept. 1961

DYNAMIC ANALYSIS OF THE  
LEM FLIGHT CONTROL SYSTEM

[U]

(NASA-CR-117567) DYNAMIC ANALYSIS OF THE  
LEM FLIGHT CONTROL SYSTEM (Grumman Aircraft  
Engineering Corp.) 246 p

N79-76445

Inclas  
11434

00/18

(CODE)

10  
2  
12

NASA-CR-117567  
(NASA CR OR TMX OR AD NUMBER)

(CATEGORY)

AVAILABLE TO U.S. GOVERNMENT AGENCIES  
AND CONTRACTORS ONLY





C65-8629

**AVAILABLE**

DO NOT REMOVE THIS COPY

**THE**





~~CONFIDENTIAL~~

## TABLE OF CONTENTS

<u>Section</u>		<u>Page</u>
	LIST OF ILLUSTRATIONS-----	vi
	LIST OF TABLES-----	xi
	LIST OF SYMBOLS-----	xii
1	SUMMARY-----	1
2	INTRODUCTION-----	9
	2.1 Purpose of Report-----	10
	2.2 Control System Configuration-----	10
	2.3 Scope-----	14
3	REACTION JET CONTROL SYSTEM ANALYSIS-----	16
	3.1 Introduction-----	19
	3.2 Propellant Flow Rate-----	19
	3.2.1 Introduction-----	19
	3.2.2 Normal Limit Cycle Propellant Flow Rate-----	20
	3.2.3 Disturbed Limit Cycle Propellant Flow Rate-----	23
	3.2.4 Propellant Required for Large Maneuvers-----	23
	3.2.5 Summary-----	24
	3.3 Modulator Study-----	24
	3.3.1 Introduction-----	24
	3.3.2 On-off Control-----	24
	3.3.3 Induced Rate Modulator-----	36
	3.3.4 Pulse Modulators-----	45
	3.3.4.1 Modified on-off-----	45
	3.3.4.2 Pulse Frequency Modulator (PFM)-----	46
	3.3.4.3 Pulse Width Modulator (PWM)-----	49
	3.3.4.4 Pulse Ratio Modulator (PRM)-----	50
	3.3.4.5 Non Linear PRM-----	61
	3.3.4.6 Piecewise-linear PRM-----	61
	3.3.4.7 General-----	61
	3.4 Simulation Results-----	65
	3.4.1 Introduction-----	65
	3.4.2 Limit Cycle-----	65
	3.4.3 Disturbed Limit Cycle-----	66

~~CONFIDENTIAL~~

## TABLE OF CONTENTS (Continued)

<u>Section</u>	<u>Page</u>
3.4.4 Response to Large Errors-----	71
3.4.5 Conclusion-----	71
3.5 Attitude Control Propellant Requirements for IEM Mission-----	72
3.6 Control System Deadbands-----	74
4 REACTION JET SELECT LOGIC-----	90
4.1 Introduction-----	91
4.2 Control Degradation Modes-----	91
4.3 Minimum Jet-Off Failures Resulting in Maximum Control Degradation-----	92
4.4 Logic Mechanization Concepts-----	93
4.4.1 Modulated Logic-----	93
4.4.2 Proportional Logic-----	95
4.5 Three Types of Jet-Failure Cutoff-----	96
4.5.1 Quad Cutoff-----	96
4.5.2 Logic-Coupled Jet-Pair Cutoff-----	96
4.5.3 Logic-Uncoupled Jet-Pair Cutoff-----	96
4.5.4 Logic-Coupled vs. Logic-Uncoupled-----	96
5 THRUST VECTOR CONTROL-----	100
5.1 Introduction and Summary-----	103
5.2 Powered Descent Control With Additional RCS Jets-----	103
5.3 Fuel Management Trim System-----	104
5.4 The Gimballed Engine IEM Attitude Control System Analysis-----	105
5.4.1 Derivation of the Linear Open Loop Transfer Function-----	109
5.4.2 Derivation of the Transfer Function Parameter Constraints-----	112
5.4.3 Gimballed Engine Actuator Constraints-----	116
5.4.4 Stability Criteria Summary-----	118
5.4.5 Evaluation of Actuator Response Requirements---	120
5.4.6 Simplified Gimballed Engine Control System Transfer Function Derivation-----	120
5.5 Closed Loop (Feedback Stabilized) Gimballed Engine Trim Systems-----	125

~~CONFIDENTIAL~~

~~CONFIDENTIAL~~

## TABLE OF CONTENTS (Continued)

<u>Section</u>	<u>Page</u>
5.5.1 The Necessity of Integral Compensation-----	125
5.5.2 Linear (Proportional) Servo Actuators and Engine - LEM Inertia Coupling-----	125
5.5.3 Constant Speed (Full On) Servo Actuators and Irreversible Drive (No Inertia Coupling)-----	130
5.6 Open Loop Gimbal Engine Trim Systems with Constant Speed Actuators and Irreversible Drive-----	135
5.6.1 Uncompensated (Unstable) Trim Systems-----	135
5.6.1.1 Introduction-----	135
5.6.1.2 Non-Linear (RCS) Pulse Ratio Modulators-----	136
5.6.1.3 Linear Pulse Ratio Modulators-----	141
5.6.1.4 RCS Deadzone Variation-----	142
5.6.1.5 Results-----	142
5.6.2 Phase-Lead Stabilized Trim Systems-----	143
5.6.2.1 Linear (Dipole) Stabilization-----	143
5.6.2.2 Non-Linear Relay Stabilization-----	144
5.6.2.3 Mechanization Concepts for Non-Linear (Relay) Stabilization-----	150
5.6.2.4 Maximum Stabilization-----	153
5.7 Ascent Thrust Vector Control-----	153
5.8 Conclusions-----	156
6 ATTITUDE CONTROL WITH GUIDANCE FEEDBACK-----	157
6.1 Introduction-----	160
6.2 Integral Compensation-----	160
6.3 Pendulous Accelerometer Study ( $T_1$ Abort Guidance Law)-	165
6.4 Quantized Attitude Feedback (Strap-down Attitude Reference Feasibility Study)-----	173
7 PARASITIC MODES ANALYSIS-----	183
7.1 Introduction-----	186
7.2 Propellant Sloshing-----	186
7.2.1 Introduction-----	186
7.2.2 Stability Analysis-----	190

~~CONFIDENTIAL~~

~~CONFIDENTIAL~~

## TABLE OF CONTENTS (Continued)

<u>Section</u>	<u>Page</u>
7.2.3 Transient Response-----	195
7.2.4 Method of Propellant Damping-----	196
7.2.5 Baffle Configuration-----	197
7.3 Elastic Airframe-----	198
7.4 Conclusion-----	206
8 BIBLIOGRAPHY-----	232

~~CONFIDENTIAL~~

~~CONFIDENTIAL~~

## LIST OF ILLUSTRATIONS

<u>Figure</u>	<u>Title</u>	<u>Page</u>
1-1	Control System Analysis Block Diagram-----	8
2-1	RCS Jet Thruster Configuration-----	15
3-1	Electrical Pulse Width Versus Specific Impulse ( $I_{sp}$ )-----	21
3-2	Symmetrical Limit Cycle-----	22
3-3	Electrical Pulse Width Versus Total Impulse and Propellant Flow Rate-----	25
3-4	Disturbed Limit Cycle-----	26
3-5	Single Axis Attitude Control Loop-----	27
3-6	On-off and Induced Rate Modulator Characteristics-----	28
3-7	Rate Gyro Input-Output Characteristics for a Ramp Input ( $\dot{\theta}$ Constant)-----	31
3-8	Thrust Function Characteristics-----	31
3-9	On-off Limit Cycle, $K_R = 0.05$ seconds-----	32
3-10	On-off Limit Cycle, $K_R = 0.1$ seconds-----	33
3-11	On-off Limit Cycle, $K_R = 0.2$ seconds-----	34
3-12	On-off Disturbed Limit Cycle, $K_R = 0.1$ seconds-----	37
3-13	On-off Disturbed Limit Cycle, $K_R = 0.2$ seconds-----	38
3-14	On-off Disturbed Limit Cycle, $K_R = 0.4$ seconds-----	39
3-15	On-off Transient Response to a $5^\circ$ Step, $K_R = 0.05$ seconds---	40
3-16	On-off Transient Response to a $5^\circ$ Step, $K_R = 0.1$ seconds---	41
3-17	On-off Transient Response to a $5^\circ$ Step, $K_R = 0.2$ seconds---	42
3-18	Single Axis Attitude Control Loop with Rate Gyro Deadzone---	43
3-19	Limit Cycle Characteristics for the Determination of $\dot{\theta}_{RG}$ ---	44
3-20	Modified On-off Modulator Characteristics-----	47
3-21	PFM Characteristics-----	48
3-22	PWM Characteristics-----	51
3-23	PRM Characteristics-----	52
3-24	Piecewise Linear PRM Characteristics-----	53
3-25	Non Linear PRM Characteristics-----	54
3-26	Phase Plane Thresholds for Pulse Modulators-----	55
3-27	Limit Cycle Characteristics for Determining One Pulse Limit Cycle Boundary-----	56
3-28	$t_{\Delta\theta}$ and $T_p$ Versus $\dot{\theta}_{RG}$ for PWM-----	57

~~CONFIDENTIAL~~

~~CONFIDENTIAL~~

## LIST OF ILLUSTRATIONS (Continued)

<u>Figure</u>	<u>Title</u>	<u>Page</u>
3-29	$t_{\Delta\theta}$ and $T_P$ Versus $\dot{\theta}_{RG}$ for PFM-----	58
3-30	PRM Limit Cycle with $\lambda_{ON} = 0$ ms and $K_R = 0$ seconds-----	59
3-31	Moment Unbalance Limit Cycle Characteristics-----	60
3-32	Moment Unbalance Limit Cycle Characteristics to Determine Boundary Between Switch Line and Desired Limit Cycles-----	63
3-33	Example of a Wandering Limit-----	64
3-34	$K_R$ Versus $\dot{\theta}_A$ for On-off Modulator-----	67
3-35	$K_R$ Versus $\dot{\theta}_A$ for Delay Type PWM-----	68
3-36	$K_R$ Versus $\dot{\theta}_A$ for Piecewise Linear PRM-----	69
3-37	$K_R$ Versus $D$ for Piecewise Linear PRM-----	70
3-38	Moment Unbalance Versus Average Attitude-----	78
3-39	Moment Unbalance Versus Angular Rate Peak to Peak Oscillations-----	79
3-40	Moment Unbalance Versus Attitude Peak to Peak Oscillations--	80
3-41	Moment Unbalance Versus Propellant Flow Rate-----	81
3-42	Piecewise Linear PRM Transient Response to a $10^\circ$ Step, $K_R = 0.12$ seconds-----	82
3-43	Induced Rate Modulator Response to a $17^\circ$ Step, $K_R = 0.05$ seconds-----	83
3-44	PRM Transient Response to a $10^\circ$ Step, $\Omega = 0.1^\circ$ , $K_R = 0.1$ seconds-----	84
3-45	PRM Transient Response to a $10^\circ$ Step, $\Omega = 0.1^\circ$ , $K_R = 0.2$ seconds-----	85
3-46	Moment Unbalance Versus Limit Cycle Period-----	86
3-47	Single Axis Configuration of LEM Attitude Control System----	87
3-48	Phase Plane Boundaries with $\Omega_a = 0$ -----	88
3-49	Phase Plane Boundaries with $\Omega_a \neq 0$ -----	89
4-1	RCS Jet Thruster Configuration-----	94
4-2	Logic Block Diagrams-----	99
5-1	Gimballed Engine Planar Free Body Diagrams-----	107
5-2	Descent Control System Feedback Diagram-----	108
5-3	Root Locus for Gimbal Engine Control-----	114
5-4	Root Locus of Gimbal Engine Control System Example-----	115

~~CONFIDENTIAL~~

~~CONFIDENTIAL~~

## LIST OF ILLUSTRATIONS (Continued)

<u>Figure</u>	<u>Title</u>	<u>Page</u>
5-5	Gimballed Engine Attitude Control Loop and Gimballed Engine Attitude Control Loop with $\delta/\delta_c$ and $\psi/\delta$ Transfer Functions Inserted-----	122
5-6	Simplified Gimballed Engine Planar Dynamics-----	123
5-7	Schematic of the Closed Loop Linear-Actuator Trim System and RCS Attitude Control-----	128
5-8	Root Locus for Closed Loop Gimbal Engine Trim System with Linear Servo Actuators-----	129
5-9	Feedback Stabilized Gimbal Trim System (GTS) with Constant Speed Nonlinear Servo Actuator-----	132
5-10	Analytically Equivalent Feedback Stabilized GTS with Describing Function Nonlinearity-----	132
5-11	Root Locus for Closed Loop Gimbal Trim System with Constant Speed Servo Actuators and Irreversible Drive-----	133
5-12	Root Locus Example for Constant Speed Gimbal Trim System----	134
5-13	The Open Loop Trim System Representation as the Prime Attitude Control-----	137
5-14	Analytically Equivalent Trim System Representation (with Describing Function Nonlinearity)-----	137
5-15	Root Locus of the Open Loop Trim System as the Prime Attitude Control-----	138
5-16	Nonlinear Pulse Ratio Modulator-Powered Descent RCS Propellant Consumption-----	139
5-17	Linear Pulse Ratio Modulator-Powered Descent Propellant Consumption-----	140
5-18	Root Locus Sketch of the Open Loop Trim Attitude Control System with Linear Phase Lead Stabilization-----	145
5-19	Root Locus Plot of the Open Loop Trim System with 30 Gain Linear Stabilization-----	146
5-20	Describing Function Analysis of the Normalized Open Loop Trim System with Nonlinear Phase Lead Stabilization-----	147
5-21	A Concept Basis for Mechanizing the Nonlinear Phase Lead Stabilization-----	148
5-22	Stabilization Mechanization-----	151
5-23	Trim System with Maximum Stabilization-----	152

~~CONFIDENTIAL~~

~~CONFIDENTIAL~~

## LIST OF ILLUSTRATIONS (Continued)

<u>Figure</u>	<u>Title</u>	<u>Page</u>
6-1	Schematic of Planar RCS Attitude Control with Attitude Error Integral Compensation-----	161
6-2	Integral Compensation Effect on Limit Cycle Error Signal-----	162
6-3	Attitude Control System with Pendulous Accelerometer-----	167
6-4	Accelerometer Locations-----	168
6-5	Pendulous Accelerometer Root Loci-----	168
6-6	Accelerometer Constant Versus Minimum Damping Ratio and Time Constant-----	171
6-7	Quantized Attitude Control System-----	172
6-8	PFM Characteristics Assumed for Quantized Attitude Control System-----	175
6-9	Quantized Attitude Control System with Continuous Rate Feedback-----	176
6-10	Comparison of Attitude Response with Quantized and Unquantized Angle Feedback-----	177
6-11	Typical Limit Cycles for Continuous (a) and Quantized (b) Attitude Hold Mode-----	178
6-12	Limit Cycling for the conditions: $I = 10,000 \text{ slug-ft}^2$ , $k_f = 11.7 \text{ PPS/mr}$ and $f_o = 20.4 \text{ PPS}$ -----	179
6-13	Effects of Quantization Size and Minimum Frequency on Pulse Frequency-----	180
6-14	Limit Cycling Using Quantized Angle with Continuous Rate- $I = 10,000 \text{ slug-ft}^2$ , $k_f = 11.7 \text{ PPS/mr}$ , $f_o = 20.4 \text{ PPS}$ -----	181
6-15	Limit Cycling Using Quantized Angle with Continuous Rate- $I = 2000 \text{ slug-ft}^2$ , $f_o = 50 \text{ PPS}$ , $\Delta \theta = 0.03 \text{ deg.}$ -----	182
7-1	Linearized Control System-----	207
7-2	Control System Programmed for Analog Slosh Study-----	208
7-3	Reaction Jet Thrust Characteristics-----	209
7-4	Model Parameters for Ascent Tanks-----	210
7-5	Model Parameters for Descent Tanks-----	211
7-6	Sloshing Mass Versus Ascent, Descent Burn Time-----	212
7-7	Descent Yaw (No Jet Delay) - $h/2R = 1.0$ , $K_R = 0.8 \text{ sec}$ , $\mathcal{S} = 0$ -----	213
7-8	Descent Yaw (Jet Delay) - $h/2R = 0.5$ , $K_R = 0.8 \text{ sec}$ , $\mathcal{S} = 0$ -----	214

~~CONFIDENTIAL~~



~~CONFIDENTIAL~~

## LIST OF ILLUSTRATIONS (Continued)

<u>Figure</u>		<u>Page</u>
7-9	Descent Yaw (No Jet Delay) - $h/2R = 0.5$ , $K_R = 0.8$ , $\mathcal{J} = 0$ -----	215
7-10	Descent Yaw - $h/2R = 0.4$ , $K_R = 0.8$ sec, $\mathcal{J} = 0$ -----	216
7-11	Descent Roll (Jet Delay) - $h/2R = 1.0$ , $K_R = 0.8$ sec, $\mathcal{J} = 0.05$ --	217
7-12	Descent Roll (No Jet Delay) - $h/2R = 0.4$ , $K_R = 0.8$ sec, $\mathcal{J} = 0$ --	218
7-13	Ascent Yaw - $h/2R = 0.65$ , $K_R = 0.4$ sec, $\mathcal{J} = 0$ -----	219
7-14	Ascent Yaw - $h/2R = 0.35$ , $K_R = 0.4$ sec, $\mathcal{J} = 0$ -----	220
7-15	Ascent Roll - $h/2R = 0.65$ , $K_R = 0.4$ sec, $\mathcal{J} = 0$ -----	221
7-16	Ascent Roll - $h/2R = 0.35$ , $K_R = 0.4$ sec, $\mathcal{J} = 0$ -----	222
7-17	Transient Response to a Unit Step Input - Descent Yaw - Gain = $K_O/2$ , $h/2R = 1.0$ -----	223
7-18	Transient Response to a Unit Step Input - Descent Yaw - Gain = $K_O/2$ , $h/2R = 0.5$ -----	224
7-19	Transient Response to a Unit Step Input - Descent Yaw - Gain = $K_O/2$ , $h/2R = 0.4$ -----	225
7-20	Transient Response to a Unit Step Input - Ascent Yaw - Gain = $K_O/2$ , $h/2R = 0.65$ -----	226
7-21	Transient Response to a Unit Step Input - Ascent Yaw - Gain = $K_O/2$ , $h/2R = 0.35$ -----	227
7-22	Schematic Model of LEM Structure-----	228
7-23	Maximum Describing Gain Ratio Versus Saturation Deadband Ratio	229
7-24	Location of Open Loop Roots in Complex Plane-----	230
7-25	Block Diagram of Attitude Control Loop Including Structural Dynamics-----	231
7-26	Ascent Stage Propellant Tank Configuration-----	188
7-27	Descent Stage Propellant Tank Configuration-----	189

~~CONFIDENTIAL~~LIST OF TABLES

<u>Table</u>	<u>Title</u>	<u>Page</u>
1-1	Control System Parameters-----	6
1-2	Summary of RCS Propellant Requirements-----	7
3-1	Mass Property History-----	72
3-2	Modulator Parameters for Moment Unbalance Study-----	73
3-3	Propellant Requirements - Attitude Control and Rotational Maneuvering Breakdown-----	77
4-1	A Comparison Between the Logic Coupled and Logic Uncoupled Jet-pair Cutoff Schemes-----	98
5-1	Gimballed Engine Force Equilibrium Equations-----	106
5-2	Gimbal Trim System Propellant Requirements-----	142
5-3	Parameter Values-----	155
6-1	System Constants-----	164
7-1	Descent Yaw Axis Damping-----	193
7-2	Descent Roll Axis Damping-----	193
7-3	Ascent Roll Axis Damping-----	194
7-4	Ascent Yaw Axis Damping-----	194
7-5	Descent Yaw Axis Transient Response-----	195
7-6	Ascent Yaw Axis Transient Response-----	196
7-7	System Parameters-----	202
7-8	Numerical Results-----	203
7-9	Single Axis Sloshing Dynamics Equations for LEM Vehicle-----	191

~~CONFIDENTIAL~~

~~CONFIDENTIAL~~

## LIST OF SYMBOLS

<u>Section</u>	<u>Page</u>
1,2-----	2
3-----	17
5-----	101
6-----	158
7-----	184

~~CONFIDENTIAL~~



~~CONFIDENTIAL~~

PAGE 1

SECTION 1

SUMMARY:

~~CONFIDENTIAL~~

GRUMMAN AIRCRAFT ENGINEERING CORPORATION

REPORT NO. LED-500-3

DATE 30 Sept. 1964

~~CONFIDENTIAL~~SYMBOLS USED IN SECTIONS 1 & 2

<u>Symbol</u>	<u>Definition</u>	<u>Units</u>
a	gimbal trim system error rate threshold	rad/sec.
D <sub>1</sub>	gimbal trim system error threshold	rad.
D	deadband	rad.
e <sub>P</sub>	yaw axis total error	rad.
e <sub>Q</sub>	pitch axis total error	rad.
e <sub>R</sub>	roll axis total error	rad.
e <sub>1</sub>	modulator operating range	rad.
K <sub>R</sub>	rate gain	sec.
p	yaw axis body rate	rad/sec
p <sub>e</sub>	yaw axis rate error	rad/sec
p <sub>c</sub>	yaw axis rate command	rad/sec
p <sub>L</sub>	yaw axis rate limit	rad/sec
q	pitch axis body rate	rad/sec
q <sub>e</sub>	pitch axis rate error	rad/sec
q <sub>c</sub>	pitch axis rate command	rad/sec
q <sub>L</sub>	pitch axis rate limit	rad/sec
r	roll axis body rate	rad/sec
r <sub>e</sub>	roll axis rate error	rad/sec
r <sub>c</sub>	roll axis rate command	rad/sec
r <sub>L</sub>	roll axis rate limit	rad/sec
t <sub>on min</sub>	modulator minimum electrical pulse width	sec.
φ <sub>b</sub>	yaw axis attitude error	rad.
θ <sub>b</sub>	pitch axis attitude error	rad.
ψ <sub>b</sub>	roll axis attitude error	rad.
1C <sub>b</sub>	vehicle attitude in guidance coordinates	rad.
1C <sub>c</sub>	attitude command in guidance coordinates	rad.
1C <sub>e</sub>	attitude error in guidance coordinates	rad.
1C <sub>s</sub>	body axis attitude error	rad.
[M <sub>S</sub> ]	transformation matrix from guidance coordinates to body axes	

Code 26512 Eng-23-1A

~~CONFIDENTIAL~~

~~CONFIDENTIAL~~SYMBOLS USED IN SECTIONS 1 & 2

<u>Symbol</u>	<u>Definition</u>	<u>Units</u>
$\omega_n$	rate gyro natural frequency	rad/sec
$\omega_f$	filter natural frequency	rad/sec
$\zeta_n$	rate gyro damping ratio	
$\zeta_f$	filter damping ratio	
$\delta$	gimbal actuator gain	rad/sec
$\tau$	gimbal actuator time constant	sec.
$\lambda$	modulator nonlinearity factor	
$\epsilon_{QN}$	filtered pitch axis error	rad.
$\epsilon_{RN}$	filtered roll axis error	rad.
$\dot{\epsilon}_{QA}$	trim system pitch axis error rate	rad/sec.
$\dot{\epsilon}_{RA}$	trim system roll axis error rate	rad/sec.

Code 26512 Eng-23A

~~CONFIDENTIAL~~REPORT LED-500-3  
DATE 30 Sept. 1964

GRUMMAN AIRCRAFT ENGINEERING CORPORATION

~~CONFIDENTIAL~~

This report presents the results of a series of analyses performed from January 1963 to June 1964 which have been conducted to enable selection of a functional configuration (Figure 1-1) for the attitude control portion of the LEM Flight Control System. These analyses are concerned primarily with the stability and response of the vehicle in the automatic control modes and with the compatibility between the automatic and manual modes.

The attitude control system accepts attitude and thrust vector commands from the Navigation and Guidance System (primary or abort) and manual commands from the astronaut. Control torques are generated by a combination of 16 reaction jets and a gimballed rocket engine for the descent stage, but only by the 16 reaction jets (fixed ascent rocket engine) for the ascent stage.

Figure 1-1 presents schematically the LEM attitude control system, its operating modes and logic inputs. Table 1-1 summarizes the values recommended for the attitude control system parameters. These parameter values were determined from the various analyses performed to determine the attitude control system configuration. Based upon these control system parameters, the RCS propellant requirements for attitude control for a typical LEM mission were estimated. These propellant requirements are tabulated in Table 1-2.

Non-linear pulse ratio modulators have been selected to generate the rotation torque thrust commands to be delivered to the reaction jets. These modulators were selected because they yield satisfactory attitude control for normal limit cycle, disturbed limit cycle and large transient response operation while minimizing the number of thruster operations. The non-linear PRM assures convergence to a minimum impulse limit cycle (coasting periods) in the presence of vehicle inertia variation, jet time delays and control system lags. It provides excellent propellant economy and jet pulsing frequency control for moment unbalance operation (thrusting periods) by virtue of the long pulse widths generated, and requires the minimum number of changes of control system parameters during the LEM mission. Also, a single deadband on the total error in each axis ( $e_p$ ,  $e_Q$  and  $e_R$ ) rather than two deadzones (one on the total error and one on the attitude error ( $\phi_b$ ,  $\theta_b$  and  $\psi_b$ )) was selected to avoid undesirable limit cycles.

A descent rocket engine gimbal servo was selected which is a constant speed, irreversible drive, non-linear phase lead stabilized open loop actuator. This low response trim system was selected because of the inherent simplicity and reliability advantages of the constant speed actuators over proportional actuators, of irreversible drive over reversible drive, and of open loop actuator control over closed loop actuator control. Maneuvering control is provided by the reaction jets.

For ascent thrust vector control, it was concluded that the reaction jets alone will provide adequate maneuver and trim control for the expected levels of disturbance torques.

To meet the requirements of the Abort Guidance System (AGS) with the  $T_1$  compensation law, it was found that the attitude offset error due to control system response to moments generated by the vehicle c.g. offset when thrusting with the ascent engine must be removed. Addition of integral compensation

Code 26512

Eng-23-1A



~~CONFIDENTIAL~~

on the attitude error signal will remove the offset, thereby, satisfying  $T_1$  compensation requirements. It was shown that satisfactory control stability could be attained with proper choice of the integral gain. However, it was also determined that integral compensation should not be used during coasting periods in order to avoid deterioration of the coasting limit cycles.

Integral compensation will provide control of attitude offset errors during ascent engine burn times, but the  $T_1$  compensation law also requires control of the total thrust vector alignment error. The thrust vector must be controlled because thrust vector misalignment with respect to the inertial reference axes will introduce position and velocity errors into the abort guidance law. A pendulous accelerometer was selected to provide the necessary information to control the thrust vector with respect to the reference axes. To select accelerometer parameters, which will insure control system stability, a stability analysis was performed on the resultant control system. It was found that parameters for the accelerometer could be specified which will provide both satisfactory alignment response and control system stability.

The use of quantized attitude information in place of continuous attitude information was studied as part of a strap-down guidance feasibility study. This study showed that for the range of vehicle moments of inertia considered it is possible to use quantization levels of at least 0.03 degree without a great penalty in coasting limit cycle propellant consumption, provided that continuous rate information is used. It was also verified that satisfactory transient response is obtained when the attitude feedback is quantized.

Analyses were performed to determine control system stability in the presence of an elastic airframe and propellant sloshing. The analyses verified that LEM control system is stable for the vehicle and tank configurations considered. It was also concluded that anti-slosh baffles are necessary in both ascent and descent tanks to improve transient response damping.

It should be noted that all data presented in this report was generated prior to June 1964.

~~CONFIDENTIAL~~

GRUMMAN AIRCRAFT ENGINEERING CORPORATION

REPORT LED-500-3  
DATE 30 Sept. 1964

~~CONFIDENTIAL~~

TABLE 1 - 1

Control System Parameters

(1 June 1964)

PARAMETER	DESCENT		ASCENT		UNITS
	Nominal Value	Tolerance	Nominal Value	Tolerance	
$K_R$	1.5	$\pm 5\%$	0.4	$\pm 5\%$	sec
$P_L$	5	$\pm 5\%$	5	$\pm 5\%$	deg/sec
$q_L$	10	$\pm 5\%$	10	$\pm 5\%$	deg/sec
$r_L$	5	$\pm 5\%$	5	$\pm 5\%$	deg/sec
D	0.1 or 5.0	$\pm 10\%$	0.1 or 5.0	$\pm 10\%$	degrees
$\delta$	0.2	$\pm 10\%$	--	$\pm 10\%$	deg/sec
$\tau$	0.1	--	--	--	sec
$\omega_n$	125	$\pm 20\%$	125	$\pm 20\%$	rad/sec
$\omega_f$	113	$\pm 20\%$	113	$\pm 20\%$	rad/sec
$\zeta_n$	0.7	$\pm 0.1$	0.7	$\pm 0.1$	--
$\zeta_f$	0.8	--	0.8	--	--
$\lambda$	0.1	--	0.1	--	--
$t_{onmin}$	$10 \times 10^{-3}$	--	$10 \times 10^{-3}$	--	sec
$e_1$	0.5	--	0.5	--	deg
a	0.00	$\pm .01$	--	--	deg
$D_1$	0.09	$\pm .01$	--	--	deg

Code 26512

Eng-23-1A

~~CONFIDENTIAL~~

TABLE 1-2

Summary of RCS Propellant Requirements\*\*

Mission Phase	Limit Cycle			Maneuvers***
	Time (sec)	Dead Zone (deg)	Propellant (lbs)	Propellant (lbs)
<u>DESCENT</u>				
Separation	78	.1	.2	5.6 (2)
Orientation and Insertion Prep.	792	.1	2.0	22.7 (8)
Coast to Pericynthion	3600	5.0	.2	8.1 (3)
Automatic Powered	710	.1	39.2	8.1 (2)
<u>ASCENT</u>				
Powered	430	.1	172.7*	2.3 (2)
Contingency Stay	600	.1	15.9	6.8 (20)
Coast	5400	5.0	3.0	1.9 (9)
Rendezvous	847 600	5.0 .1	.5 15.9	— —

\* 170# of the 172.7# provides a useful  $\Delta V = 226$  ft/sec, which is equivalent to 128# of ascent main tank propellant.

\*\* Manual landing and docking propellant requirements are not included.

\*\*\* Number of maneuvers assumed is shown in parentheses.

Code 26512 Eng-23A



GIMBAL TRIM SYSTEM

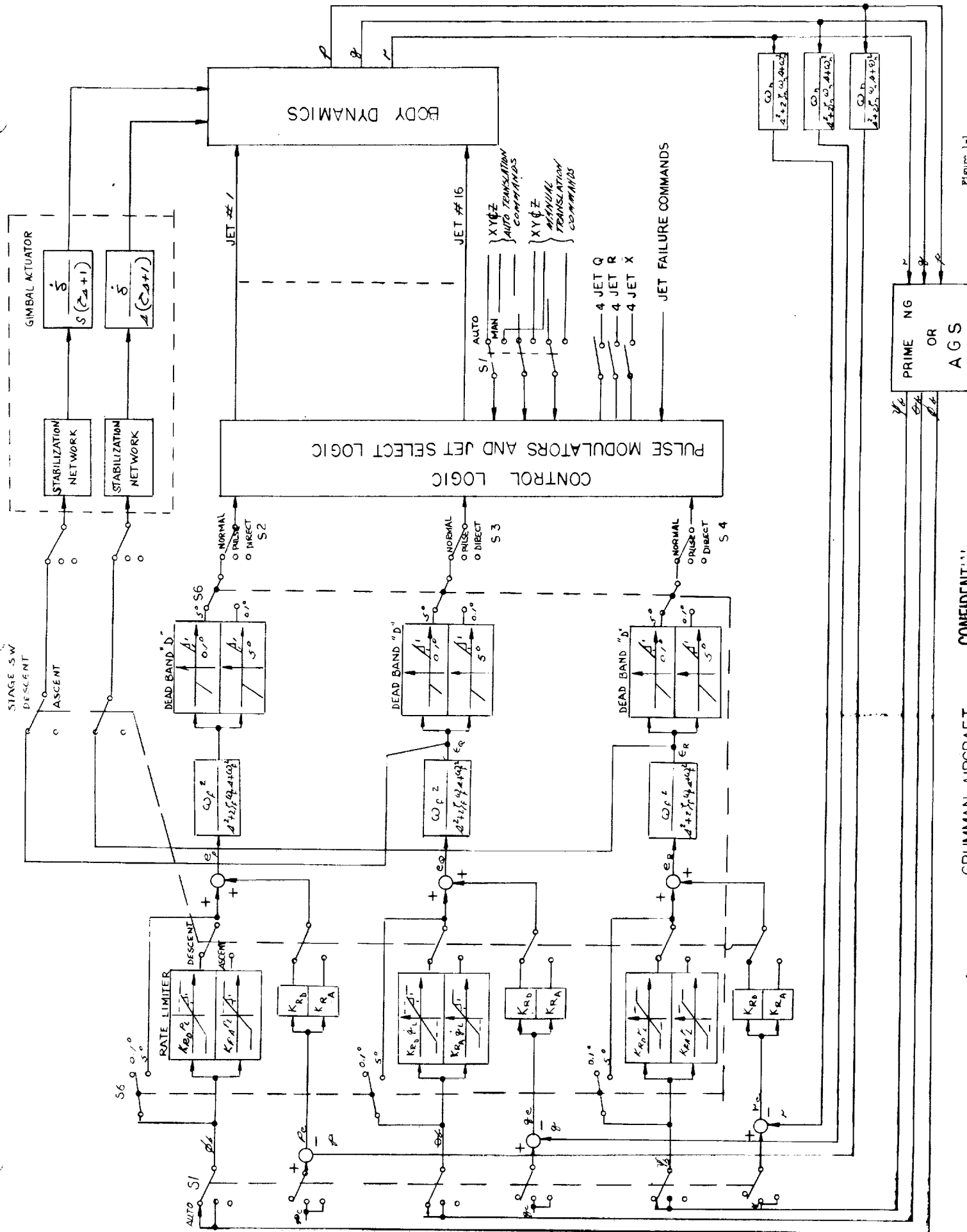


Figure 1-1  
CONTROL SYSTEM ANALYSIS BLOCK DIAGRAM



~~CONFIDENTIAL~~

PAGE 9

SECTION 2

INTRODUCTION

~~CONFIDENTIAL~~

GRUMMAN AIRCRAFT ENGINEERING CORPORATION

REPORT NO. LED-500-3

DATE 30 Sept. 1964

~~CONFIDENTIAL~~

## 2.1 PURPOSE OF REPORT

This report presents the results of a series of analyses performed from January 1963 to June 1964 which have been conducted to enable selection of a functional configuration for the attitude control portion of the LEM Flight Control System. These analyses are concerned primarily with the stability and response of the vehicle in the automatic control modes and with the compatibility between the automatic and manual modes, and apply to lunar landing mission.

## 2.2 CONTROL SYSTEM CONFIGURATION

The attitude control system accepts attitude and thrust vector commands from the Navigation and Guidance System (primary or abort), manual commands from the astronaut and provides the required vehicle control response and stability.

The LEM attitude is maintained by the control torque produced from sixteen reaction jets located on the LEM as shown in Figure 2-1. The attitude control system generates thrust commands for the reaction jets based upon control error signals, directs each command to the proper jets, and thereby maintains attitude control. The jet commands are generated and directed by the control logic which consists of error dependent pulse modulators and a jet select logic. For some of the manual modes of control, the astronaut replaces the modulator and separate jet select logic is made an integral part of the rotational control stick. During powered descent attitude is maintained in the pitch and roll axes by the descent engine gimbal trim system.

The attitude control system is functionally depicted by the block diagram in Figure 1-1.\* References 1, 2, 3 and 4 accurately define the Flight Control System in terms of the overall functional diagram (1)\*\* and the component specifications (2, 3, 4).

The block diagram in Figure 1-1 presents schematically the LEM attitude control system and its operating modes and logic inputs. The operating modes are:

A - Rotational Operating Modes (These modes may be selected independently for each axis)

1 - Normal (closed loop)

- a) Automatic control mode
- b) Rate command with attitude hold control mode
- c) Rate command control mode

Note: For either a, b or c, all axes are selected simultaneously.  
b and c are manual modes.

2 - Pulse Mode (open loop) - manual mode which generates a fixed train of reaction jet thrust pulses. All jets are selected by jet select logic.

\* See section 1 for list of symbols

\*\* Numbers in parentheses correspond to reference numbers in Bibliography (Section 8).

~~CONFIDENTIAL~~



- 3 - Direct (open loop) - manual mode which bypasses jet select logic; i.e., the control stick is hard wired to RC jet emergency coils and is gated by a jet select logic which is an integral part of the control stick.
  - 4 - Direct Override - four jet direct rotation is obtained by full deflection of control stick. This control mode overrides normal, pulse and direct modes.
- B - Translational Operating Modes - all translation signals pass thru jet select logic.
- 1 - Automatic
  - 2 - Manual - a combination pulse and on-off; i.e., a fixed pulse train is generated for a given range of stick rotation while on-off control is generated for all larger rotations.

All operating modes are selected manually by the astronaut. The rotational operating mode select switches (S2, S3, and S4) select independently for all three axes the normal, pulse and direct modes. The normal control modes, automatic, rate command attitude hold and rate command, are manually selected simultaneously for all three axes by the attitude mode control switch (S1). Manual translation commands are selected simultaneously for all axes by the automatic-manual translation switch (S1). The pitch and roll rotation and the X axis translation response level (2 or 4 jet) are manually and individually selected by the astronaut while the deadband (large or small) is selected manually by S6 for all three axes simultaneously. The small value of deadband is also automatically selected (not shown) for all three axes whenever the ascent or descent engines are thrusting.

When the control system is put in the automatic (normal) rotational control mode (Figure 1-1), attitude errors are generated by the Navigation and Guidance System (prime or abort) steering equations; that is the guidance steering equations must form the error vector

$$\vec{\Omega}_e = \vec{\Omega}_c - \vec{\Omega} \quad (2 - 1)$$

in its own coordinate system between vehicle attitude and desired attitude. In order for the control system to properly respond to this guidance steering error,  $(\vec{\Omega}_e)$ , a transformation matrix is required to transform  $\vec{\Omega}_e$  from guidance coordinates into body axes, autopilot commands; i.e.

$$\vec{\omega}_b = \begin{bmatrix} \phi_b \\ \theta_b \\ \psi_b \end{bmatrix} = [M_S] \vec{\Omega}_e \quad (2 - 2)$$

Code 26512 Eng-23A

~~CONFIDENTIAL~~

This transformation is accomplished by the CDU and LGC on LEM. Therefore, the total control error becomes

$$e_p = \Phi_b + p_e K_R$$

$$e_Q = \Theta_b + q_e K_R$$

(2 - 3)

$$e_R = \Psi_b + r_e K_R$$

In the rate command attitude hold (normal) mode,  $\eta_e$  is maintained at zero by the Navigation and Guidance System when the control stick is out of detent; i.e.  $\Phi_b$ ,  $\Theta_b$  and  $\Psi_b$  are zero in equations 2-3. This rapid followup permits the control error for each axis to be dependent solely on the rate commands and the vehicle body rates. Therefore, equations 2-3 become

$$e_p = K_R(p_c - p)$$

$$e_Q = K_R(q_c - q)$$

(2 - 4)

$$e_R = K_R(r_c - r)$$

However, equations 2-3 still hold when the control stick is in detent. For the rate command mode equations 2-4 will hold since  $\Phi_b$ ,  $\Theta_b$ , and  $\Psi_b$  are disabled (Figure 1-1).

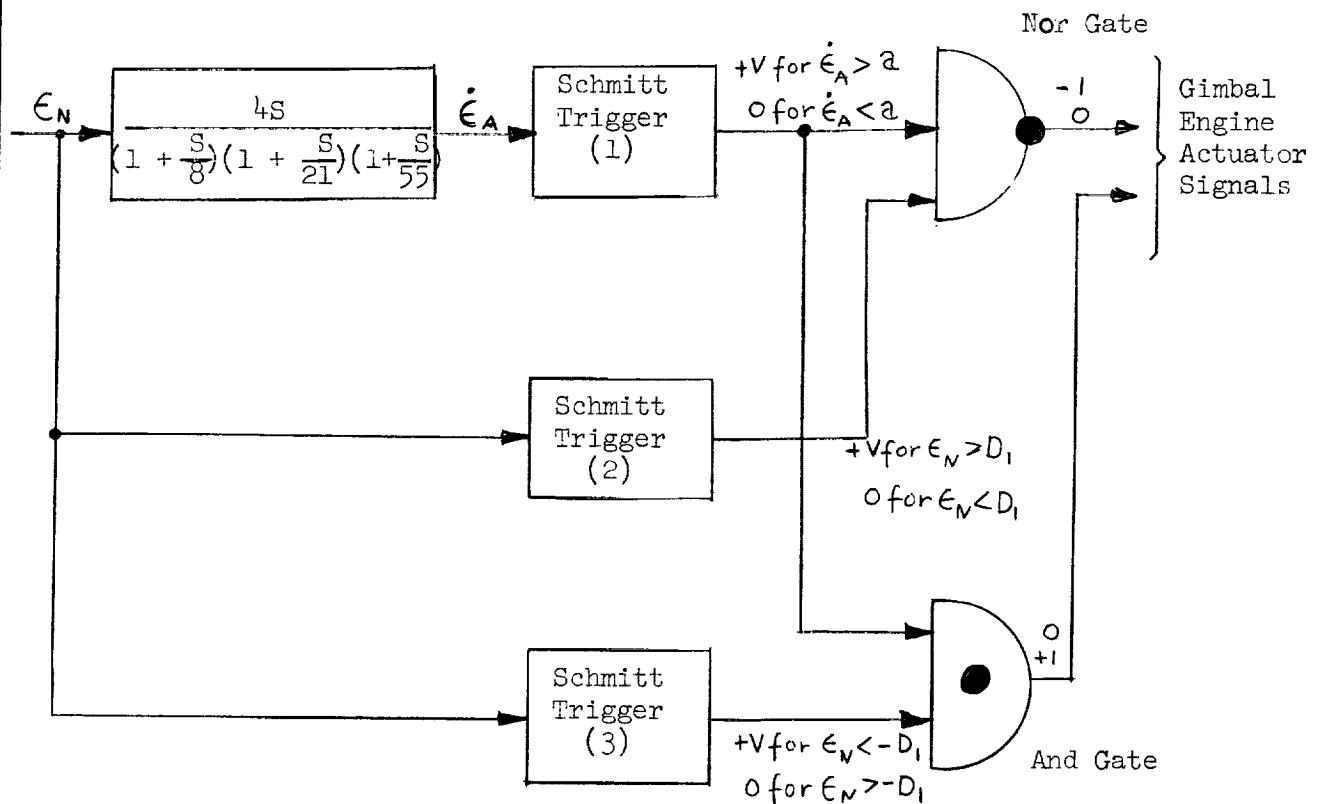
The logic equations which state the conditions which cause each of the 16 reaction jets to fire in response to error signals in the flight control system are discussed in detail in section 4. In a normal mode, the logic provides optimum control torques and translation forces in response to any combination of simultaneous rotation and translation commands. The input to the logic equations is comprised of pitch, yaw and roll rotation command signals; X, Y and Z translation commands; an astronaut executed 2 or 4 jet X-axis translation force level selection; astronaut selected 2 or 4 jet pitch and roll rotation torque levels, and astronaut activated jet failure logic switches. The jet failure logic switches accomplish the dual function of "RCS fuel and oxidizer isolation" and failure logic command. These switches will automatically change the control logic to take advantage of the remaining jets for any combination of simultaneous rotation and translation commands.

The rotation torque thrust commands consist of a train of constant amplitude pulses of varying width and frequency of occurrence, which are produced by non-linear pulse ratio modulators. In the direct modes of control system operation the pulse ratio modulator is replaced by a direct on-off signal. During control system automatic attitude hold operation, the system will limit cycle and the modulators will produce a typical electrical pulse of 10 ms.

~~CONFIDENTIAL~~

(10 ms pulse will generate the reaction jet minimum impulse).

The descent engine gimbal trim system (GTS) is required for thrust vector control during powered descent because the unbalance torques that can be generated by a fixed descent engine exceeds the torque capability of the RCS. However, the GTS will align the descent engine thrust vector so that it will pass near the vehicle CG and thereby reduce the unbalance torque. The GTS is implemented as shown in control system block diagram (Figure 1-1), and it is enabled only during powered descent phases of the IEM mission. The GTS stabilization network shown in Figure 1-1 is mechanized as shown below. A detailed discussion of the GTS is given in Section 5.



~~CONFIDENTIAL~~

### 2.3 SCOPE

This report has been written in a manner such that each section can be read without having to read any previous section, thereby permitting the reader to read only the section that is of particular interest to him. A summary of material covered in each section is given below.

Sections 3 and 4 contain the reaction jet control system analyses. In section 3, the selection of a pulse modulator, the vehicle attitude control propellant requirements and the control system deadzone analysis are considered while various reaction jet select logic schemes are presented in section 4. Section 5 presents various methods of thrust vector control for powered phases of the LEM mission. The descent engine gimbal trim system is discussed in great detail in this section.

The attitude control system stability in the presence of guidance feedback is considered in section 6 while section 7 presents the effects of propellant sloshing and elastic airframe on control system stability.

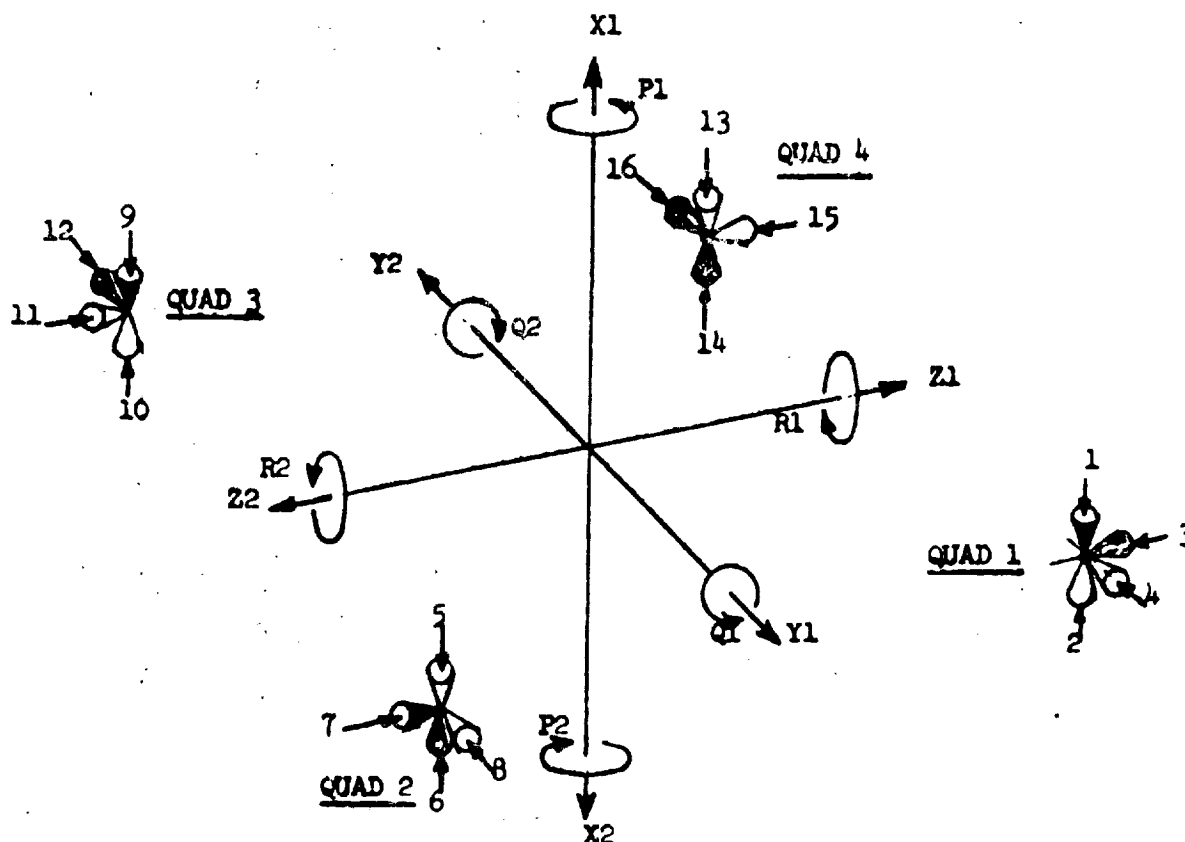
Code 26512

Eng-23-1A

REPORT LED-500-5  
DATE 30 Sept. 1964

~~CONFIDENTIAL~~

GRUMMAN AIRCRAFT ENGINEERING CORPORATION



CODE:

Subscript 1: Positive Rotation or Translation

Subscript 2: Negative Rotation or Translation

▲ Fuel System "A"

▲ Fuel System "B"

Figure 2-1

RCS JET THRUSTER CONFIGURATION



~~CONFIDENTIAL~~

SECTION 3

REACTION JET CONTROL SYSTEM ANALYSIS

Code 26512 Eng-23A

~~CONFIDENTIAL~~

GRUMMAN AIRCRAFT ENGINEERING CORPORATION

REPORT LED-500-3  
DATE 30 Sept. 1964

~~CONFIDENTIAL~~

## SYMBOLS USED IN SECTION 3

<u>Symbol</u>	<u>Definition</u>	<u>Units</u>
A	induced rate modulator output level	
D	duty factor	
e	modulator input signal	rad.
F	thrust per reaction jet	lbs.
f	modulator pulse repetition frequency	pulses/sec
h	hysteresis	rad.
I	vehicle moment of inertia	slug-ft <sup>2</sup>
I <sub>sp</sub>	specific impulse	sec.
I <sub>T</sub>	reaction jet total impulse	lb.-sec.
K	induced rate modulator feedback gain	rad./sec.
K <sub>θ</sub>	attitude feedback gain	
K <sub>R</sub>	rate feedback gain	sec.
L	reaction jet moment arm	ft.
M <sub>c</sub>	control moment	ft.-lbs.
M <sub>u</sub>	unbalance moment	ft.-lbs.
PFM	Pulse Frequency Modulator	
PRM	Pulse Ratio Modulator	
PWM	Pulse Width Modulator	
t <sub>on</sub>	electrical pulse width	sec.
t <sub>off</sub>	electrical off time	sec.
T <sub>p</sub>	time to next pulse	sec.
T <sub>w</sub>	thrust on time	sec.
X <sub>..</sub>	normalized error signal	
α, θ	vehicle acceleration	rad/sec <sup>2</sup>
α <sub>c</sub>	vehicle control acceleration	rad/sec <sup>2</sup>
α <sub>u</sub>	vehicle unbalance acceleration	rad/sec <sup>2</sup>
ζ <sub>u</sub>	rate gyro damping ratio	
θ	vehicle attitude	rad.
θ <sub>c</sub>	attitude command	rad.
θ <sub>AV</sub>	average vehicle attitude	rad.
θ <sub>coast</sub>	angle vehicle coasts in normal limit cycle	rad.
θ <sub>osc p-p</sub>	peak to peak attitude excursion	rad.
θ	vehicle body rate	rad/sec

Code 26512 Eng-23-1A

~~CONFIDENTIAL~~



~~CONFIDENTIAL~~

## SYMBOLS USED IN SECTION 3 (Continued)

<u>Symbol</u>	<u>Definition</u>	<u>Units</u>
$\dot{\theta}_A$	normal limit cycle coasting rate (residual rate)	rad/sec
$\dot{\theta}_B$	rate gyro bias	rad/sec
$\dot{\theta}_C$	rate command	rad/sec
$\dot{\theta}_{RG}$	rate gyro deadzone	rad/sec
$\dot{\theta}_{RL}$	rate limit	rad/sec
$\theta_{osc \text{ p-p}}$	peak to peak rate oscillation	rad/sec
$\lambda$	PRM nonlinearity factor	
$\tau_p$	modulator integrating time for first pulse	sec.
$\tau_{on}$	thrust "on delay"	sec.
$\tau_{off}$	thrust "off delay"	sec.
$\tau_G$	rate gyro delay	sec.
$\tau_l$	induced rate modulator feedback time constant	sec.
$\Omega$	deadzone on total vehicle error	rad.
$\Omega_a$	deadzone on attitude error	rad.
$\dot{w}$	propellant	lbs.
$\dot{w}$	propellant flow rate	lbs/sec
$\omega_n$	rate gyro natural frequency	rad/sec

Code 26512 Eng-23A

~~CONFIDENTIAL~~

GRUMMAN AIRCRAFT ENGINEERING CORPORATION

REPORT LED-500-3  
DATE 30 Sept. 1964

~~CONFIDENTIAL~~

### 3.1 Introduction

LEM attitude control is maintained by the control torque produced from sixteen one-hundred pound reaction jets located on LEM as shown in Figure 2-1. Four reaction jets will be available for rotation about each axis provided the astronaut activates the appropriate 2-4 jet switches. However, two jet control will be considered normal for all rotations in the analyses. Error dependent modulators, which will yield the desired attitude and attitude rates throughout the LEM mission, are required to control the jets in conjunction with an appropriate jet select logic.

To insure that the best modulator or combination of modulators is selected to control LEM attitude for disturbed limit cycle operation, normal limit cycle operation and rotational maneuvers, it was necessary to study many types of modulators. Each modulator was studied with respect to the following:

- a) Normal (undisturbed) limit cycle rates, attitude excursions, and propellant flow rate. Also considered was the value of rate gyro deadzone which can be tolerated without deteriorating the limit cycle.
- b) Moment unbalance (disturbed) limit cycle peak to peak (P-P) rate changes, P-P attitude changes, average attitude offset and propellant requirements.
- c) Transient response to large rate and attitude commands.

Both analytical and simulation results of the modulators studied will be presented in the following sections.

Aside from the modulator study the control system attitude deadband constraints and mission propellant requirements were also considered. A rigid body, single axis rotation, with all cross-coupling terms neglected was assumed for the LEM for the purposes of studying the above and evaluating the various modulators to be considered. Also, the effects of the rate gyro dynamics, reaction jet thrust "on" and "off" delays, reaction jet specific impulse variation and vehicle moment of inertia variations on limit cycle operation are considered.

The reaction jet select logic techniques are discussed in detail in section 4.

### 3.2 Propellant Flow Rate

3.2.1 Introduction It is a prime consideration from a weight point of view to minimize reaction jet propellant flow rates for normal limit cycle,

Code 26512

Eng-23-1A

REPORT  
DATELED-500-3  
30 Sept. 1964~~CONFIDENTIAL~~

GRUMMAN AIRCRAFT ENGINEERING CORPORATION

disturbed limit cycle and maneuvers. In this section the relations for propellant flow rate for the above and the criteria for minimizing propellant flow rate are determined.

### 3.2.2 Normal Limit Cycle Propellant Flow Rate

Propellant flow rate for normal limit cycle (2 jets) is given by (5)

$$\dot{\omega} = \frac{2F}{I_{sp}} D \quad (3-1)$$

where  $\dot{\omega}$  - propellant flow rate -lbs/sec  
 $F$  - thrust per reaction jet -lbs  
 $I_{sp}$  - specific impulse -sec  
 $D$  - duty factor

Duty factor ( $D$ ) is defined as the ratio of electrical pulse width and the sum of electrical pulse width ( $t_{on}$ ) and electrical off-time ( $t_{off}$ ).  
 $I_{sp}$  variation as a function of electrical pulse width is shown in Figure 3-1.

Assuming a symmetrical limit cycle as shown in Figure 3-2 we have

$$D = \frac{t_{on}}{t_{on} + t_{off}} \quad (3-2)$$

$$\text{where } t_{off} = (t_1 - t_o) + (t_4 - t_3) \quad (3-3)$$

$$\theta_1 = \Omega - \frac{K_R (\Delta \dot{\theta})}{2} \quad (3-4)$$

$$\theta_2 = \Omega - (K_R - \tau_{on}) \frac{\Delta \dot{\theta}}{2} \quad (3-5)$$

$$t_1 - t_o = 2 (\theta_1 + \theta_2) / \Delta \dot{\theta} \quad (3-6)$$

$$t_4 - t_3 = \tau_{off}; t_2 - t_1 = \tau_{on} \quad (3-7)$$

$$\Delta \dot{\theta} = 2 \int_{t_o}^{t_{on}} \left\{ \frac{F(t) L}{I} \right\} dt = 2 \frac{I_T L}{I} \quad (3-8)$$

where  $F(t)$  - reaction jet thrust as a function of time -lbs.  
 $L$  - reaction jet moment arm -ft.  
 $I$  - vehicle moment of inertia -slug-ft<sup>2</sup>  
 $I_T$  - reaction jet total impulse -lb.sec.  
 $\tau_{on}$  - jet on delay  
 $\tau_{off}$  - jet off delay

Substituting (3-2) thru (3-8) into (3-1) we get

$$\dot{\omega} = \frac{2F}{I_{sp}} \left[ \frac{2 t_{on} I_T L}{4 \Omega I + 2 I_T L (t_{on} + \tau_{off} + \tau_{on} - 2 K_R)} \right] \quad (3-9)$$

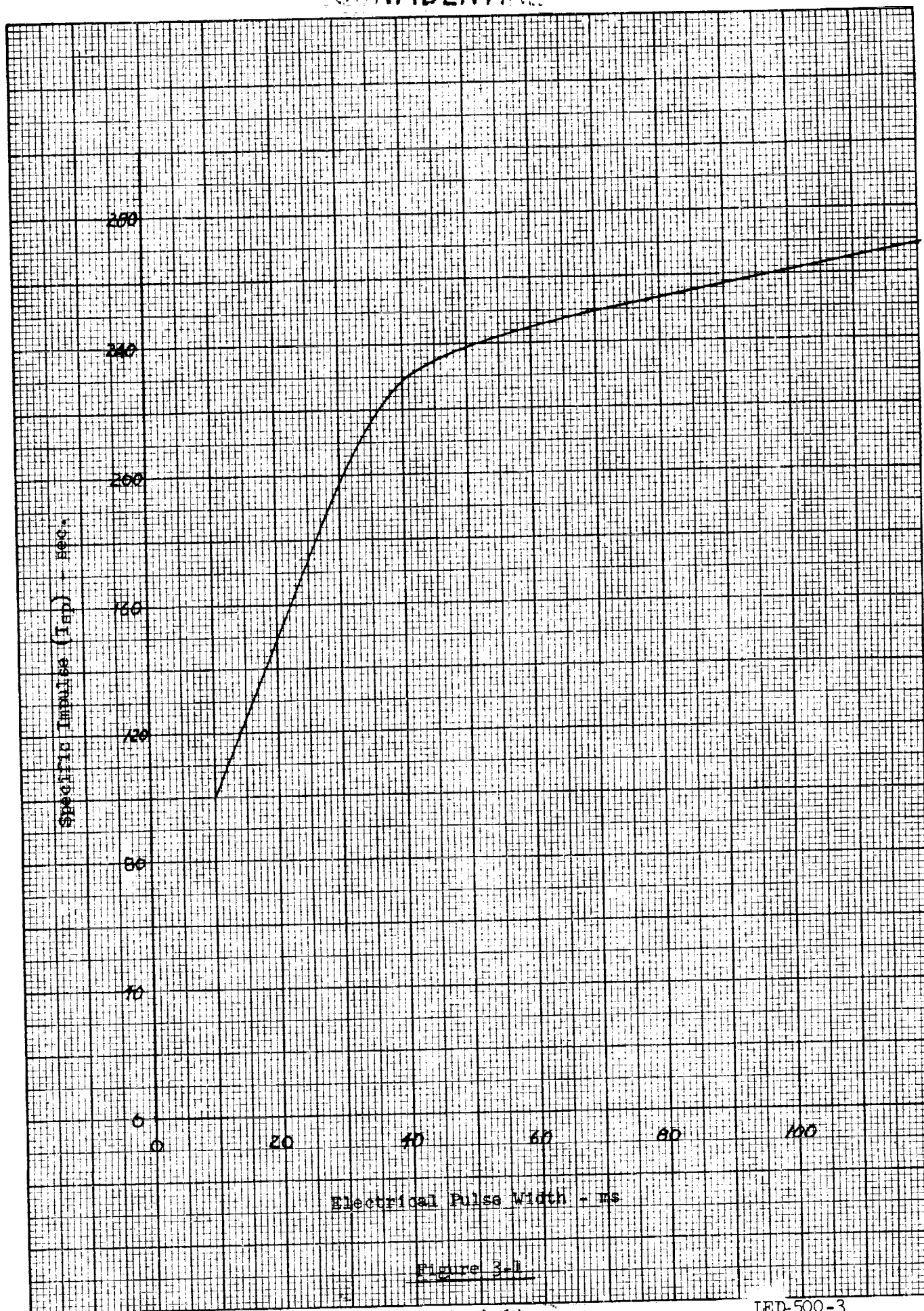


Figure 3-1

K&W 10 X 10 TO THE 1/2 INCH 359T-11  
KEUFFEL & ESSER CO. MADE IN U.S.A.  
ALBANY, N.Y.

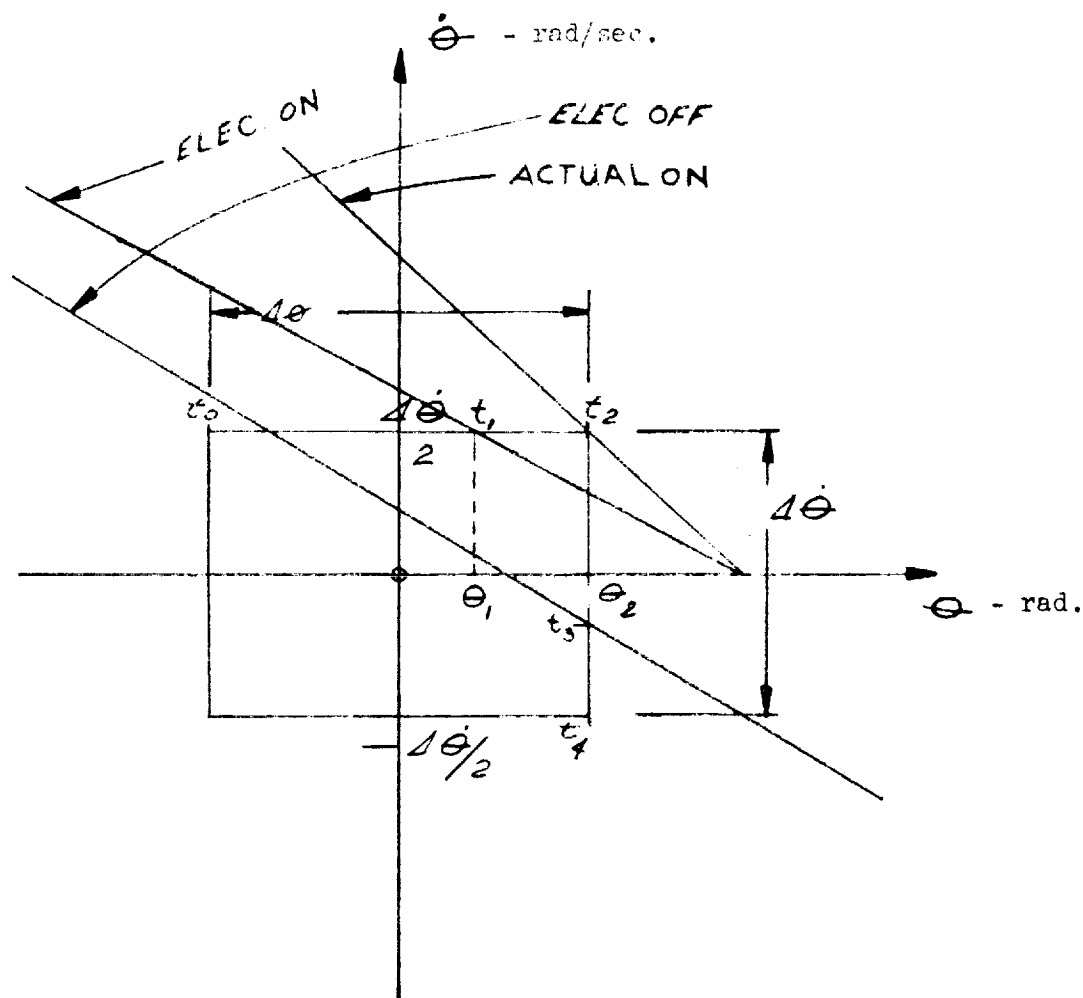


Figure 3-2 - Symmetrical Limit Cycle

~~CONFIDENTIAL~~

$$\text{or } \dot{\omega} = \frac{2F}{I_{sp}} \left[ \frac{t_{on} \Delta \dot{\theta}}{4 \Omega + \Delta \theta (t_{on} + \tau_{off} + \tau_{on} - 2K_R)} \right] \quad (3-10)$$

$I_{sp}$  and  $I_T$  versus electrical pulse width are plotted in Figures 3-1 and 3-3a respectively.

From equation (3-9) it can be seen that if  $t_{on}$  is minimized limit cycle propellant flow rate will be minimized; i.e., a minimum total impulse limit cycle yields the minimum propellant usage limit cycle (See Figure 3-3b).

3.2.3 Disturbed Limit Cycle Propellant Flow Rate - Propellant flow rate for limit cycle in the presence of a large disturbance is obtained from Figure 3-4, and is given by the following

$$\dot{\omega} = \frac{2F}{I_{sp}} \left[ \frac{|M_u| \left[ 1 + \frac{(\tau_{on} - \tau_{off}) |M_c - M_u|}{I(\Delta \dot{\theta})} \right]}{|M_c|} \right] \quad (3-11)$$

where  $M_u$  - moment unbalance-ft-lbs

$M_c$  - control moment -ft-lbs

Equation (3-11) is obtained by substituting

$$D = \frac{t_{on}}{t_{on} + t_{off}}$$

into equation (3-1) where

$$t_{on} = \frac{I(\Delta \dot{\theta})}{|M_c - M_u|} + \tau_{on} - \tau_{off} \quad (3-12)$$

$$t_{off} = \frac{I(\Delta \dot{\theta})}{|M_u|} + \tau_{off} - \tau_{on} \quad (3-13)$$

where  $\tau_{on}$  and  $\tau_{off}$  are defined in Figure 3-4. However, since  $\tau_{off} \approx \tau_{on}$ , equation (3-5) can be written as follows:

$$\dot{\omega} \approx \frac{2F}{I_{sp}} \frac{|M_u|}{|M_c|} \quad (3-11a)$$

From equation (3-11), it can be seen that propellant flow rate can be minimized only by maximizing  $I_{sp}$ .  $I_{sp}$  can be maximized by making  $t_{on}$  as large as possible. However,  $t_{on}$  cannot be arbitrarily increased since its value (i.e.  $(\Delta \dot{\theta})$ ) must be consistent with modulator switch lines as will be discussed in a following section.

3.2.4 Propellant Required for Large Maneuvers - Propellant required to complete each large maneuver is

$$\omega = 2F \sum_{j=1}^n \frac{t_j}{I_{sp_j}} \quad (3-14)$$

where 
$$t_j = \left[ \frac{(\Delta \dot{\theta})_j}{|\ddot{\theta}|} + \tau_{on} \right] \quad (3-15)$$

and  $(\Delta \dot{\theta})_j$  - is  $j^{th}$  vehicle rate change -rad/sec

$\ddot{\theta}$  - vehicle angular acceleration -rad/sec

$\tau_j$  -  $j^{th}$  electrical on time -sec.

$\ddot{\theta}$   
 $\theta$  is determined by vehicle inertias and is not controllable. Therefore, to minimize propellant consumed by rotational maneuvers  $\Delta \theta$  must be limited to a small value ( $\theta_{RL}$ ) consistent with allowable time for completion of maneuvers.

3.2.5 Summary - From the preceding, it is evident that to minimize propellant requirements for the LEM mission the following criteria must be satisfied:

- a) minimum impulse normal limit cycle must be generated by the error dependent modulators
- b) for disturbed limit cycle  $t_{on}$  must be as large as possible and still yield a limit cycle consistent with the modulator switch line characteristics.
- c)  $\theta_{RL}$  must be as small as possible for large maneuvers and still permit maneuvers to be completed in allotted time.

### 3.3 MODULATOR STUDY

3.3.1 Introduction To select a suitable modulator for the LEM attitude control system the single axis control loop shown in Figure 3-5 was assumed to determine limit cycle performance and transient response characteristics of the control system for each modulator. The modulators which were evaluated are:

- a) On-off modulator
- b) Induced rate modulator
- c) Pulse modulators

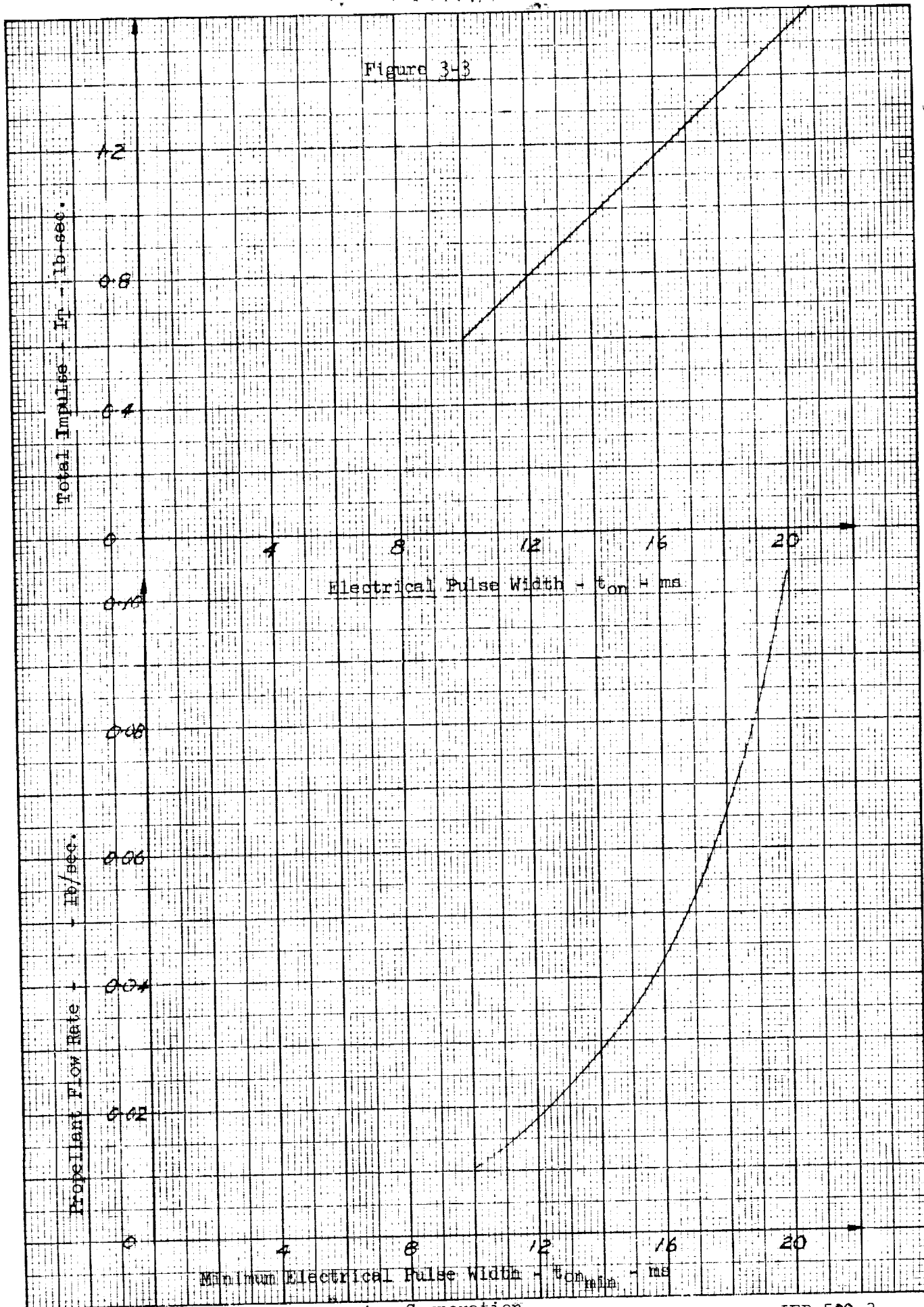
3.3.2 On-off Control - For on-off control the modulator in the RCS control loop is replaced by the relay characteristic shown in Figure 3-6a. The limit cycle characteristics for this modulator are determined entirely by the phase plane "jet-on" and "jet-off" switch lines for disturbed and undisturbed limit cycles. The equations defining the jet switch lines include the effects of rate gyro dynamics which are represented as a pure delay (Figure 3-7) and thrust function characteristics (Figure 3-8). For normal (undisturbed) limit

Code 26512

Eng-23A

10 X 10 TO THE 1/2 INCH  
KEUFFEL & ESSER CO.  
ALBANY, N.Y.

Figure 3-3





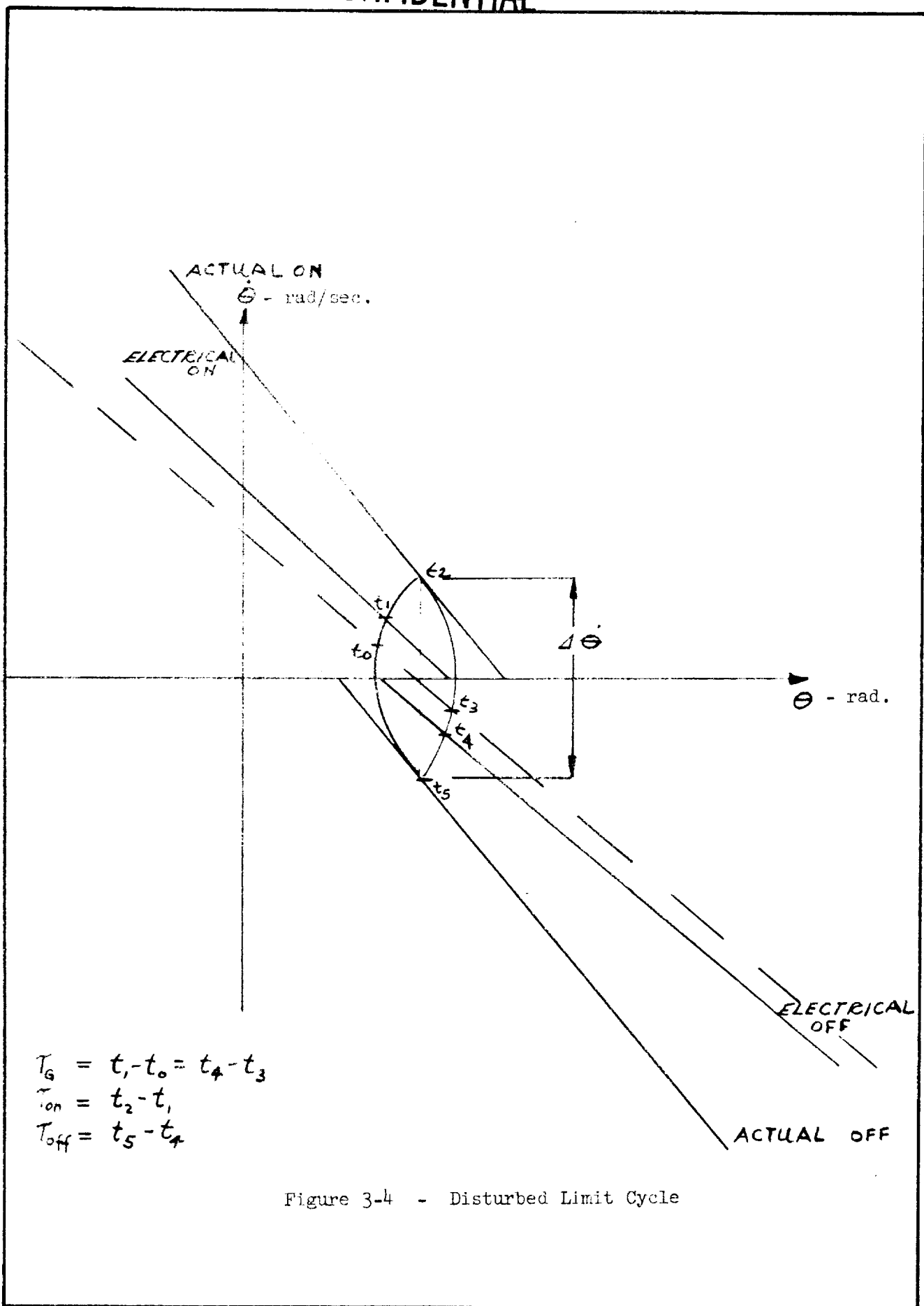
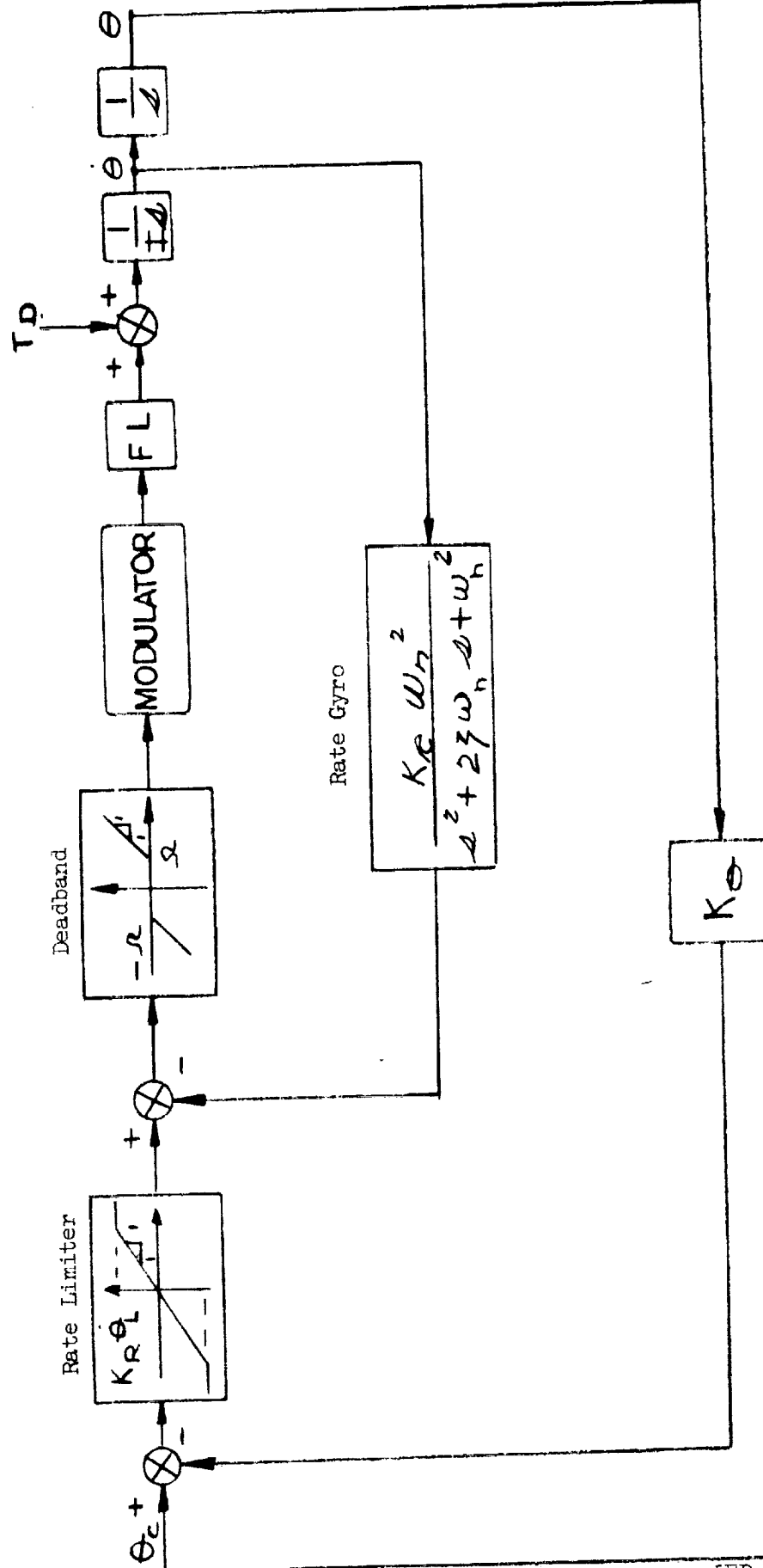


Figure 3-5 - Single Axis Attitude Control Loop



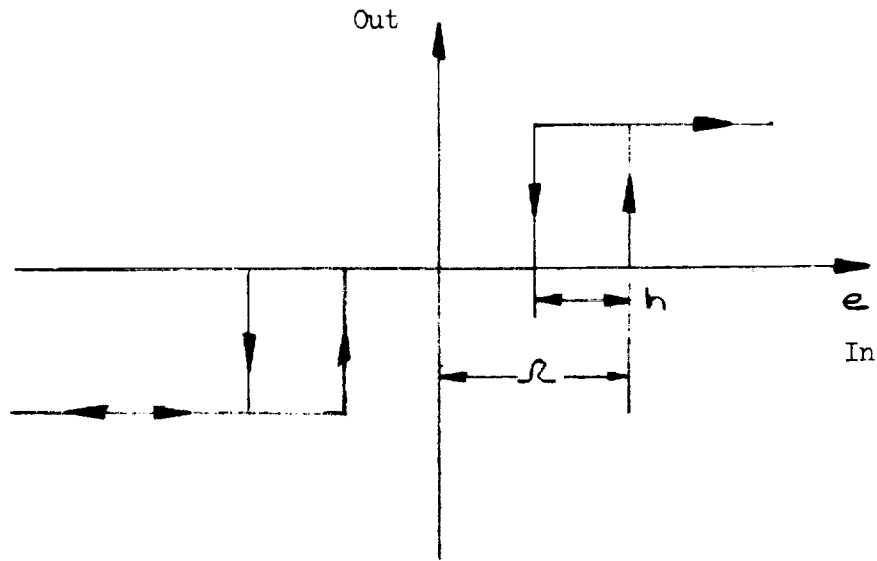


Figure 3-6a - On-off Modulator Characteristics

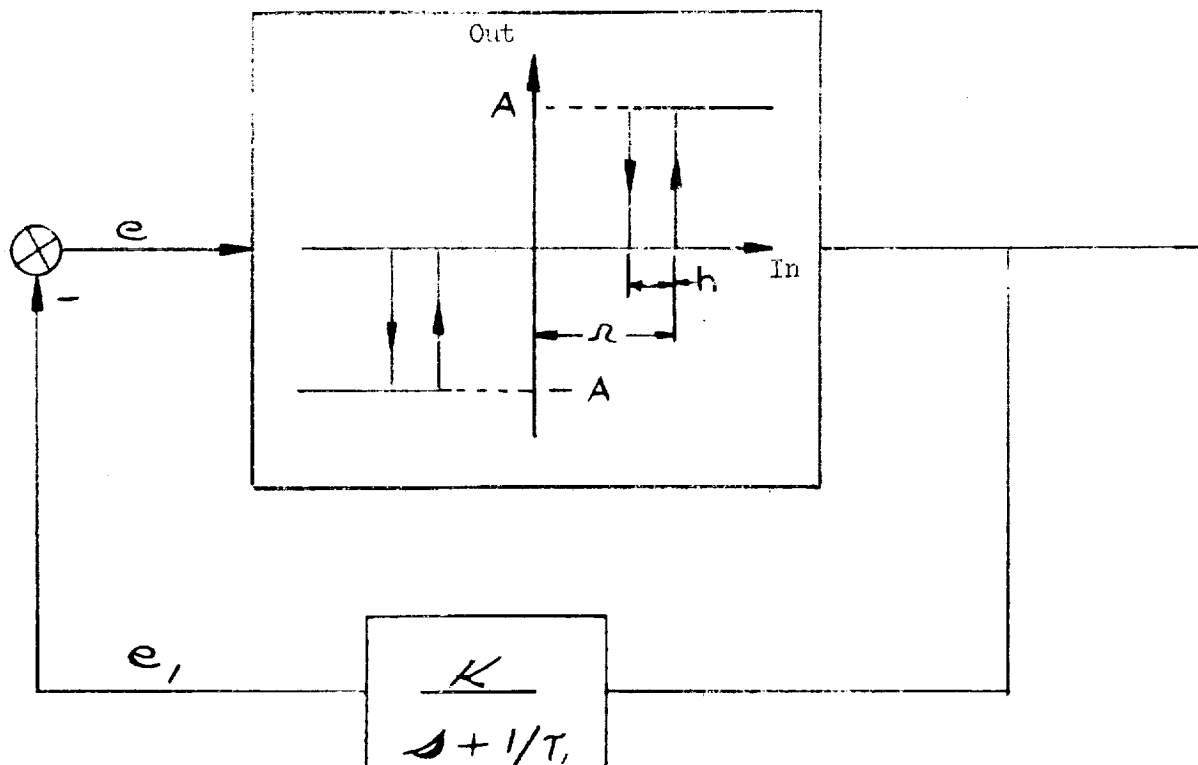


Figure 3-6b - Induced Rate Modulator Characteristics

~~CONFIDENTIAL~~

cycle the switch line equations can be obtained from Figure 3-5. They are:

On Switch Lines - Normal Limit Cycle

$$\text{Electrical} \quad K_R \dot{\theta} + K_\theta \theta = \pm \Omega \quad (3-16)$$

$$\text{Actual} \quad (K_R - K_\theta \tau_{on}) \dot{\theta} + K_\theta \theta = \pm \Omega \quad (3-17)$$

Off Switch Lines - Normal Limit Cycle

$$\text{Electrical} \quad K_R \dot{\theta} + K_\theta \theta = \pm h + \dot{\theta} K_R \tau_G \pm \Omega \quad (3-18)$$

$$\text{Actual} \quad (K_R - K_\theta \tau_{off}) \dot{\theta} + K_\theta \theta = \pm \Omega \pm h + \dot{\theta} A \quad (3-19)$$

$$\text{where} \quad A = K_R (\tau_{on} + \tau_G) - \frac{K_\theta \tau_{off}^2}{2} \quad (3-20)$$

From equations 3-17, 3-19 and 3-20 it can be seen, that for normal limit cycle on-off control, the following are true:

- $K_R = 0$  - system is unstable since slope of "on" and "off" switch lines are positive and equal to  $1/\tau_{on}$  and  $1/\tau_{off}$  respectively.  $K_R = 0$  also clearly shows the destabilizing effects of forward loop delays.
- $K_R = K_\theta \tau_{on}$  and  $K_R = K_\theta \tau_{off}$  define the infinite slope values for the actual on and off switch lines respectively.  $K_R$  must be greater than  $K_\theta \tau_{on}$  and  $K_\theta \tau_{off}$  for stability.
- "A" defines the change in location of the "off" switch line (equation 3-19) due to changes in  $\tau_{off}$ ,  $\tau_G$ ,  $K_\theta$  and vehicle acceleration ( $\dot{\theta}$ ). Figures 3-9, 3-10 and 3-11 show the effect of  $K_R$  variation on "off" switch line location. It can be seen from the figures that as  $K_R$  increases (A increases also) both coasting rate and attitude excursions decrease. As  $K_R$  (A) is increased further a point will be reached where thrusting will be continuous (first positive torque and then negative torque). The value of  $K_R$  for continuous operation is given by the following equation

$$K_{R_c} = \left[ \frac{2|\Omega|}{|\dot{\theta}|} + \frac{K_\theta \tau_{off}^2}{2} \right] \frac{1}{\tau_{off} + \tau_G} \quad (3-21)$$

which is obtained by equating equations 3-17 and 3-19 for plus and minus  $\Omega$  respectively.

Code 26512 Eng-23-1A

From the above it is apparent that  $K_R$  must be chosen greater than  $K_\theta \tau$  ( $\tau$  is  $\tau_{on}$  or  $\tau_{off}$ , whichever is larger) but less than the value given by equation 3-21. That is

$$\max (K_\theta \tau_{on}, K_\theta \tau_{off}) < K_R < K_{R_c} \quad (3-22)$$

The only remaining quantity of interest for normal limit cycle operation is propellant flow rate ( $\dot{\omega}$ ). It is desired to minimize  $\dot{\omega}$  for the LEM mission. From equation 3-10

$$\dot{\omega} = \frac{2F}{I_{sp}} \left[ \frac{t_{on} \Delta \dot{\theta}}{4 \Omega + \Delta \dot{\theta} (t_{on} + \tau_{on} + \tau_{off} - 2 K_R)} \right]$$

but  $t_{on} = \frac{\Delta \dot{\theta}}{|\ddot{\theta}|} + \tau_{on} - \tau_{off}$  (3-23)

$\therefore \dot{\omega} = \frac{2F}{I_{sp}} \left[ \frac{\Delta \dot{\theta} [\Delta \dot{\theta} + |\ddot{\theta}|] (\tau_{on} - \tau_{off})}{4 \Omega |\ddot{\theta}| + \Delta \dot{\theta} [\Delta \dot{\theta} + 2 |\ddot{\theta}| (\tau_{on} - K_R)]} \right]$  (3-24)

or  $\dot{\omega} = \frac{2F}{I_{sp}} \left[ \frac{\Delta \dot{\theta} [\Delta \dot{\theta} + |\ddot{\theta}|] (\tau_{on} - \tau_{off})}{4 |\ddot{\theta}| \theta_2 + (\Delta \dot{\theta})^2} \right]$  (3-24a)

From figures 3-9, 3-10 and 3-11 it can be seen that equation (3-24a) is not minimized for the minimum value of  $\Delta \dot{\theta}$  obtained by varying  $K_R$  since  $\theta_2$  (Figure 3-2) decreases as  $K_R$  increases. It can therefore be concluded that the  $K_R$  required for  $\dot{\omega}_{min}$  and  $\dot{\theta}_A min$  for a particular value of  $\ddot{\theta}$  will not agree, and that  $K_R$  must be selected to yield  $\dot{\omega}_{min}$  or  $\dot{\theta}_{min}$  for various mission phases.

For disturbed (moment unbalance) limit cycle operation, the switch lines are:

On Switch Lines - Disturbed Limit Cycle

Electrical  $K_R \dot{\theta} + K_\theta \theta = \pm \Omega + \ddot{\theta} \tau_G K_R$  (3-28)

Actual  $(K_R - K_\theta \tau_{on}) \dot{\theta} + K_\theta \theta = \pm \Omega + \ddot{\theta} \left[ K_R (\tau_{on} + \tau_G) - \frac{K_\theta \tau_{on}^2}{2} \right]$  (3-29)

Off Switch Lines - Disturbed Limit Cycle

Electrical  $K_R \dot{\theta} + K_\theta \theta = \pm \Omega + h + \ddot{\theta} K_R \tau_G$  (3-18)

Actual  $(K_R - K_\theta \tau_{off}) \dot{\theta} + K_\theta \theta = \pm \Omega + h + \ddot{\theta} \left[ (\tau_{off} + \tau_G) K_R - \frac{K_\theta \tau_{off}^2}{2} \right]$  (3-30)

Code 26512 Eng-23A

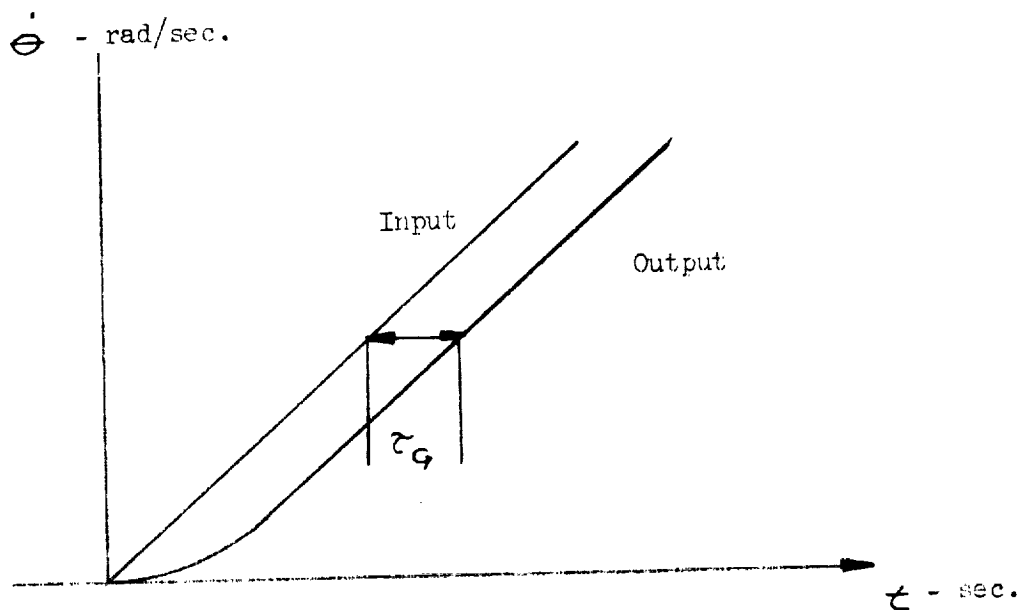


Figure 3-7 - Rate Gyro Input-Output Characteristics  
For A Ramp Input ( $\dot{\theta}$  Constant)

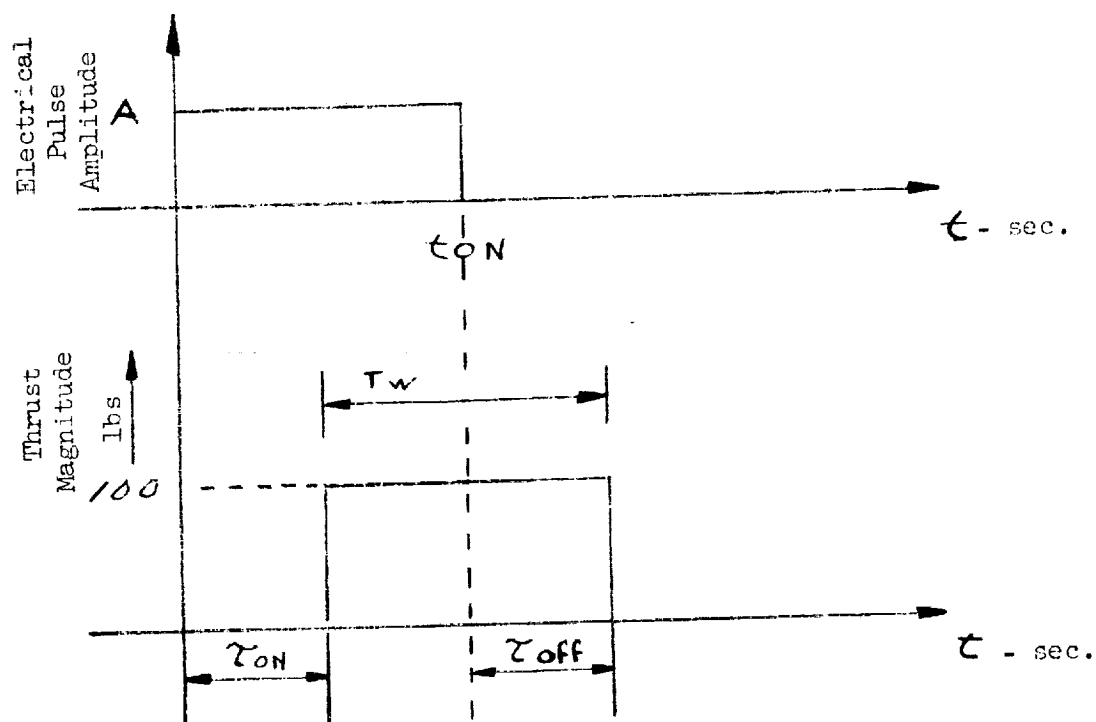


Figure 3-8 - Thrust Function Characteristics

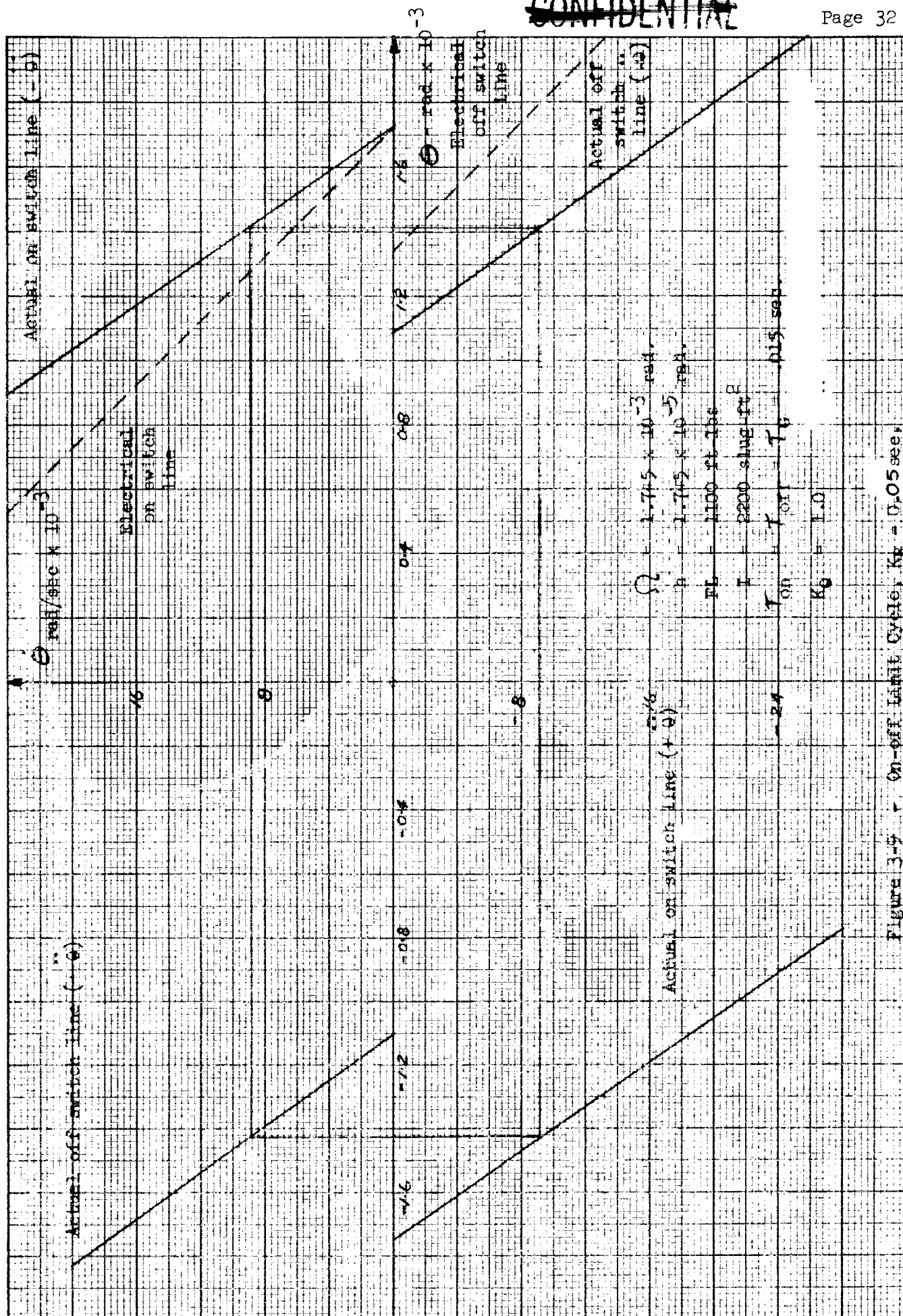
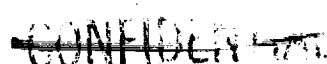


Figure 3-9 On-off Limit Cycle,  $K_F = 0.05$  sec.

Grumman Aircraft Engineering Corporation



LED-500-3  
30 Sept. 1964



~~CONFIDENTIAL~~

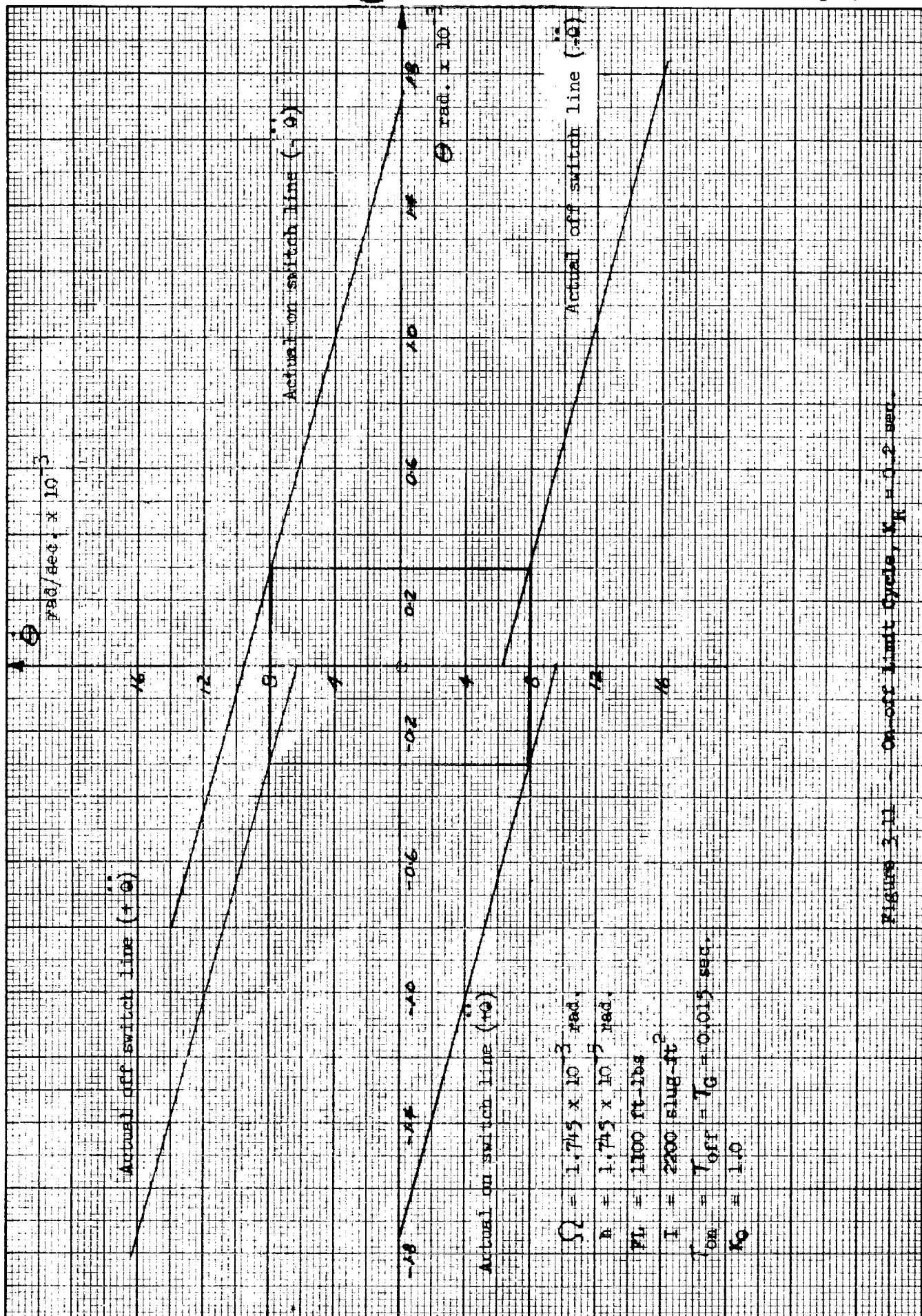


Figure 3-11 On-off limit cycle,  $K_G = 0.2 \text{ sec.}$

~~CONFIDENTIAL~~

From equations 3-29 and 3-30 the following can be seen:

- $K_R = 0$  — system is unstable since slope of "on" and "off" switch lines is positive.
- $K_R$  must be greater than  $K_\theta \tau_{on}$  and  $K_\theta \tau_{off}$  to insure stability; i.e.,  $K_R > \max(K_\theta \tau_{on}, K_\theta \tau_{off})$ .
- Jet on time increases with an increase in any or all delays ( $\tau_{on}$ ,  $\tau_{off}$ , and  $\tau_G$ ) for a fixed  $K_R$ .
- Location of switch lines varies with  $\ddot{\theta}$  and is therefore dependent upon vehicle inertias, control moment and unbalance moment.
- For fixed values of  $K_\theta$ ,  $\tau_G$ ,  $\tau_{off}$ ,  $\tau_{on}$  and  $\ddot{\theta}$  the disturbed limit cycle is plotted in Figures 3-12, 3-13 and 3-14 for various values of  $K_R$ . From the figures it can be seen that  $K_R$  effects  $\theta_{osc}$  p-p only slightly but has a marked effect on  $\theta_{AV}$ .

From equation 3-11a we have

$$\dot{\omega} = \frac{2F}{I_{sp}} \frac{|M_u|}{|M_c|}$$

for a disturbed limit cycle. As was discussed previously the only quantity in the above equation that can change  $\dot{\omega}$  is the specific impulse ( $I_{sp}$ ) since all other quantities are fixed. Therefore, it is obvious that a large on-time is desirable to minimize propellant flow rate, but the on-time for "on-off" moment unbalance control is solely determined by the relay hysteresis and vehicle parameters ( $\tau_{on}$ ,  $\tau_{off}$ ,  $\tau_G$  and  $\ddot{\theta}$ ) and cannot be controlled.

The switch lines for transient response are given by equations 3-16 thru 3-20. However, since the LEM body rates will be limited, an additional switch line must be considered. The switch line is an "off" line defined by the following equation

$$\text{Electrical} \quad \dot{\theta} = \pm \dot{\theta}_L \pm |\ddot{\theta}| \tau_G \quad (3-31)$$

$$\text{Actual} \quad \dot{\theta} = \pm \dot{\theta}_L \pm |\ddot{\theta}| (\tau_{off} + \tau_G) \quad (3-32)$$

Typical large transient trajectories are shown in Figures 3-15, 3-16 and 3-17. It is apparent from the figures that a large  $K_R$  is desirable for good trans-

Code 26512 Eng-23-1A

REPORT LED-500-3

DATE 30 Sept. 1964

~~CONFIDENTIAL~~  
GRUMMAN AIRCRAFT ENGINEERING CORPORATION

ient response and that actual rate limit will vary with vehicle inertia ( $\theta$ ).

The total propellant required for a transient maneuver is given by equation 3-14 which is

$$\omega = 2F \sum_{j=1}^n \frac{t_j}{I_{spj}}$$

An example is given in Figure 3-17.

If a rate gyro deadzone (Figure 3-18) is considered a value must be selected for the deadzone such that the limit cycle is undisturbed or an increase in propellant consumption will arise. The permissible rate gyro deadzone for the on-off modulator is given by the following equation

$$\dot{\theta}_{RG} = 2 \left[ \frac{h - \theta_{\min} [K_R(\tau_{\text{off}} + \tau_G) + \tau_{\text{off}}^2/2]}{2K_R - \tau_{\text{on}} - \tau_{\text{off}}} \right] \quad (3-33)$$

where  $K_\theta = 1$  and  $K_R$  must be less than  $K_{Rc}$  (equation 3-21).

**3.3.3 Induced Rate Modulator** From equation 3-10 it is obvious that propellant consumption during normal limit cycle operation will be minimized if the quantity  $t_{\text{on}} \Delta\theta$  is minimized. This can be accomplished by generating a minimum impulse limit cycle which will yield the smallest possible  $\Delta\theta$  and  $t_{\text{on}}$  possible for a particular value of  $K_R$ .

The "Induced Rate" modulator is such a device. A minimum impulse is generated for slowly varying signals by the addition of a feedback network  $K/(s + 1/\tau_1)$  to the "on-off" relay characteristic as shown in Figure 3-6b. The impulse width (on time) generated is dependent upon  $K, \tau_1, h, \theta, K_R$  and  $\tau_{\text{on}}$ . Because of the pulse width dependence upon  $\theta$  the minimum electrical pulse generated during normal limit cycle by this device will vary with vehicle inertia. Therefore,  $K$  must be varied during the LEM mission to compensate for inertia changes to achieve minimum impulse limit cycle throughout the mission.

When the modulator error( $e$ ) exceeds  $AK\tau_1$  a continuous thrusting condition will occur. However, for  $\Omega \leq e \leq AK\tau_1$  the pulse width generated will vary from a minimum pulse to a continuous thrusting pulse dependent upon the magnitude of  $e$ . This modulator will give the same results as the "on-off" modulator for large transients and moment unbalances since the error magnitude will exceed the feedback network output in these cases.

The permissible rate gyro deadzone for the "Induced Rate" modulator was not evaluated. However, it can be seen from Figure 3-19 that the time to traverse  $\Delta\theta$  after the thrust pulse must be less than the time it takes for the induced rate network output ( $e_1$ ) to reach a level such that  $\Omega \leq e - e_1$ . The largest vehicle inertia will present the most stringent requirement on the rate gyro deadzone.

Code 26512 Eng-23A

K&E  
KEULEY & ESSLER CO.  
ATTN: ENGINEERING  
10 X 10 TO THE INCH  
3291-11

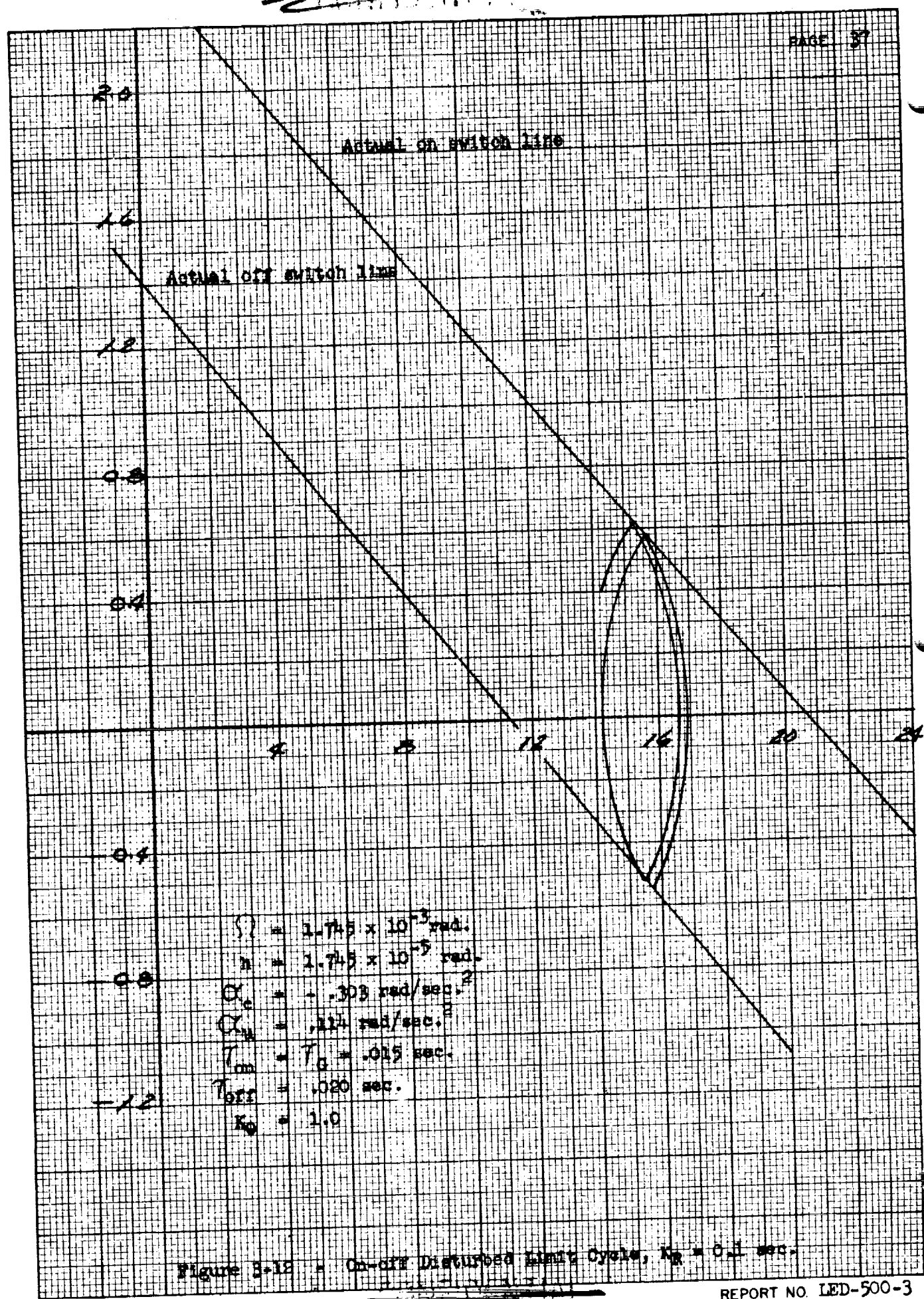


Figure 3-12 - On-off Disturbed Limit Cycle,  $K_R = 0.1$  sec.

~~CONFIDENTIAL~~

PAGE 38

11-7022 K&E  
KUEHLER & ESSER CO.  
ALBANY, N.Y.  
10 X 10 TO THE 1/2 INCH

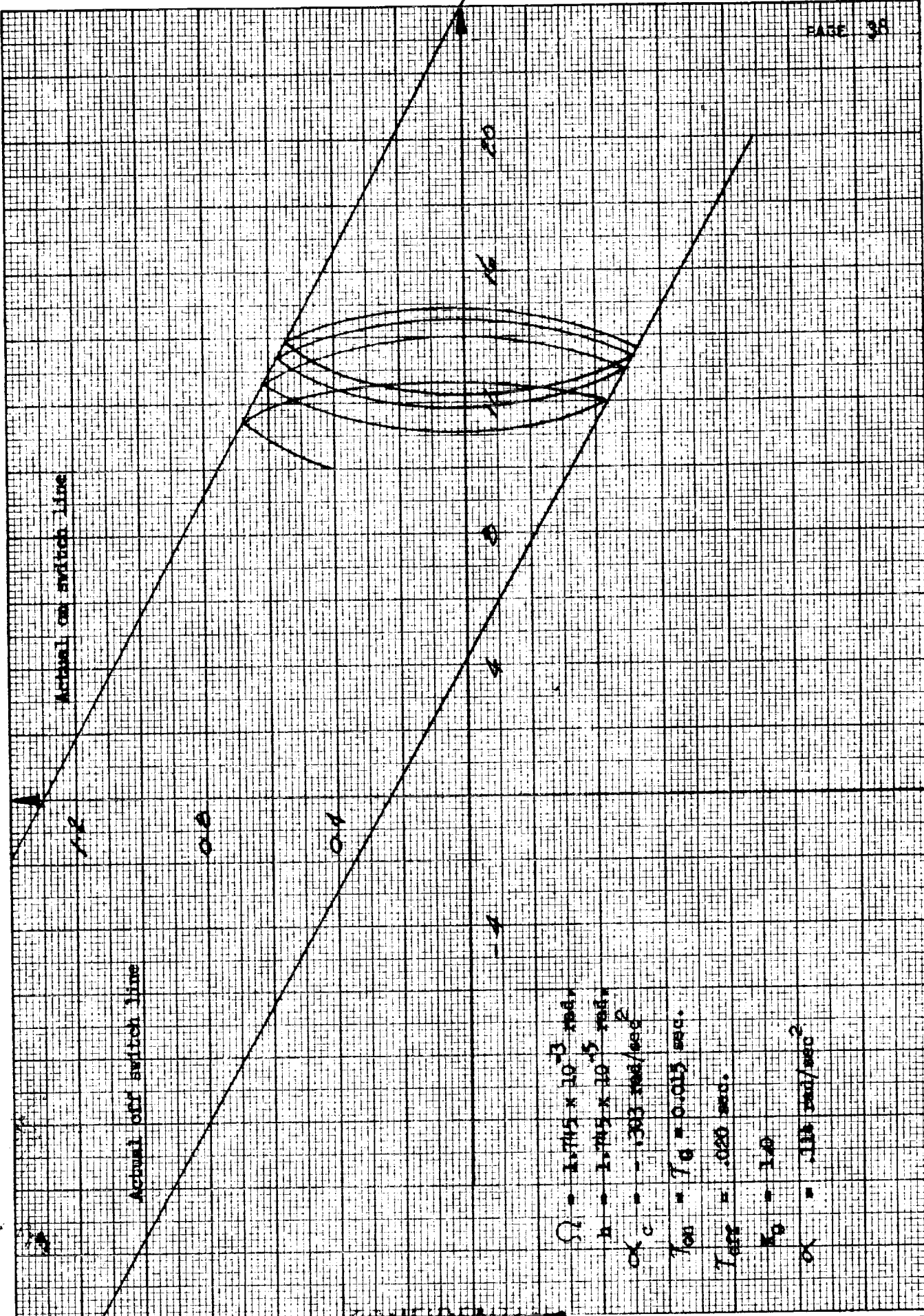




Figure 3-13 - On-off Disturbed Limit Cycle,  $K_R = 0.2$

ENG 435  
8 62

GRUMMAN AIRCRAFT ENGINEERING CORPORATION

REPORT NO. LED-500-3  
30 Sept. 1964




**ALBANYENE** 
  
**KENNEL & ESSER CO.**
  
**10 X 10 TO THE 1/8 INCH**
  
**MADE IN U.S.A.**
  
**32501-11**

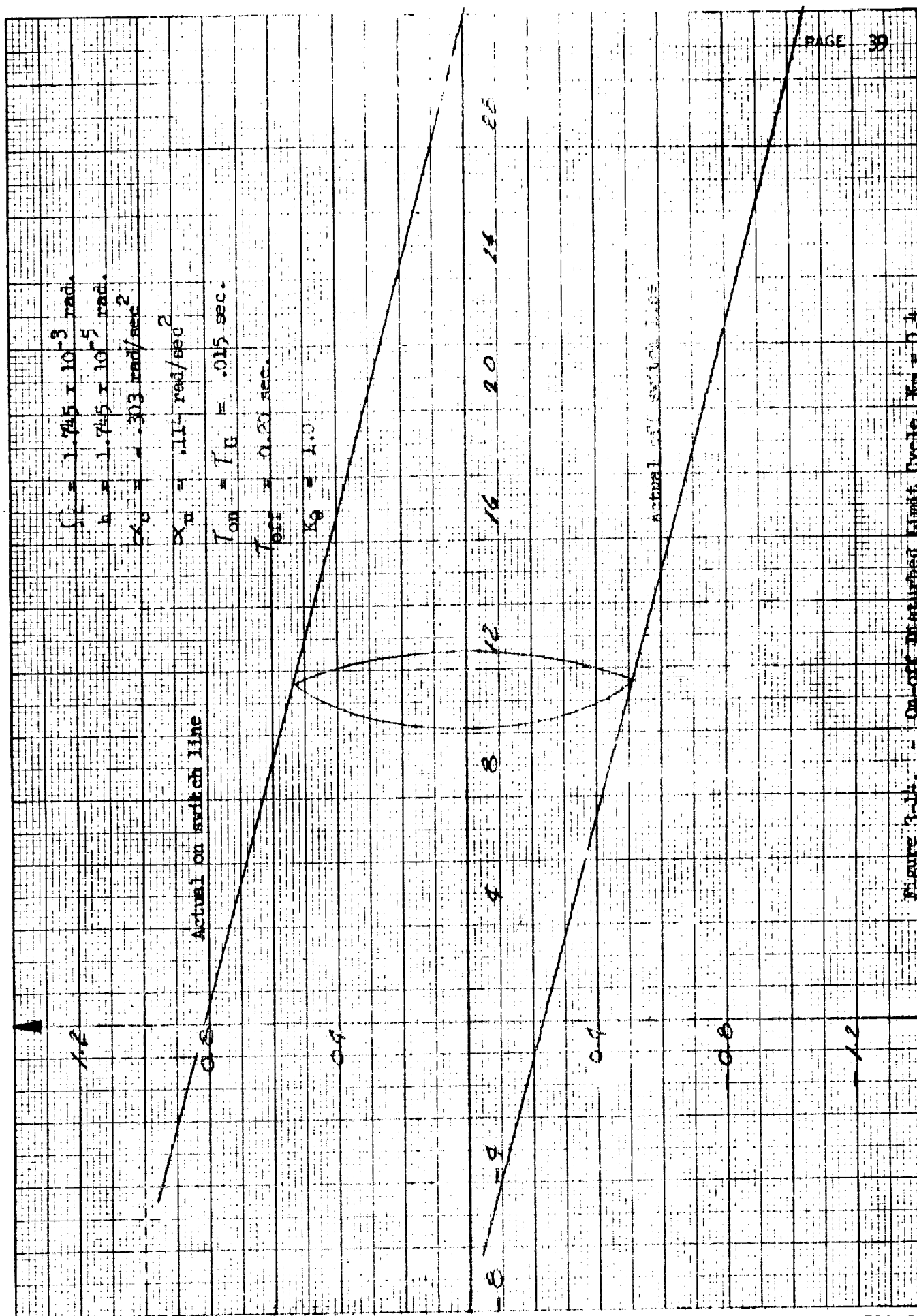


Figure 3-14, - On-off Disturbed Limit Cycle,  $K_F = 0.4$

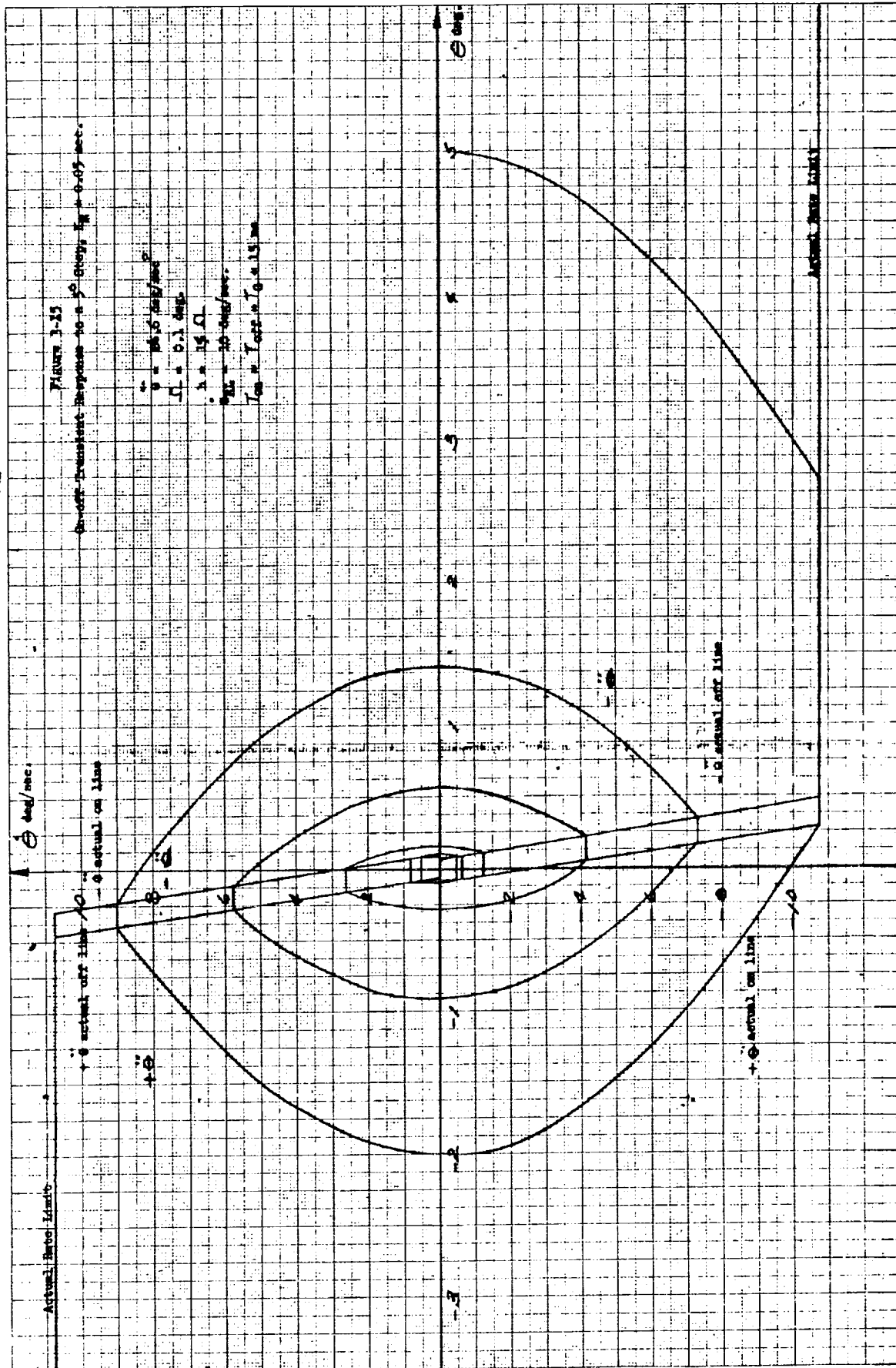






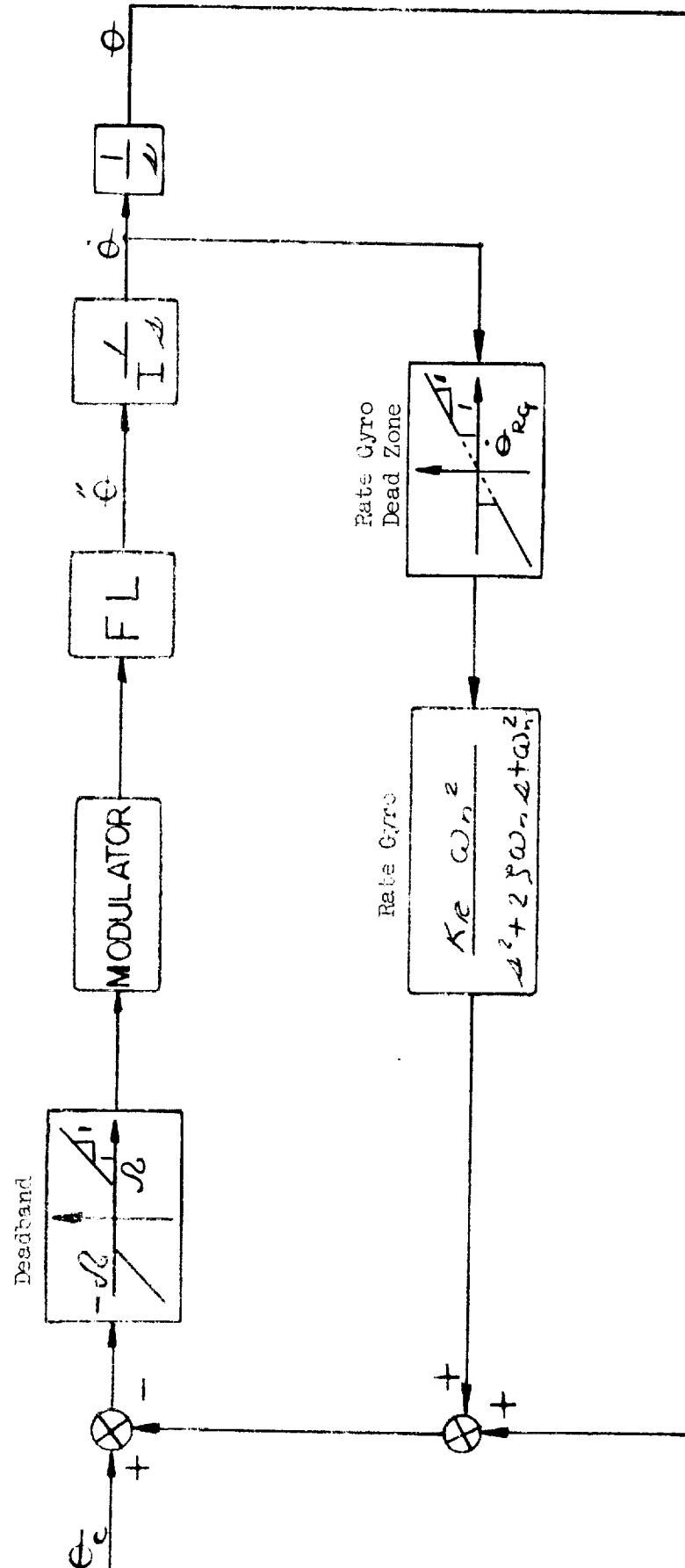








Figure 3-18 - Single Axis Attitude Control Loop With Rate Gyro Deadzone



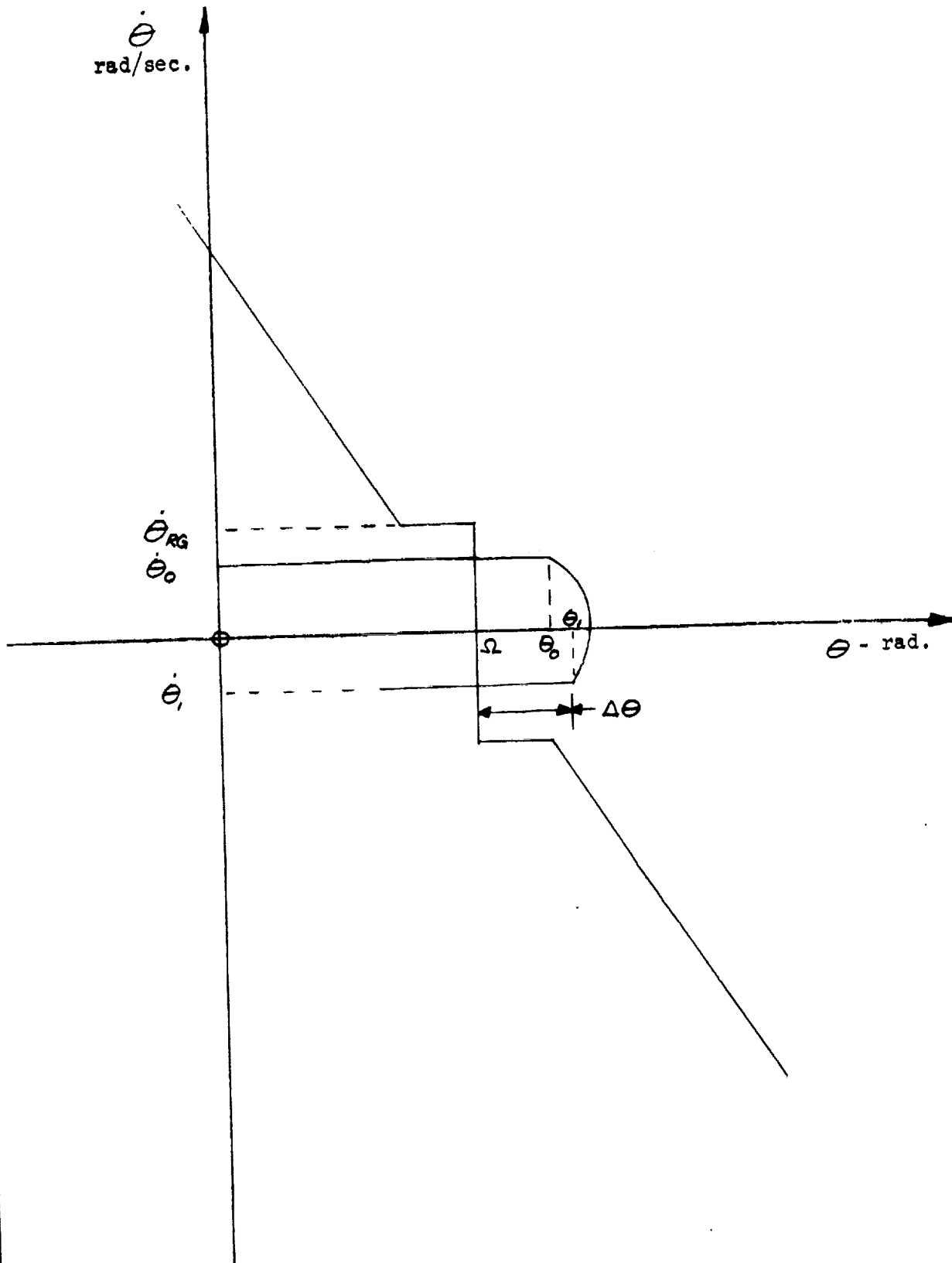


Figure 3-19 - Limit Cycle Characteristics for the Determination of  $\dot{\theta}_{RG}$

~~CONFIDENTIAL~~

3.3.4 Pulse Modulators All remaining modulators of interest are of the pulse modulation type which convert the input error signal into a fixed amplitude pulse train output. The pulse modulators considered are:

- a) modified on-off
- b) Pulse Frequency Modulator (PFM)
- c) Pulse Width Modulator (PWM)
- d) Pulse Ratio Modulator (PRM)
- e) non-linear PRM
- f) piecewise-linear PRM

Each of the above modulators have the capability of generating a minimum impulse for normal limit cycle operation independent of vehicle inertia, and thereby will yield a minimum propellant limit cycle. However, the modulators can be constructed as a pulse on demand modulator (first pulse is generated as soon as "electrical on" switch line is crossed) or delay modulator (first pulse is generated a definite time after "electrical on" switch line is crossed). The minimum impulse limit cycle is generated by all demand pulse modulators. Only the PFM and the modified on-off yield minimum impulse limit cycle for both demand and delay type modulators.

The functioning of each pulse modulator is discussed below:

3.3.4.1 Modified on-off The characteristics of the modified on-off modulator are shown in Figure 3-20. From the figure it can be seen that this modulator generates a pulse train with constant pulse repetition frequency and pulse width for all errors less than  $e_1$ . The pulse width ( $t_{on}$ ) should be set equal to  $t_{onmin}$  (pulse width that generates minimum impulse) such that minimum propellant limit cycle is generated. All errors greater than  $e_1$  cause continuous thrusting.

Phase plane thresholds (electrical switch lines) are shown in Figure 3-26. They are described by

$$K_R \dot{\theta} + K_\theta \theta = \pm \Omega \quad (3-34)$$

$$K_R \dot{\theta} + K_\theta \theta = \pm e_1 \pm \Omega \quad (3-35)$$

in the absence of acceleration, and

$$K_R \dot{\theta} + K_\theta \theta = \pm \Omega + \ddot{\theta} (K_R \tau_G) \quad (3-36)$$

$$K_R \dot{\theta} + K_\theta \theta = \pm e_1 \pm \Omega + \ddot{\theta} K_R \tau_G \quad (3-37)$$

Code 26512 Eng-23-1A

~~CONFIDENTIAL~~

~~CONFIDENTIAL~~

in the presence of acceleration.

To insure a one pulse limit cycle the following relationship (assuming no rate gyro deadzone) should be satisfied

$$K_R > \frac{T_W}{2} + \frac{\dot{\theta}_o}{\theta T_W} \left[ T_W + \tau_{off} + \frac{1}{f_p} \right] \quad (3-38)$$

Equation 3-38 is sufficient but not necessary to guarantee a one pulse limit cycle and is obtained from Figure 3-27 by solving for  $y < \alpha T_W$ . The limit cycle propellant flow rate is given by equation 3-9 where

$$t_{on} = T_W + \tau_{on} - \tau_{off}$$

If  $t_{on}$  is selected to be  $t_{onmin}$  the minimum impulse limit cycle will be obtained.

For large moment unbalances and rotational commands the modified on-off modulator functions as the on-off modulator. However, the rate gyro deadzone requirement is different for the modified on-off modulator. The permissible rate gyro deadzone for the modified on-off modulator is derived from Figure 3-19 where  $t_{\Delta\theta}$  must be less than  $T_p$  to insure that normal limit cycle is not changed. The equations defining  $T_p$  and  $t_{\Delta\theta}$  are (6):

$$t_{\Delta\theta} = T_W \left[ \frac{\alpha T_W/2 + \dot{\theta}_o (1 + \tau_{on}/T_W + \tau_{pmax}/T_W)}{|\alpha T_W + \dot{\theta}_o|} \right] \quad (3-39)$$

$$T_p = \frac{1}{f} - \tau_{on} \quad (3-40)$$

where  $\tau_{pmax}$  is worst delay due to modulator characteristics ( $\tau_{pmax} = 0$  for demand type modulator).  $\dot{\theta}_o = \dot{\theta}_{RG}$  and  $\alpha = \dot{\theta}_{min}$  will be the worst case to consider. Equations 3-39 and 3-40 are plotted in Figure 3-28 for this case.

**3.3.4.2 Pulse Frequency Modulator (PFM)** The characteristics of the PFM are shown in Figure 3-21. As can be seen from the characteristic curves, the PFM varies pulse repetition frequency while maintaining a constant pulse width as a function of error magnitude. Also shown is the linear duty factor variation as a function of error. The phase plane boundaries are shown in Figure 3-26.

As for the modified on-off modulator  $K_R$  should satisfy the relationship of equation 3-38 to guarantee a one pulse limit cycle. Therefore, if  $t_{on}$  is selected equal to  $t_{onmin}$  a minimum impulse limit cycle and therefore minimum propellant limit cycle will be generated by the PFM. However, propellant consumption for limit cycle in the presence of a large moment unbalance will

Code 26512

Eng-23A

~~CONFIDENTIAL~~

REPORT LED-500-3  
DATE 30 Sept. 1964

GRUMMAN AIRCRAFT ENGINEERING CORPORATION



Figure 3-20 - Modified on-off Modulator Characteristics

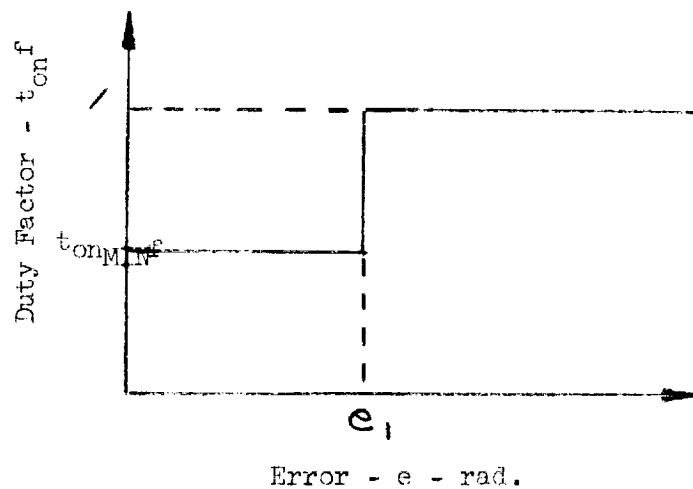
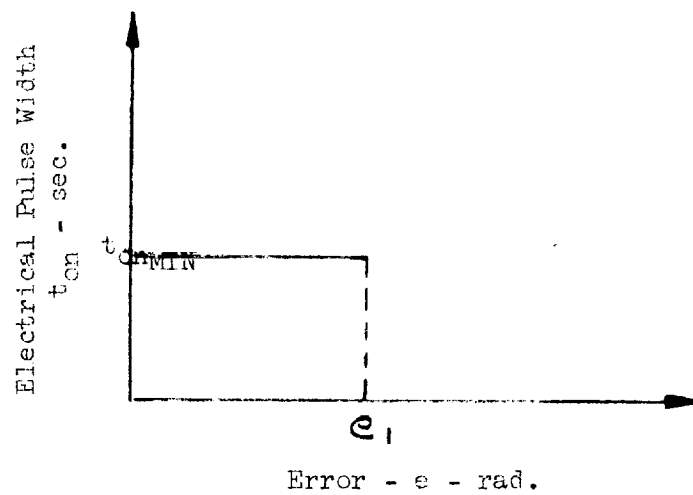
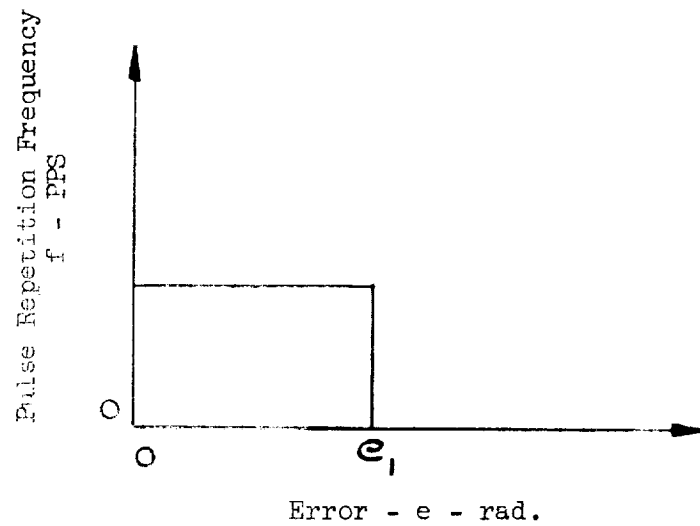
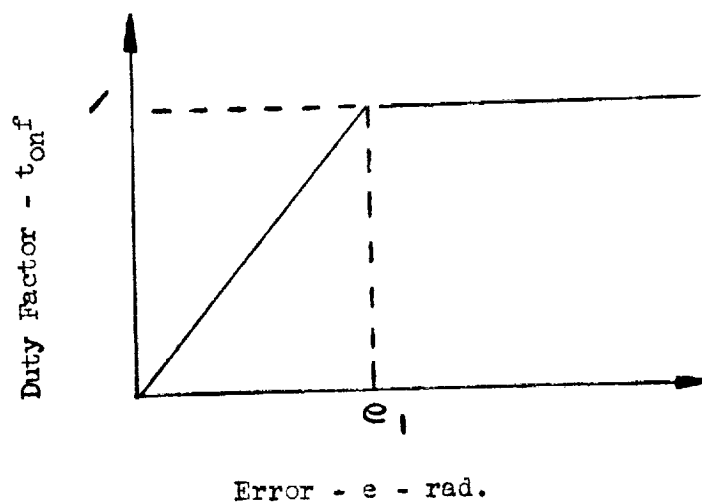
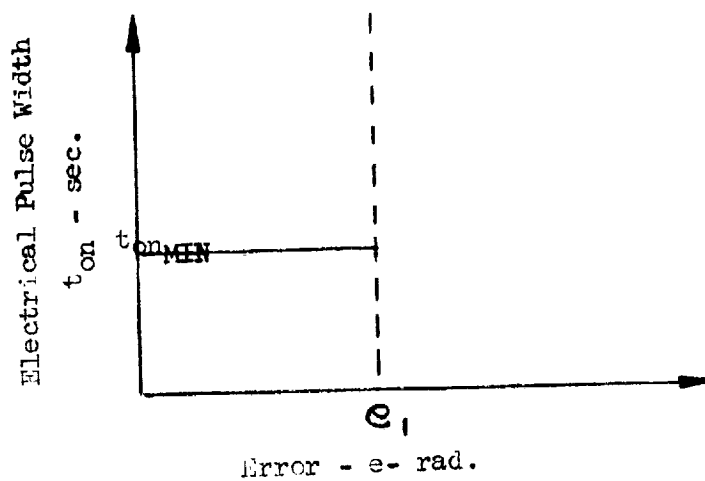
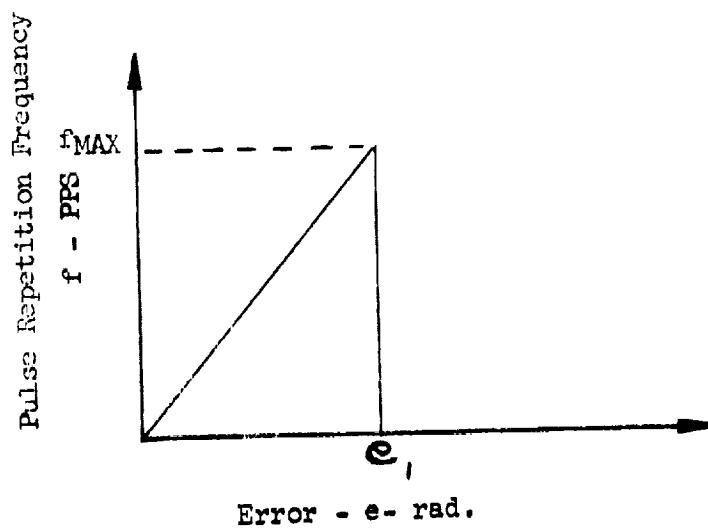


Figure 3-21 - PFM Characteristics



~~CONFIDENTIAL~~

be excessively large. This is due to the fact that  $t_{on}$  is fixed at  $t_{onmin}$  which yields the smallest  $I_{sp}$  value and therefore the largest propellant consumption rate (see equation 3-11a).

Response to large rotational commands will be similar to that of the on-off modulator.

The permissible rate gyro deadzone is again determined from Figure 3-19 where  $t_{\Delta\theta} < T_p$  to insure that normal limit cycle is not changed. The PFM equations for  $t_{\Delta\theta}$  and  $T_p$  are (6):

$$t_{\Delta\theta} = T_w \frac{\alpha T_w/2 + \dot{\theta}_o (1 + \tau_{on}/T_w + \tau_p/T_w)}{|\alpha T_w + \dot{\theta}_o|} \quad (3-41)$$

$$T_p = \left[ \frac{\theta_1 - \Omega + f_1/K_f}{|\dot{\theta}_1|} \right] \left[ -1 + \frac{2|\dot{\theta}_1|}{K_f [(\theta_1 - \Omega) + f_1/K_f]^2} \right] \quad (3-42)$$

where  $T_w = t_{on} - \tau_{on} + \tau_{off}$  and  $K_f$  and  $f_1$  are defined in Figure 3-21. Equations (3-41) and (3-42) are plotted in Figure 3-29 for  $\alpha = \dot{\theta}_{min}$ .

**3.3.4.3 Pulse Width Modulator (PWM)** - The PWM characteristics are shown in Figure 3-22. From the curves it can be seen that the PWM generates pulses of varying width with a constant pulse repetition frequency as a function of error signal. Also shown is the linear duty factor variation as a function of error signal. The phase plane boundaries are the same as for the PFM (Figure 3-26).

If the PWM is of the "pulse on demand" type  $t_{on}$  will equal  $t_{onmin}$  to yield a minimum propellant limit cycle. However, if the PWM is of the "delay" type  $t_{on} \neq t_{onmin}$  and the minimum propellant limit cycle cannot be obtained, but can be approached if  $e_1$  is made very large (decrease PWM gain). The value of  $K_R$  selected for normal limit cycle should satisfy equation 3-38 to guarantee one pulse limit cycle.

Both "delay" and "demand" type PWM will yield good propellant consumption rates for large moment unbalances since  $f$  can be chosen to yield large pulse widths and therefore large  $I_{sp}$  values. Response to large rotational commands will be similar to "on-off" modulator for the large values of modulator gain being considered (small  $e_1$ ).

As with the PFM  $t_{\Delta\theta}$  and  $T_p$  will determine the permissible rate gyro deadzone. That is,  $t_{\Delta\theta} < T_p$  to insure a normal limit cycle. The equations for  $t_{\Delta\theta}$  and

Code 26512 Eng-23-1A

~~CONFIDENTIAL~~

~~CONFIDENTIAL~~

$T_p$  for the demand PWM are given by the following (6):

$$T_p = \frac{1}{f} - t_{on} \quad (3-43)$$

$$t_{on} = T_w \left[ \frac{\alpha T_w/2 + \dot{\theta}_o (1 + T_{on}/T_w + T_p/T_w)}{|\alpha T_w + \dot{\theta}_o|} \right] \quad (3-44)$$

The above equations are plotted in Figure 3-28. The permissible rate gyro deadzone was not evaluated for the delay type PWM.

3.3.4.4 Pulse Ratio Modulation (PRM) The PRM varies both pulse width and pulse repetition frequency as a function of error signal. Duty factor, pulse width and pulse frequency static characteristics as a function of error are plotted in Figure 3-23. The dynamic equations used to determine pulse width and frequency of the PRM (3) for varying error signals are:

$$t_{on_{min}} = \int_0^{t_{on}} (1-x) dt ; x = f(t) \quad (3-45)$$

$$t_{on_{min}} = \int_{t_{on}}^{T_p} x dt \quad (3-46)$$

where  $x$  is the normalized error signal. See Figure 3-26 for the phase plane boundaries.

A "demand" PRM will satisfy equation 3-45 first whenever the PRM threshold is crossed; i.e., the "demand" PRM starts delivering a pulse as soon as  $x$  exceeds zero. Upon satisfying 3-45, 3-46 will be satisfied to determine  $T_p$  using previous  $t_{on}$  as lower limit on the integral. However, if during the evaluation of  $T_p$  the PRM input is reduced to zero the PRM will reset in order that 3-45 will be satisfied when input exceeds zero again; but, if the input is reduced to zero while 3-45 is being satisfied, the PRM stops delivering the pulse ( $t_{on}$  cannot be less than  $t_{on_{min}}$ ) and resets to satisfy 3-45 when  $x$  exceeds zero again.

The "delay" PRM operates on a continuous clock basis; i.e., it does not reset either  $t_{on}$  or  $T_p$  integrals when  $x$  is zero. The delay PRM solves equation 3-46 when  $x$  exceeds zero using the previous value of  $t_{on}$  for the lower limit on the integral. Upon satisfying 3-46, 3-45 is satisfied to determine  $t_{on}$ . When  $x$  is reduced to zero while satisfying 3-45 the PRM will stop delivering a pulse ( $t_{on}$  cannot be less than  $t_{on_{min}}$ ) and will satisfy 3-46 when  $x$  exceeds zero again. If 3-46 is being satisfied when  $x$  is reduced to zero, 3-46 will be completed when  $x$  exceeds zero again; i.e., off time is accumulated until 3-46 is satisfied.

As for the "demand" PWM, a pulse on "demand" PRM will generate a minimum propellant limit cycle since  $t_{on}$  will equal  $t_{on_{min}}$ . The "delay" type PRM unlike the delay PWM will generate a near minimum propellant limit cycle

~~CONFIDENTIAL~~

REPORT LED-500-3  
DATE 30 Sept. 1964

Figure 3-22 - PWM Characteristics

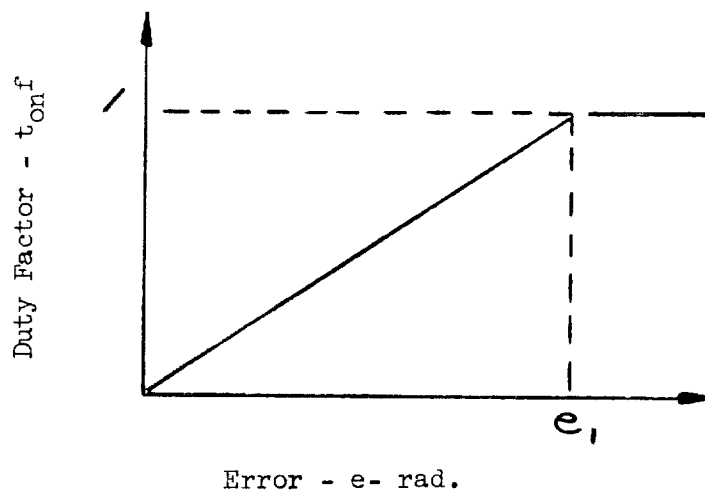
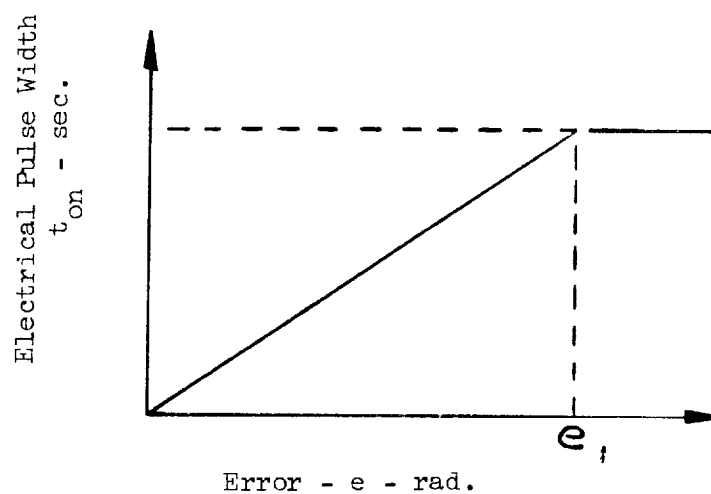
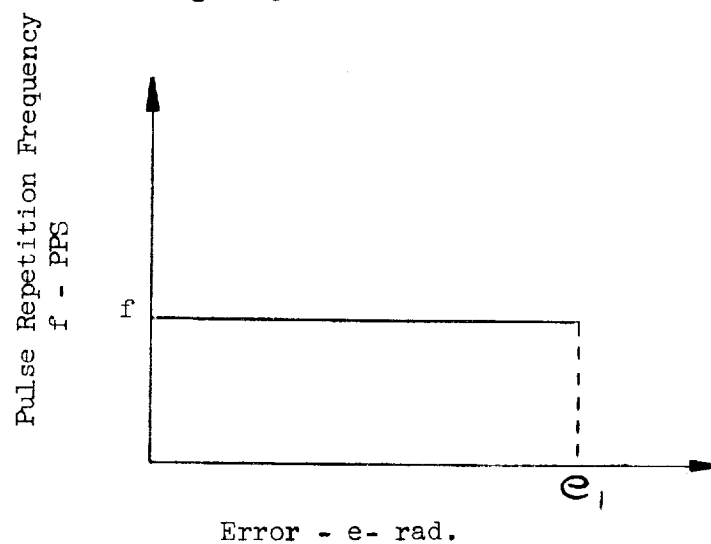


Figure 3-23 - PRM Characteristics

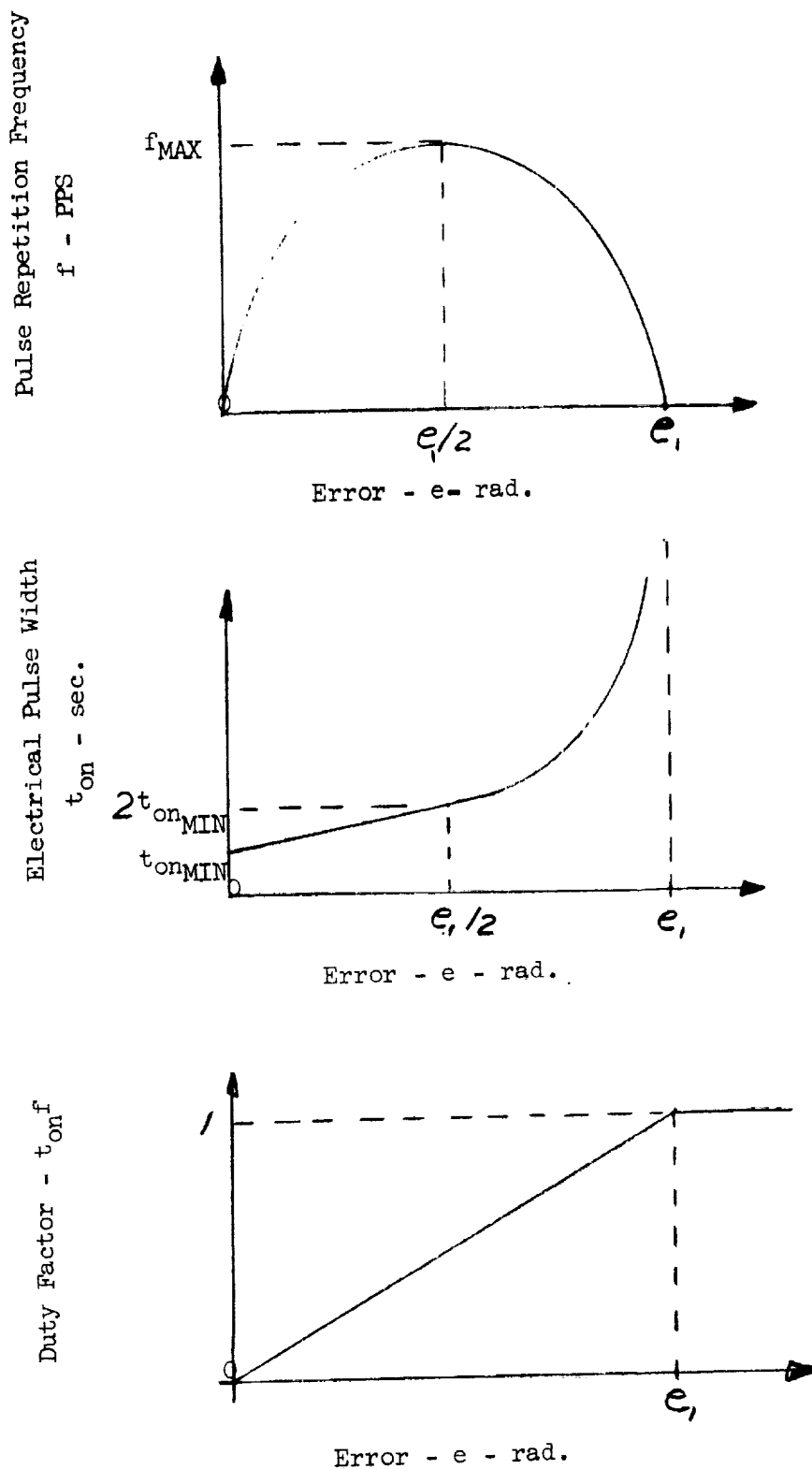


Figure 3-24 - Piecewise Linear PRM Characteristics

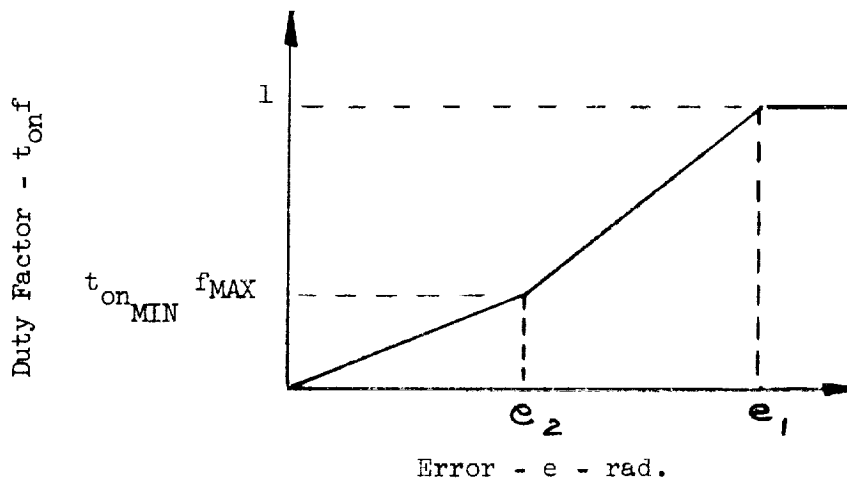
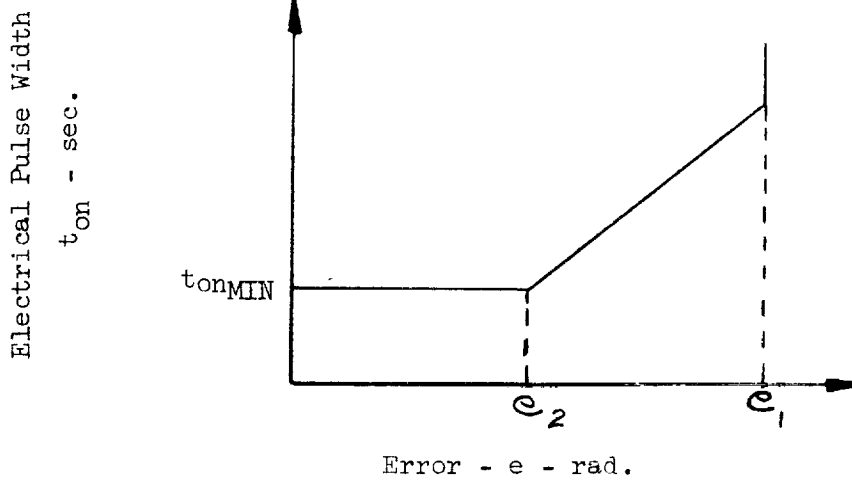
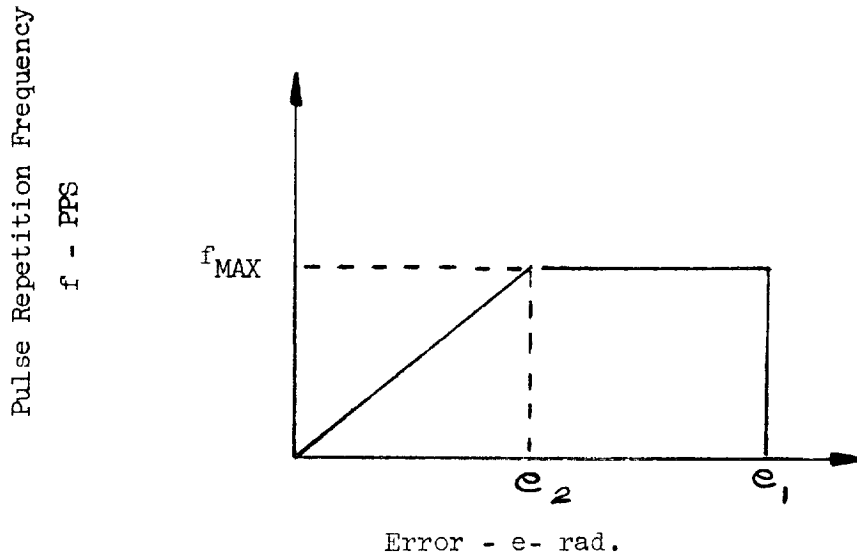
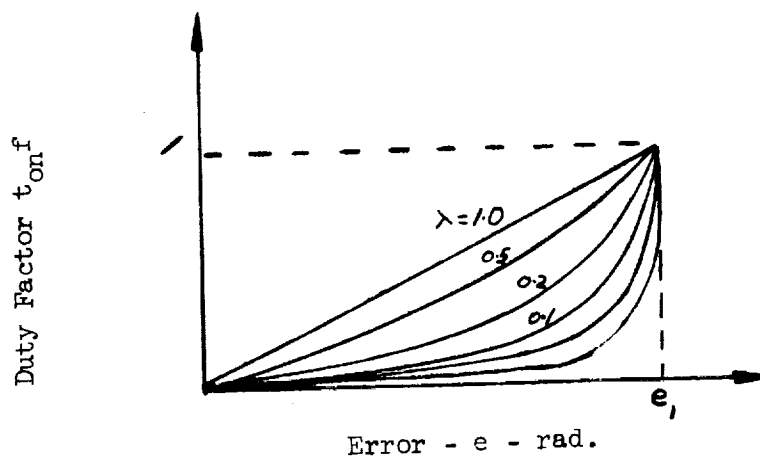
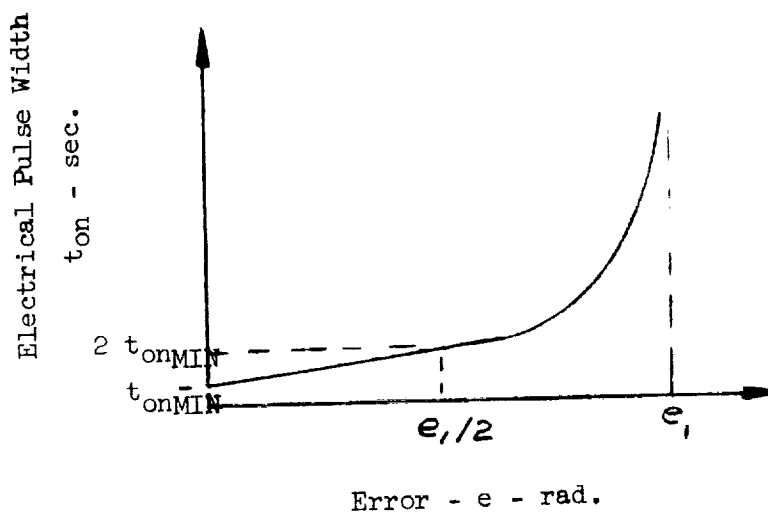
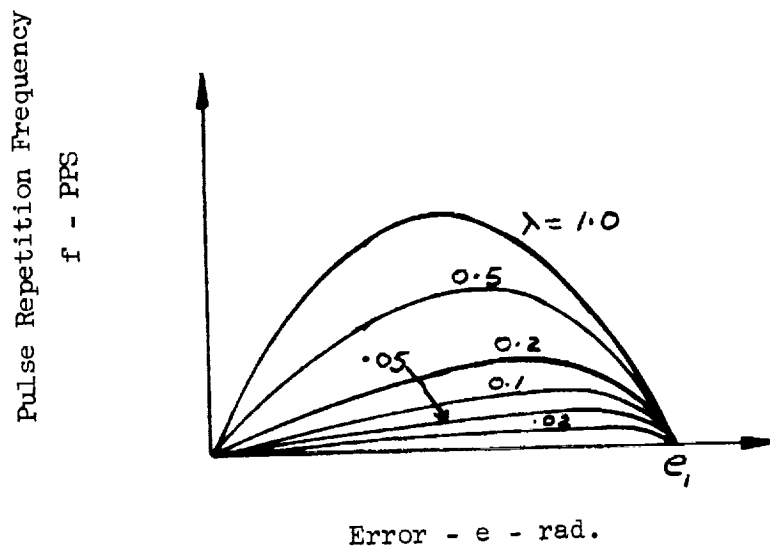


Figure 3-25 - Non-Linear PRM Characteristics





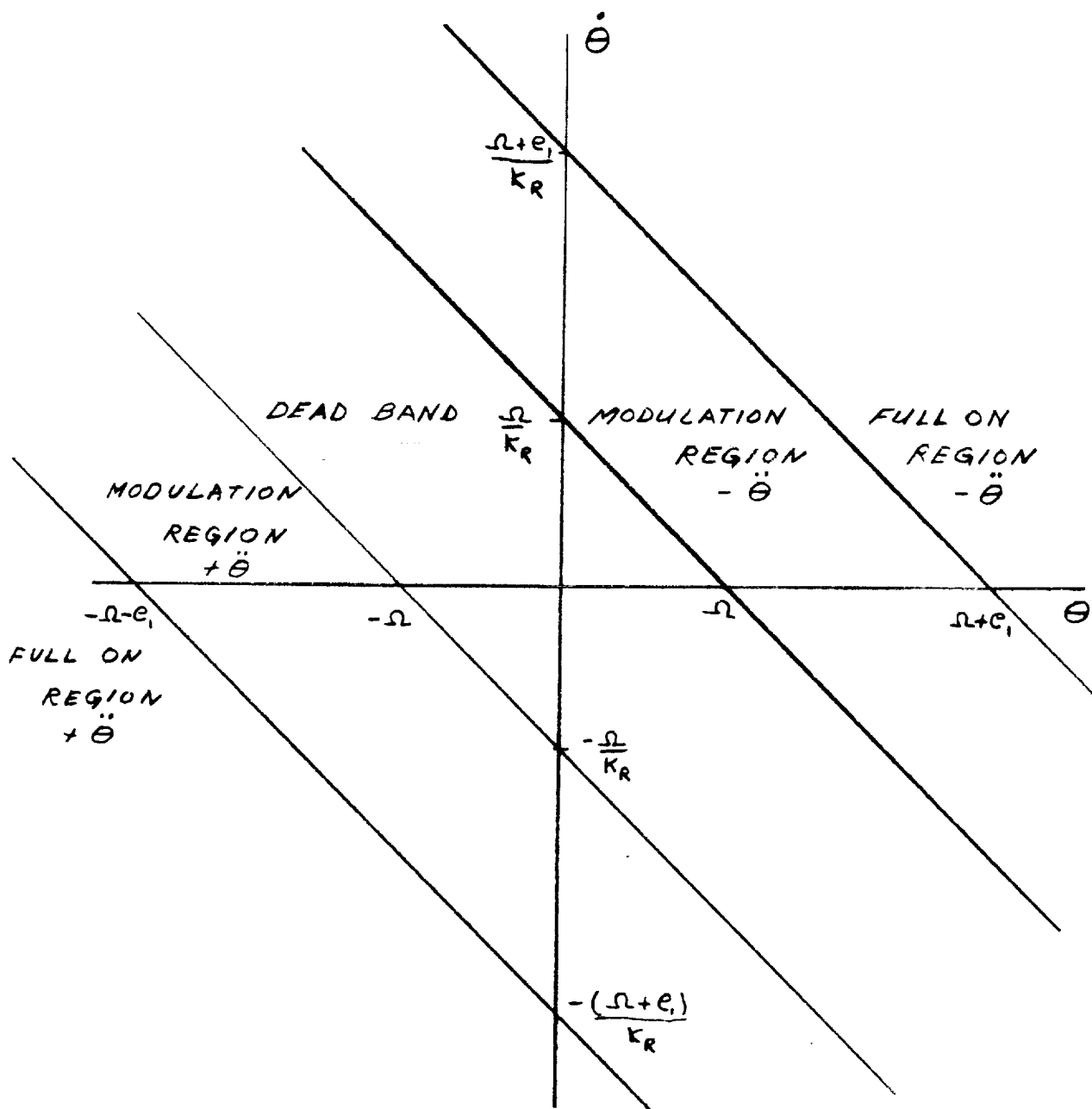


Figure 3-26 - Phase Plane Thresholds For Pulse Modulators

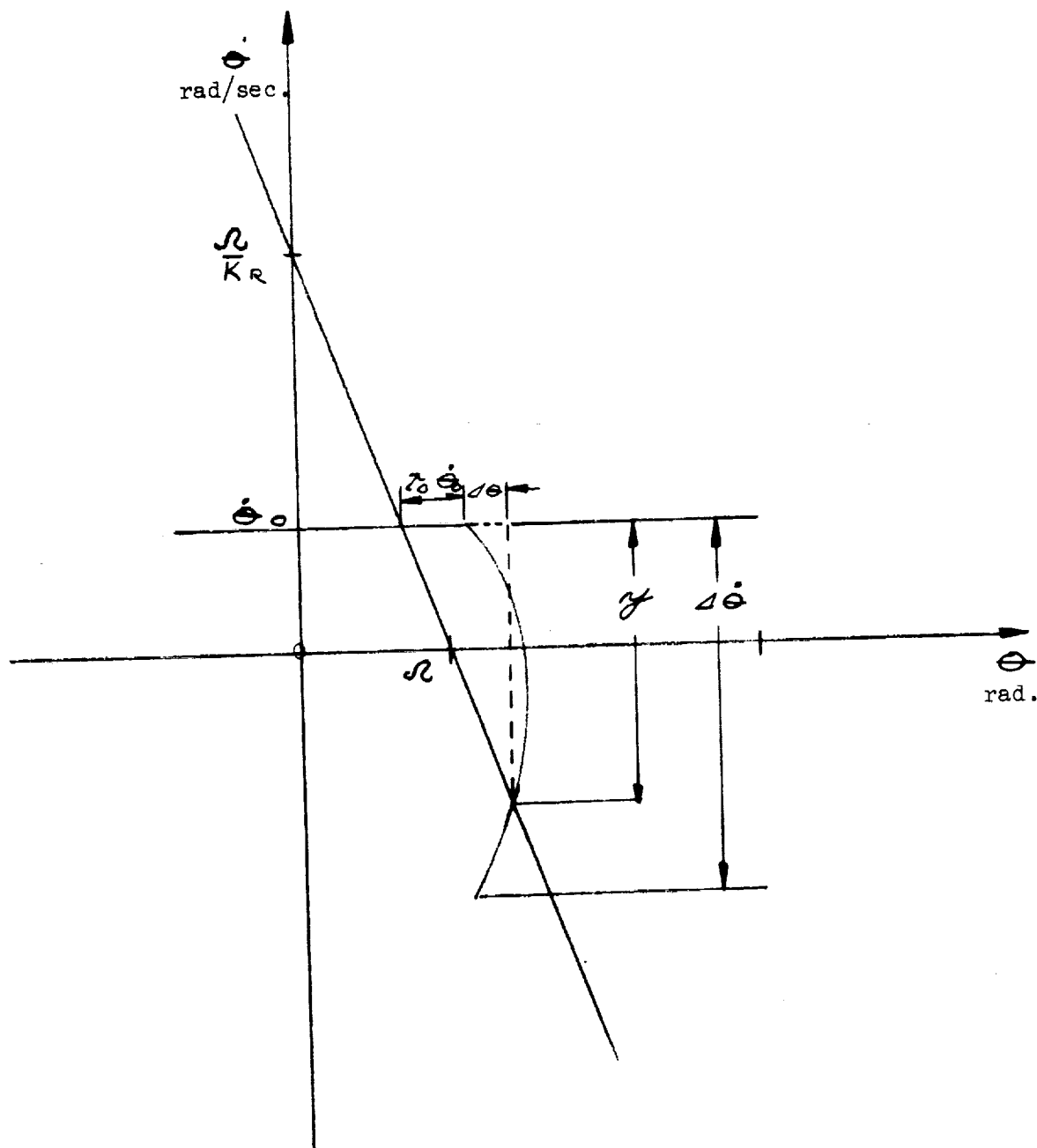


Figure 3-27 - Limit Cycle Characteristics for Determining One Pulse Limit Cycle Boundary

~~CONFIDENTIAL~~

$\ddot{\phi} = 0.06 \text{ rad/sec}^2$

$\tau = 12 \text{ msec}$

011

Time (t) sec.

0.14

0.12

0.10

0.08

0.06

0.04

0.02

$\frac{1}{f} = 0.10 \text{ sec}$

$T_p = 0.09 \text{ sec}$

$t_{10}$

0.6 1.2 1.8 2.4 3.0 3.6

Rate Gyro Deadzone -  $\dot{\phi}_{R0}$  (Rad/sec  $\times 10^{-14}$ )

Figure 3-28 -  $t_{10}$  and  $T_p$  Versus  $\dot{\phi}_{R0}$  for PWM

~~CONFIDENTIAL~~

~~CONFIDENTIAL~~

$\alpha = 0.06 \text{ rad/sec}^2$

PAGE 58

Time (t) sec.

$C_0 = 12 \text{ mo}$

$T_p$

$t_{\Delta\theta}$

$C_0 = 12 \text{ mo}$

Rate Gyro Deadzone -  $\dot{\theta}_{RG}$  (Rad/sec  $\times 10^{-4}$ )

Figure 3-29 -  $t_{\Delta\theta}$  and  $T_p$  Versus  $\dot{\theta}_{RG}$  for FGM

~~CONFIDENTIAL~~

REPORT NO. LED-500-3

30 Sept. 1964

GRUMMAN AIRCRAFT ENGINEERING CORPORATION

~~CONFIDENTIAL~~

PAGE 59

$\alpha = 0.06 \text{ rad/sec}^2$   
 $\epsilon = 1.745 \times 10^{-3} \text{ rad}$   
 $t_{ON} = 0 \text{ ms}$

$\dot{\theta}$   
(rad/sec  $\times 10^{-4}$ )

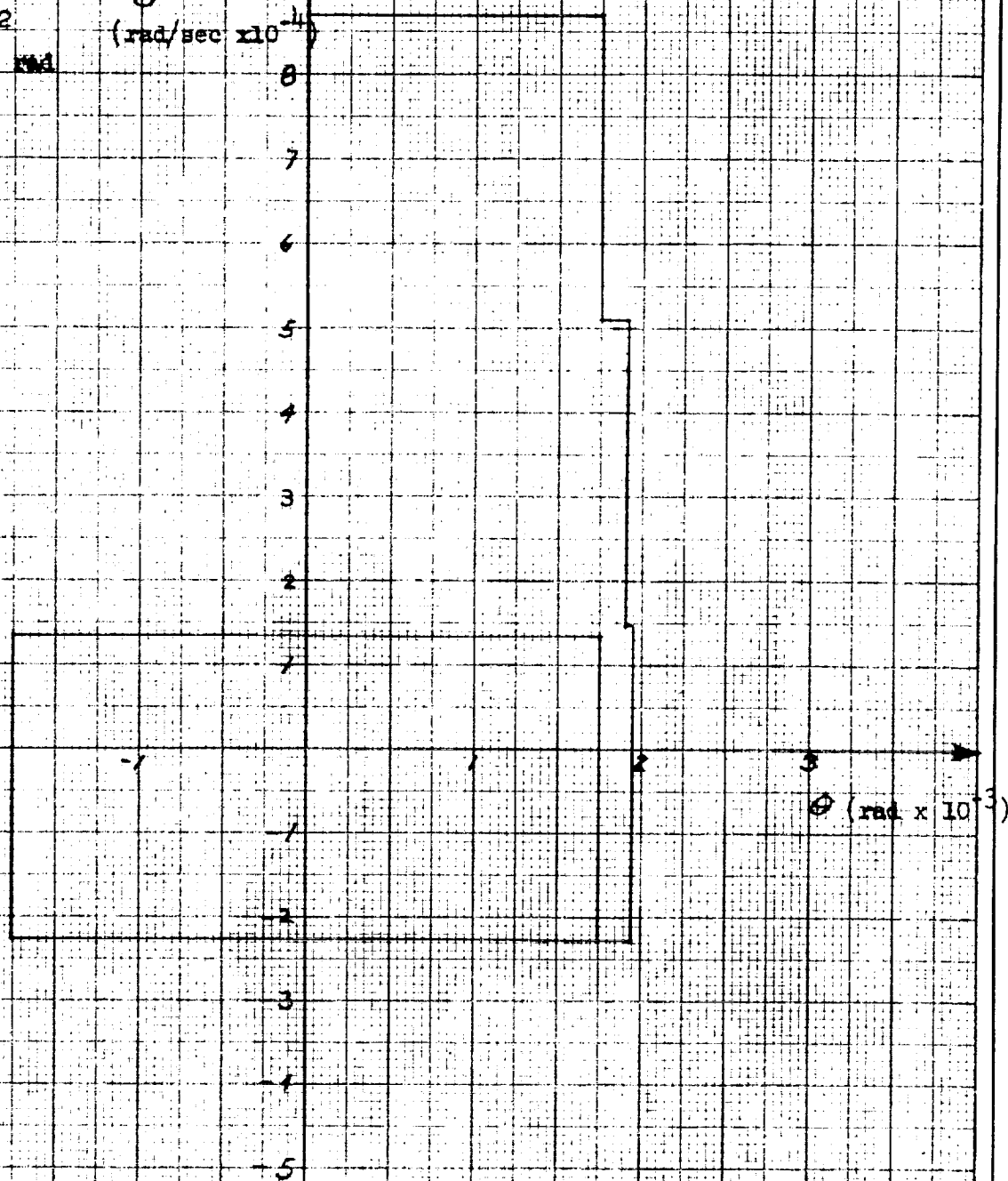


Figure 3-30 - PPM Limit Cycle With  $t_{ON} = 0 \text{ ms}$  and  $K_g = 0 \text{ sec}$ .

~~CONFIDENTIAL~~

GRUMMAN AIRCRAFT ENGINEERING CORPORATION

REPORT NO. LED-500-3

30 Sept. 1964

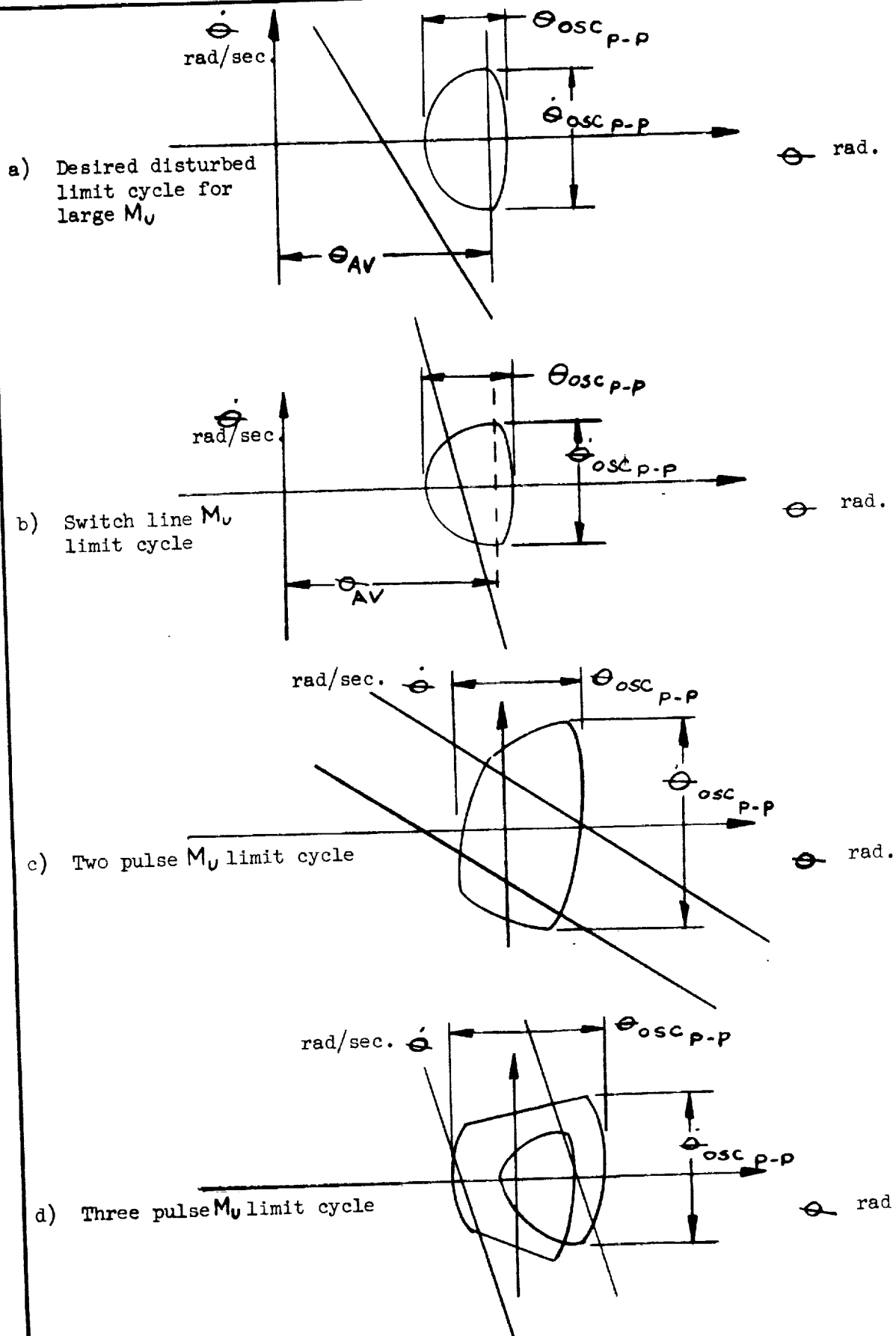


Figure 3-31 - Moment Unbalance Limit Cycle Characteristics

FORM G328 5-63 (ENG 23, ENG 26)

~~CONFIDENTIAL~~

GRUMMAN AIRCRAFT ENGINEERING CORPORATION

REPORT LED-500-3  
DATE 30 Sept. 1964  
CODE 26512

~~CONFIDENTIAL~~

because  $t_{on} \approx t_{on_{min}}$  due to the pulse width characteristic of the PRM (Figure 3-23). However, it is this same pulse width characteristic that causes poor propellant flow rates for moment unbalance control when  $M_u < 0.5 M_c$ . This is due to the small values of  $I_{sp}$  caused by the small pulse widths. (For  $M_u = 0.5 M_c$ ;  $t_{on} = 2t_{on_{min}}$ ). For  $M_u > 0.5 M_c$ , the pulse width increases rapidly and better  $I_{sp}$  values are obtained.

Response to large rotational commands of the PRM is, as for all other pulse modulators, similar to that of the on-off modulator.

The permissible rate gyro deadzone for a pulse on "demand" PRM was determined by digital techniques (6) to be 0.05 deg/sec. for the IEM. A typical limit cycle with  $K_R = 0$  is shown in Figure 3-30. A permissible rate gyro deadzone has not been evaluated for the "delay" PRM.

**3.3.4.5 Non Linear PRM** In order to improve the PRM moment unbalance limit cycle propellant flow rate, its static pulse repetition frequency characteristics are modified to yield a nonlinear PRM as shown in Figure 3-25. Also shown are the static duty factor and pulse width characteristics of the nonlinear PRM. It should be noted that the pulse width characteristics are unchanged. The integral equations for the nonlinear PRM are:

$$t_{on_{min}} = \int_0^{t_{on}} (1-x) dt; x = f(t) \quad (3-47)$$

$$t_{on_{min}} = \int_{t_{on}}^{T_p} \lambda x dt \quad (3-48)$$

For decreasing values of the non-linearity factor ( $\lambda$ ) larger pulse widths will be required to control a given moment unbalance. Therefore, large values of  $I_{sp}$  and lower propellant flow rates will be obtained along with a lower pulse repetition frequency by use of non-linear PRM for large moment unbalance control. However, an increased average attitude offset will have to be tolerated, but normal limit cycle operation will not be changed by introducing  $\lambda$  due to the modulator pulse width characteristics.

As with the other pulse modulators response to large rotational commands will be similar to that of the "on-off" modulator.

**3.3.4.6 Piecewise-linear PRM** The characteristics of the piecewise-linear PRM are shown in Figure 3-24. It can be seen from the characteristic curves that for  $e < e_2$  this modulator is a PFM and for  $e_2 < e < e_1$  it is a PWM. Therefore, its normal limit cycle operation is identical to that of the PFM and its large moment unbalance limit cycle operation is that of PWM. Also, the piecewise-linear PRM permissible rate gyro deadzone is identical to that of a PFM.

**3.3.4.7 General** Other than the characteristics discussed for each pulse modulator in the preceding sections, there are several characteristics which are common to all "delay" and/or "demand" modulators. These common characteristics are discussed below:

~~CONFIDENTIAL~~

~~CONFIDENTIAL~~

- a) "Demand" type pulse modulators will yield switch line limit cycles for small moment unbalances (on the order of 100 ft-lbs) as shown in Figure 3-31b. For this type of limit cycle  $t_{on} = t_{onmin}$  and therefore wastes propellant and should be avoided if possible. From Figure 3-32 it can be seen that if

$$\dot{\theta}_y - \dot{\theta}_x < \frac{|M_c| - |M_u|}{I} (t_{onmin} - T_{on} + T_{off}) = \Delta \dot{\theta} \quad (3-49)$$

a switch line limit cycle will be generated by the control system.  $\theta_x$  and  $\theta_y$  are given by the following equations:

$$\dot{\theta}_y = \alpha_u (T_{on} + T_G) + \dot{\theta}_o \quad (3-50)$$

$$\dot{\theta}_x = K_R \alpha_T \left[ -1 + \sqrt{1 - \frac{C}{\alpha_T^2 K_R^2}} \right] \quad (3-51)$$

where

$$C = \alpha_T \alpha_u (T_{on} + T_G)^2 + 2 \alpha_T [\dot{\theta}_o (T_{on} + T_G) + \theta_o - \Omega] - [\dot{\theta}_o + \alpha_u (T_{on} + T_G)]^2 \quad (3-52)$$

$$\alpha_T = \alpha_u + \alpha_c \quad (3-53)$$

$$\alpha_u = M_u / I \quad (3-54)$$

$$\alpha_c = (M_c - M_u) / I \quad (3-55)$$

From the above equations the value of  $M_u$  which is the boundary between a limit cycle on the switch line or in the modulation region can be determined.

- b) "Delay" pulse modulators tend to alleviate the switch line moment unbalance problem for small moment unbalances because equation 3-50 increases; i.e.

$$\dot{\theta}_y = \alpha_u (T_{on} + T_G + T_p) + \dot{\theta}_o$$

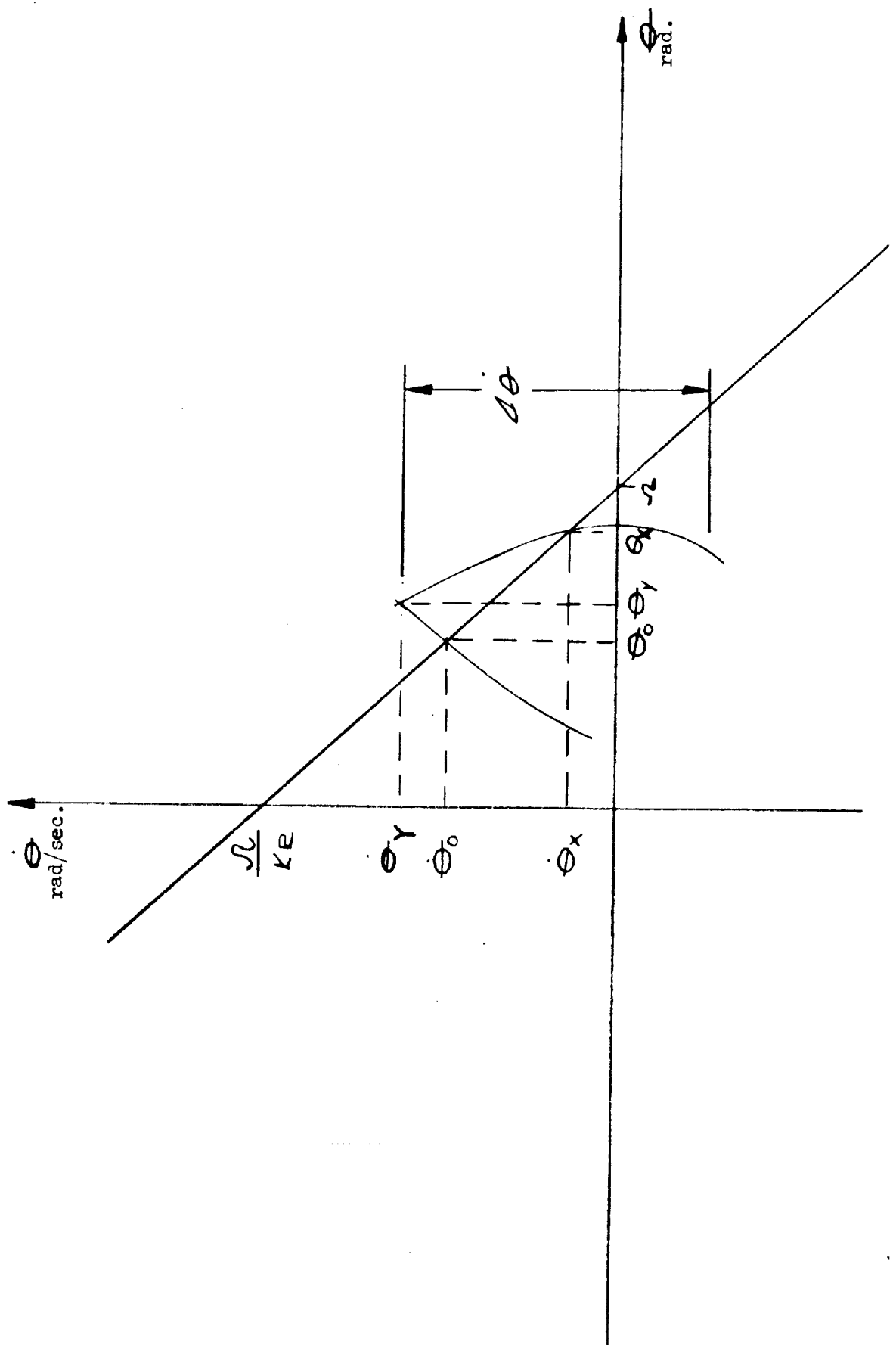
where  $T_p$  is the integrating delay of the modulator.

- c) All pulse modulators give good transient response for attitude commands less than one degree with the high gain linear modulators yielding the best response.

~~CONFIDENTIAL~~

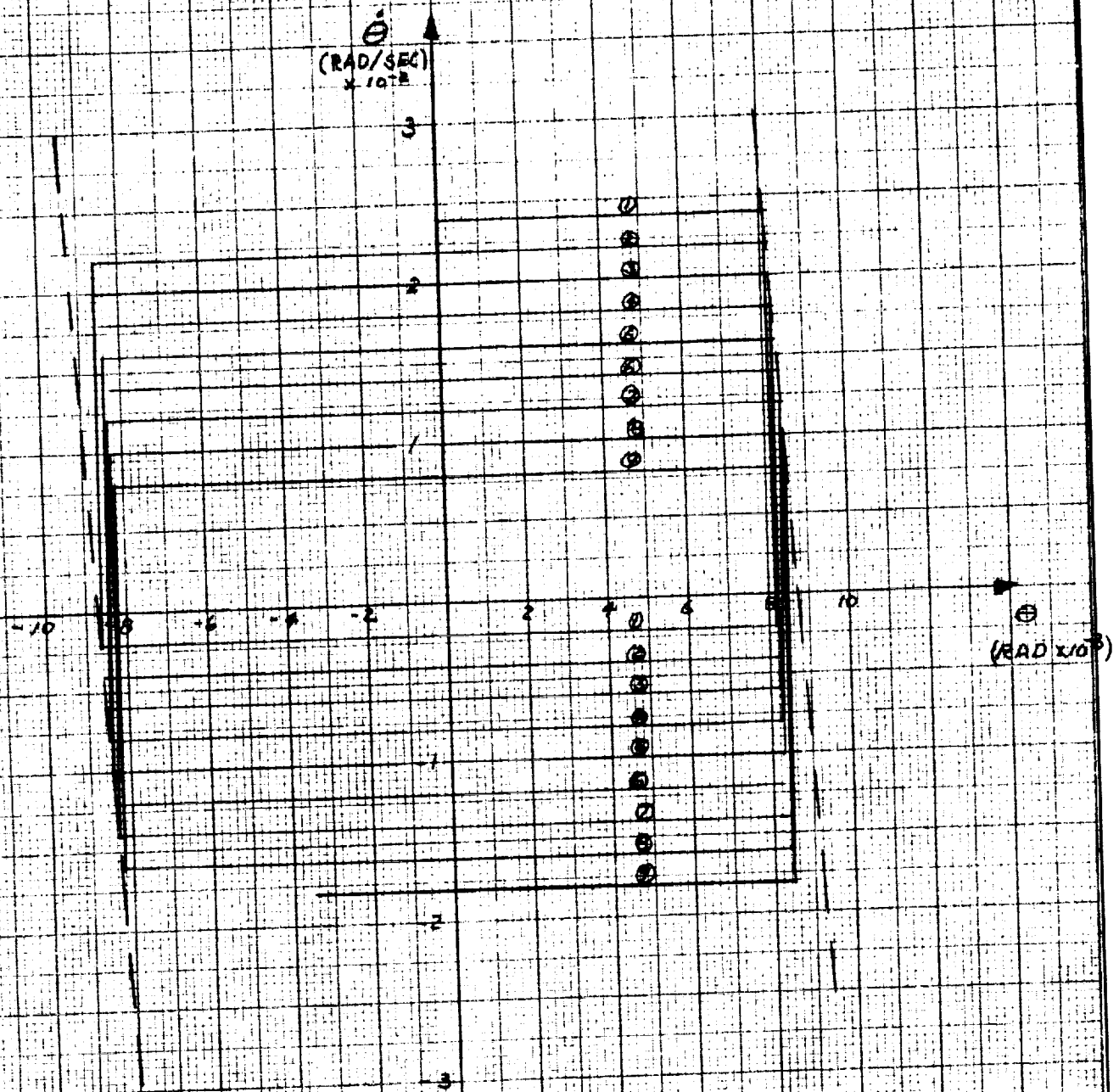


Figure 3-32 - Moment Unbalance Limit Cycle Characteristics to Determine Boundary Between Switch Line and Desired Limit Cycles



~~CONFIDENTIAL~~

PAGE 64



~~CONFIDENTIAL~~

- d) For large moment unbalances the PWM and PRM will deliver increasingly larger pulse widths.  $K_R$  must be selected in order that the limit cycle shown in Figure 3-31 c or d does not occur for the range of moment unbalances expected for LEM in order that RCS propellant is not wasted by thrusting in such a way that the control acceleration adds to the moment unbalance acceleration.
- e) "Demand" pulse modulators are susceptible to noise and will therefore generate extraneous pulses while "delay" pulse modulators serve as noise filters and therefore will not generate extraneous pulses during normal limit cycle.
- f) All pulse modulators will generate a wandering limit cycle (8) as shown in Figure 3-33. This phenomena will occur because of different moments generated for plus and minus rotations.

### 3.4 Simulation Results

3.4.1 Introduction The results to be presented in this section were obtained from both analog and digital computer simulations. An analog simulation of the single axis control system (Figure 3-5) was used to study the following:

- a) On-off modulator
- b) Induced-rate modulator
- c) Piecewise-linear PRM
- d) PWM

A digital simulation of the control system (Figure 3-5) was used to study the following:

- a) PRM
- b) Non-linear PRM

To facilitate the presentation of the simulation data the LEM control requirements will be separated into the following:

- a) limit cycle operation
- b) limit cycle operation with moment unbalance applied
- c) response to large errors

3.4.2 Limit Cycle To investigate limit cycle operation, in the absence of disturbance moments, the following modulators were used:

- a) on-off modulator
- b) induced rate modulator

~~CONFIDENTIAL~~

~~CONFIDENTIAL~~

- c) piecewise-linear PRM (delay type)
- d) PWM (delay type)

Plots of  $K_R$  vs.  $\dot{\theta}_A$  and the parameters assumed are shown in Figures 3-34, 3-35, and 3-36 for the on-off, pulse width and piecewise-linear PRM respectively. From these figures, it is apparent that only the piecewise-linear PRM is not heavily dependent upon  $K_R$  for the minimum value of  $\dot{\theta}_A$ . It is also evident that the piecewise-linear PRM generates the minimum impulse limit cycle. The PFM, PRM, non-linear PRM, modified on-off modulators and demand PWM will also display an independence to  $K_R$  variation with respect to  $\dot{\theta}_A$ .

The induced rate modulator was simulated with  $T_i = \infty$ , and it was verified that with the proper value of  $K$  for each inertia a minimum impulse limit cycle will be generated.

Although  $\dot{\theta}_A$  is independent of  $K_R$  for pulse modulators,  $D$  is not, due to dependence of  $\theta_{\max}$  on  $K_R$ , as can be seen from Figure 3-37 and it will therefore be necessary to vary  $K_R$  for all modulators during the LEM mission. However, only two values of  $K_R$  appear to be necessary (one value for ascent and one value for descent) for the pulse modulators while many would have to be required for the on-off modulator (induced rate modulator also requires many  $K$  changes).

From the preceding, it is obvious that a pulse modulator, other than the delay PWM, should be used for limit cycle control because:

- a) a pulse modulator provides minimum or near minimum impulse limit cycle and therefore minimum propellant for any value of  $K_R$  chosen.
- b) only two values of  $K_R$  will be required for the LEM mission assuming mass properties in Table 3-1.
- c) a pulse modulator yields minimum possible values of  $\dot{\theta}_A$  and will therefore satisfy the desired maximum rate for docking (9) that

$$\dot{\theta} = 2\dot{\theta}_A < 0.5 \text{ deg/sec.}$$

3.4.3 Disturbed Limit Cycle To study limit cycle operation in the presence of moment unbalances, the following modulators were used:

- a) on-off modulator
- b) induced rate modulator
- c) PWM
- d) piecewise-linear PRM
- e) PRM
- f) non-linear PRM

~~CONFIDENTIAL~~

REPORT LED-500-3  
DATE 30 Sept. 1964

Figure 3-34  
 $K_A$  vs.  $\theta_A$  for On-off Modulator

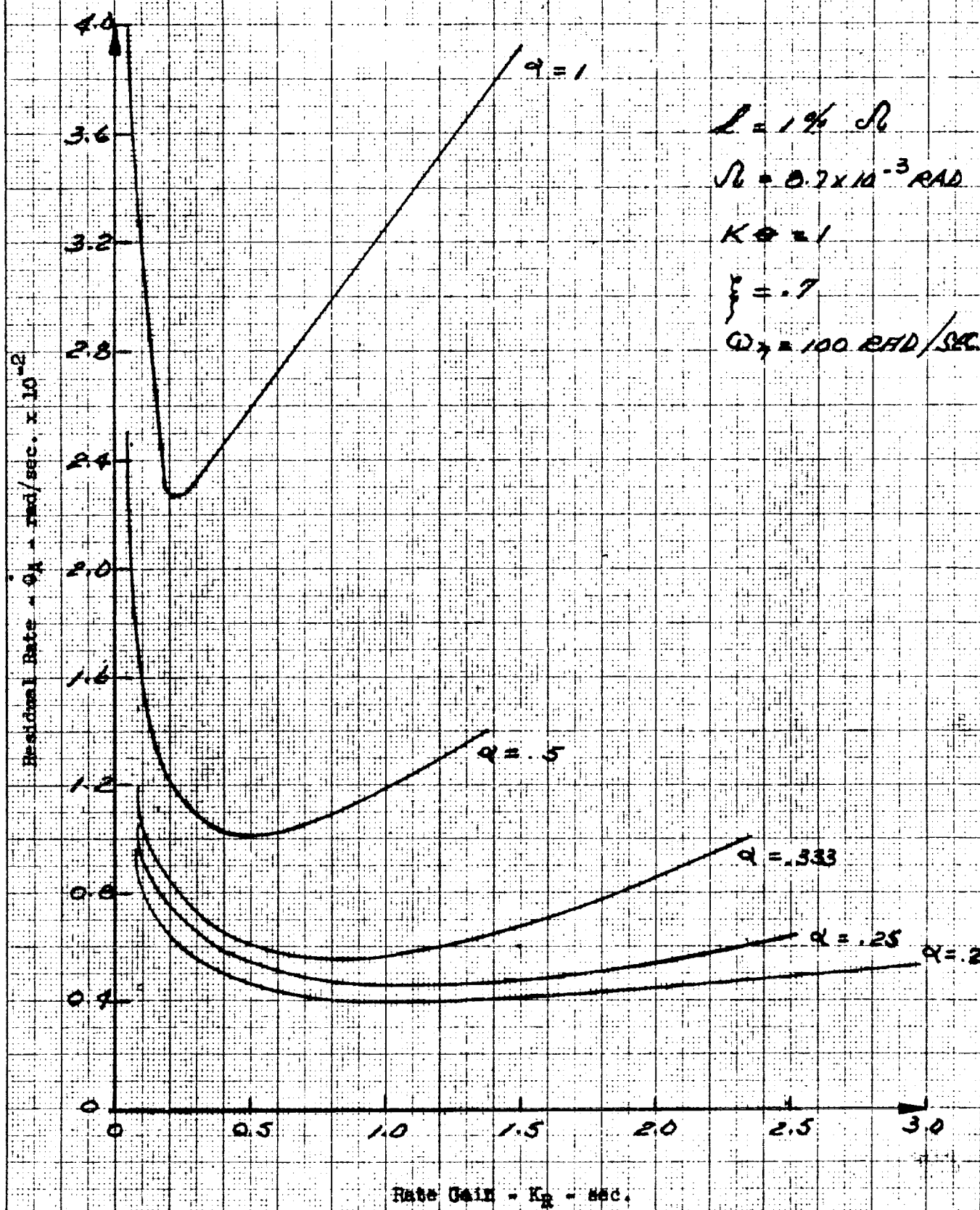
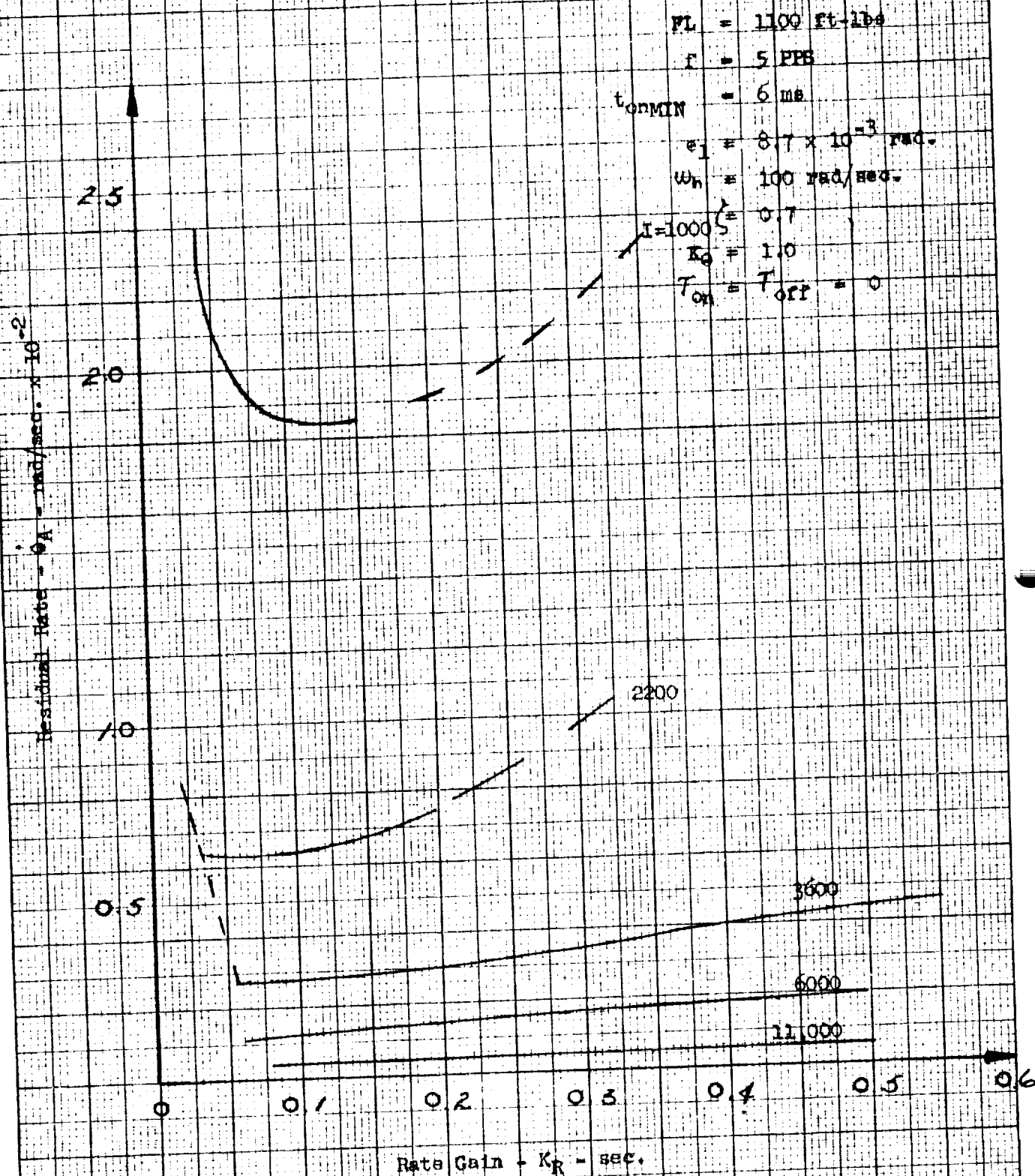


Figure 3-35

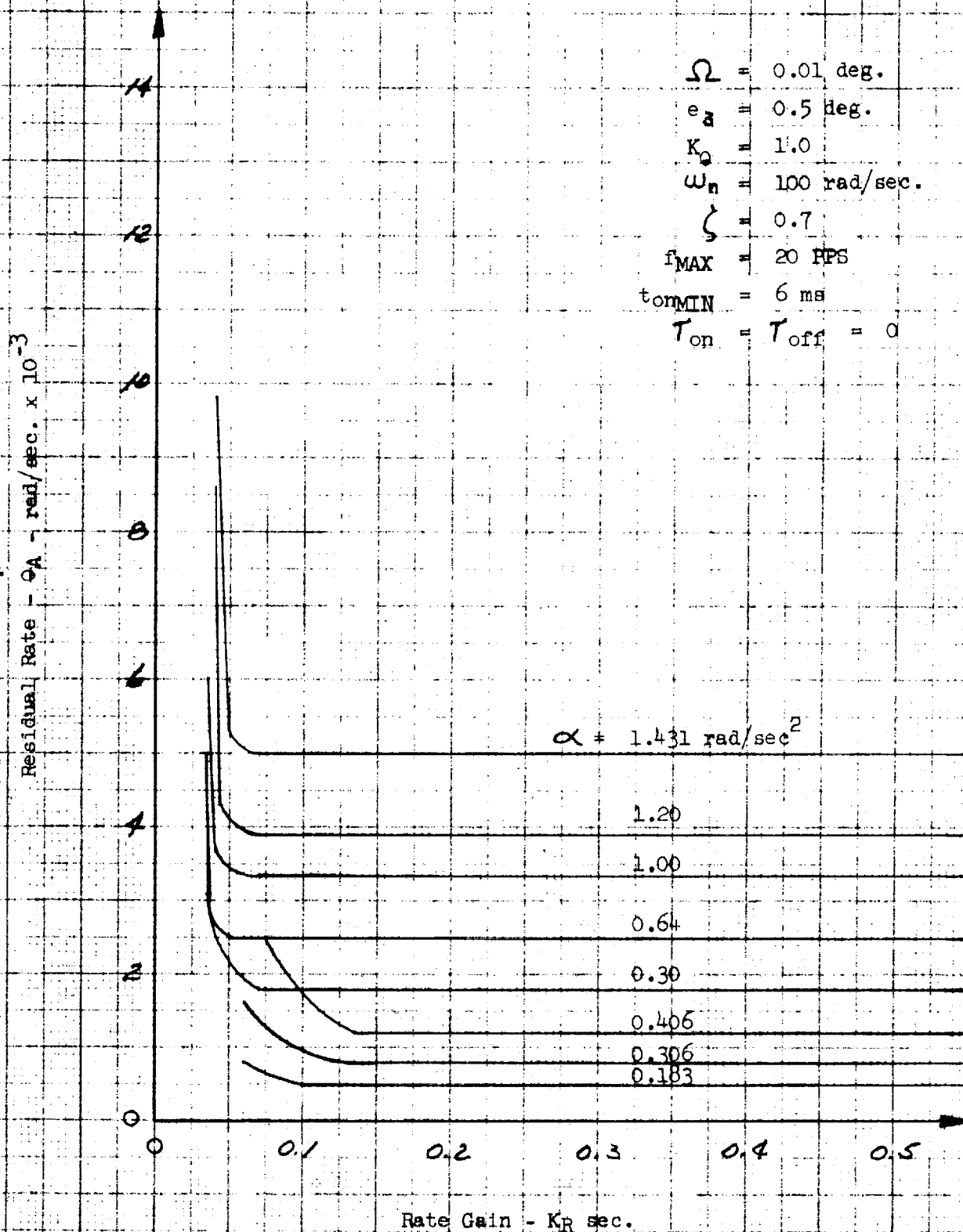
 $K_R$  vs.  $\phi_A$  for Delay Type PWM

~~CONFIDENTIAL~~

Figure 3-36

PAGE 69

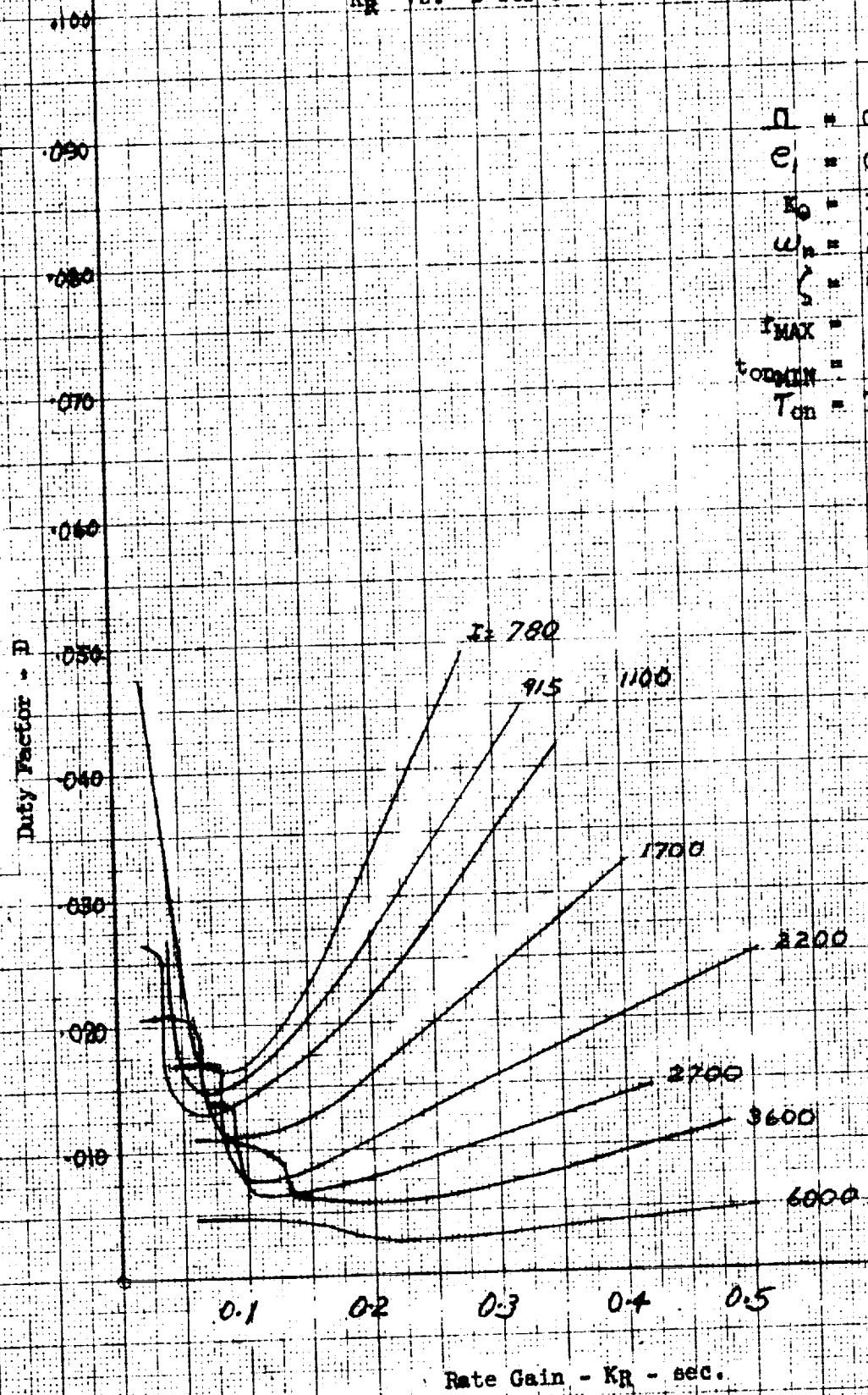
$K_R$  vs.  $\theta_A$  for Piecewise Linear PRM



~~CONFIDENTIAL~~

Figure 3-37

$K_R$  vs.  $D$  for Piecewise Linear PWM



$\Delta = 0.01$  deg.  
 $e_1 = 0.5$  deg.  
 $K_0 = 1.0$   
 $\omega_n = 100$  rad/sec.  
 $\zeta = 0.7$   
 $f_{MAX} = 20$  FPS  
 $t_{ONMIN} = 6$  ms  
 $T_{on} = T_{off} = 0$

K-E  
 10 X 10 TO THE CM. 359T-14G  
 KEUFFEL & ESSER CO. MADE IN U.S.A.  
 ALBANY, N.Y.



~~CONFIDENTIAL~~

Disturbed limit cycle characteristics are defined in Figure 3-32 (only desired and switch line limit cycles were obtained). Plots of  $M_u$  versus these quantities are shown in Figures 3-38, 3-39 and 3-40 while  $M_u$  versus  $\dot{\omega}$  is plotted in Figure 3-41 (for all modulators listed above). The parameters used for the modulators are tabulated in Table 3-2.

It is evident from Figure 3-41 that a non-linear PRM ( $\lambda = 0.1$ ) or a PWM should be used to control large moment unbalances during powered ascent to minimize propellant consumption. A delay type PWM or a delay type non-linear PRM will yield improved limit cycle operation for  $25 < M_u < 100$  as can be seen from the delay PWM and  $\lambda = 0.1$  non-linear demand PRM curves for  $M_u$  vs.  $\dot{\omega}$  in Figure 3-41. The delay non-linear PRM improvement can be seen by extending the curve on the right of  $M_u = 100$  to the curve to the left of  $M_u = 100$  as shown in the Figure 3-41. It can be seen from this dashed curve that the delay non-linear PRM ( $\lambda = 0.1$ ) will yield the smallest propellant requirements.

To obtain the small values of propellant flow rate, obtained by selecting the non-linear PRM, larger values of  $\theta_{AV}$ ,  $\dot{\theta}_{osc}$  and  $\theta_{osc}$  for  $M_u > 100$  ft-# must be tolerated. However, the guidance system can compensate for these quantities.

**3.4.4 Response to Large Errors** As can be seen from Figures 3-42, 3-43, 3-44, and 3-45, there is little difference in the response of on-off or pulse modulator control systems. However, the effect of  $K_R$  on overshoot and therefore propellant consumption is quite evident. Also, it is evident that the non-linear PRM gives better response than the "on-off" modulator due to its region of varying pulses.

**3.4.5 Conclusion** It can be concluded from the discussion presented in section 3.3 and the simulation results presented in this section that PRM or non-linear PRM provide suitable overall control system operation. However, PRM is desirable for normal operation because of its higher gain and therefore better response to small attitude commands, and "delay" non-linear PRM is desired to control moment unbalance during powered ascent. Therefore, a non-linear "delay" PRM with the capability of varying  $\lambda$  such that  $\lambda = 1$  (PRM) and  $\lambda < 1$  (non-linear PRM) would be ideal since it would yield the best overall attitude control system. However, a fixed non-linear "delay" PRM with  $\lambda < 1$  is recommended for use in the IEM control system because it yields satisfactory overall system response and presents a simpler system since switching of  $\lambda$  will not be required.

The number of thruster operations during the IEM mission is also of interest in selecting the type of PRM to be used in the attitude control system. From a reliability point of view, it is desirable to minimize the number of thruster operations required. Moment unbalance operation is the condition of interest here since there is no appreciable difference between linear and non-linear PRM with respect to the number of thruster operations for normal limit cycle and large transient response operation. As can be seen from Figure 3-46, the moment unbalance limit cycle period decreases (frequency increases) for all modulators as moment unbalance increases; i.e., the number of thruster operations increases with increasing moment unbalance. From the curves plotted in Figure 3-46, it is apparent that the "delay" PRM ( $\lambda = 0.1$ ) will yield the least number of thruster operations. Also notice that  $\dot{\omega} \propto f/\tau_{on}$  (Figures 3-41, 3-46 and 3-1); i.e., high frequency moment unbalance limit cycle yields small

Code 26512 Eng-23-1A

~~CONFIDENTIAL~~

TABLE 3-1  
MASS PROPERTY HISTORY

Mission Phase	Weight Earth Lbs	Center of Gravity			Moments of Inertia		
		sta	in	in	Slug - ft <sup>2</sup>		
		X	Y	Z	I <sub>xx</sub>	I <sub>yy</sub>	I <sub>zz</sub>
Start of Separation	29,870	190	-0.4	0.1	20,455	22,314	21,965
Start of Powered Descent	29,458	190	-0.4	0.1	20,173	22,006	21,662
Start of Hover	15,618	212	-0.8	0.2	11,524	12,080	13,977
Touchdown	13,805	221	-0.9	0.2	10,290	10,729	12,668
Liftoff	10,500	242	-0.3	0.8	6,414	3,381	5,576
Start of Rendezvous	5,511	254	-0.6	1.6	3,133	3,048	1,730
Docked	5,129	254	-0.6	1.7	2,916	2,837	1,610

$t_{on}$  values and therefore large values of  $\dot{\omega}$ . Therefore, small values of  $f$  (large  $T$ ) which yield large rate excursions (Figure 3-39) are desired for minimum propellant consumption and minimum number of thruster operations. It can therefore be concluded that a non-linear PRM with  $\lambda < 1$  should be used for the LEM attitude control system.

### 3.5 Attitude Control Propellant Requirements for LEM Mission (10, 11)

The RCS propellant requirement for LEM attitude control was evaluated assuming the simplified LEM control system with cross-coupling terms neglected (Figure 3-5). It was also assumed that a PRM was used for reaction jet control. The propellant requirements were evaluated as follows:

- a. Propellant required for limit cycle operations:

~~CONFIDENTIAL~~

TABLE 3-2  
MODULATOR PARAMETERS FOR MOMENT UNBALANCE STUDY

MODULATOR				
On-Off	Induced Rate	Piecewise Linear PRM	PWM	PRM Nonlinear PRM
$\Omega = 0.1$ deg $h = 2\%$ $\Omega$ $I = 2200$ slug-ft <sup>2</sup> $T_c = 667$ ft-lbs $K_R = 0.2$ sec. $K_\theta = 1.0$ $\zeta = 0.7$ $\tau_{on} = 15$ ms $\tau_{off} = 20$ ms	$\Omega = 0.1$ deg $h = 1\%$ $\Omega$ $I = 2500$ slug-ft <sup>2</sup> $T_c = 1100$ ft-lbs $K_R = 0.05$ sec. $K_\theta = 1.0$ $\omega_h = 100$ rad/sec $\zeta = 0.7$ $\tau_L = 0$ $K = 0.13$ sec $\tau_{on} = 15$ ms $\tau_{off} = 20$ ms	$\Omega = 0.01$ deg $e_3 = 0.5$ deg $I = 2200$ slug-ft <sup>2</sup> $T_c = 1100$ ft-lbs $K_R = 0.12$ sec $K_\theta = 1.0$ $\omega_h = 100$ rad/sec $\zeta = 0.7$ $f_{pmax} = 20$ pps $\tau_{onmin} = 6$ ms $e_2 = 0.25$ deg $\tau_{on} = 0$ $\tau_{off} = 0$	$\Omega = 0.01$ deg $e_1 = 0.5$ deg $I = 2200$ slug-ft <sup>2</sup> $T_c = 1100$ ft-lbs $K_R = 0.12$ sec $K_\theta = 1.0$ $\omega_h = 100$ rad/sec $\zeta = 0.7$ $f_p = 5$ pps $\tau_{onmin} = 6$ ms $\tau_{on} = 0$ $\tau_{off} = 0$	$\Omega = 0.1$ deg $e_1 = 0.5$ deg $I = 2200$ slug-ft <sup>2</sup> $T_c = 1100$ ft-lbs $K_R = 0.4$ sec $K_\theta = 1.0$ $\omega_h = 125$ rad/sec $\zeta = 0.8$ $\tau_{onmin} = 10$ ms $\tau_{on} = 12$ ms $\tau_{off} = 7$ ms

Code 26512 Eng-23-1A

 REPORT LED-500  
 DATE 30 Sept 1960
~~CONFIDENTIAL~~

GRUMMAN AIRCRAFT ENGINEERING CORPORATION

~~CONFIDENTIAL~~

- 1- during coasting phases of LEM mission using equation 3-9
- 2- during powered phases of LEM mission using equation 3-11a for ascent (see section 2 for powered descent estimate)
- b. Propellant required for large angular rotations using equation 3-14 assuming a  $50^\circ/\text{sec.}$  rate limit

The total propellant required for attitude control was evaluated based upon the above assumptions and is tabulated in Table 3-3 for the mass properties in Table 3-1. Any major change in mission plan will require that the propellant requirements be re-estimated.

### 3.6. Control System Deadbands (12)

Use of two deadbands were considered (Figure 3-47), one in the forward loop, and one on the attitude signal, with respect to their effects on minimum rate command and limit cycle operation. Also considered is the effect of rate gyro bias on limit cycle operation. However, the rate gyro deadband of  $0.01^\circ/\text{sec.}$  was neglected because it is smaller than the minimum possible rate change of  $0.02^\circ/\text{sec.}$

A phase plane technique was used to determine the effects of the additional attitude deadband and the rate gyro bias on limit cycle operation of a single axis LEM attitude control system with cross coupling terms neglected (Figure 3-47).

For the attitude deadzone ( $\Omega_a$ ) equal to zero the phase plane boundaries are plotted in Figure 3-48 for both attitude hold and rate command modes. The following relationships are obtained from Figure 3-48.

$$a) \dot{\theta}_{cmin} > 2\Omega/K_R > \Delta \dot{\theta}_{min} \quad (3-56)$$

must be satisfied to insure a rate change and a final rate value in the deadband;

$$b) \theta_{coast} < 2\Omega \quad (3-57)$$

states that total attitude change cannot exceed  $2\Omega$  during limit cycle;

$$c) \theta_{AV} = K_R \dot{\theta}_B$$

states that  $\dot{\theta}_B$  causes limit cycle to have an average value.

Equation 3-56 is the critical equation. It must be satisfied for all values of  $\Omega$  and  $K_R$ . For ascent coast which is the worst case,  $K_R = 0.4 \text{ sec.}$  and  $\theta_{coast} \approx 0.32^\circ/\text{sec.}$ ; therefore, from equation 3-56

$$\dot{\theta}_{cmin} > 0.5^\circ/\text{sec.} > 0.32^\circ/\text{sec.} \text{ for } \Omega = 0.1^\circ$$

$$\text{and } \dot{\theta}_{cmin} > 25^\circ/\text{sec.} > 0.32^\circ/\text{sec.} \text{ for } \Omega = 5.0^\circ$$

~~CONFIDENTIAL~~

~~CONFIDENTIAL~~

For  $\Omega = 0.1^\circ$  we have a satisfactory control system. However, for  $\Omega = 5.0^\circ$  the control system is unacceptable since a  $\dot{\theta}_{c\min}$  of  $25^\circ/\text{sec.}$  exceeds rate gyro limits, the desired maximum command rate and is too coarse for vehicle control. Therefore, to use the  $\Omega_a = 0$  scheme it will be necessary to switch to  $\Omega = 0.1^\circ$  whenever a rate command is given.

With the inclusion of  $\Omega_a$  the phase plane boundaries change as shown in Figure 3-49. The following relationships are obtained from Figure 3-49:

$$a) \quad \dot{\theta}_{c\min} > 2 \Omega / K_R > \Delta \dot{\theta}_{\min} \quad (3-56)$$

to insure a rate change and a null within the deadband.

$$b) \quad \theta_{\text{coast}} < 2 \Omega + \Omega_a \quad (3-59)$$

for limit cycle if

$$\dot{\theta}_{\min} < \Omega / K_R - |\dot{\theta}_\beta| \quad (3-60)$$

$$c) \quad \theta_{\text{coast}} < 2 \Omega \quad (3-61)$$

for limit cycle if

$$|\dot{\theta}_\beta| \geq \Omega / K_R \quad (3-62)$$

$$d) \quad \theta_{AV} = K_R \dot{\theta}_\beta \quad \text{if (57) is true} \quad (3-58)$$

$$e) \quad \theta_{AV} = \pm [|\Omega_a| + |K_R \dot{\theta}_\beta|] \quad \text{is true} \quad (3-63)$$

Again equation 3-56, for ascent conditions, is critical. For ascent  $\dot{\theta}_{\min} = 0.32^\circ/\text{sec.}$  and  $K_R = 0.4 \text{ sec.}$  From equation 3-56 we get

$$\Omega > \frac{(0.32)(0.4)}{2} = 0.064^\circ/\text{sec}$$

Selecting  $\Omega = 0.1^\circ$  we get the following

$$\dot{\theta}_{c\min} > 0.5^\circ/\text{sec.} > 0.32^\circ/\text{sec.}$$

$$\Omega_a = 0^\circ \text{ for } 0.1^\circ \text{ coast}$$

$$\Omega_a = 4.9^\circ \text{ for } 5.0^\circ \text{ coast}$$

Therefore, for tight attitude ( $\Omega_a = 0$ ) the system of Figure 3-49 becomes the simplified system shown in Figure 3-48.

Code 26512 Eng-23-1A

REPORT  
DATE

LED-500  
30 Sept. 1964

~~CONFIDENTIAL~~

GRUMMAN AIRCRAFT ENGINEERING CORPORATION

At present  $\dot{\theta}_{B_{max}} = 0.2^\circ/\text{sec}$  (4) Therefore, from inequality 3-60  $\Delta \dot{\theta}_{min} < 0.05^\circ/\text{sec}$ . but, actually  $\Delta \dot{\theta}_{min} = 0.32^\circ/\text{sec}$ . and therefore inequality 3-60 is not true. Inequality 3-62 is not true since it requires  $|\dot{\theta}_B| \geq 0.25^\circ/\text{sec}$ . but  $|\dot{\theta}_B| = 0.2^\circ/\text{sec}$ . with present gyro characteristics. Since both inequalities 3-60 and 3-62 are not satisfied a limit cycle with both values of  $\theta_{coast}$  and  $\theta_{AV}$  will occur.

The addition of  $\Omega_a$  in the attitude error signal offers the possibility of achieving a small  $\dot{\theta}_{cmin}$  independent of the value of the total attitude dead-zone. During coast large attitude deadbands are desired to minimize fuel consumption. However, for  $\Omega_a \neq 0$  and for the range of  $\dot{\theta}_B$  possible, undesirable limit cycle periods due to decreased  $\theta_{coast}$  values will occur. This will result in increased RCS propellant consumption. Also with  $\Omega_a \neq 0$ , the possibility of having  $\theta_{AV}$  oscillate between  $K_R \dot{\theta}_B$  and  $[|\Omega_a| + |K_R \dot{\theta}_B|]$  where  $\Omega_a = 5^\circ$ , is highly undesirable.

When  $\Omega_a = 0$  for the entire LEM mission,  $\Omega$  alone will control the total attitude deadband.  $\Omega$  must be set equal to  $5^\circ$  for coast phases to minimize propellant consumption. However, this results in an unacceptably large  $\dot{\theta}_{cmin}$ . Therefore, it will be necessary to switch to the smaller value of  $\Omega$  whenever a rate command is given. This will yield the desired small value for  $\dot{\theta}_{cmin}$  and also yield the desired values for  $\theta_{coast}$  and  $\theta_{AV}$ .

It is therefore concluded that the control system with  $\Omega_a \equiv 0$  and the inclusion of the capability to switch to the smaller value of  $\Omega$  for rate commands should be used because:

1. Only one value of  $\theta_{AV}$  exists and its maximum value is

$$\theta_{AV_{max}} = K_R \dot{\theta}_{B_{max}}$$

2. Only one range of  $\theta_{coast}$  is possible. That is

$$\theta_{coast} < 2 \Omega$$

3. Reasonable values of  $\dot{\theta}_{cmin}$  will be obtained.

Since pilot maneuvers during coast periods are few and pre-planned, it appears acceptable to depend upon manual selection of the small  $\Omega$  prior to the maneuver. Automatic  $\Omega$  selection by means of the detent switch on the control stick is also acceptable.

TABLE 3-3

Attitude Control And Rotational Maneuvering Propellant Breakdown

Mission Phase	Limit Cycle			Maneuvers***
	Time (sec)	Dead Zone (deg)	Propellant (lbs.)	Propellant (lbs.)
DESCENT				
Separation	78	.1	.2	5.6 (2)
Orientation and Insertion Prep.	792	.1	2.0	22.7 (8)
Coast to Pericynthion	3600	5	.2	8.1 (3)
Automatic Powered	710	.1	39.2	8.1 (2)
ASCENT				
Powered	430	.1	172.7*	2.3 (2)
Contingency Stay	600	.1	15.9	6.8 (20)
Coast	5400	5	3.0	1.9 (9)
Rendezvous	847 600	5 .1	.5 15.9	-- --

\* 170# of the 172.7# provides a useful  $\Delta V = 226$  ft/sec, which is equivalent to 128# of ascent main tank propellant.

\*\* Manual landing and docking propellant requirements are not included.

\*\*\* Number of maneuvers assumed is shown in parentheses.

Code 26512  
Eng-23A

Figure 3-38

See Table 3-2  
for modulator  
parameters

Average Attitude -  $\theta_{AV}$  - deg.

0.6

0.5

0.4

0.3

0.2

0.1

Demand PWM  $\lambda = 0.1$

Piecewise Linear Plot

Delay PWM

On-off

100

200

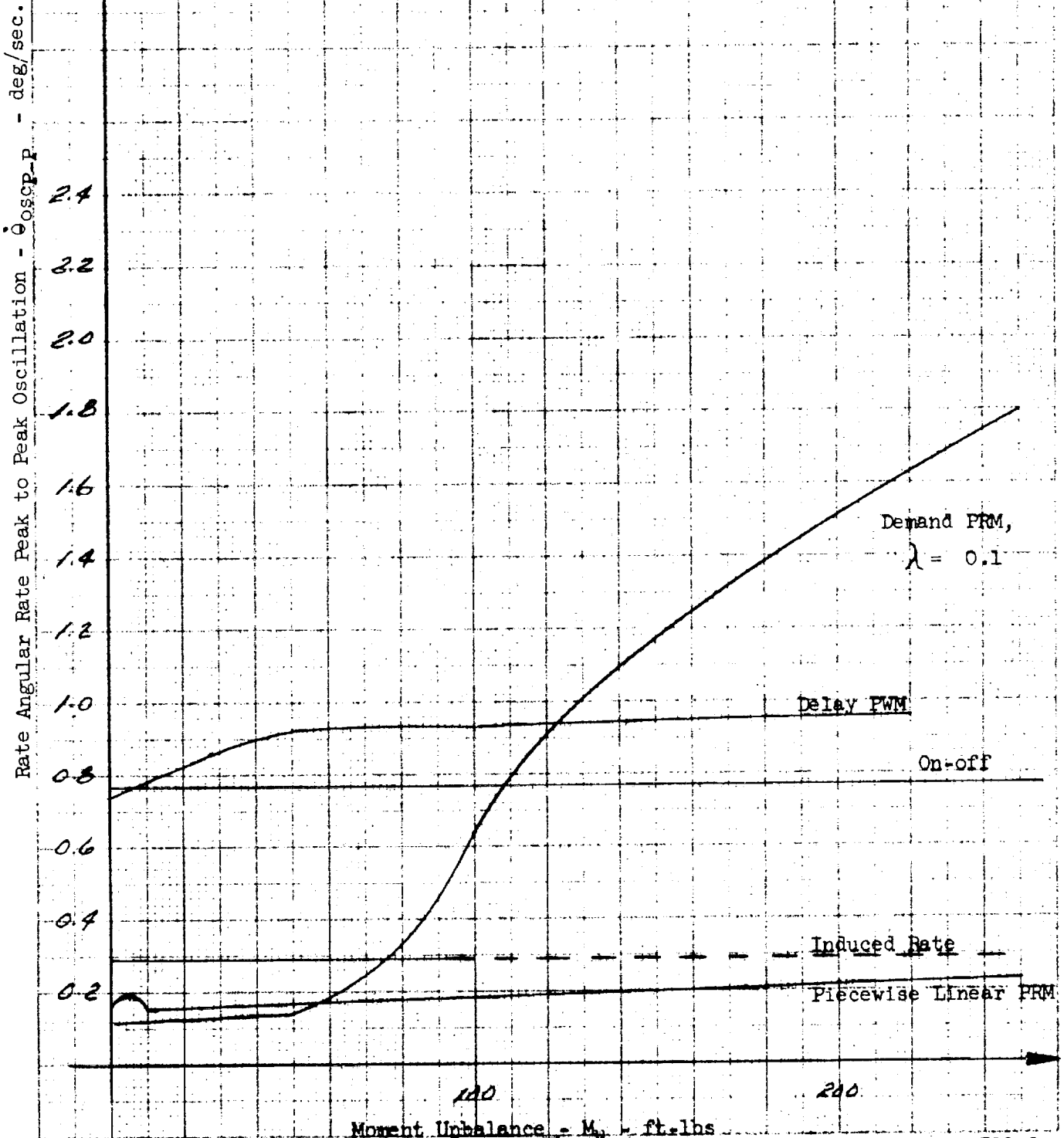
Moment Unbalance -  $M_u$  - ft-lbs

K&E  
KLEINER & KLEINER CO.  
10 X 10 TO THE 1" INCH  
3201-11



Figure 3-39

See Table 3-2 for  
modulator parameters



See Table 3-2 for  
modulator parameters

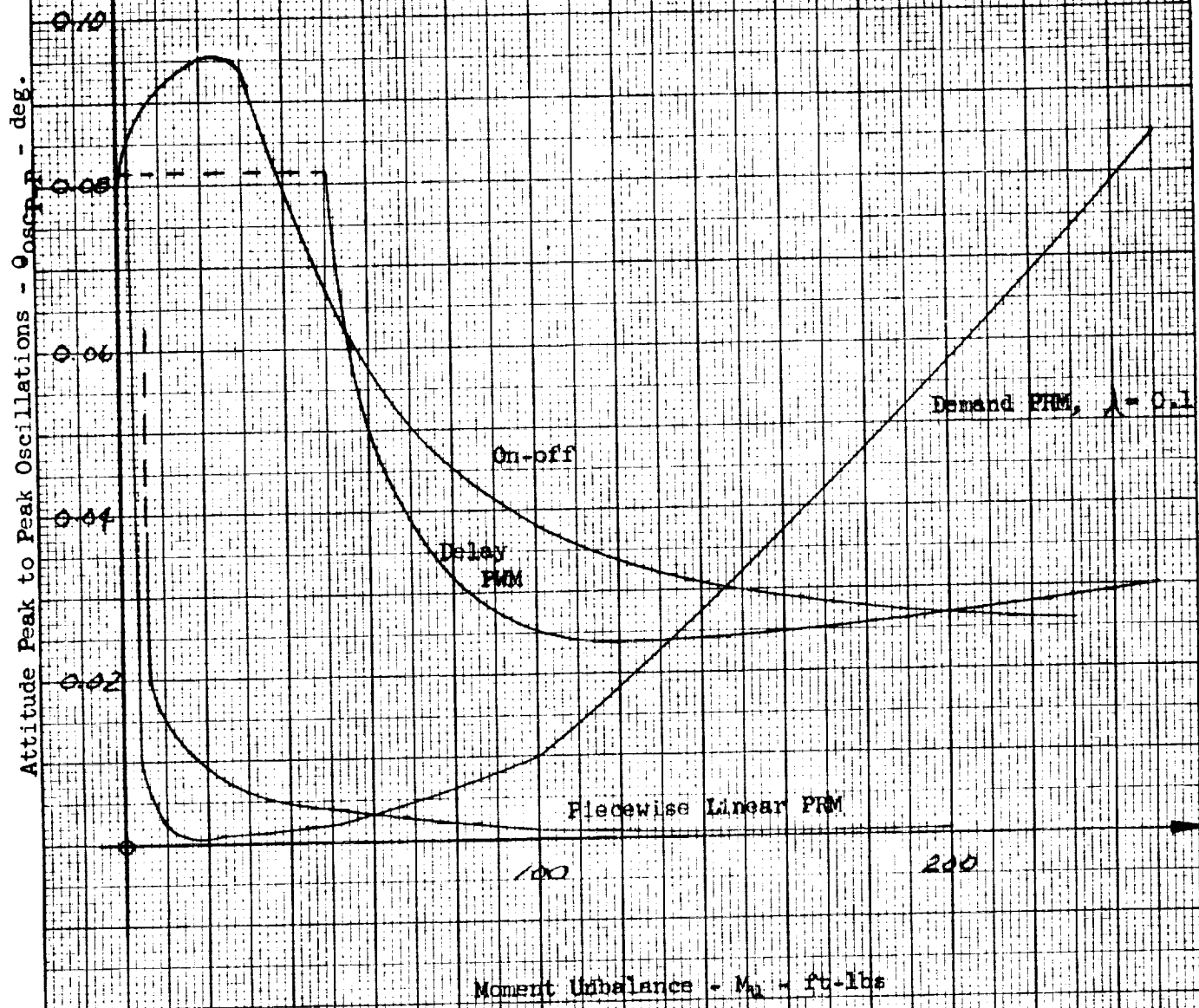


Figure 3-40

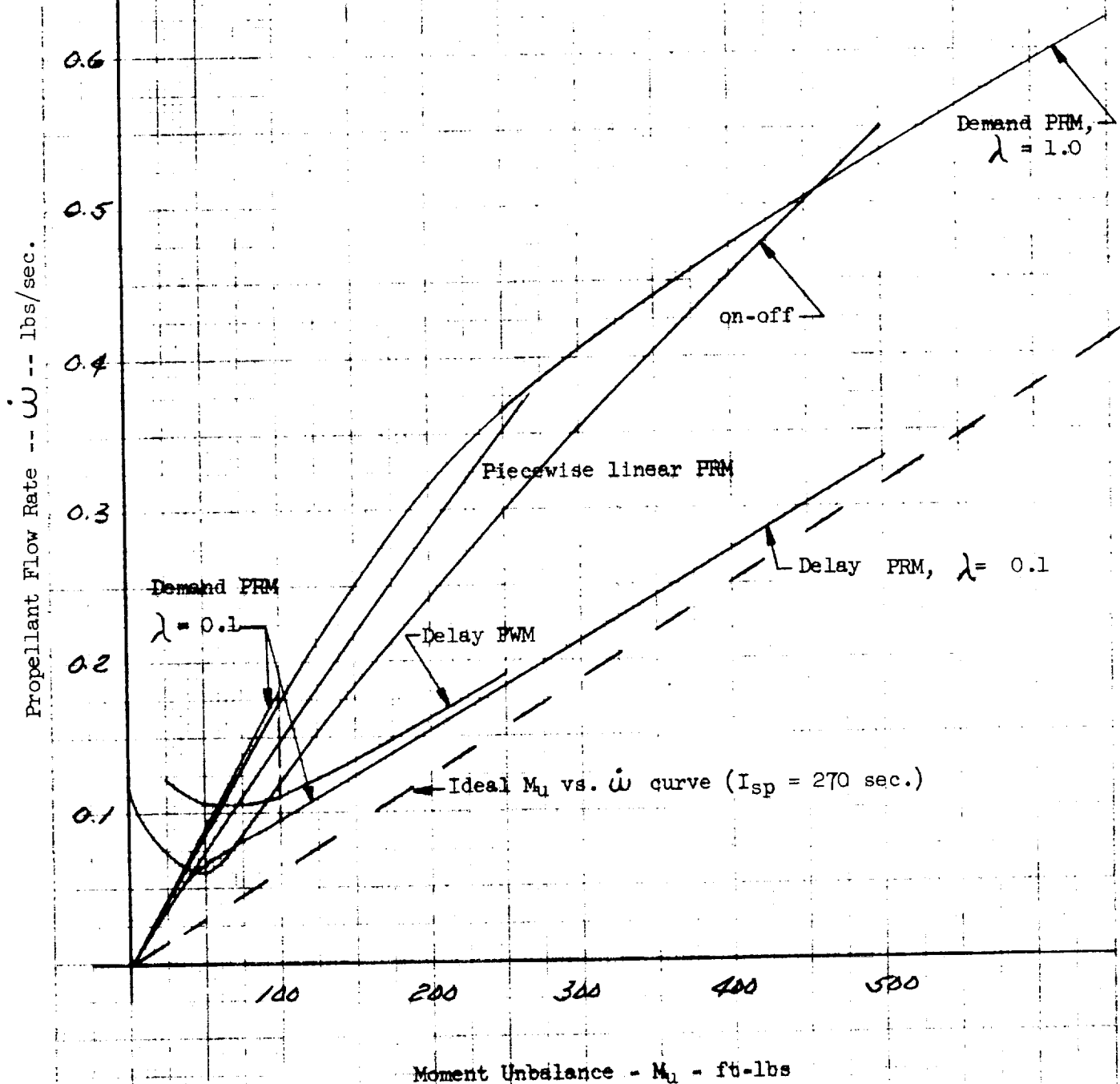
K&E  
KENTLETT & EPPER CO.  
10 X 10 1/2 INCH  
3201-11

~~CONFIDENTIAL~~

PAGE 81

Figure 3-41

See Table 3-2 for  
modulator parameters



~~CONFIDENTIAL~~

GRUMMAN AIRCRAFT ENGINEERING CORPORATION

REPORT NO. LED-500-3

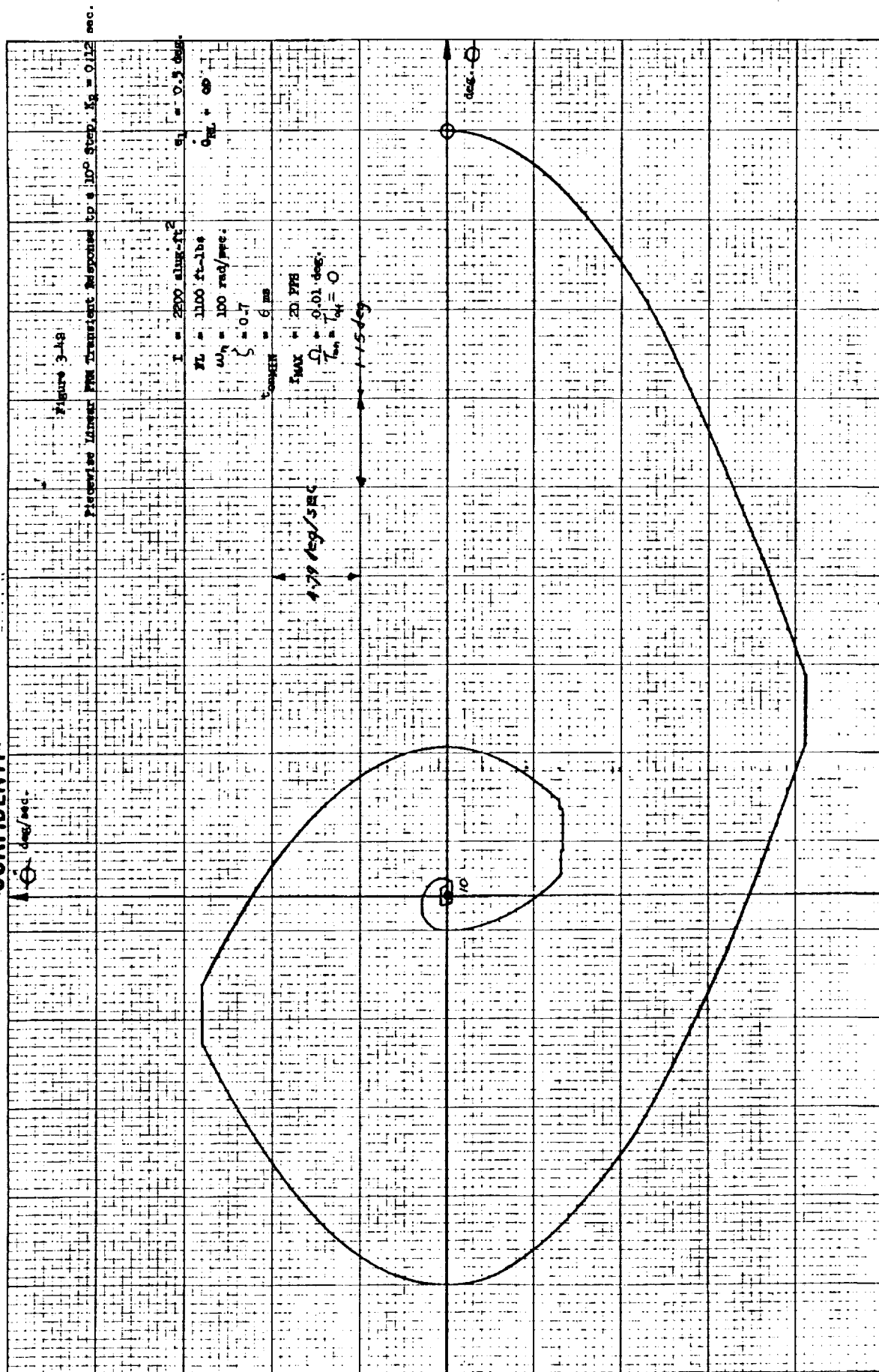
30 Sept. 1964

ENG 435  
9 62

QB 1099



CONFIDENTIAL



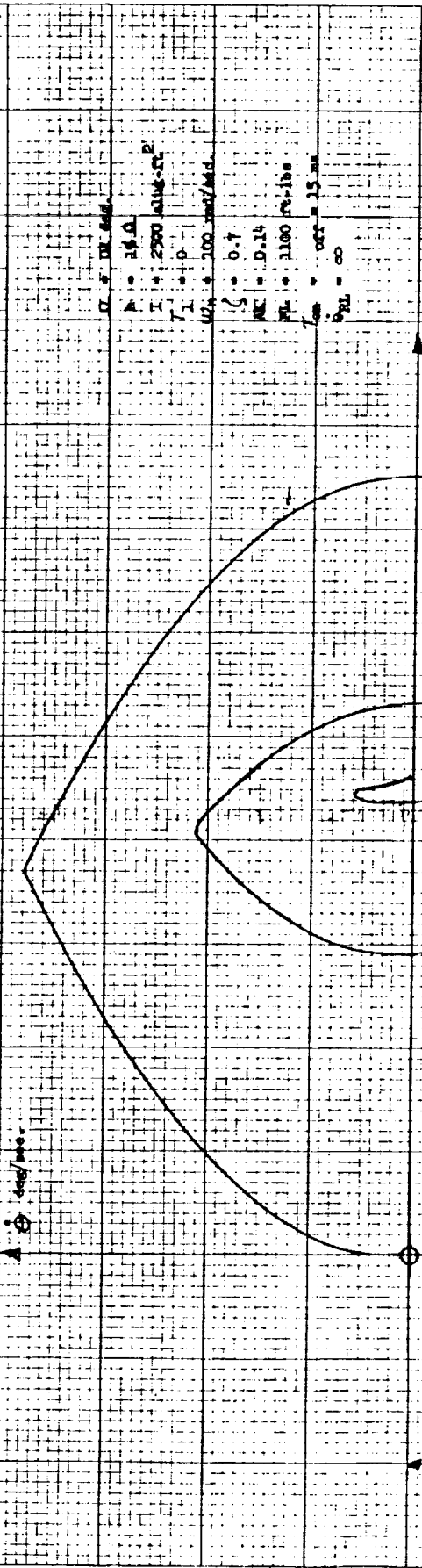
CONFIDENTIAL



**CONFIDENTIAL**

Figure 3-13

Induced Ramjet Oscillator Transient Response to a 17° Step,  $\eta = 0.05$  sec.



$\Delta \phi$  deg/sec

10 sec/sec

20 sec/sec

30 sec/sec

40 sec/sec

50 sec/sec

60 sec/sec

70 sec/sec

80 sec/sec

90 sec/sec

100 sec/sec

110 sec/sec

120 sec/sec

130 sec/sec

140 sec/sec

150 sec/sec

160 sec/sec

170 sec/sec

180 sec/sec

190 sec/sec

200 sec/sec





~~CONFIDENTIAL~~

$I = 2200 \text{ slug-ft}^2$   
 $PL = 1100 \text{ ft-lbs}$   
 $\omega_n = 125 \text{ rad/sec.}$   
 $t_{OPMIN} = 10 \text{ ms}$   
 $\zeta = 0.8$   
 $T_{OP} = 12 \text{ ms}$   
 $T_{VMIN} = 5 \text{ ms}$

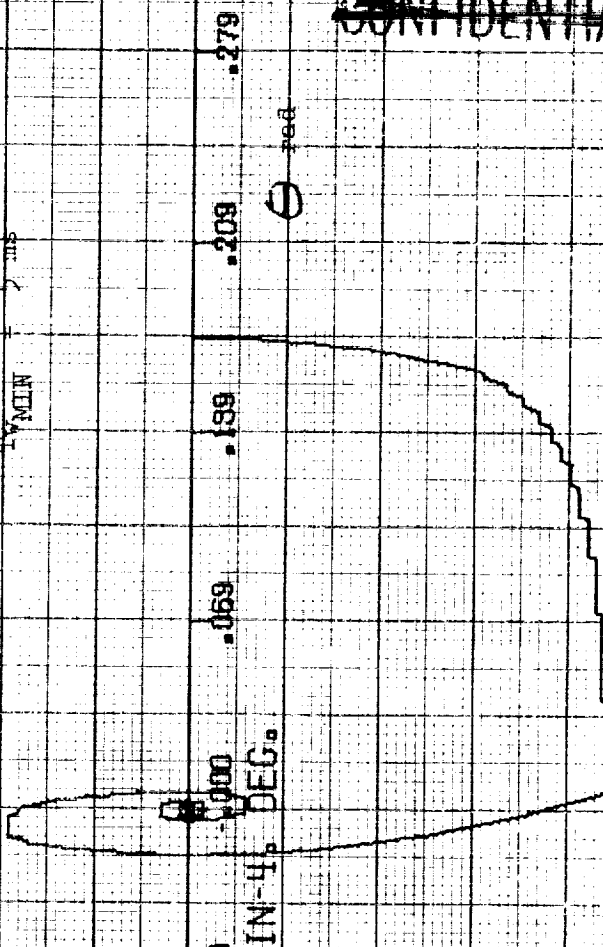


Figure 3.44 - PRM Transient Response to a 100 step,  
 $\lambda = 0.1, K_R = 0.1 \text{ sec.}$

Grumman Aircraft Engineering Corporation

LED-500-3  
30 Sept. 1964

~~CONFIDENTIAL~~

CONFIDENTIAL

$I = 2200 \text{ slug-ft}^2$   
 $FL = 1100 \text{ ft-lbs}$   
 $\omega_h = 125 \text{ rad/sec.}$   
 $\zeta = 0.8$   
 $t_{dMIN} = 10 \text{ ms}$   
 $T_{on} = 12 \text{ ms}$   
 $T_{dMIN} = 5 \text{ ms}$

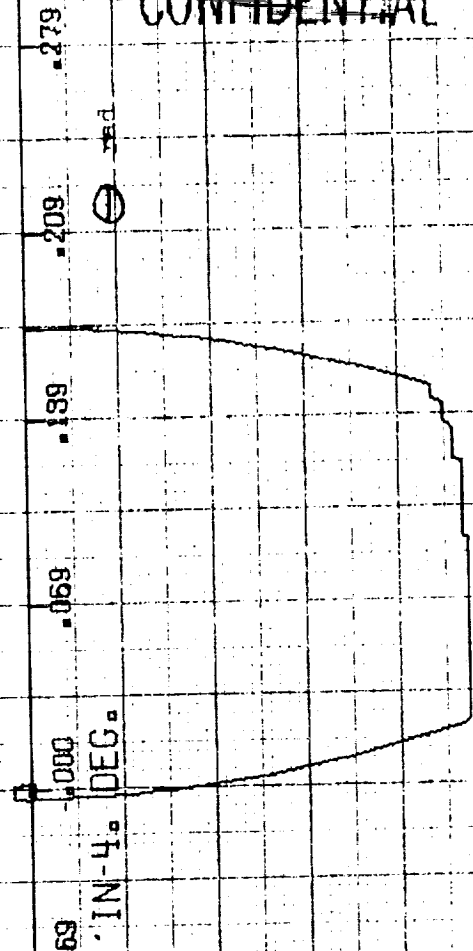
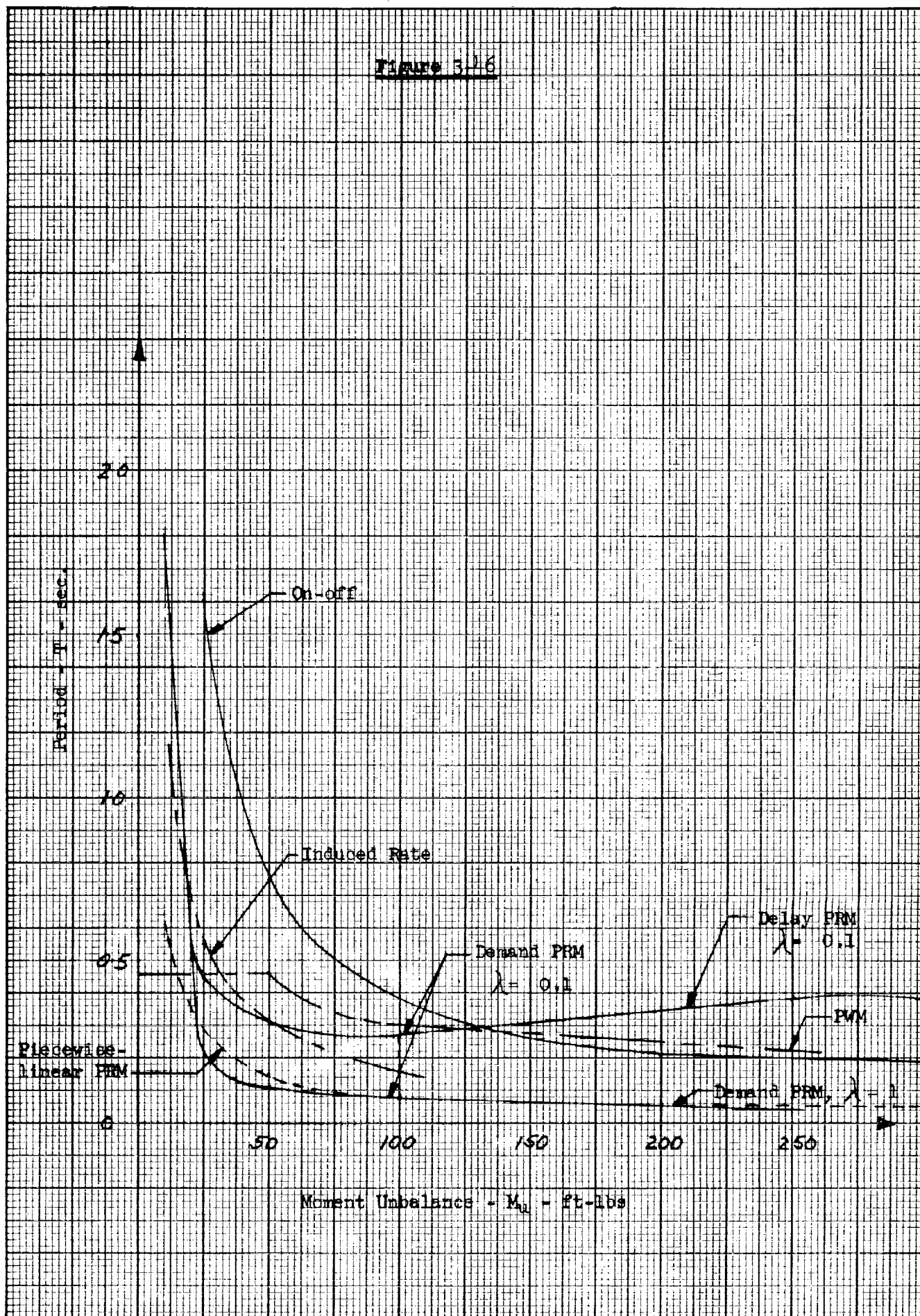


Figure 3-45 - FRM Transient Response to a 10° Step,  $\lambda = 0.1$ ,  $K_F = 0.2 \text{ sec.}$

FIGURE 3.16



~~CONFIDENTIAL~~

87

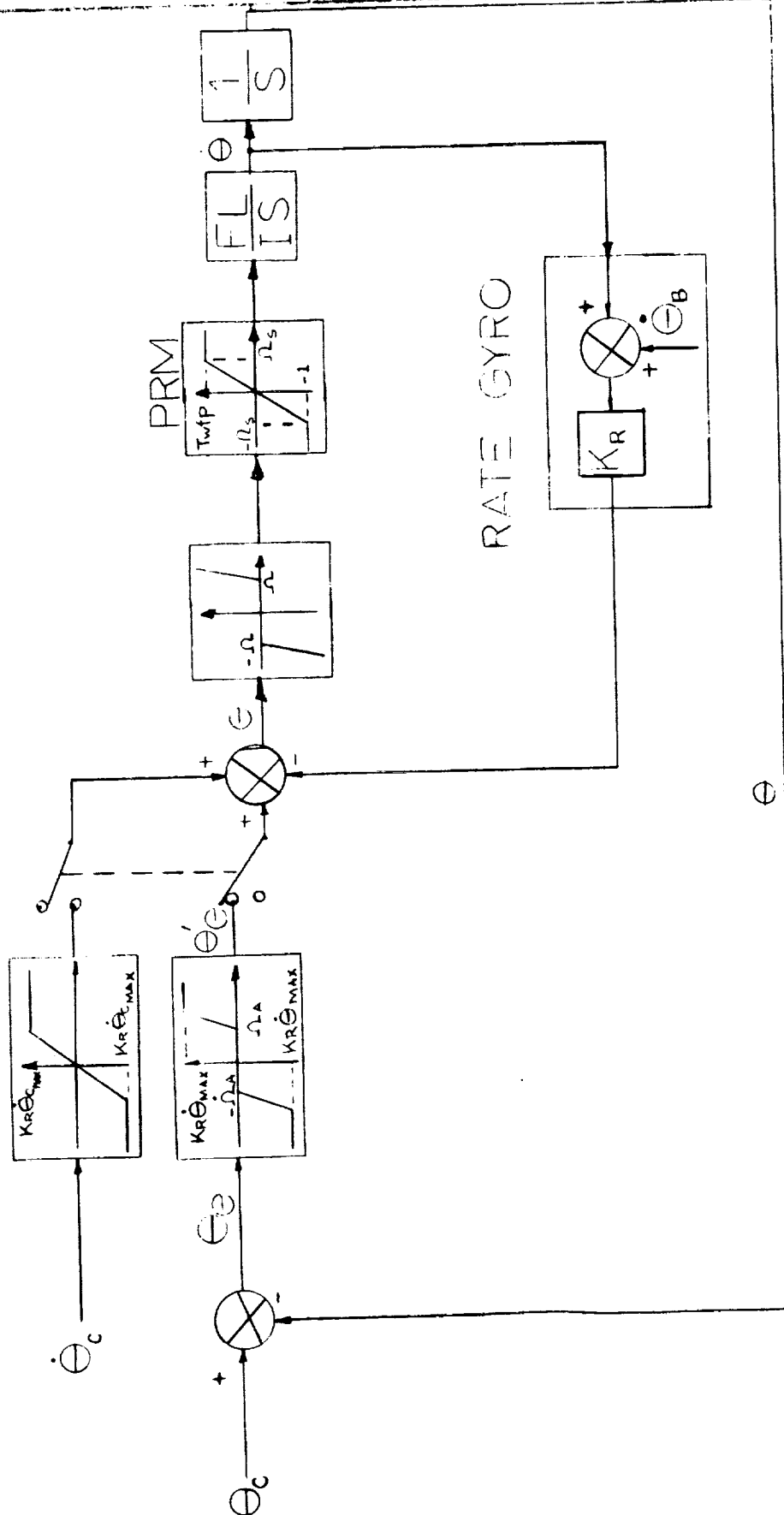


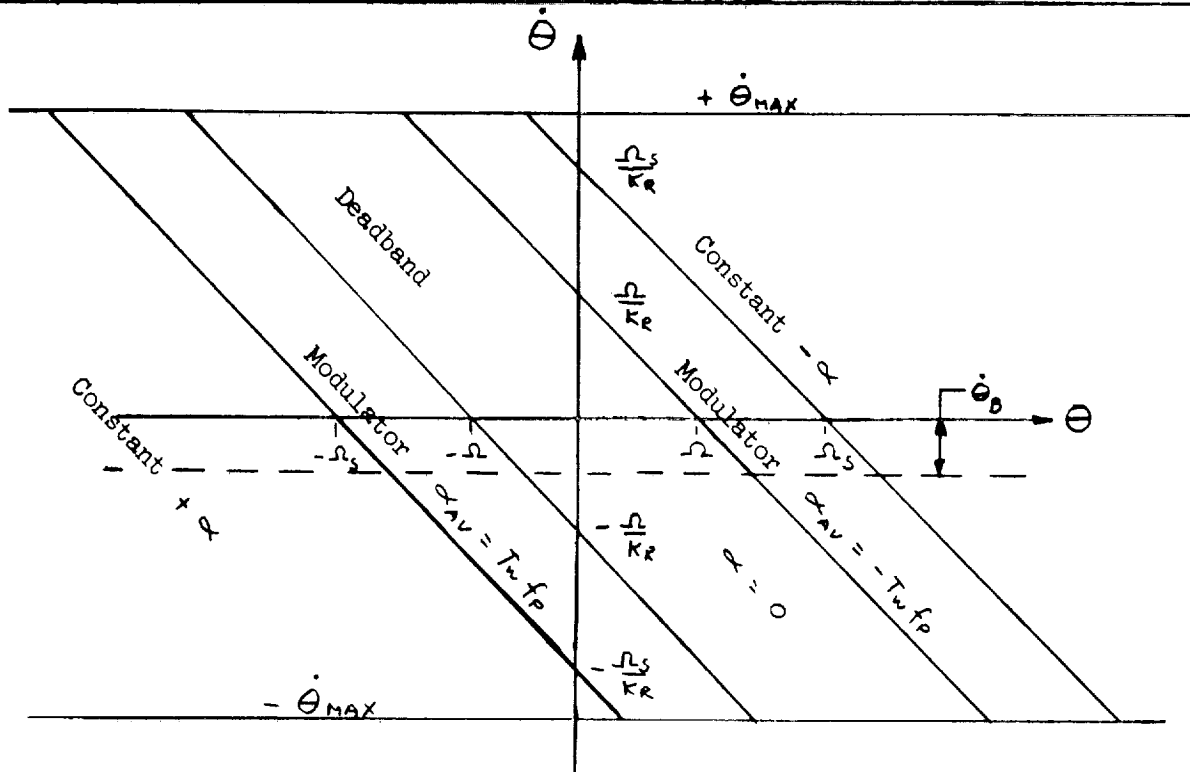
Figure 3-47 - Single axis configuration of LEM Attitude Control System.

~~CONFIDENTIAL~~

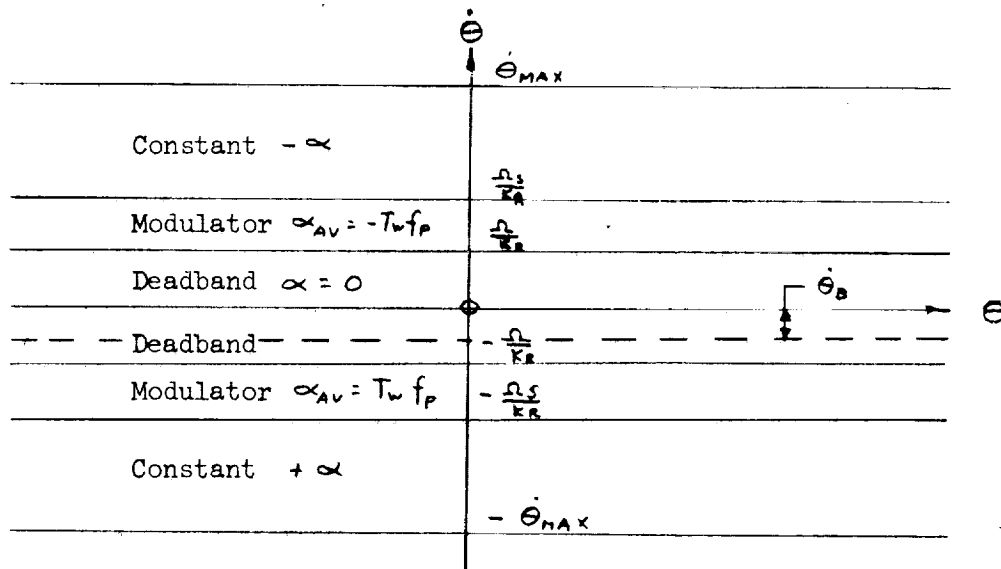
GRUMMAN AIRCRAFT ENGINEERING CORPORATION

REPORT: LED-500-3  
DATE: 30 Sept. 1964

QB 1037

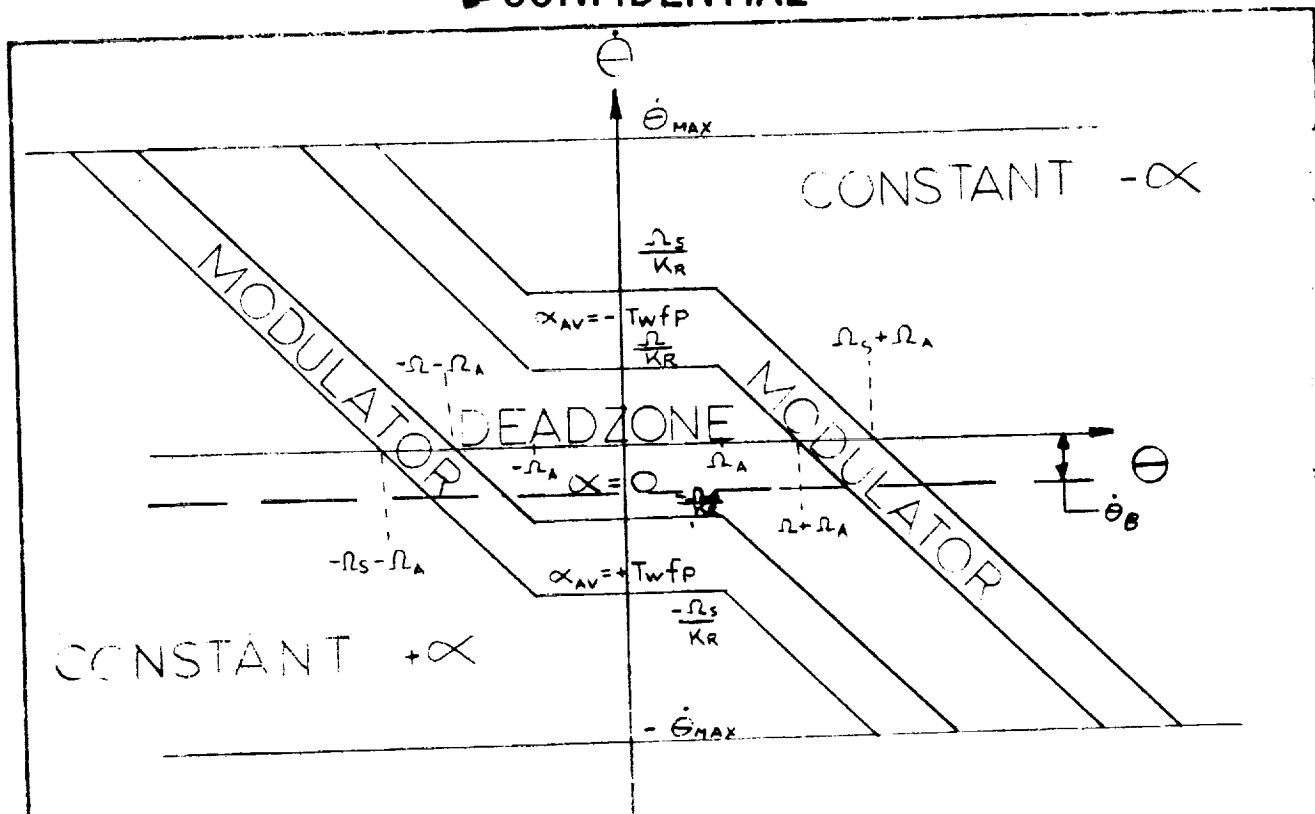


a) Attitude hold mode

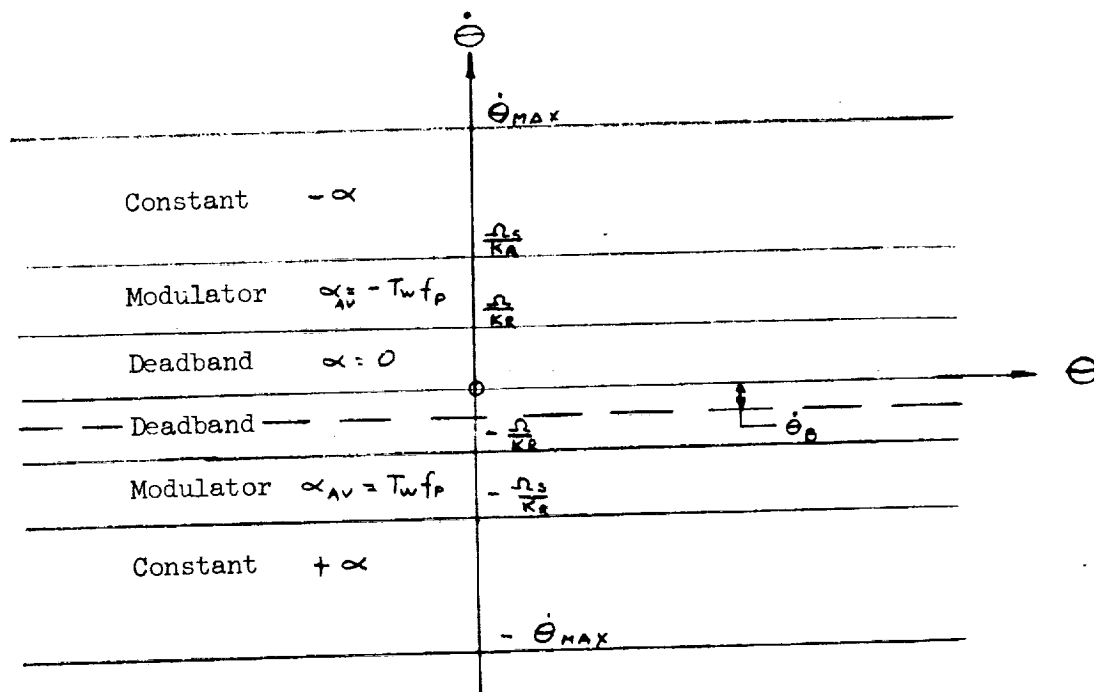


b) Rate command mode

Figure 3-48 - Phase Plane Boundaries With  $\Omega_a = 0$



a) Attitude hold mode



b) Rate command mode

Figure 3-49 - Phase Plane Boundaries With  $\Omega_a \neq 0$

~~CONFIDENTIAL~~

PAGE 90

SECTION 4

REACTION JET SELECT LOGIC

Code 26512 Eng-23A

~~CONFIDENTIAL~~

REPORT LED-500-3  
DATE 30 Sept. 1964

GRUMMAN AIRCRAFT ENGINEERING CORPORATION

~~CONFIDENTIAL~~

#### 4.1 - Introduction

Vehicle maneuver commands may consist of any combination for simultaneous translation and rotation. Theoretically it is possible that six commands, one for every rigid body degree of freedom could be generated at once. Thus, an acceptable jet-select logic should provide full control for any combination of rotation and translation commands. This "mode" of operation is called "normal"

However, when one or more jets are not available for control purposes because of failure(s), the normal mode of operation is no longer possible. The response to some combination of commands will be degraded in performance. Ideally, the jet logic for the LEM could be selected on the basis of providing the minimum of control degradation for multiple jet failures. In practice, other considerations (weight, reliability, etc.) predominate in the selection of the jet logic. However, a complete appreciation of the characteristics of any logic scheme cannot be achieved without an understanding of the control performance degradation it provides for multiple jet failures.

This section presents some basic concepts that were developed during the analysis and synthesis of different jet-select logic schemes.

#### 4.2 - Control Degradation Modes

The following defines four modes of control degradation that could occur from jet-off failures.

##### Mode I

The first mode is merely a degradation in the magnitude (or quantity) of the control capability, while retaining the ability to respond (or quality) to all combined commands in rotation and almost all in translation. This level of degradation does not require the disconnect of the LEM guidance automatic control.

##### Mode II

The second mode of degradation represents the inability to respond correctly to many combined commands while retaining the capability of sequential

Code 26512 Eng-23-1A

~~CONFIDENTIAL~~



single-axis rotation about all three axes, and sequential single-axis translation with attitude hold, along any two axes. In this mode the automatic control system mode cannot operate, but manual control may be accomplished.

#### Mode III

In the third degradation mode the vehicle is uncontrollable with translation commands, but the capability of sequential single-axis attitude control remains. In this mode the command module must perform the rendezvous and docking maneuvers.

#### Mode IV

This level of degradation would represent the loss of all attitude control capability. If the LEM rotation rate is excessive this mode could be catastrophic. Even if the rotation rate is not excessive, normal docking cannot occur. The astronauts must exit from the LEM into space and 'fly' to the command module.

#### 4.3 - Minimum Jet-Off Failures Resulting in Maximum Control Degradation

As defined in the previous section, a Mode IV control degradation can be catastrophic, and must be avoided at all cost. At maximum failure, when all jets are inoperative, a Mode IV degradation has occurred. However, the minimum failure that will cause a Mode IV degradation is of great significance. In fact, the minimum failures that cause each of the modes of degradation, assuming a "best" jet select logic scheme, must be appreciated for an adequate understanding of the capabilities and limitations of the reaction jet controls, and for an adequate evaluation of any jet logic scheme.

It simplifies the understanding of the minimum failure considerations to recognize that the reaction jets controlling the Q-R-X motions are logically uncoupled from those jets controlling the P-Y-Z motions. Thus, no jet aligned to thrust parallel to the X-axis can possibly correct a P-rotation error or provide Y or Z translation, and no jet aligned to thrust parallel to the Y or Z axes can possibly correct a Q or R rotation error or provide X translation.\* (Figure 4-1)

#### Mode IV

A brief study of the jet orientation diagram (Figure 4-1) will verify that only two jet-off failures need occur for complete loss of control (Mode IV). The failure of any two oppositely-oriented X-aligned jets in diagonal quads (i.e. any one of the following four pair: 1-10, 2-9, 5-14, 6-13) will cause a Mode IV degradation. This is actually not as bad as it appears at first glance.

---

\* Assuming the LEM c.g. to be at the center of the RCS thruster coordinate system, in Figure 4.1

~~CONFIDENTIAL~~

Taken one at a time, there are 120 combinations of jet pairs. Thus assuming a two-jet off failure, any two jets equally probable, the chance is only 1/30 that this pair would cause a Mode IV degradation.

### Mode III

When considering the minimum failures for a Mode III degradation it is simpler to first analyze the Q-R-X and P-Y-Z controls separately. For Q-R-X control, the ability to translate along the X axis, while maintaining attitude hold, is lost if any two similarly-oriented X-aligned jets in adjacent quads are failed off. For example, if jets 1-5 are failed off it will be impossible to translate in the X2 direction without losing attitude control. For P-Y-Z control, the ability to control translation along Y or Z is lost if any two similarly-oriented Y-or-Z-aligned jets in adjacent quads are inoperative. (For example, 4-8 for Y, or 3-15 for Z) Since manual rendezvous maneuvers are currently planned to be accomplished with two axes of translation control, a Mode III degradation would occur, for example, if at least any two of the following three jet pairs were rendered inoperative; (1-5, 3-15, 4-8).

### Mode II

If only the jet pair 1-5 were out, rendezvous could be accomplished manually by translating along Y and Z. If 3-15 were out, X and Y translation control could still be available. And if 4-8 were out, X and Z translation would still be possible. Thus, a Mode II degradation occurs whenever any two similarly-oriented X-or-Y-or-Z aligned jets in adjacent quads are inoperative. (It also occurs with four Y-Z jet failures where none are similarly aligned.)

### Mode I

The following failures of X-aligned jets can be tolerated with a little loss of Q-R-X control quality, although control quantity (or strength) will be compromised: any single jet failure, any two jets similarly-oriented in diagonal quads, any two jets oppositely-oriented in adjacent quads, and, any three or four jets that are similarly-oriented in diagonal quads and oppositely-oriented in adjacent quads (i.e. 1-6-9-14, or 2-5-10-13). It might be noted that the latter failure corresponds to the loss of an entire fuel system for Q-R-X control.

The following failures of Y-and Z-aligned jets can be tolerated: any single jet failure, any two jet failures where the jets are not similarly aligned in adjacent quads, and any three jet failures where none are similarly aligned in adjacent quads.

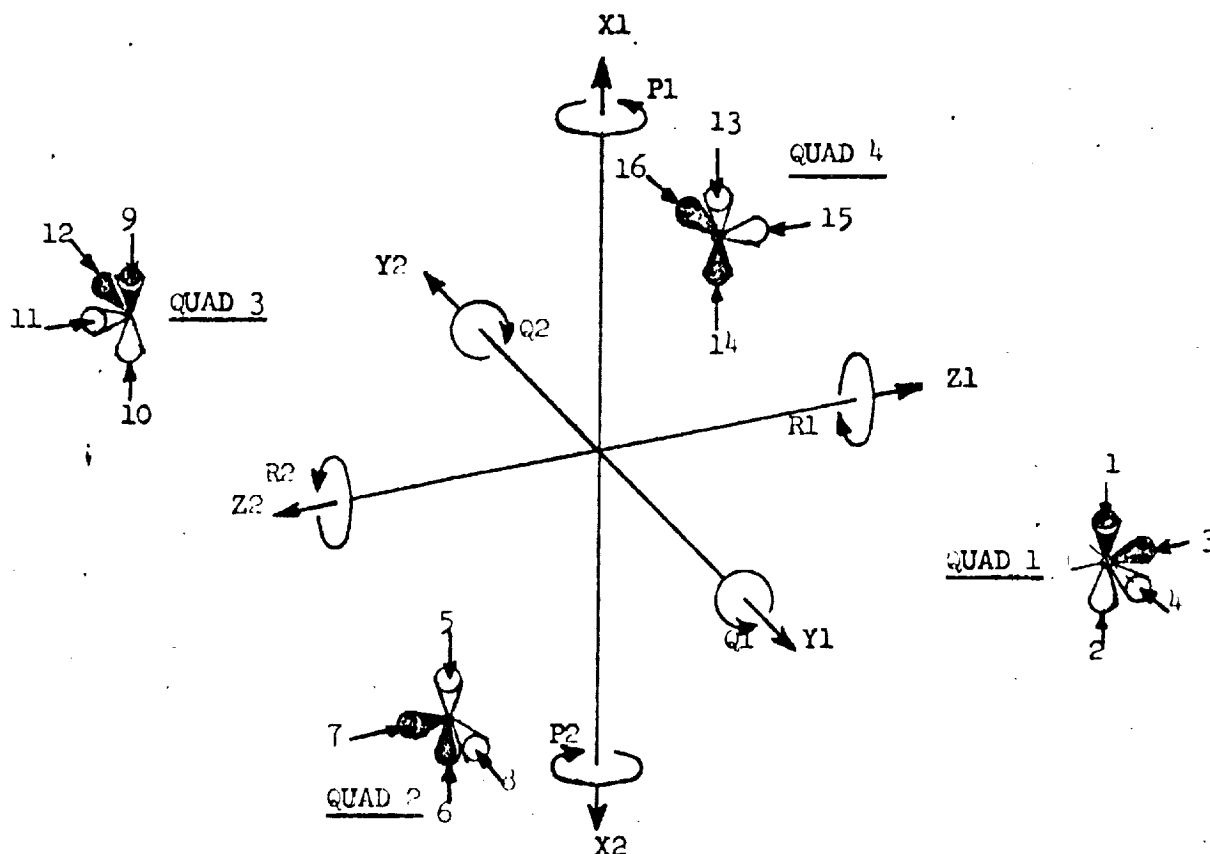
## 4.4 - Logic Mechanization Concepts

4.4.1 - Modulated Logic - The earliest LEM logic schemes developed at GAEC (sometimes referred to as "series" logic) employed modulated attitude error signal inputs, as illustrated in Figure 4-2a. The three proportional attitude error signals (P, Q, R) are independently modulated by three pulse-ratio

Code 26512

Eng-23-1A

~~CONFIDENTIAL~~



CODE:

Subscript 1: Positive Rotation or Translation

Subscript 2: Negative Rotation or Translation

△ FUEL SYSTEM "A"

▲ FUEL SYSTEM "B"

Figure 4-1

RCS JET THRUSTER CONFIGURATION

~~CONFIDENTIAL~~

modulators. Each of the modulated error signals then enters the logic. The on-off logic output then signals the jets. Since the logic receives pulse-train commands it must rapidly and frequently switch outputs from one jet combination to another. This logic mechanization has been employed for the GAEC Manned Abort Simulator (13) and the GAEC Manned Rendezvous Simulator. It has been proven that this scheme provides satisfactory attitude control.

To illustrate this system operation, consider an (R1, X1) command with full-on translation response. The full-on X1 command continuously signals the jet select logic. The R1 command, however, is modulated as a function of the proportional error signal. Thus, at some times an R1 command and an X1 command both signal the select logic and the logic selects the R1, X1 jets 10, 14. At the other times only the X1 command signals the select logic and the logic selects the X1 jets 2, 10, or 6, 14, or 2, 6, 10, 14.

4.4.2 Proportional Logic - By letting the logic accept the proportional attitude error signal inputs and putting the proportional output of the logic into the pulse-ratio modulators one achieves a "proportional" logic mechanization (also referred to as "parallel" logic) as illustrated in Figure 4-2b. Since this logic receives proportional signals, rather than pulse-trains, it ideally should perform a much lower order of magnitude of switching operations compared with the modulated scheme. However, where the modulated logic requires three pulse-radio modulators for the three attitude error signals, the proportional logic requires eight pulse-ratio modulators, one for each pair of opposing jets, and eight summing amplifiers.

As an illustration of the operation of the proportional logic scheme, consider again the (R1, X1) command with full-on X translation. The full-on X1 command will call for a set of jets with a full-on signal (for example, jets 2, 10). The proportional R1 command will call for another set of jets with an equal-to or less-than full-on signal (for example, jets 1, 14). Thus, jet 10 will be full-on, jet 14 will be modulated-on as a function of the proportional attitude error signal, and jet 2 will be modulated-on as a function of the summed (magnitude difference) opposite-signed signals, of saturation amplitude for jet 2 and proportional amplitude for jet 1.

One of the most readily apparent differences between the operating characteristics of the two logic schemes is the synchronous jet output of the modulated logic vs. the unsynchronous output of the proportional logic. Because the entire logic is modulated in the modulated scheme, the logic output to each of the selected jets is modulated the same way, and each of the selected jets fires in synchronism with the others. On the other hand, the proportional logic outputs are proportional inputs to separate modulators, one modulator to each selected jet. Since the modulators are unsynchronized, the jet firings are unsynchronized and the instantaneous pattern of jet firings appears somewhat random in nature.

Another difference is the apparent efficiency of the proportional logic for Q-R diagonal-axis moments. Because the modulated logic selects jet combinations

Code 26512 Eng-23-1A

~~CONFIDENTIAL~~

on a pulse-by-pulse basis, it (effectively) splits a diagonal moment unbalance into two orthogonal components along the Y-Z control axis, and then operates on these components (except for the relatively infrequent times when Q-R pulses occur simultaneously). The proportional logic scheme, however, will "attempt" to fire only those jets along the most efficient axis of moment application. There is a possibility, though, that the unsynchronous firings of the proportional logic will negate this efficient performance.

An extensive dynamic simulation would be required before a complete performance comparison between the two schemes could be made. However, either the proportional or the modulated logic schemes could meet the minimum control performance requirements. Therefore, the proportional logic scheme was selected for the ATCA design (2) on the basis of other considerations, such as circuit mechanization, redundancy requirements, and partial failure effects.

#### 4.5 - Three Types of Jet-Failure Cutoff

4.5.1 - Quad Cutoff - If a jet-on failure occurs, the failed jet must be rendered inoperative under penalty of a catastrophic mode of degradation. The Reaction Control System is designed to provide a shut-off of the flow of propellant to the failed jet. One way of doing this is to shut down the entire quad. This is undesirable for the following reason. Assuming two jet failures in two different quads where both quads must be shut down, the chance is  $1/3$  that the quads will be diagonal, thus causing a Mode IV degradation. Even if the two quads are adjacent, the Mode III degradation will occur.

However, it is unnecessary to disconnect an entire quad. The system is designed such that each quad has two pairs of jets, each pair associated with one of the two fuel systems. Thus, it is as easy to cut off a pair of jets as it is to cut off a quad. It may be firmly stated that quad jet-failure cutoff has only disadvantages when compared with pair jet cutoff. The only remaining problem then is to select the optimum jet-pairs in the quad to cut off.

4.5.2 - Logic-Coupled Jet-Pair Cutoff - If the jet pairs consist of both jets aligned along the X-axis or both jets aligned along the Y and Z axes, (i.e. the jet pairs 1,2; 3,4; 5,6; 7,8; ... etc.) then each of the two jets in the jet pair is associated with the same select logic (i.e. Q-R-X or P-Y-Z) and they might be thus referred to as being logic-coupled. This type of jet-pair cutoff has been employed in the GAEC abort simulation.

4.5.3 - Logic-Uncoupled Jet-Pair Cutoff - If the jet pairs consist of a jet aligned along the X-axis and a jet aligned along the Y or Z axis (i.e. the jet pairs 1,3; 2,4; 5,8; 6,7; ... etc.) then each of the two jets in the jet pair is associated with a different select logic (i.e., Q-R-X and P-Y-Z) and they must be thus referred to as being logic-uncoupled. This type of jet pair cutoff is employed in the ATCA (2) and RCS design.

4.5.4 - Logic-Coupled vs. Logic-Uncoupled - Since an optimum logic would provide only a Mode I degradation for a single jet-pair cutoff of either logic-coupled or logic-uncoupled type, a selection between the two systems

~~CONFIDENTIAL~~

must be made on the basis of multiple jet-pair failure considerations. This has been done in Table 4-1 which compares the logic-coupled and logic-uncoupled schemes on the basis of the probabilities of the occurrence of the various modes of control degradation, assuming the occurrence of two jet-pair off failures (with the possibility of any two jet-pair failure combinations assumed equally probable).

Considering the logic-coupled cutoff approach, there are six combinations of two jet-pairs in the P-Y-Z logic and another six combinations in the Q-R-X logic, for a total of 12 two jet-pair combinations. A Mode I degradation occurs if any two jet-pairs in the P-Y-Z logic in diagonal quads fails off. There are only two combinations of this failure (3-4, 11-12 or 7-8, 15-16) and thus the probability of a Mode I failure is  $2/13 = .167$ . A Mode II degradation occurs for failures of any two jet-pairs in adjacent quads in the P-Y-Z (3-4, 7-8, or 7-8, 11-12, or 11-12, 15-16 or 15-16, 3-4), or in the Q-R-X (1-2, 5-6 or 5-6, 9-10 or 9-10, 13-14 or 13-14, 1-2) logic. Since there are eight combinations of these failures, the probability of a Mode II degradation is  $8/12 = .666$ . A Mode IV degradation occurs for any two jet-pair failures in diagonal quads in the Q-R-X logic (1-2, 9-10 or 5-6, 13-14). Since there are only two combinations, the probability of a Mode IV degradation is  $2/13 = .167$ .

With similar arguments the probability of occurrence of the various modes of degradation can be derived for the logic-uncoupled jet-pair cutoff scheme, as presented in Table 4-1. Comparing the two jet-pair cutoff schemes, it can be seen that the probability of losing the capability of prime guidance automatic control is .833 for logic coupled pair cutoff and only .572 for the logic uncoupled system. In addition, the probability of total loss of control is .167 for the former and .143 for the latter. On the basis of these considerations, it is concluded that the logic-uncoupled scheme is superior to the logic-coupled scheme.

REPORT  
DATELED-500-2  
30 Sept. 1954~~CONFIDENTIAL~~

GRUMMAN AIRCRAFT ENGINEERING CORPORATION

~~CONFIDENTIAL~~

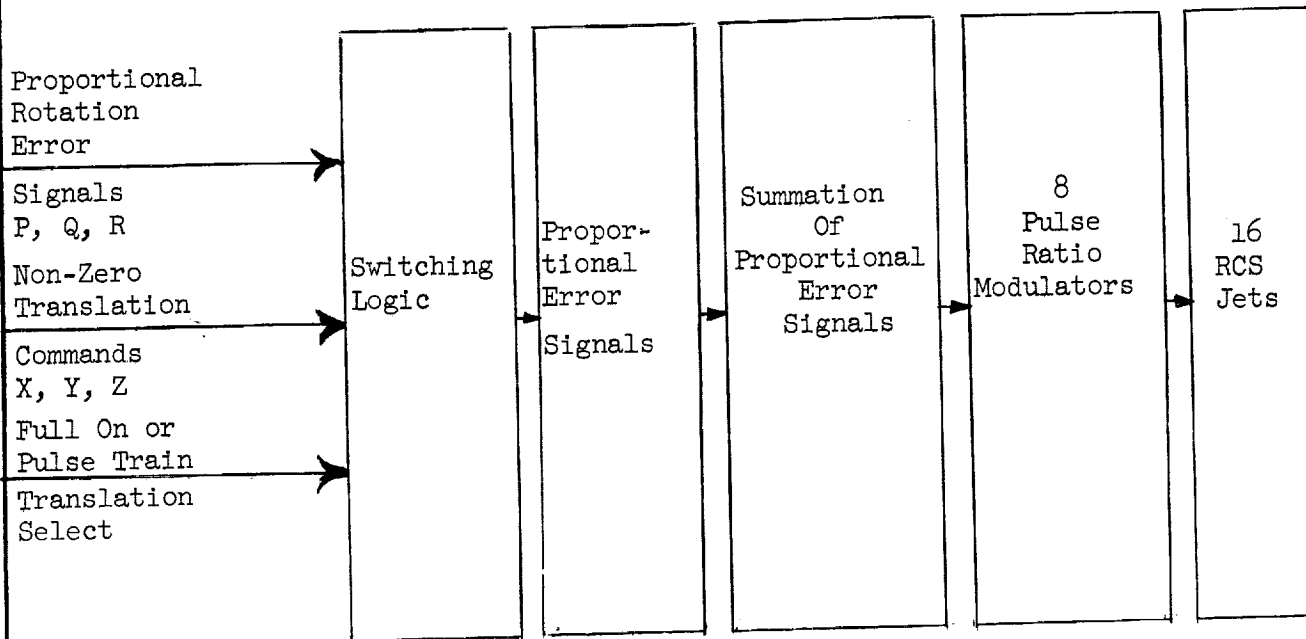
TABLE 4 - 1

A comparison between the logic coupled and logic uncoupled jet-pair cutoff schemes through an evaluation of the probability of magnitudes of control degradation for combinations of two jet-pair failures\*

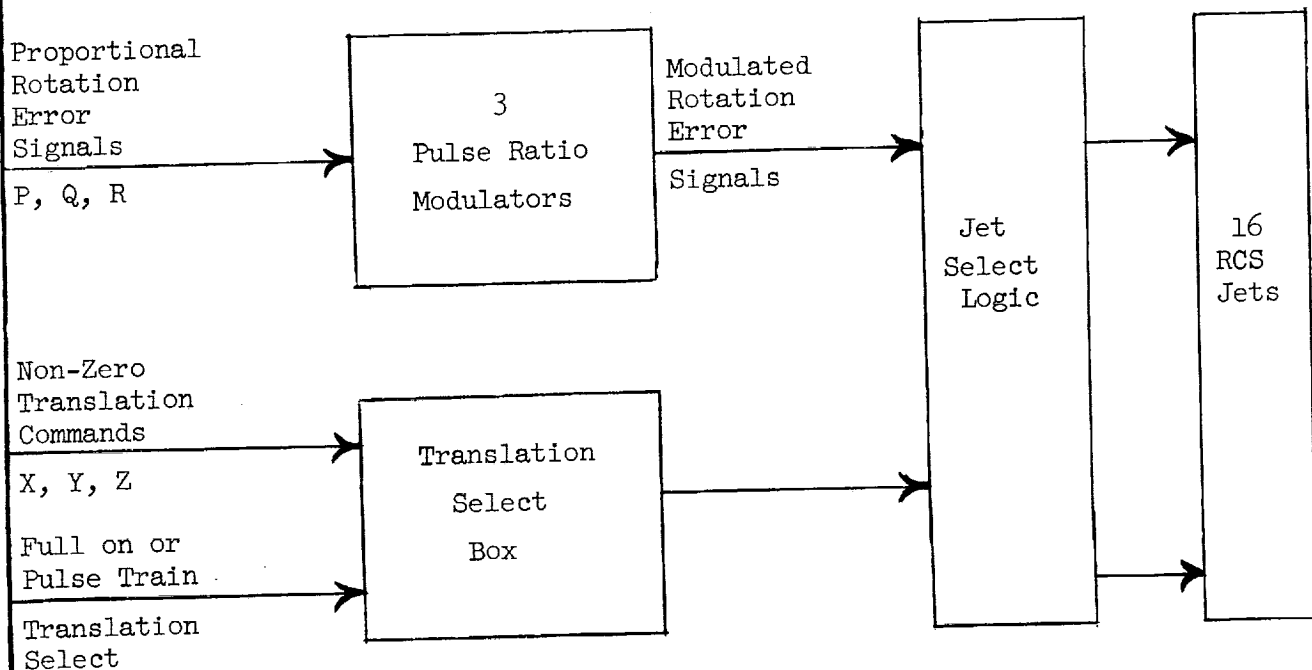
Pair Cutoff Scheme	Degradation ( ) = Number of Jet Pair Combinations				Degradation Probability			
	I	II	III	IV	I	II + III + IV $\frac{4 + 8 + 4}{28}$	II	IV
Logic Uncoupled Jet-Pair Cutoff	Single Quad, (4) A or B Jets; Adjacent Quads (4) Diagonal Quads (4) Total (12)	A or B Adj (4) A and B Adj (8) (12)	0	A and B Jets Diag. Quads (4)	$\frac{12}{28}$ .429	.572	$\frac{12}{28}$ .429	$\frac{4}{28}$ .143
Logic Coupled Jet Pair Cutoff	QRX			Diag. Quads (2)	$\frac{2}{12}$ .167	$\frac{4 + 4 + 2}{12}$ .833	$\frac{8}{12}$ .666	$\frac{2}{12}$ .167
	PYZ	Diagonal Quads (2)						

\* Any two jet-pair failure combinations have been assumed to the equally probable

~~CONFIDENTIAL~~

~~CONFIDENTIAL~~

(b) - Proportional or "parallel" logic  
(Presently in ATCA)



(a) Modulated or "series" logic  
(Employed during initial simulation studies)

Figure 4- 2

Logic Block Diagrams

~~CONFIDENTIAL~~

REPORT LED-500-3  
DATE 30 Sept. 1964



~~CONFIDENTIAL~~

SECTION 5

THRUST VECTOR CONTROL

~~CONFIDENTIAL~~

GRUMMAN AIRCRAFT ENGINEERING CORPORATION

REPORT LED-500-3  
DATE 30 Sept. 1964

~~CONFIDENTIAL~~

## SYMBOLS USED IN SECTION 5

<u>Symbol</u>	<u>Definition</u>	<u>Units</u>
A	perturbation amplitude	rad.
a	Schmitt trigger deadzone	rad.
D	Schmitt trigger deadzone	rad.
$D_1$	average RCS duty factor in ascent	
F	descent engine thrust	lbs.
$F_m$	ascent engine thrust	lbs.
$F_R$	RCS thrust	lbs.
f	frequency	pulses/sec
$g_o$	earth gravity	ft/sec <sup>2</sup>
$I, I_2$	total vehicle moment of inertia	slug-ft <sup>2</sup>
$\bar{I}_e$	gimballed engine moment of inertia	slug-ft <sup>2</sup>
$I_e$	gimballed engine moment of inertia about gimbal point	slug-ft <sup>2</sup>
$\bar{I}_L$	LEM body moment of inertia	slug-ft <sup>2</sup>
$K_M$	gimbal engine actuator gain	ft-lb/rad.
$K_R$	rate feedback gain	sec.
L	reaction jet moment arm	ft.
l	descent engine moment arm	ft.
$l_e, l_1$	geometric dimensions	ft.
$\bar{M}_e$	descent engine mass	slugs
$M_L$	total LEM mass	slugs
$\bar{M}_L$	LEM body mass	slugs
$M_o$	lunar liftoff mass	slugs
$M_1$	ascent burnout mass for zero moment unbalance	slugs
$M_2$	ascent burnout mass when unbalance exists	slugs
$\dot{m}_1$	ascent engine mass flow rate	slugs/sec
$\dot{m}_2$	RCS mass flow rate	slugs/sec
$P_{MAX}$	maximum power	watts
POD	pulse on demand	
R	inverse of rate gain	sec <sup>-1</sup>
$T_a$	gimbal actuator torque	ft-lb

~~CONFIDENTIAL~~

~~CONFIDENTIAL~~

## SYMBOLS USED IN SECTION 5 (CONT'D)

<u>Symbol</u>	<u>Definition</u>	<u>Units</u>
$T_{MAX}$	maximum control torque	ft-lb.
$T_{RJ}$	reaction jet torque	ft-lb.
$v$	gimbal actuator velocity constant	ft-lb-sec
$W_A$	actual weight of propellant saved	lbs.
$W_{RCS}$	propellant required to control moment unbalance	lbs.
$X, Y$	body coordinates	ft.
$X_e, Y_e$	descent engine coordinates	ft.
$\ddot{X}_L, \ddot{Y}_L$	body acceleration in X and Y directions	ft/sec <sup>2</sup>
$\ddot{X}_e, \ddot{Y}_e$	descent engine acceleration in $X_e$ and $Y_e$ directions	ft/sec <sup>2</sup>
$Y_{cg}$	cg offset in Y direction	ft.
$\Delta V$	required ascent velocity increment	ft/sec
$\alpha, \ddot{\psi}$	LEM angular acceleration	rad/sec <sup>2</sup>
$\ddot{\alpha}$	control gain	rad <sup>2</sup> /sec <sup>2</sup>
$\delta$	gimbal angle	rad.
$\delta_c$	gimbal angle command	rad.
$\dot{\delta}$	gimbal angle rate	rad/sec
$\ddot{\delta}$	gimbal angle acceleration	rad/sec <sup>2</sup>
$\zeta_R$	rate gyro damping ratio	
$\zeta_F$	filter damping ratio	
$\theta, \psi$	LEM attitude	rad.
$\theta_c$	attitude command	rad.
$\theta_E$	error signal	rad.
$\dot{\theta}_R$	error signal rate	rad/sec
$\lambda$	modulator nonlinearity factor	
$\Sigma F_X$	sum of forces in X direction	lbs.
$\Sigma F_Y$	sum of forces in Y direction	lbs.
$\Sigma T_\delta$	sum of torques applied to gimbal engine	ft-lbs.
$\Sigma T_\psi$	sum of torques applied to LEM body	ft-lbs.
$\tau$	gimbal actuator time constant	sec.

~~CONFIDENTIAL~~  
 GRUMMAN ENGINEERING CORPORATION

REPORT LED-500-3  
 DATE 30 Sept. 1964

~~CONFIDENTIAL~~

## SYMBOLS USED IN SECTION 5 (CONT'D)

<u>Symbol</u>	<u>Definition</u>	<u>Units</u>
$\psi, \theta$	LEM attitude	rad.
$\ddot{\psi}, \alpha$	LEM angular acceleration	rad/sec <sup>2</sup>
$\omega_D$	frequency below which trim system is unstable	rad/sec.
$\omega_F$	filter natural frequency	rad/sec.
$\omega_P$	frequency above which trim system is unstable	rad/sec.
$\omega_R$	rate gyro natural frequency	rad/sec.
$\omega_1$	stabilization network zero	rad.
$\omega_2$	stabilization network pole	rad.

5.1 - Introduction and Summary

Estimates made of the probable LEM center of gravity (cg) offset from the nominal thrust axis have indicated magnitudes on the order of two inches for both descent and ascent (29). At a descent thrust of 10,500 pounds and an ascent thrust of 3,500 pounds, this offset would induce a torque unbalance magnitude of about 1,700 ft-lbs during descent and 600 ft-lbs during ascent. The thrust vector control problem is to compensate for these potential torque unbalances while minimizing structural weight, propellant consumption, maximizing reliability, and providing adequate maneuver control.

Some of the techniques that were considered for controlling the thrust vector (torque unbalances) during powered descent phases of the LEM mission are:

- a- use of additional RCS jets
- b- fuel management
- c- gimballed engine LEM attitude control system
- d- gimballed engine trim system

Each of the above is considered in the following sections. While the techniques a-, b-, d- can only provide torque unbalance trim control, technique c- could, in addition, provide stable LEM attitude control and augment the RCS attitude control system. Techniques a- and b- are briefly considered in the following sections. The analysis of technique c- is presented in detail, and some practical disadvantages of its implementation are discussed and illustrated. The bulk of this chapter is devoted to the analysis and investigation of some different possibilities inherent in technique d-.

The results of these investigations have shown that technique d- has significant advantages with regard to weight, power, simplicity and crew safety. Detailed studies have indicated that the gimbal trim system has superior performance characteristics when it is mechanized as an open loop system with irreversible-drive constant-speed actuators and with phase lead stabilization. Therefore, the recommended trim control system, and the system employed in present control assembly specifications, is an open loop nonlinear stabilized gimballed engine trim system.

Since the torque unbalance magnitude predicted for powered ascent is well within the control capability of the RCS jets, the thrust vector control scheme chosen for powered ascent was the use of the existing RCS jets.

5.2 - Powered Descent Control with Additional RCS Jet Thrusters

The moment unbalance time history (30) indicates that normal disturbances during

~~CONFIDENTIAL~~

~~CONFIDENTIAL~~

powered descent will be on the order of 1500 ft-lbs, and a maximum of 2200 ft-lbs is possible.

In order to trim this magnitude of moment unbalance with RCS jets, eight additional jets of 100 lb. thrust at a lever arm distance of 5.5 ft. are required. The support structures and fuel and oxidizer lines from the main descent tanks are also needed.

From reference 30, 562 lb. of propellant would be required for c.g. trimming during powered descent. If a positive X-axis thrust logic (see section 5-7) is used, most of this propellant would provide trajectory impulse as well, and the only additional main tank propellant requirement would be 128 lb.

If the gimbal structure weight is the same as that of the additional jets and associated structure, this scheme would result in a net increase in weight of 128 lb. For this reason, no further effort was made in this area.

### 5.3 - Fuel Management Trim System

Another way of minimizing the thrust vector-to-c.g. offset is through moving the c.g. by drawing upon fuel (oxidizer) unequally from the pair of tanks, while the descent engine is firing. Thus, the c.g. of the fuel is shifted to compensate for the c.g. eccentricity of the LEM structure, thrust vector misalignment, etc. This is accomplished by putting the error signal (that would normally actuate the gimbal trim system) into a logic system that flips various valves on and off, shunting the main engine propellant flow from one tank to another.

If the fuel management trim system is assumed to be compensating for a large c.g. offset, then fuel would be drained from one tank to the exclusion of the other. The fuel drained from one side of the vehicle, would cause the c.g. to move away from that side and closer to the thrust vector. Thus the torque unbalance on the vehicle would be reduced almost linearly with time. Therefore, the simplified dynamic response of the fuel management trim system is essentially similar to that of gimballed engine trim system with constant speed actuators and irreversible drive (sec 5.5.2). A planar digital simulation with a simplified representation of fuel management trim has verified the trim control ability of this system.

Initial considerations of this system have indicated the following disadvantages

- a- The pressure transients in the descent engine propellant feed lines will cause the oxidizer-fuel ratio to deviate from the optimum (by an unestimated magnitude) thus causing increased propellant consumption.
- b- To insure reliability, a multiple redundancy of valves will be required. Preliminary estimates have indicated that the resulting weight, reliability, and power advantages will not be significantly greater than (but may be appreciably less than) the gimballed engine trim system (section 5.5).
- c- Development time might be excessive for this trim control system since an extensive investigation is necessary to accurately determine the dynamic stability criteria of this system.

Code 26512 Eng-23A

~~CONFIDENTIAL~~

REPORT LED-500-3  
DATE 30 Sept. 1964

~~CONFIDENTIAL~~

d- Near the end of the descent phase the fuel in one tank can be zero while the fuel in the opposite tank is needed to trim out the system. As this last portion of fuel is employed the system will become increasingly out-of-trim. At best this would only waste RCS fuel. At worst it could cause a torque unbalance that saturates the RCS jets, thus causing unstable attitude control.

e- The unbalance correction rate capability of the fuel management trim system is about half of what has been estimated as being desirable in any trim system.

Because of these disadvantages, it has been concluded that fuel management may provide at best, a very small advantage with respect to a gimballed engine trim system, but that more conclusive studies would possibly prove it to be very much worse.

#### 5.4 - The Gimballed Engine LEM Attitude Control System Analysis

Figure 5-1 represents the analytical model of the LEM with a gimballed engine acting as a LEM attitude control system (with proportional linear servo actuators). Force and torque equilibrium equations developed from this model are presented in Table 5-1 (Equations 5-1 through 5-4). These equations, plus the gimballed engine actuator servo-motor equation (Equation 5-5), form the "LEM Dynamics" relationships that define the forward loop response of the control system.

The feedback diagram of Figure 5-2 illustrates the system dynamics that were incorporated in an analog computer investigation. Function switches in the diagram emphasize some of the variations tested: attitude control, rate control, gimballed engine control, reaction jet control, coupled engine-jet control, etc.

To facilitate the execution of a control system synthesis, the analytical problem was executed in two overlapping phases. In the first phase the linearized gimballed engine control system parameters were thoroughly investigated. In this phase, the gimballed engine system was considered as the sole control, except during the very last portion of the phase where it was briefly investigated in concurrent operation with a linearized representation of a pulse-modulated reaction jet control system.

In the second phase, the system equations were mechanized on analog computers and the non-linear system performance was optimized. Among many other characteristics, it was found that the high power requirements of the gimballed engine control system actuators could be substantially reduced if lead-lag stabilization networks were inserted within the attitude feedback loop. In addition, it was demonstrated that the transient LEM response to attitude commands was highly satisfactory, with the gimballed engine control system acting alone or acting in conjunction with the RCS.

Because of reliability, power requirements, and weight considerations, the fast-response gimballed engine control system was discarded in favor of the slow response gimballed engine trim system soon after the analog studies were completed (31). Thus a detailed explanation of the computer studies will not be presented in this report. However, the linearized Gimballed Engine Control

TABLE 5-1

GIMBALED ENGINE FORCE EQUILIBRIUM EQUATIONS

$$\Sigma F_X = 0 : (\bar{M}_L + \bar{M}_e) \ddot{X}_L + \bar{M}_e Y_{CG} \ddot{\psi} = F$$

$$\Sigma F_Y = 0 : (\bar{M}_L + \bar{M}_e) \ddot{Y}_L - \bar{M}_e (\ell_L + \ell_e) \ddot{\psi} + \bar{M}_e \ell_e \ddot{\delta} + F \delta = 0$$

$$\Sigma T_{\psi} = 0 : \bar{M}_e Y_{CG} \ddot{X}_L - \bar{M}_e \ell_L \ddot{Y}_L + \left\{ \bar{I}_L + \bar{M}_e [\ell_L (\ell_L + \ell_e) + Y_{CG}^2] \right\} \ddot{\psi} - \bar{M}_e \ell_e \ell_L \ddot{\delta} - F \ell_L \delta = T_a + Y_{CG} F + T_{RJ}$$

$$\Sigma T_{\delta} = 0 : \bar{M}_e \ell_e \ddot{Y}_L - [\bar{I}_e + \bar{M}_e \ell_e (\ell_L + \ell_e)] \ddot{\psi} + [\bar{I}_e + \bar{M}_e \ell_e^2] \ddot{\delta} + \bar{M}_e \ell_e (\ddot{X}_L + Y_{CG} \ddot{\psi}) \delta = T_a$$

where :

$$\begin{aligned} \ddot{X}_e &= \ddot{X}_L + Y_{CG} \ddot{\psi} \\ \ddot{Y}_e &= \ddot{Y}_L - (\ell_L + \ell_e) \ddot{\psi} + \ell_e \ddot{\delta} \end{aligned}$$

let :  $\bar{M}_L + \bar{M}_e = M_L, \quad M_e \ell_e = M_{ee}, \quad M_e (\ell_L + \ell_e) = M_{eL}$

$$\bar{I}_L + \bar{I}_e + \bar{M}_e (\ell_L + \ell_e)^2 = I_L, \quad \bar{I}_e + M_e \ell_e (\ell_L + \ell_e) = I_{eL}$$

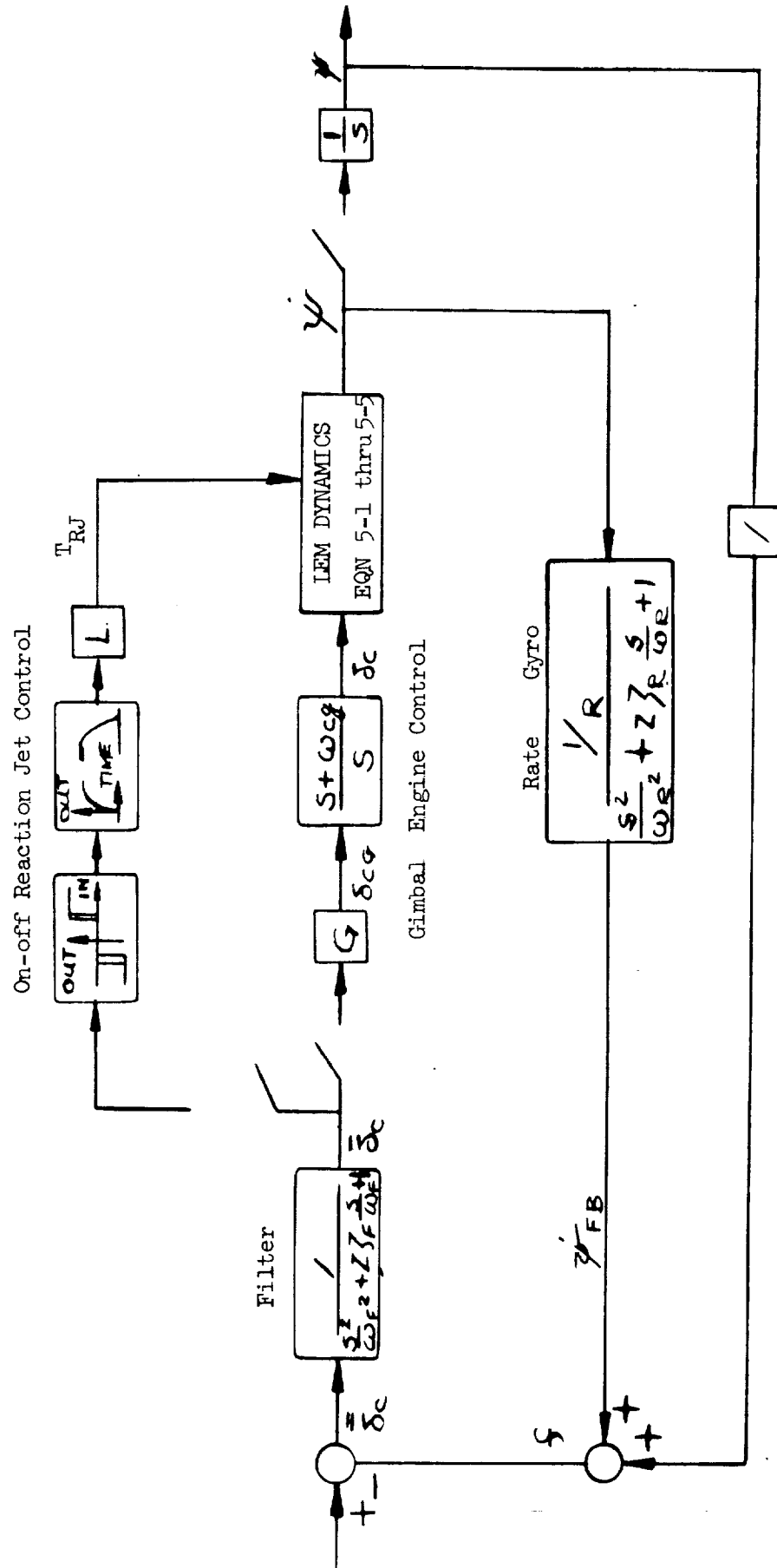
$$\bar{I}_e + \bar{M}_e \ell_e^2 = I_e$$

$+M_L \ddot{X}_L$	0	$+\bar{M}_e Y_{CG} \ddot{\psi}$	0	=	F	(1)
0	$+M_L \ddot{Y}_L$	$-M_{eL} \ddot{\psi}$	$+M_{ee} \ddot{\delta} + F \delta$	=	0	(2)
$+\bar{M}_e Y_{CG} \ddot{X}_L$	$-\bar{M}_e \ell_L \ddot{Y}_L$	$(\bar{I}_L - I_{eL} + \bar{M}_e Y_{CG}^2) \ddot{\psi}$	$-(M_{ee} \ell_L \ddot{\delta} + F \ell_L \delta)$	=	$T_a + Y_{CG} F + T_{RJ}$	(3)
0	$+M_{ee} \ddot{Y}_L$	$-I_{eL} \ddot{\psi}$	$+I_e \ddot{\delta} + M_{ee} (\ddot{X}_L + Y_{CG} \ddot{\psi}) \delta$	=	$T_a$	(4)
GIMBALED ENGINE ACTUATOR EQUATION:			$K_M (\delta_C - \delta) - v \dot{\delta}$	=	$T_a$	(5)





FIGURE 5-2 DESCENT CONTROL SYSTEM FEEDBACK DIAGRAM



~~CONFIDENTIAL~~

analysis is presented in the following pages. This analysis defined the basic system stability criteria, which was later verified by computer studies.

5.4.1- Derivation of the Linear Open Loop Transfer Function (Engine Control Only)--In performing the linearized analysis, equations 5-1 through 5-5 are operated upon in the following sequence:  $Y_{cg}$  and  $T_{PJ}$  are set equal to zero. The solution of  $X$  from equation 5-1 is inserted into equation 5-4 to form equation 5-4A. Equation 5-4A is subtracted from equation 5-3 to form equation 5-3A. Equation 5-5 is subtracted from equation 5-4A to form equation 5-4B. Thus, written in operator and matrix notations, one obtains:

$$\begin{bmatrix} M_L S^2 & -M_{eL} S^2 & M_{ee} S^2 + F \\ -M_{eL} S^2 & I_L S^2 & -I_{eL} S^2 + F \ell_L (1 + \epsilon) \\ M_{ee} S^2 & -I_{eL} S^2 & I_e S^2 + vS + F \ell_L \left( \frac{K_M}{F \ell_L} + \epsilon \right) \end{bmatrix} \begin{bmatrix} Y_L \\ \psi \\ \delta \end{bmatrix} = \begin{bmatrix} 0 \\ 0 \\ K_M \delta_C \end{bmatrix} \quad (5-2)$$

where:  $\frac{\ell_e M_e}{\ell_L M_L} = \epsilon$

Now, let

$$\begin{bmatrix} a_{11} a_{12} a_{13} \\ a_{21} a_{22} a_{23} \\ a_{31} a_{32} a_{33} \end{bmatrix} \begin{bmatrix} Y_L \\ \psi \\ \delta \end{bmatrix} = \begin{bmatrix} 0 \\ 0 \\ K_M \delta_C \end{bmatrix} \quad \text{And let } \Delta = \begin{vmatrix} a_{11} a_{12} a_{13} \\ a_{21} a_{22} a_{23} \\ a_{31} a_{32} a_{33} \end{vmatrix} = S^4 (B_2 S^2 + B_1 S + B_0)$$

The fundamental forward loop transfer function of the linearized gimballed engine control system can now be represented as:

$$\frac{\psi}{\delta_C} = \frac{-K_M \begin{vmatrix} a_{11} a_{12} \\ a_{21} a_{22} \end{vmatrix}}{\Delta} = \frac{K_M (A_2 S^2 + A_0)}{S^2 (B_2 S^2 + B_1 S + B_0)}$$

~~CONFIDENTIAL~~

While this transfer function is in straight-forward polynomial form, the coefficients of the polynomials are complicated functions of the system parameters. In an attempt to simplify these coefficients, they were expanded in terms of the system parameters. Numerical values were substituted for fixed parameters (masses, inertias, etc.) and the variable parameters (thrust, masses, inertias, etc.) were evaluated at extreme values.

Two operational conditions were analyzed to bracket the extremes of operational range: orbit insertion at minimum thrust and touchdown at maximum thrust. An inspection of the numerical contributions of the various parameters to the magnitude of the coefficients led to the conclusion that the transfer function could be represented as,

$$\frac{\psi}{\delta C} = \frac{K_M (M_L I_{eL} S^2 + M_L F \ell_L)}{S^2 \left\{ I_e M_L I_L S^2 + v M_L I_L S + M_L I_L \left( K_M - F \ell_L \frac{I_{eL}}{I_L} \right) \right\}} \quad (5-6)$$

where the coefficients are numerically accurate within about five percent.

Making the following substitutions,

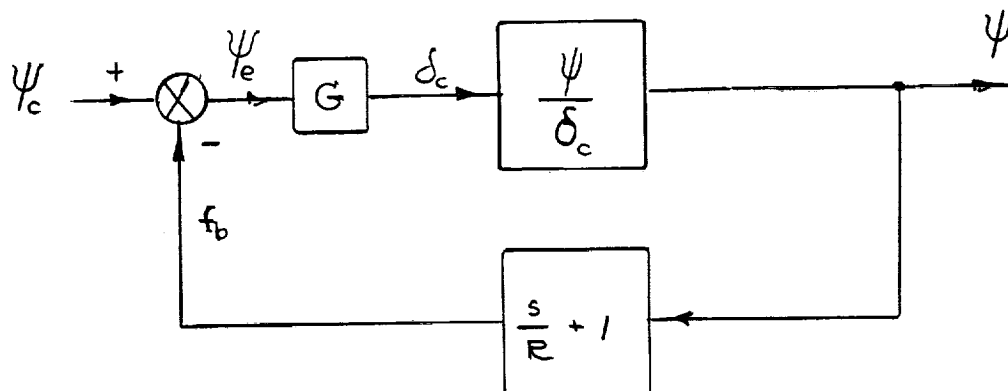
$$\alpha = \frac{F \ell_L}{I_L}, \quad \omega_o^2 = \frac{F \ell_L}{I_{eL}}, \quad \beta = \left( 1 - \alpha \frac{I_{eL}}{K_M} \right), \quad \bar{K}_M = K_M \beta \quad (5-7)$$

$$\omega_L \omega_H = \frac{\bar{K}_M}{I_e}, \quad \omega_L = \frac{\bar{K}_M}{v}, \quad \therefore \omega_H = \frac{v}{I_e}$$

one obtains the final form of the linearized gimballed engine control system transfer function:

$$\frac{\psi}{\delta C} = \frac{\alpha \left( \frac{S^2}{\omega_o^2} + 1 \right)}{S^2 \left( \frac{S^2}{\omega_L \omega_H} + \frac{S}{\omega_L} + 1 \right)} \quad (5-8)$$

When the forward loop transfer function, Equation 5-8, is substituted into a simplified feedback diagram as shown below:



The following open-loop transfer function is obtained:

$$\frac{f_b}{\psi_e} = G \frac{\alpha}{s^2} \frac{\left( \frac{s^2}{\omega_o^2} + 1 \right) \left( \frac{s}{R} + 1 \right)}{\left( \frac{s^2}{\omega_L \omega_H} + \frac{s}{\omega_L} + 1 \right)}$$

If it is assumed that  $\omega_L \ll \omega_H^*$  then the open loop transfer function may be written as:

\* The inequality constraints presented in the succeeding pages will indicate the feasibility of this assumption.

~~CONFIDENTIAL~~

$$\frac{f_b}{\psi_e} = G \frac{\alpha \left| \frac{S^2}{\omega_o^2} + 1 \right| \left| \frac{S}{R} + 1 \right|}{\beta S^2 \left| \frac{S}{\omega_L} + 1 \right| \left| \frac{S}{\omega_H} + 1 \right|} \quad (5-9)$$

The root locus of this transfer function is sketched in Figure 5-3. It can be seen that this system will be stable for all gains if the following inequalities are satisfied:

$$R \ll \omega_{o\text{MIN}} , \quad R \ll \omega_L , \quad \omega_{o\text{MAX}} \leq \omega_H$$

#### 5.4.2 - Derivation of the Transfer Function Parameter Constraints

In the derivation of equation 5-8 from 5-6, a parameter  $\beta$  was introduced, which actually is the constant in the quadratic polynomial denominator of equation 5-8. This constant may be negative or positive. Since equation 5-8 will soon be shown to incorporate the major dynamic characteristics of the open loop gimballed engine control system transfer function, a negative  $\beta$  will provide a pole in the right half plane of the open loop transfer function. Thus for stability purposes  $\beta$  should be positive. Moreover, it will be seen that stability of the control loop is enhanced by maintaining sufficiently large values of the quadratic denominator singularities, and therefore, keeping  $\beta$  as large as possible. Because of these constraints, it may reasonably be specified that

$$\beta \cong 1, \text{ or } \alpha \frac{I_{eL}}{K_M} \ll 1, \text{ or } K_M \gg \alpha I_{eL}$$

Note that the transfer function gain ( $\alpha$ ) and the (tail-wags-dog) LEM zeros ( $\omega_o$ ) are functions of numerically pre-determined system parameters.

The parameters  $\alpha$  and  $\omega_o$  are determined by the structure and operating characteristics of the LEM. Control system optimization must evolve around these parameters. The following defines the variation extremes of these parameters:

Orbit Insertion, Minimum Thrust:

$$\alpha = \frac{Fl}{I} = \frac{1000 \text{ (lbs)} \cdot 2 \text{ (ft)}}{20,000 \text{ (lb-ft-sec}^2\text{)}} = 0.1 \left( \frac{\text{rad.}}{\text{sec.}^2} \right) \quad (5-10A)$$

$$\omega_o = \sqrt{\frac{Fl}{I_{eL}}} = \sqrt{\frac{1,000 \text{ (lbs)} \cdot 2 \text{ (ft)}}{40 \text{ (lb-ft-sec}^2\text{)}}} = 7.1 \left( \frac{\text{rad.}}{\text{sec.}} \right)$$

Touchdown, Maximum Thrust:

$$\alpha = \frac{Fl}{I} = \frac{10,000 \text{ (lbs)} \cdot 5 \text{ (ft)}}{10,000 \text{ (lb-ft-sec}^2\text{)}} = 5.0 \left( \frac{\text{rad.}}{\text{sec.}^2} \right)$$

~~CONFIDENTIAL~~

$$\omega_o = \sqrt{\frac{Fl}{I_{eL}}} = \sqrt{\frac{10,000 \text{ (lbs)} \cdot 5 \text{ (ft)}}{40 \text{ (lb-ft-sec}^2)}} = 35 \left(\frac{\text{rad.}}{\text{sec.}}\right) \quad (5-10B)$$

Thus, if  $I_{eL} = 40 \text{ (lb-ft-sec}^2)$  and  $\alpha_{\max} = 5.0 \text{ (rad/sec}^2)$

$$\text{then, for stability, } K_M \gg \alpha I_{eL} = 200 \left(\frac{\text{ft-lb}}{\text{rad.}}\right) \quad (5-10C)$$

Since

$$\omega_{b_{\max}} = 35 \frac{\text{rad.}}{\text{sec.}}, \quad \omega_{o_{\min}} = 7.1 \left(\frac{\text{rad.}}{\text{sec.}}\right)$$

$$\therefore R \ll \omega_{o_{\min}} = 7.1 \text{ (rad/sec)}$$

$$\omega_L \gg R \ll 7.1 \text{ (rad/sec)}$$

We may assume that

$$1.0 \geq R \geq 0.5$$

$\therefore$  we can state that, roughly,

$$\frac{K_M}{V} = \omega_L \geq 5.0 \left(\frac{\text{rad.}}{\text{sec.}}\right) \quad (5-11)$$

$$\text{Also we know that } \frac{v}{I_e} = \omega_H \geq \omega_{o_{\max}} = 35 \left(\frac{\text{rad.}}{\text{sec.}}\right) \quad (5-12)$$

Therefore, the open loop transfer function may be written as

$$\frac{\alpha G \left(\frac{S^2}{\omega_o^2} + 1\right) \left(\frac{S}{0.5} + 1\right)}{S^2 \left(\frac{S}{5.0} + 1\right) \left(\frac{S}{35} + 1\right)} \quad (5-13)$$

and the root locus may be plotted, as shown in Figure 5-4. Also from Figure 5-4, this system is stable for all operating gains ( $\alpha$ ) within the range defined by equations 5-10A and B when the electrical gain ( $G$ ) is about 1.0. However, the assumed break frequencies of equation 5-13 might require performance characteristics (specifically, magnitudes of power, response rise time, and maximum rate of motion) that are highly unacceptable. In fact, the results of computer studies (31) have indicated that reasonable performance characteristics result in a system that requires special circuitry to maintain stability over all operating gains and compensate for the destabilizing effects of system nonlinearities.

~~CONFIDENTIAL~~5.4.3 - Gimballed Engine Actuator Performance Constraints

At this point the actuator response requirements will be related to the previously-derived system stability requirements. From equation 5-12, for  $I_e = 40$  (lb-ft-sec<sup>2</sup>),

$$V \geq 1400 \text{ (lb-ft-sec)} \quad (5-14A)$$

Applying the above inequality to equation 5-11,

$$K_M \geq 7200 \left( \frac{\text{ft-lb}}{\text{rad.}} \right) \quad (5-14B)$$

Equation 5-14B, being the more stringent, would pre-empt equation 5-10C as the performance requirement.

To develop the actuator response requirements, we will consider the "open loop" actuator characteristic. Rewriting the actuator equation,

$$K_M (\delta_c - \delta) - v \dot{\delta} = T_a$$

Because of the relative magnitude of LEM inertia to gimballed engine inertia,

$$T_a \cong -I_e \ddot{\delta}$$

$$K_M (\delta_c - \delta) - v \dot{\delta} = -I_e \ddot{\delta}$$

$$\text{or} \quad I_e \ddot{\delta} + v \dot{\delta} + K_M \delta = K_M \delta_c$$

Or, in operator notation:

$$\left( \frac{I_e}{K_M} s^2 + \frac{v}{K_M} s + 1 \right) \delta = \delta_c$$

Thus, the "closed loop" actuator characteristic is

$$\frac{\delta}{\delta_c} = \frac{1}{\frac{I_e}{K_M} s^2 + \frac{v}{K_M} s + 1}$$

and the "open loop" is

$$\frac{\delta}{\delta_e} = \frac{K_M/v}{s \left( \frac{I_e}{v} s + 1 \right)}$$

(where  $\delta_e = \delta_c - \delta$ )

$$\text{or} \quad \frac{\dot{\delta}}{\delta_e} = \frac{K_M/v}{\left( \frac{I_e}{v} s + 1 \right)}$$

~~CONFIDENTIAL~~

However, the linear open loop gain of the actuator,  $K_M/v = G_a$ , has been numerically defined by equation 5-11, and the linear open loop rise time constant (rise time to a steady state velocity),  $I_e/v = \tau_a$ , has been defined by equation 5-12. In order to minimize the actuator power consumption and performance requirements, it is necessary to minimize the actuator gain and maximize the actuator time constant. Thus for minimum actuator power and maximum control stability, (within the constraints of the previously defined stability inequalities) the actuator open loop (linear) transfer function may be written as

$$\frac{\dot{\delta}}{\delta_e} = \frac{5.0}{\left(\frac{s}{35} + 1\right)} \quad (5-15)$$

The non-linear actuator characteristics are represented by a saturation velocity,  $|\dot{\delta}|_{\max}$ , and a saturation torque,  $|T_a|_{\max}$ . From equation 5-15, the steady-state saturation velocity may be written as

$$|\dot{\delta}|_{\max} = 5.0 |\delta_e|_{\max}$$

The non-linear saturation characteristics of the gimballed engine control system cannot be completely determined from the linear stability-requirement inequalities. Thus, the level of error signal input at which the actuator response will saturate will be defined as  $\delta_{\text{ELIN}}$  where

$$\delta_{\text{ELIN}} = .7 |\delta_e|_{\max} \quad (5-16)$$

We will assume that a minimum linear range of control must be defined with respect to the  $\pm 6^\circ$  nominal gimbaling range. The results of analog computer studies have indicated the desirability of a linear range magnitude of a few degrees. The following linear range will be assigned:

$$\begin{aligned} \delta_{\text{ELIN}} &= 3.0^\circ \\ |\delta_e|_{\max} &= 4.29^\circ \\ |\dot{\delta}|_{\max} &= 21.5^\circ/\text{sec.} = 0.375 \text{ (rad/sec)} \end{aligned}$$

Moreover, applying equation 5-16 to equation 5-5 at  $\dot{\delta} = 0$

$$T_a = |T_a|_{\max} = K_M |\delta_e|_{\max} = \frac{K_M}{.7} \delta_{\text{ELIN}} \quad (5-6)$$

Applying equation 5-12A to equation 5-6:

$$|T_a|_{\max} \geq \frac{7200}{.7} \left(\frac{\text{ft-lb}}{\text{rad}}\right) \times 3.0^\circ \times \frac{\pi \text{ rad.}}{180^\circ} = 540 \text{ (ft-lb)}$$



~~CONFIDENTIAL~~

Since the actuator power requirements can be expressed as:

$$\begin{aligned} P(t) &= T(t) \left( \frac{\text{ft-lb}}{\text{rad}} \right) \times \dot{\delta} \left( \frac{\text{rad.}}{\text{sec.}} \right) \\ &= T(t) \dot{\delta}(t) \left( \frac{\text{ft-lb}}{\text{sec.}} \right) \end{aligned}$$

$$\text{and, } T(t) = T_{\max} \left( 1 - \frac{\dot{\delta}(t)}{\dot{\delta}_{\max}} \right)$$

$$\therefore P_{\max} = \frac{1}{4} T_{\max} \dot{\delta}_{\max}$$

Assuming a thrust-pivot misalignment of  $\frac{1}{4}$ "

$$T_{\text{TPM}} = \frac{1}{4} (\text{in.}) \cdot 10,500 (\text{lb}) \cdot \frac{1 (\text{ft})}{12 (\text{in})} = 220 (\text{ft-lb})$$

Assuming a c.g.-pivot eccentricity of 3 inches, engine weight of 400 lbs, LEM acceleration of 1 g.

$$T_g = 400 (\text{lbs}) \cdot 3 (\text{in}) \cdot 1(\text{g}) \cdot \frac{1 (\text{ft})}{12 (\text{in})} = 100 (\text{ft-lb})$$

Assuming miscellaneous restraints such that  $T_{\text{misc}} = 100 \text{ ft. lb.}$

$$\begin{aligned} \text{then } T_{\max} &= T_{\max} + T_{\text{TPM}} + T_g + T_{\text{misc}} \\ \text{total} &= 540 + 220 + 100 + 100 = 960 \text{ ft-lb} \end{aligned}$$

$$P_{\max} \geq \frac{1}{4} \times 960 (\text{ft-lb}) \times .375 (\text{rad/sec})$$

$$\geq 90.0 \left( \frac{\text{ft-lb}}{\text{sec}} \right)$$

or  $P_{\max} \geq 122$  watts per actuator (assuming perfectly efficient actuators)

#### 5.4.4 - Stability Criteria Summary

The linearized system open loop transfer function is:

~~CONFIDENTIAL~~

$$\frac{y_e}{f_b} = G \frac{\alpha}{\beta s^2} \frac{\left(\frac{s^2}{\omega_o^2} + 1\right) \left(\frac{s}{R} + 1\right)}{\left(\frac{s}{\omega_L} + 1\right) \left(\frac{s}{\omega_H} + 1\right)}$$

where:

$$\alpha = \frac{F l}{I_L}, \quad \beta = \left(1 - \alpha \frac{I_{eL}}{K_M}\right)$$

$$\omega_o = \sqrt{\frac{F l}{I_{eL}}}, \quad \omega_L = \frac{K_M}{v}, \quad \omega_H = \frac{v}{I_e}; \quad \omega_H \gg \omega_L$$

and  $0.1 \leq \alpha \leq 5.0$  (rad/sec<sup>2</sup>)

$7.1 \leq \omega_o \leq 35.0$  (rad/sec)

For stability  $K_M \gg 200 \left(\frac{\text{ft-lb}}{\text{rad}}\right)$  or,  $B \cong 1$

$$R \ll \omega_{o\min} = 7.1 \text{ (rad/sec)}$$

$$\omega_L \gg R \text{ (rad/sec)}$$

$$\omega_H \gg \omega_{o\max} = 35 \text{ (rad/sec)}$$

Assuming:  $1.0 \geq R \geq 0.5$  (rad/sec)

$$\therefore \omega_L \geq 5.0 \text{ (rad/sec)}$$

$$v \geq 1400 \text{ (lb-ft-sec)}$$

Assuming:

$$\beta \cong 1.0, \quad \therefore K_M \geq v_{\min} \omega_{L\min} = 7200 \left(\frac{\text{ft-lb}}{\text{rad.}}\right)^*$$

$$\omega_H = 1/\gamma$$

$$\gamma \leq 1/35 \text{ (sec)}$$

Assuming:  $\delta_{e\text{Lin}} \cong 3.0(^{\circ})$

\* Being more stringent, the second inequality of  $K_M$  controls.

~~CONFIDENTIAL~~

then  $T_{\max} \geq 540 \text{ (ft-lb)}$

$$\dot{\delta}_{\max} \geq 21.5^\circ/\text{sec.}$$

For a thrust-pivot misalignment of  $\frac{1}{4}$ ", an engine c.g.-pivot eccentricity of 3 inches, etc.

$$P_{\max} \geq 122 \text{ watts output per actuator}$$

#### 5.4.5 - Evaluation of Actuator Response Requirements

It should be recognized that the actuator performance constraints for system stability must be satisfied while complying with LEM weight and power allotment constraints. A dynamic torque capability of 540 ft-lb will more than double the torque requirements with respect to static considerations, which is not desirable. A response time constant of 1/35 second, in all directions and for extreme static unbalance conditions, may be difficult to provide. Output power requirements, of over 120 watts per actuator, are very high.

These requirements may be relaxed to a great extent, but only by compromising control system stability. It is conceivable, however, that by restricting the attitude control system performance requirements, a lower performance gimbal servo system might be successfully employed (31).

#### 5.4.6 - Simplified Gimballed Engine Control System Transfer Function Derivation

The final result of the linear analysis stability criteria was the development of a feasible forward loop transfer function for the gimballed engine LEM attitude control system. This function was developed from an inclusive free-body diagram planar representation which provided a five-parameter matrix of differential equations. This matrix was subsequently simplified to a three-parameter matrix for linear analysis purposes. (Section 5.4.1) The linear analysis resulted in a complete gimbal-control-inertia transfer function for the entire gimballed engine LEM attitude control system forward loop. A numerical evaluation of parameter magnitudes then led to the conclusion that the transfer function could be represented by a limited number of significant parameters. A stability criteria investigation indicated further constraints on the parameters, enabling further simplifications.

However, because of the lengthy (but rigorous) analytical path employed to reach the final transfer function, an appreciation of the physical origin of some of the basic dynamic characteristics has been sacrificed. To rectify this situation, the open loop transfer function will be re-derived in a much simpler manner by making all the simplifying assumptions initially (using the results of the rigorous development as justification).

To analyze the stable gimballed engine trim system as an attitude hold device within the RCS deadzone, we can neglect the RCS. Thus, the assumed attitude hold system is as illustrated in Figure 5-5. Assuming the gimballed engine mass and inertia characteristics to be much less than the rest of the LEM, then the actuator torque can be expressed as:

~~CONFIDENTIAL~~

$$T = I_e \ddot{\delta} = K_M (\delta_C - \delta) - v \dot{\delta}$$

Where the actuator open loop transfer function is

$$\frac{\delta}{\delta_C - \delta} = \frac{K_M}{S(I_e S + v)}$$

and the closed loop actuator transfer function is

$$\frac{\delta}{\delta_C} = \frac{1}{\frac{I_e}{K_M} S^2 + \frac{v}{K_M} S + 1}$$

$$\text{Let } \omega_L = \frac{K_A}{v}, \omega_L \omega_H = \frac{K_A}{I_e} \quad \therefore \omega_H = \frac{v}{I_e}$$

Assuming  $\omega_H \gg \omega_L$

$$\therefore \frac{\delta}{\delta_C} = \frac{1}{\left(\frac{S}{\omega_H} + 1\right)\left(\frac{S}{\omega_L} + 1\right)}$$

From the simplified body dynamics illustration, Figure 5-6, assuming the gimballed engine inertia is not negligible, the following torque equilibrium equation can be written:

$$I_L \ddot{\psi} = F \ell \delta + T$$

but,  $T \cong I_e \ddot{\delta}$

$$\therefore I_L \ddot{\psi} = F \ell \delta + I_e \ddot{\delta}$$

Code 26512 Eng-23A

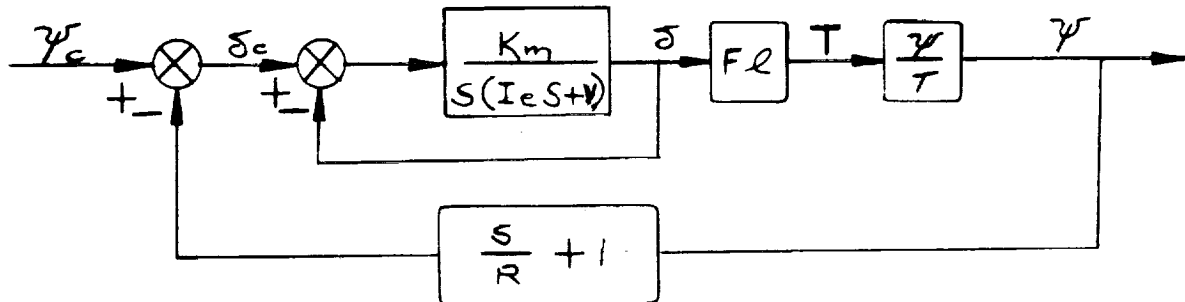


Figure 5-5A Gimballled engine attitude control loop

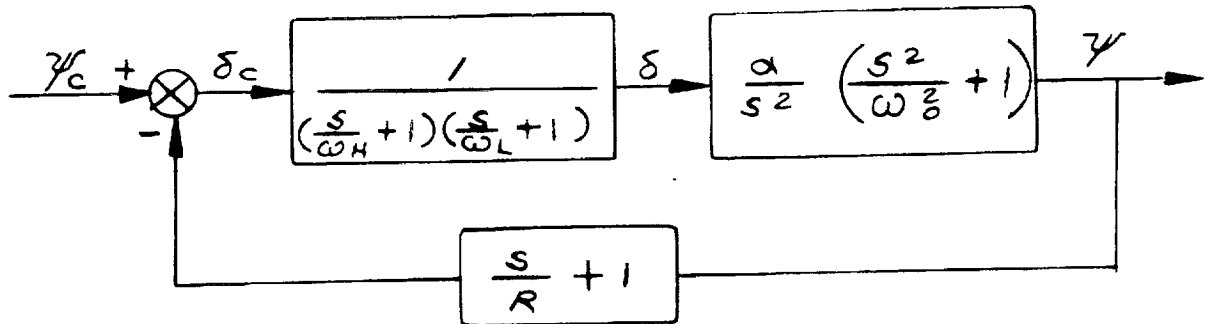


Figure 5-5B Gimballled engine attitude control loop with  $\delta/\delta_c$  and  $\psi/\delta$  transfer functions inserted

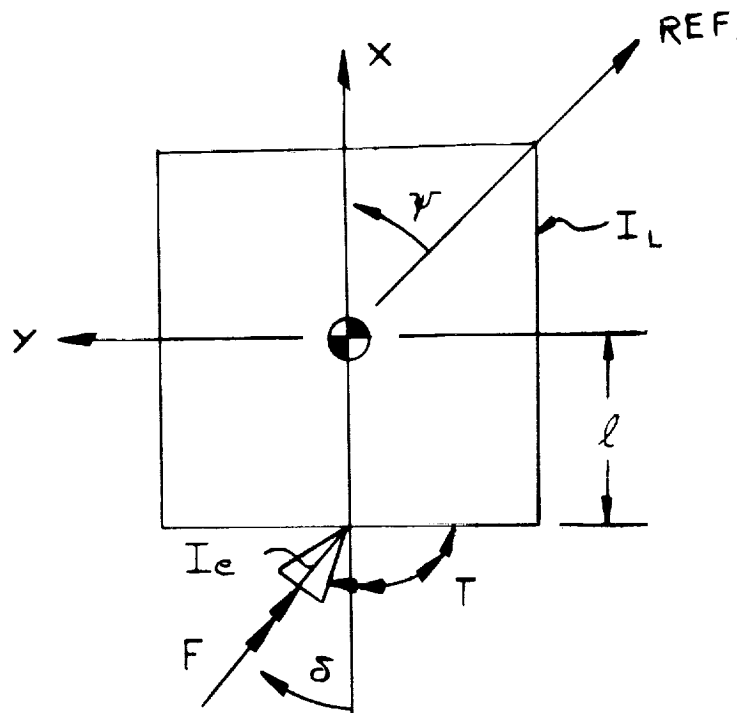


Figure 5-6 Simplified gimbaled engine planar dynamics

~~CONFIDENTIAL~~

Thus: 
$$\frac{\psi}{\delta} = \frac{(I_e s^2 + Fl)}{I_L s^2}$$

Let 
$$\omega_o^2 = \frac{Fl}{I_e}, \quad \alpha = \frac{Fl}{I_L}$$

then 
$$\frac{\psi}{\delta} = \frac{\alpha}{s^2} \left( \frac{s^2}{\omega_o^2} + 1 \right)$$

Inserting the transfer functions  $\frac{\delta}{\delta_C}$  and  $\frac{\psi}{\delta}$  into the attitude hold system of Figure 5-5 results in the system of Figure 5-6. The open loop transfer function of this system is:

$$\frac{\psi}{\delta_C} = G \frac{\alpha \left( \frac{s^2}{\omega_o^2} + 1 \right) \left( \frac{s}{R} + 1 \right)}{s^2 \left( \frac{s}{\omega_L} + 1 \right) \left( \frac{s}{\omega_H} + 1 \right)}$$

This is the same equation previously derived for Figure 5.3 (equation 5-9) with the rigorous analysis (For  $\beta = 1$ , the usual assumption).

~~CONFIDENTIAL~~

## 5.5 - Closed Loop (Feedback Stabilized) Gimballed Engine Trim Systems

### 5.5.1 - The Necessity of Integral Compensation

It must be recognized that, in general, a feedback stabilized gimballed engine will not satisfactorily null the LEM torque unbalances for acceptably small attitude errors. In order for the feedback stabilized gimballed engine systems to adequately satisfy both criteria, an integral compensation network is generally required. This is as true for fast-response feedback stabilized gimballed engine LEM attitude control systems, (discussed in the previous section) as it is for the slow response feedback stabilized trim systems discussed in this section.

Briefly, this requirement is due to the fact that the steady state LEM attitude control system transfer function (for LEM attitude "output" to torque-unbalance "input") is inversely proportional to the steady state trim control system transfer function. The steady state transfer function of a feedback stabilized trim system is a simple gain, of a magnitude determined by system stability requirements. If this gain is sufficiently large, then the attitude error will be adequately small for maximum expected torque unbalances. In general, it is not sufficiently large and integral compensation must be employed.

(Note that the steady state transfer function of an open loop trim system is a simple integrator and the steady state attitude error for a torque unbalance input is then zero. Thus, an open loop trim system does not require integral compensation.)

In the preliminary stability analysis of a trim control system, there is little loss of accuracy in neglecting the existence of a required integral compensation network. After the basic stability requirements have been defined, the system can be easily re-evaluated to include the dynamic effects of the integral compensation. The compensation network can usually be tailored to provide suitable performance with a minimum effect on control system stability.

Thus, the integral compensation was neglected in the previous presentation of the gimballed engine LEM-attitude control system, 5-4, although it was naturally incorporated in the more extensive analysis and stability optimization studies that had been performed. For illustration purposes, it has been included in the following analysis presented on the linear-actuator feedback-stabilized trim system, 5.5.2. However, it has been neglected in the analysis presented on the constant-speed actuator feedback-stabilized trim system, 5.5.3, because it would appreciably complicate the equations and presentation without providing any significant information for the purposes of this report.

### 5.5.2 - Linear (Proportional) Servo Actuators and Engine-LEM Inertia Coupling

When the fast-response gimballed engine control system was discarded because of the advantages of a slow response trim system, one of the first trim



~~CONFIDENTIAL~~

systems to be investigated was the closed loop (feedback stabilized) type. In these initial investigations, it was assumed that proportional linear servo actuators could be used, and that inertia coupling would still exist between the gimballed engine and the LEM structure.

Thus, the same equations developed for the analysis of the gimballed engine LEM attitude control system could be used to investigate this type of trim system. The major difference between the two systems is that the trim system requires a much lower gimballed engine maximum velocity, and a much lower saturation error signal. This naturally results in a much lower actuator power requirement for the trim system.

An example of this trim system, applying the gimballed engine LEM attitude control equations of Section 5.4, is presented below and illustrated in Figure 5-7.

$$\text{Let } R = 0.5 \text{ (1/sec)}$$

$$\delta_{e_{LIN}} = 0.1 (^{\circ})$$

$$\gamma = 1/35 \text{ (sec)}$$

$$\dot{\delta}_{\max} = 0.2 (^{\circ}/\text{sec})$$

$$v = \frac{I_e}{\gamma} = \frac{40 \text{ (ft-lb-sec}^2\text{)}}{1/35 \text{ (sec)}} = 1400 \text{ (ft-lb-sec)}$$

$$\text{Let: } \omega_L = 5.0 \text{ (rad/sec)}$$

$$K_m = v \omega_L = 1400 \times 5.0 = 7000 \text{ (ft-lb/rad)}$$

$$\omega_H = 1/\gamma = 35 \text{ (rad/sec)}$$

~~CONFIDENTIAL~~

~~CONFIDENTIAL~~

$$\begin{aligned}
 T_{\max} \text{ (required for control stability)} &= \frac{K_m \delta_{eLIN}}{0.7} \\
 &= \frac{7000 \text{ (ft-lb)} \times .1 (^{\circ})}{0.7} \times \frac{\pi}{180} \left( \frac{\text{rad}}{\text{deg}} \right) \\
 &= 17.5 \text{ (ft-lb)}
 \end{aligned}$$

$$\begin{aligned}
 T_{\max} \text{ (total)} &= T_{\max} \text{ (static)} + T_{\max} \text{ (dynamic)} \\
 &= 430 \text{ (ft-lb)}
 \end{aligned}$$

$$\begin{aligned}
 P_{\max} &= \frac{1}{4} T_{\max} \dot{\delta}_{\max} = \frac{1}{4} \times 430 \times 0.2 \times \frac{\pi}{180} \\
 &= .375 \left( \frac{\text{ft-lb}}{\text{sec}} \right) \\
 &= .508 \text{ (watts)}
 \end{aligned}$$

$$\begin{aligned}
 \beta_{\min} &= 1 - \alpha_{\max} \times \frac{I_e L}{K_m} = 1 - 5.0 \left( \frac{\text{rad}}{\text{sec}^2} \right) \frac{40 \text{ (lb-ft-sec}^2\text{)}}{7000 \text{ (ft-lb)}} \\
 &= 1 - \frac{200}{7000} = 1 - \frac{1}{35} = 1
 \end{aligned}$$

$$\therefore \frac{\psi}{\delta} = \frac{\alpha G}{s^2} \frac{\left( \frac{s^2}{\omega_o^2} + 1 \right) \left( \frac{s}{0.5} + 1 \right)}{\left( \frac{s}{5.0} + 1 \right) \left( \frac{s}{35} + 1 \right)} \left[ \frac{\left( \frac{s}{\omega_i} + 1 \right)}{s} \right]$$

Integral Compensation

Code 26512 Eng-23A

~~CONFIDENTIAL~~

REPORT LED-500-3  
DATE 30 Sept. 1964

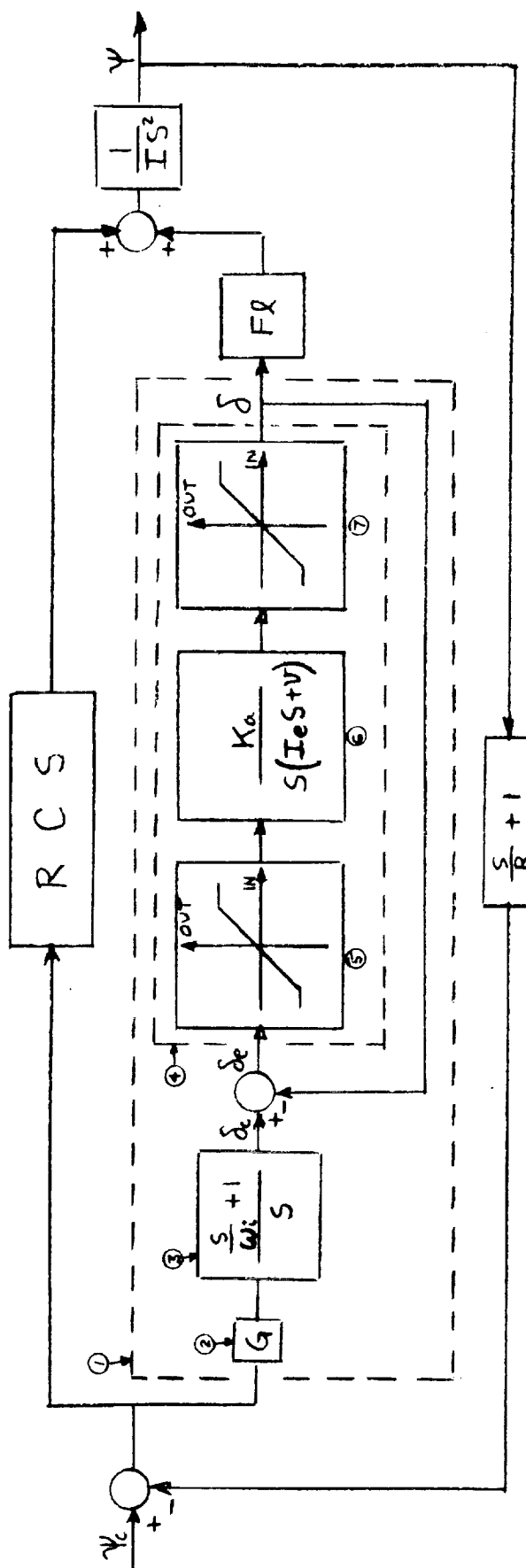


Figure 5-7  
Schematic of The  
Closed-Loop Linear-Actuator  
Trim System  
and RCS Attitude Control

Code

1. Closed Loop Trim System
2. Trim System Gain
3. Integral Compensation
4. Open Loop Trim System
5. Actuator Saturation
6. Actuator Dynamics
7. Engine Rotation Limit

~~CONFIDENTIAL~~

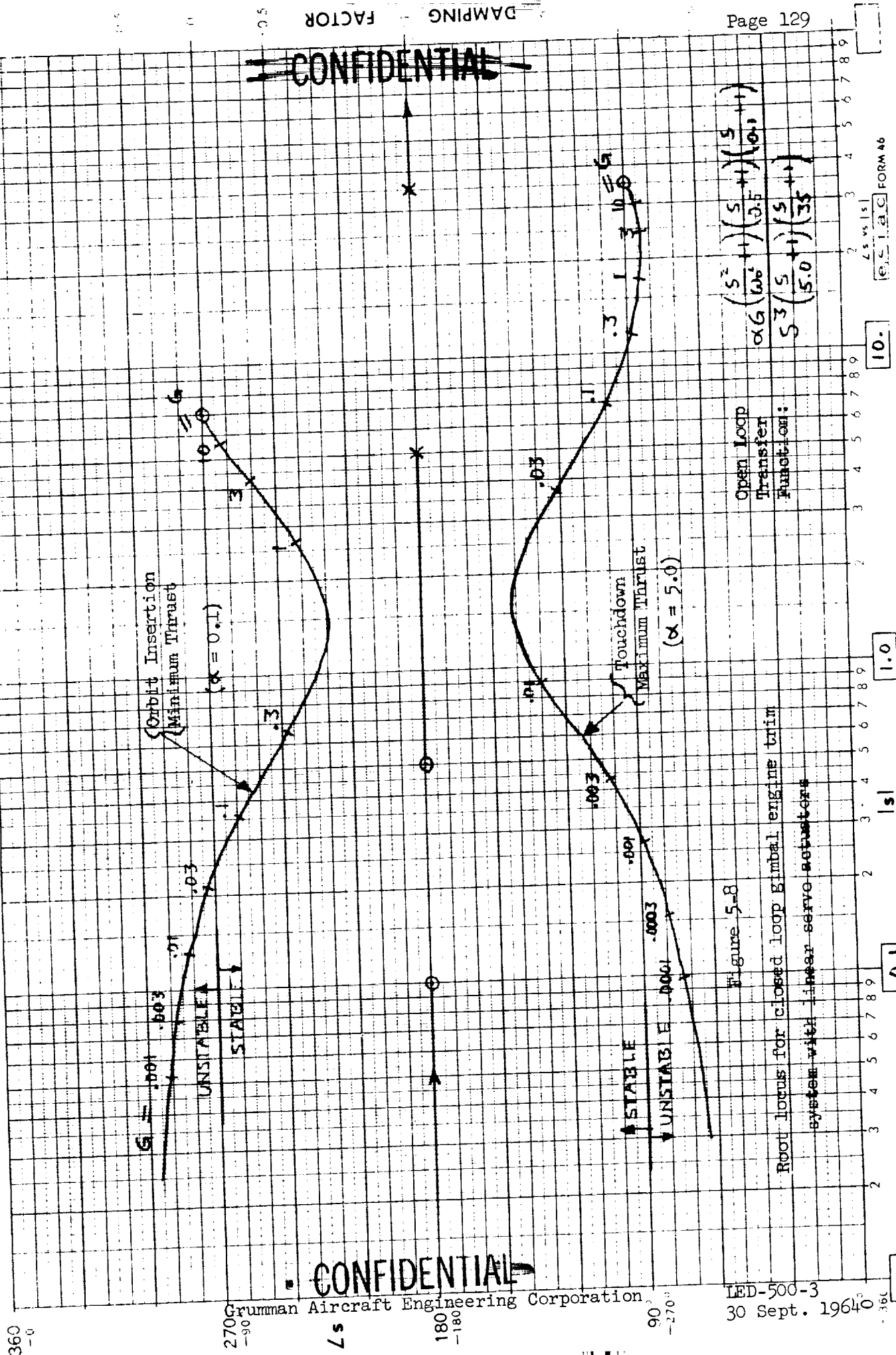


Figure 5-8

Root locus for closed loop gimbal engine trim system with linear servo actuators

Open Loop  
Transfer  
Function:

$$\alpha_G \left( \frac{S^2}{\omega_0^2} + 1 \right) \left( \frac{S}{2.5} + 1 \right) \left( \frac{S}{0.1} + 1 \right)$$

**CONFIDENTIAL**

Grumman Aircraft Engineering Corporation

LED-500-3  
30 Sept.

~~CONFIDENTIAL~~

As the value of the integral break frequency ( $\omega_i$ ) is raised, the integral compensation becomes more rapid but the trim system becomes more unstable. A magnitude of  $\omega_i = 0.1$  should provide satisfactory integral compensation without appreciably deteriorating trim control stability.

An examination of the root locus diagram of this transfer function (Figure 5-8) will suffice to prove this system stable for all operating gains, for  $G = 0.1$

#### 5.5.3 - Constant Speed (Full-on) Servo Actuators and Irreversible Drive (No Inertia Coupling)

Trade-off studies between proportional servo actuators and constant speed actuators have proven the latter to have significant advantages in terms of weight and reliability. In addition, the slow response of a trim-gimballed system, and its low power requirements, enables the use of an irreversible worm gear drive in the actuator. Thus, the actuator can rotate the engine, but engine cannot rotate itself against the actuator (via inertia forces, thrust misalignment, etc.). This irreversibility acts as a safety feature, holding the engine fixed even with a power-off failure at the actuators.

Because of this irreversibility, no appreciable dynamic coupling exists between the rigid LEM structure and the gimballed engine. Thus, in a planar analysis, the LEM can be represented as a simple inertia, as has been done in Figure 5-9. In this diagram the constant speed actuator is represented by a relay in series with the usual linear actuator (open loop) transfer function.

~~CONFIDENTIAL~~

In Figure 5-10, the system has been reduced to an analytically equivalent configuration with the non-linear actuator characteristic replaced by its describing function. The open loop transfer function of this system has been employed in the root locus diagram, Figure 5-11. Note that the system is unstable at low gains, but stable at high gains. Note also, that for a given system gain ( $\delta \alpha$ ), the root locus gain ( $4\delta \alpha / \pi A$ ) is inversely proportional to perturbation amplitude (A). Thus, for any given system gain, there will be a maximum perturbation amplitude above which the system will not converge.

Now in order for this to be a satisfactory system, the operating roots should be stable for all system gains. In order to investigate this system, the following assumptions will be made:

$$K_R = 2.0 \text{ (sec)}, \quad \dot{\delta} = 2.0 \text{ (}^\circ/\text{sec)}, \quad \tau = 0.1 \text{ (sec)}$$

Thus, the open loop transfer function can be written:

$$\frac{4(.2)}{\pi} \frac{\alpha G}{AS^3} \frac{\left( \frac{S^2}{\alpha G} + 2S + 1 \right)}{\left( \frac{S}{10} + 1 \right)} = \frac{g \left( \frac{S^2}{\alpha G} + 2S + 1 \right)}{AS^3 \left( \frac{S}{10} + 1 \right)}$$

$$\text{Where } g = \frac{4}{\pi} \dot{\delta} \alpha G \text{ (}^\circ/\text{sec}^3)$$

$$\text{But } (0.1) \leq \alpha \leq (5.0), \quad (1/\text{sec}^2) \\ \text{(Orbit Inset. Min. Thrust)} \quad \text{(Touchdown, Max. Thrust)}$$

$$@ G = 1$$

$$\alpha = .1; \left( \frac{S^2}{.1} + 2S + 1 \right) = \left[ \frac{S^2}{.316^2} + 2(.316) \frac{S}{.316} + 1 \right], \quad g = \frac{4}{\pi} \dot{\delta} \alpha G = .0255 \text{ (}^\circ/\text{sec}^3)$$

$$\alpha = 5.0; \left( \frac{S^2}{5.0} + 2S + 1 \right) = \left( \frac{S}{1.895} + 1 \right) \left( \frac{S}{.105} + 1 \right), \quad g = 1.275 \text{ (}^\circ/\text{sec}^3)$$

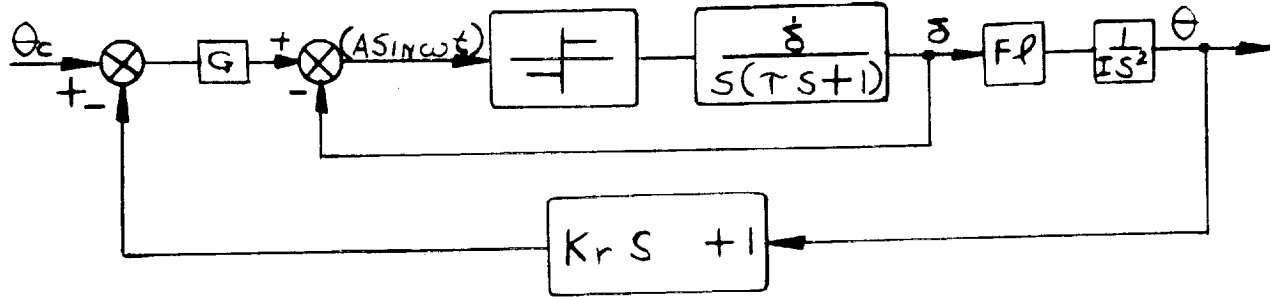
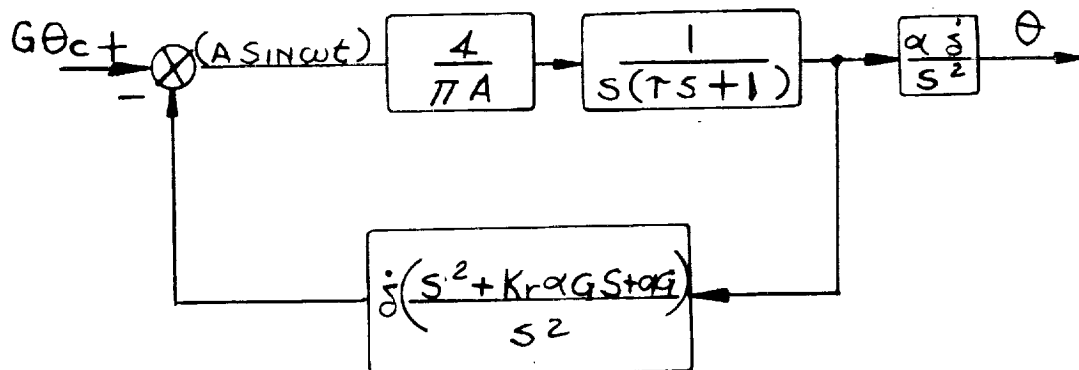


Figure 5-9 Feedback stabilized Gimbal Trim System (GTS) with constant speed nonlinear servo actuator.



Open loop transfer function: 
$$\frac{4}{\pi} \frac{\dot{\delta}}{A} \alpha G \frac{s^2 + K_R s + 1}{s^3 (\tau s + 1)}$$
  
 where  $\alpha = FL/I$

Figure 5-10 Analytically equivalent feedback stabilized GTS with describing function nonlinearity.

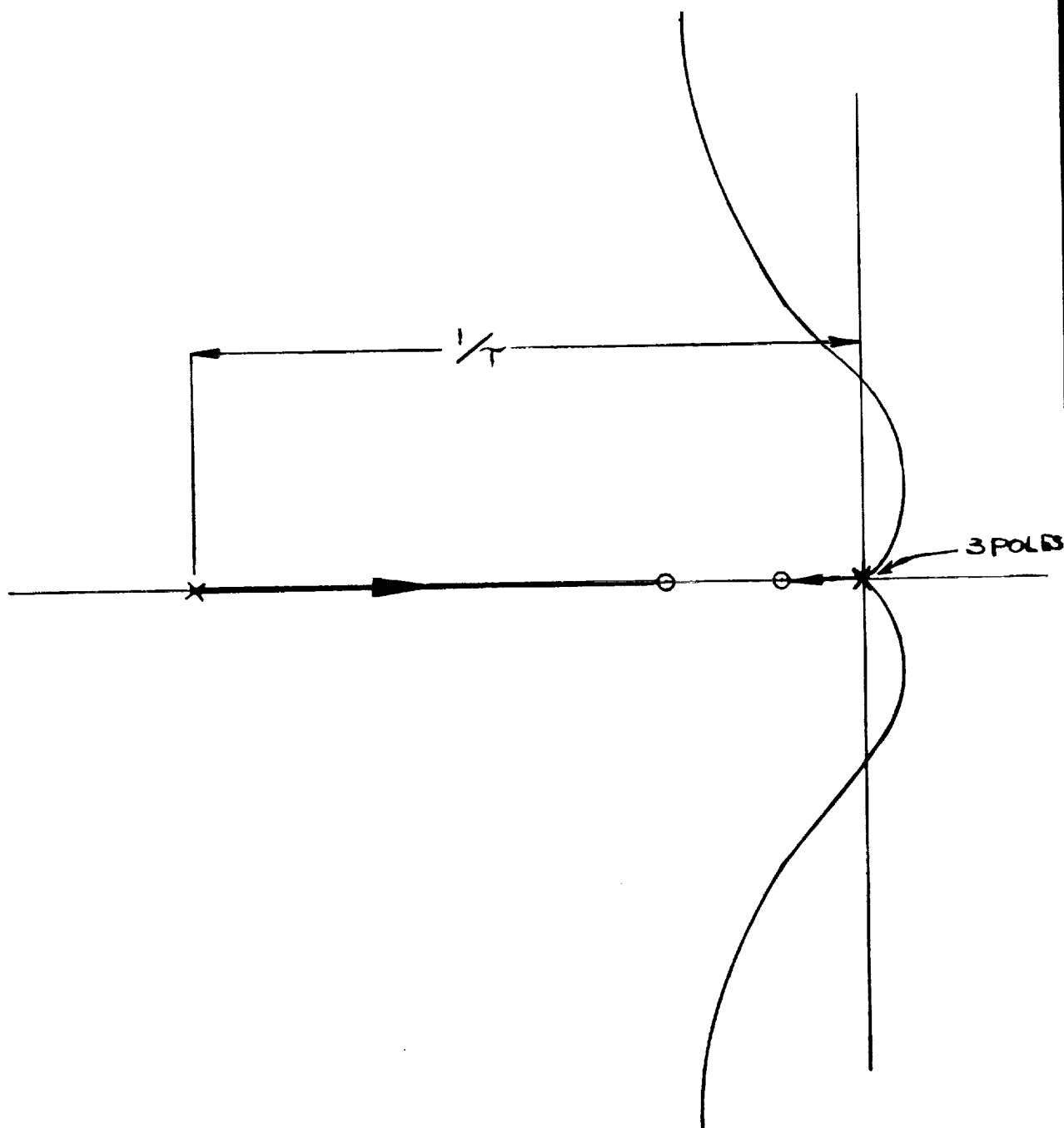
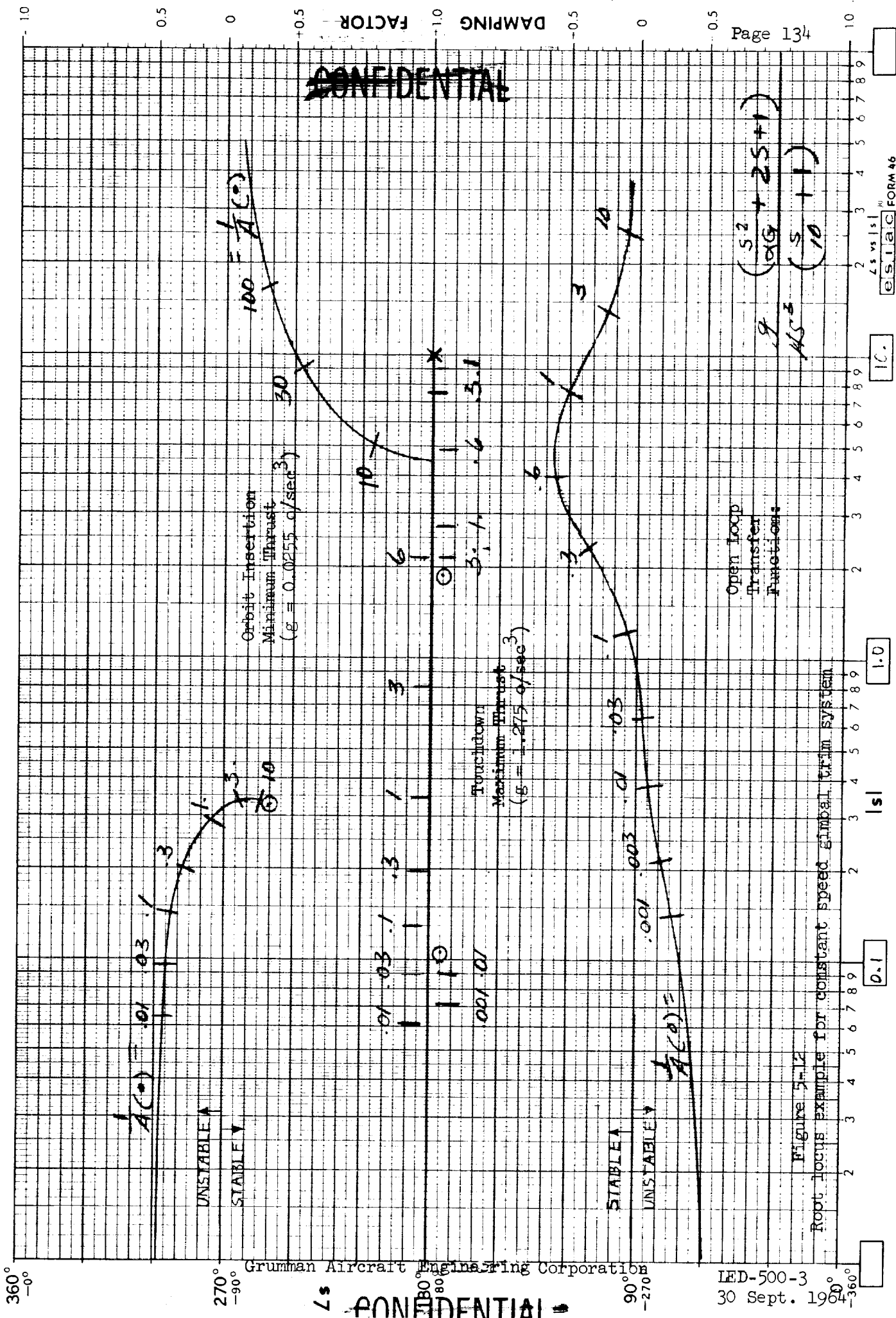


Figure 5-11 Root locus for closed loop gimbal trim system with constant speed servo actuators and irreversible drive





~~CONFIDENTIAL~~

These two root loci have been plotted in Figure 5-12. It can be seen that at orbit insertion minimum thrust, the system is stable for error perturbation amplitudes  $A \sin \omega t$  such that  $\frac{1}{A} \geq 3$ , or  $A \leq 0.33^\circ$ . Moreover, at larger amplitudes, the system will diverge with very low frequency oscillations;  $f \leq 3/2\pi$  (cps). However, at these amplitudes and frequencies the stable RCS control will predominate, and the gimballed engine control characteristics may be neglected. Similar reasoning may be applied at the other operating extreme; touchdown at maximum thrust.

## 5.6--Open Loop Gimbal Engine Trim Systems With Constant Speed Actuators and Irreversible Drive

### 5.6.1--Uncompensated (Unstable) Trim Systems

5.6.1.1--Introduction--The inherent simplicity and reliability advantages of the constant speed actuators over proportional actuators, of irreversible drive over reversible drive, and of open loop (non-feedback) actuator control over closed loop (feedback stabilized) actuator control, have resulted in the selection of a gimballed engine trim actuator which is a constant-speed, open loop actuator. Figure 5-13 represents this type trim system for the LEM, for single axis considerations and neglecting high frequency dynamics. This trim system operates in parallel with the reaction jet control system. However, to investigate the control performance characteristics of the gimballed engine, we may neglect the RCS and represent the constant speed actuator characteristic by a describing function (as in Figure 5-14). When the root locus of this system is sketched as shown in Figure 5-15, it can be seen by inspection that it is unstable at all system gains. Thus, this open loop trim system is a destabilizing influence on the LEM attitude and the RCS must be employed to maintain stable attitude control.

Therefore, this trim system will cause the RCS to use propellant at a much higher rate during powered descent than during the coasting descent phases when the trim system is not operating. One way to reduce this undesirable effect is to reduce this unstable trim system gain. The basic gimballed engine torque gain is directly proportional to the gimballed engine rotation velocity, the engine thrust level, and the gimbal-pivot to LEM- c.g. distance. Of these parameters only the gimbal rotation velocity can be designed to fit control requirements, and the assumed gimbal velocity of 0.2 degrees per second is about minimum for adequate trim characteristics.

Another way to reduce the trim system gain is by putting a dead-zone in the input signal line to the trim system. At perturbation signal amplitudes within the dead-zone the trim system has zero gain. In general, the optimum trim system dead-zone is about the same magnitude as the RCS dead-zone. At this value of gimbal dead-zone, the gimbal trim system gain (for LEM perturbation amplitudes within the RCS dead-zone) is very low and the RCS propellant (required to compensate for the unstable trim characteristic) is minimal.

~~CONFIDENTIAL~~

A high rate feedback also helps the RCS propellant consumption. As can be seen from the root locus diagram, higher rate feedback gains ( $K_R$ ) make the unstable root locus run closer to the  $j\omega$  axis, thus decreasing the phase margin of instability at the low frequency LEM perturbation amplitudes. Thus, the RCS need compensate for a lower margin, or gain, of instability and uses less propellant.

Note that this trim system can never provide stable attitude control no matter how high the rate feedback gain. Note, also, that the gimballed engine trim system cannot work with a pure rate-error-feedback input signal for the following reasons: The trim system must null quasi-static torque unbalances. For quasi-static torque unbalances, the RCS will hold the LEM at a quasi-static attitude error, with zero average attitude rate. Thus, the gimbal trim system signal input must contain attitude error information for the trim system to work at reducing the quasi-static torque unbalance.

Because the RCS propellant consumption is of major importance, and because this propellant consumption during the powered descent phase (for a specific type of unstable trim system) is strongly influenced by the RCS modulator characteristics, these modulator characteristics must be considered in detail. Thus, the following discussions in this section will consider the optimum trim system deadzones (for minimum RCS propellant consumption) for various RCS modulator characteristics.

5.6.1.2 - Nonlinear (RCS) Pulse-Ratio Modulators It has been shown (32) that a nonlinear pulse ratio modulator is required during powered ascent for minimum propellant consumption. Naturally, it would be desirable for simplicity and reliability if this same modulator could be used for all other phases of the mission, including powered descent. Figure 5-16 presents the RCS propellant consumption figures for attitude holding during all of powered descent, for various values of trim system deadzones and two values of rate feedback. The primary tool used in determining the propellant consumption figures was a digital program that was written especially for these investigations.

The propellant consumption figures were obtained by inserting the vehicle characteristics at orbit insertion, maximum thrust, into the computer program. A large transient was introduced to prevent the possibility of low-propellant-consumption oscillations if multi-stable limit-cycle regions existed. After the transient had decayed and the system was perturbing in a stable limit cycle, the RCS propellant consumption rate was calculated. This rate of propellant was assumed for two planes of control (X-Y, X-Z) and was multiplied by 600 seconds, a nominal powered descent period.

At low trim system deadzone levels, the system continuously perturbs and the gimballed engine puts a dynamic torque unbalance on the LEM, but the average torque unbalance is zero. At large trim deadzones, the RCS holds the LEM attitude error within the trim system deadzone and the LEM attitude is quasi-static. Maximum RCS propellant consumption levels can then be estimated with simple equilibrium equations.

Code 26512

Eng-23A

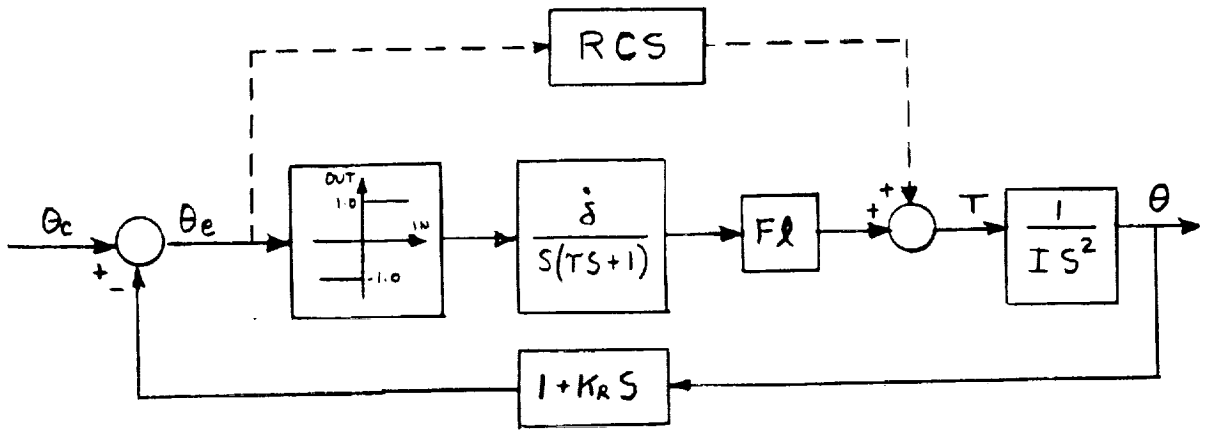


FIGURE 5-13

THE OPEN LOOP TRIM SYSTEM REPRESENTATION  
AS THE PRIME ATTITUDE CONTROL

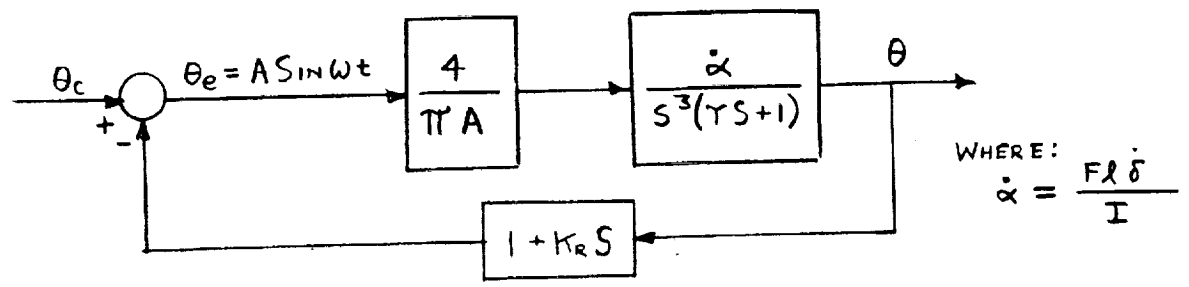
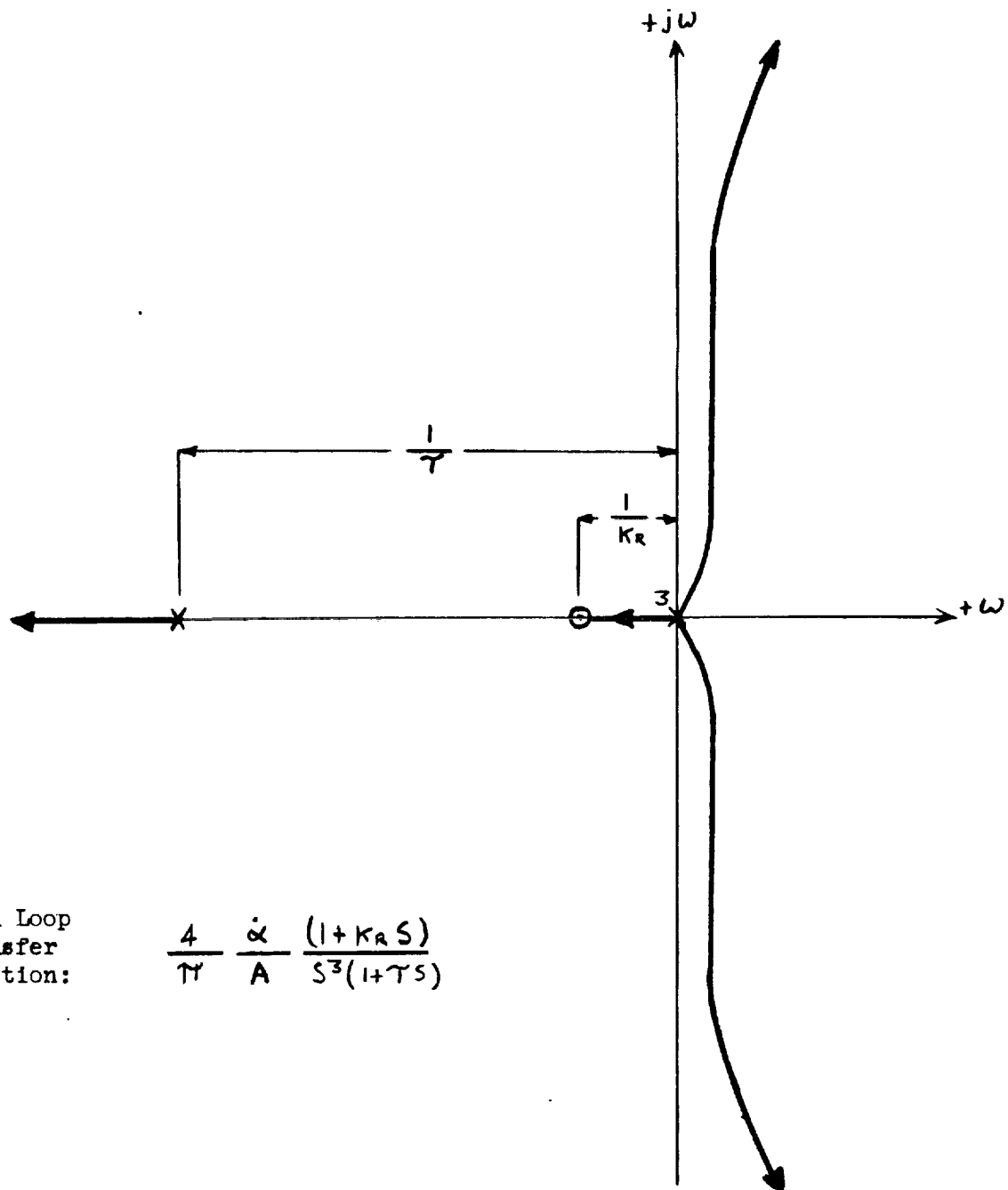


FIGURE 5-14

ANALYTICALLY EQUIVALENT TRIM SYSTEM  
REPRESENTATION  
(With Describing Function Non-Linearity)



Open Loop  
Transfer  
Function:

$$\frac{4}{\gamma} \frac{\alpha}{A} \frac{(1 + K_R S)}{S^3 (1 + \gamma S)}$$

FIGURE 5-15

ROOT LOCUS OF THE OPEN LOOP TRIM SYSTEM  
AS THE PRIME ATTITUDE CONTROL

~~CONFIDENTIAL~~

PAGE 139

Orbit Insertion Characteristics  
600 Seconds for Descent

RCS Deadzone = 0.100 Degrees

RCS Saturation = 0.6 Degrees

$\dot{\delta} = 0.2$  Degrees/Second

$\lambda = 0.1$

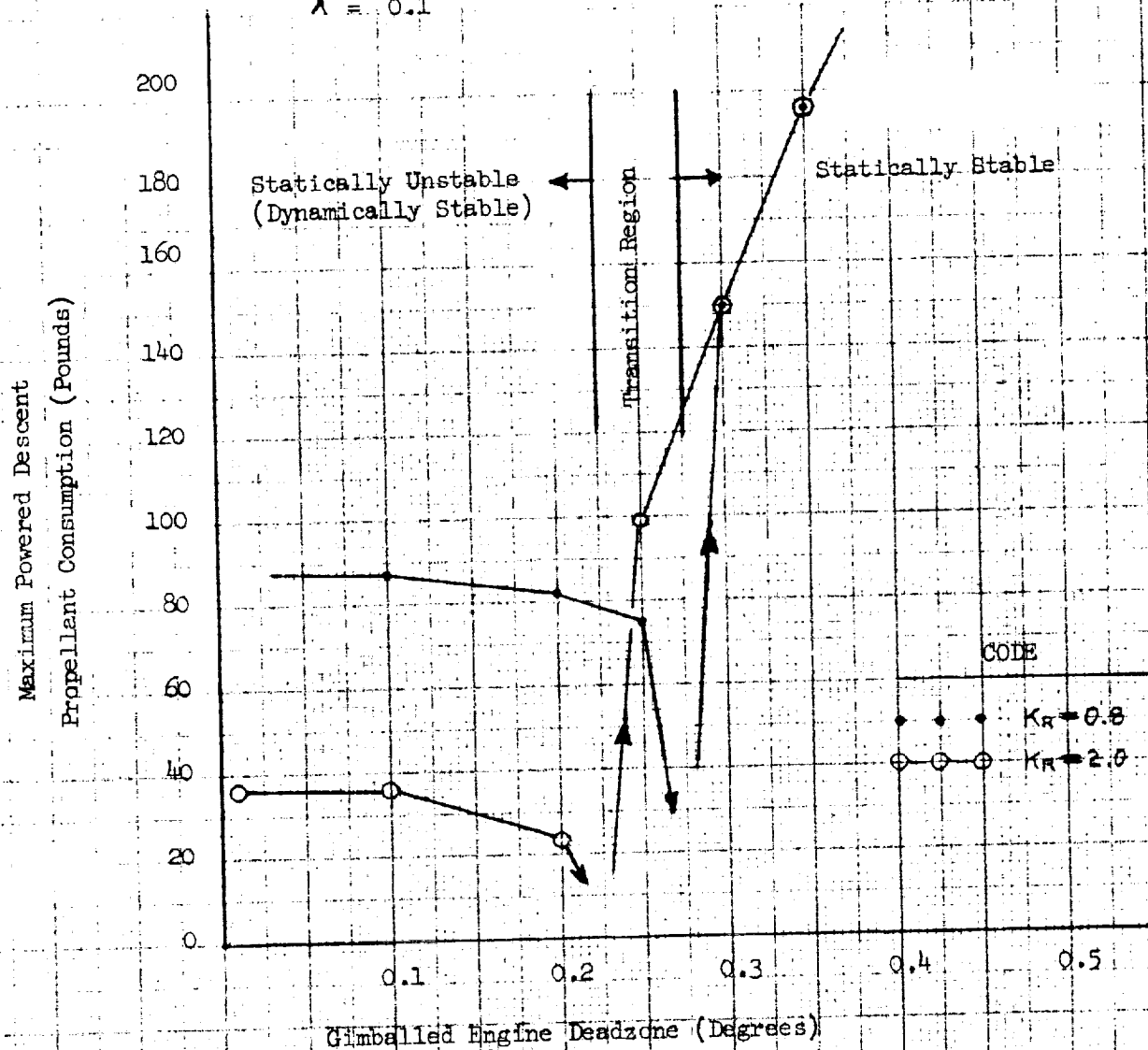


FIGURE 5-16

Nonlinear Pulse-Ratio Modulator  
Powered Descent RCS Propellant Consumption

~~CONFIDENTIAL~~

GRUMMAN AIRCRAFT ENGINEERING CORPORATION

REPORT NO. LED-500-3  
30 Sept. 1964

~~CONFIDENTIAL~~

FIGURE 5-17

LINEAR PULSE RATIO MODULATOR  
POWERED DESCENT  
PROPELLANT CONSUMPTION

NON-POD  
MODULATOR  
TRANSITION  
REGION

POD  
MODULATOR  
TRANSITION  
LINE

MAXIMUM POWERED DESCENT (ALTITUDE HOLD) RCS PROPELLANT CONSUMPTION (POUNDS)

CODE

POD,  $K_R = 0.8$   
POD,  $K_R = 1.5$   
NON-POD,  $K_R = 1.5$   
(ALL ORBIT INSERTION,  
MAXIMUM THRUST), (OI)

CODE

NON-POD,  $K_R = 1.5$ , (OI)  
NON-POD,  $K_R = 2.0$ , (OI)  
NON-POD,  $K_R = 2.0$ , (NOVER,  $F_{max}$ )

GIMBALED ENGINE THRU SYSTEM DEADEND, (DEGREES)

~~CONFIDENTIAL~~  
GRUMMAN AIRCRAFT ENGINEERING CORPORATION

~~CONFIDENTIAL~~

Note that for the nonlinear modulator with a 0.1 degree deadzone, the trim system deadzone must be set greater than 0.2 degrees before the system becomes statically stable.

Note, also, that although the propellant consumption drops as the trim system deadzone approaches the statically stable condition, it cannot be pushed too close to this condition because propellant consumption can be much higher in the static mode. Thus, even with a rate feedback gain of 2.0, the propellant consumption figure will be about 30 pounds.

5.6.1.3--Linear Pulse-Ratio Modulators--The low duty factor of the nonlinear PRM for small amplitudes decreases the relative gain of RCS loop compared to the trim loop, which is a destabilizing effect that causes larger amplitude oscillations and increased fuel consumption. We will now consider the linear pulse-ratio modulator which offers a higher RCS gain at small amplitudes. Figure 5-17 is a plot of maximum powered descent RCS propellant consumption versus trim system deadzone. These propellant consumption levels were obtained by inserting the orbit-insertion, maximum-thrust LEM characteristics into the computer program. The resulting rate of propellant consumption was considered for two planes of control and then multiplied by 600 seconds, a nominal powered descent time estimate.

The upper graph enables a comparison between two rate feedback gains, 0.8 and 1.5, for the pulse-on-demand (POD) type of pulse-ratio modulator (a modulator that resets the off-integral whenever the input signal = 0).<sup>\*</sup> It can be seen that the higher rate gain decreases the propellant consumption. Note, however, that the POD switch-line characteristic makes it mandatory to avoid a trim deadzone that is appreciably larger than the RCS deadzone. On the same graph, however, a non-POD modulator (calculates off-integral first when input signal first exceeds zero) with a rate gain of 1.5 is plotted. It can be seen that the non-POD modulator enables larger trim deadzone values since the statically-stable switch-line is further within the modulation region. Also, a comparison of figures 5-16 and 5-17 show the reduced fuel consumption obtained with the linear PRM.

Because of potential operating characteristics during powered ascent, the non-POD modulator appears to be the more desirable (section 3). Thus, the powered descent propellant consumption characteristics of the non-POD modulator have been investigated in further detail. The lower graph compares the non-POD modulator at a rate gain of 1.5 to the same system with a rate gain of 2.0, both systems with orbit insertion, maximum thrust characteristics. Note that the higher rate gain costs less propellant. Also, the propellant consumption of a non-POD, rate gain 2.0 is plotted for hover maximum thrust characteristics. Note that there is little difference of rate of RCS propellant consumption between orbit insertion and hover, at maximum thrust.

\* See Section 3.3.4.4 for a further explanation of modulator characteristics.

~~CONFIDENTIAL~~



5.6.1.4--RCS Deadzone Variation--When it is observed that most previous investigations assumed that the RCS deadzone was 0.1 degrees, and that substantial advantages are achieved with higher deadzones, the question of what happens to RCS propellant consumption at higher RCS deadzones becomes significant. An indication of the trend of this variation may be obtained from Table 5-2.

TABLE 5-2

Gimbal Trim System Propellant Requirements

RATE GAIN = 2.0		NON-POD MODULATOR	
RCS DZ = 0.300° SAT = 0.800°		RCS DZ = 0.100° SAT = 0.600°	
Gimbal D.Z.	Descent Propellant Consumption	Gimbal D.Z.	Descent Propellant Consumption
0.300	22	0.100	15
0.305	19	0.105	14
0.310	18	0.110	12
0.315	11	0.115	9
0.320	(Static)	0.120	Static

5.6.1.5--Results--This analysis has shown that, with the uncompensated trim system, RCS propellant consumption for attitude-hold during powered descent may be held within 20 pounds only if the following minimal criteria, which are estimated to be unattainable, could be satisfied:

- (a) The rate feedback gain is at least 2.0 (Preliminary vehicle handling data indicates that lower rate gains might be mandatory. Prime and abort guidance factors will also require a lower value.)

Code 26512

Eng-23A

~~CONFIDENTIAL~~

- (b) The RCS-to-trim system deadzone tolerances are within 0.005 degrees (attitude error) of the nominal. (This might be an unrealistic design criteria.)
- (c) A linear pulse ratio modulator is used (This requires switching to a nonlinear pulse ratio modulator for powered ascent).
- (d) The nominal RCS deadzone is not much more than about 0.1 degrees. (For many other system considerations, it is desirable to increase the RCS deadzone as much as possible. Preliminary guidance considerations indicate that an RCS deadzone of 0.2 or 0.3 degrees will be acceptable.)

It is further assumed that propellant slosh and elastic structure coupling will provide negligible effects on RCS propellant consumption. This assumption is required by the limitation of these preliminary analyses which only considered a rigid LEM. However, preliminary slosh considerations indicate that slosh will not increase the RCS propellant consumption during powered descent with the uncompensated trim system.

#### 5.6.2--Phase-Lead Stabilized Trim Systems

5.6.2.1--Linear (Dipole) Stabilization--As was previously shown from Figure 5-15, the basic open loop trim system always acts as a de-stabilizing influence on the attitude control, increasing the RCS rate of propellant expenditure. Thus, to minimize RCS propellant usage, a tight tolerance must be maintained between the gimballed trim system and RCS deadzones. Moreover, to hold the RCS propellant within 25 pounds, a linear PRM must be used during powered descent. However, since a nonlinear PRM must be used during powered ascent, a PRM characteristic switchover must be mechanized.

Alternatively, if the gimballed engine trim system is stabilized, no RCS propellant will be employed (for attitude holding), no tight deadzone ratio need be maintained, and the nonlinear PRM may be employed during all mission phases. The insertion of a phase-lead network in series with the trim system, as illustrated in Figure 5-18, will enable the trim system to act as a stable attitude control system within a specific range of perturbation amplitudes.

Note that at system gains below a certain level the system will be unstable below a frequency  $\omega_p$ , and at system gains above a certain amount the system will be unstable above a frequency  $\omega_p$ . However, the describing function representation of the actuator nonlinearity has shown that the system gain is inversely proportional to the amplitude (A) of the perturbing error signal. Thus, at any given control gain ( $\dot{\alpha}$ ) there will be minimum stable amplitude at which the system will perturbate at a frequency  $\omega_p$ , and a maximum stable amplitude above which the system will diverge at a frequency  $\omega_p$ . The only remaining problem is to define an adequate range of gains over which the system must be stable for satisfactory performance.

~~CONFIDENTIAL~~

The control gain  $\dot{\alpha}$  is directly proportional to main engine thrust, engine-pivot-to-LEM-c.g. distance, and inversely proportional to vehicle inertia. Main engine thrust variation is from 10,000 pounds to 1,000 pounds, a range of 10. Engine-pivot-to-LEM-c.g. distance varies from about 2 feet at orbit insertion to about 5 feet at touchdown, a range of 2.5. LEM inertia varies from about 20,000 slug-ft<sup>2</sup> at orbit insertion to about 10,000 slug-ft<sup>2</sup> at touchdown, a range of 2. Thus, the control gain range of  $\dot{\alpha}$  is about 50 to 1. Therefore, at the minimum, the root locus stability region must be stable over a 50 to 1 gain change.

Suppose we now consider an open loop trim system with linear phase lead stabilization. A reasonable frequency variation between the actuator time constant and the rate feedback gain constant is 20 to 1. We will be optimistic and assume that 30 to 1 is achievable. Suppose we assume a lead-lag stabilization network of 30 to 1 break frequency ratio, at the same frequency of the rate and actuator time constants. (This, also, is a rather extreme design.) A root locus plot of this sort of system is presented in Figure 5-19. It can be seen that this system is stable for a gain ratio of about 30 to 1.

Thus, linear network phase-lead stabilization of the open loop trim system is, perhaps, interesting, but of doubtful practical advantage because of the 50 to 1 gain variation of the trim control system operating characteristics.

5.6.2.2--Nonlinear (Relay) Stabilization--Because the gimballed engine trim system employs constant-speed actuators with, essentially, relay operating characteristics, it is possible to put a relay-type nonlinearity in the electrical input to the actuators without affecting their mode of operation. Consider, for example, the normalized trim control system with a certain type of nonlinear stabilization, as shown in Figure 5-20A. As shown in Figure 5-21, this stabilizing function, for a sinusoidal input, has an output only between 0 and  $\pi/2$ , and between  $\pi$  and  $3\pi/2$ . Thus, the describing function of this nonlinearity has a 45° phase lead as shown in Figure 5-20B. It is, therefore, possible to write the open loop transfer function of this system as shown in Figure 5-20C. Note that the actuator time constant has been expressed as a multiple of the rate feedback constant, R.

The root locus of this system has been plotted in Figure 5-20D for a frequency variation between the actuator time constant and the rate feedback constant of 10, 20, and 30. Note that, for a variation of 30, the system is stable from a gain of about 3 to 1000, a range of over 300 to 1. This is about ten times the range of the system with linear network phase lead stabilization.

Suppose we consider a system where the rate feedback gain ( $1/R$ ) equals 2.0 and the actuator time constant is 1/10 of a second. Thus, the frequency variation is 20. As shown in Figure 5-20D, the stable gain range for this frequency variation is from 3 to 300. Thus, for stability:

$$3 < \frac{\dot{\alpha}}{AR^3} < 300$$

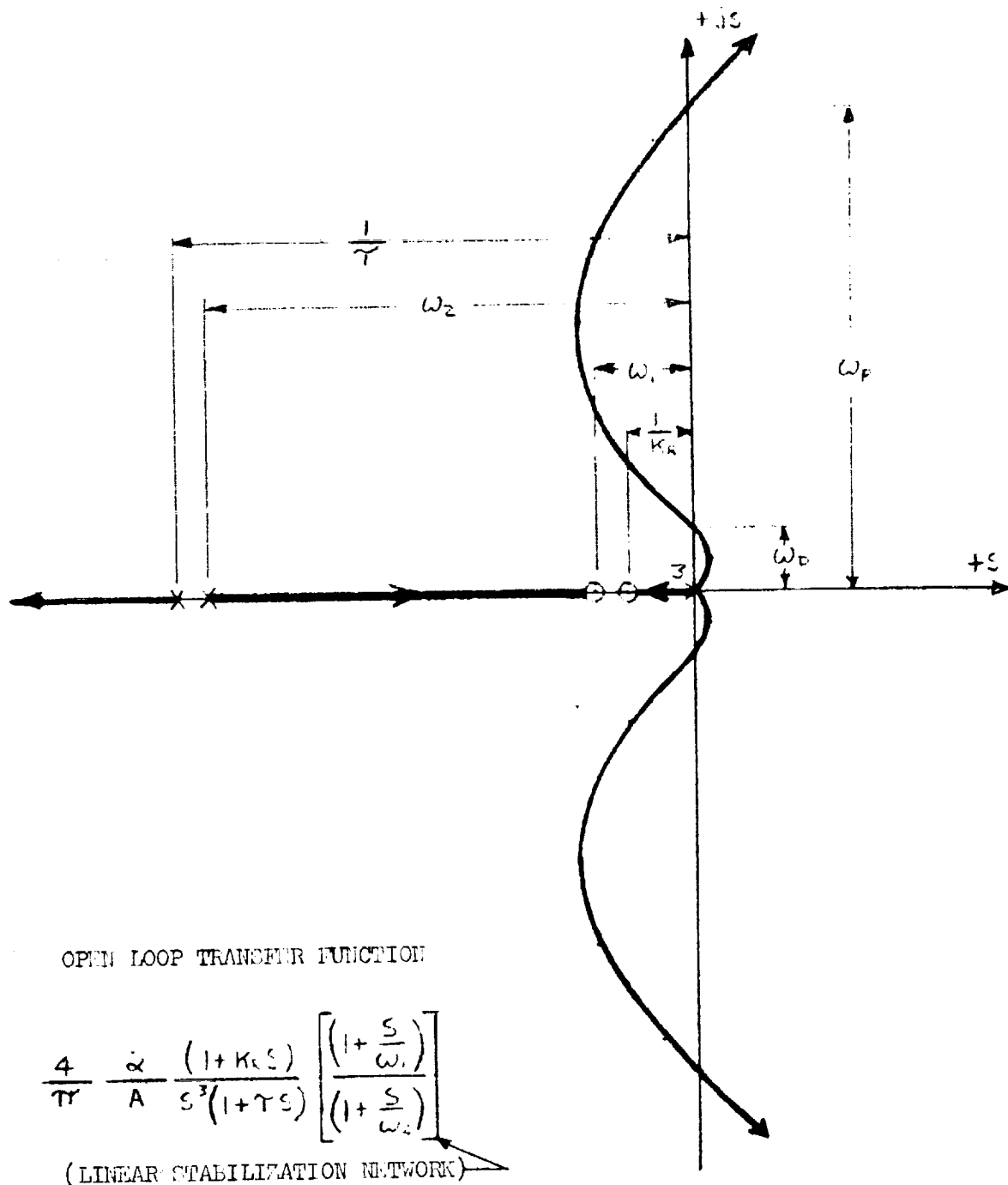
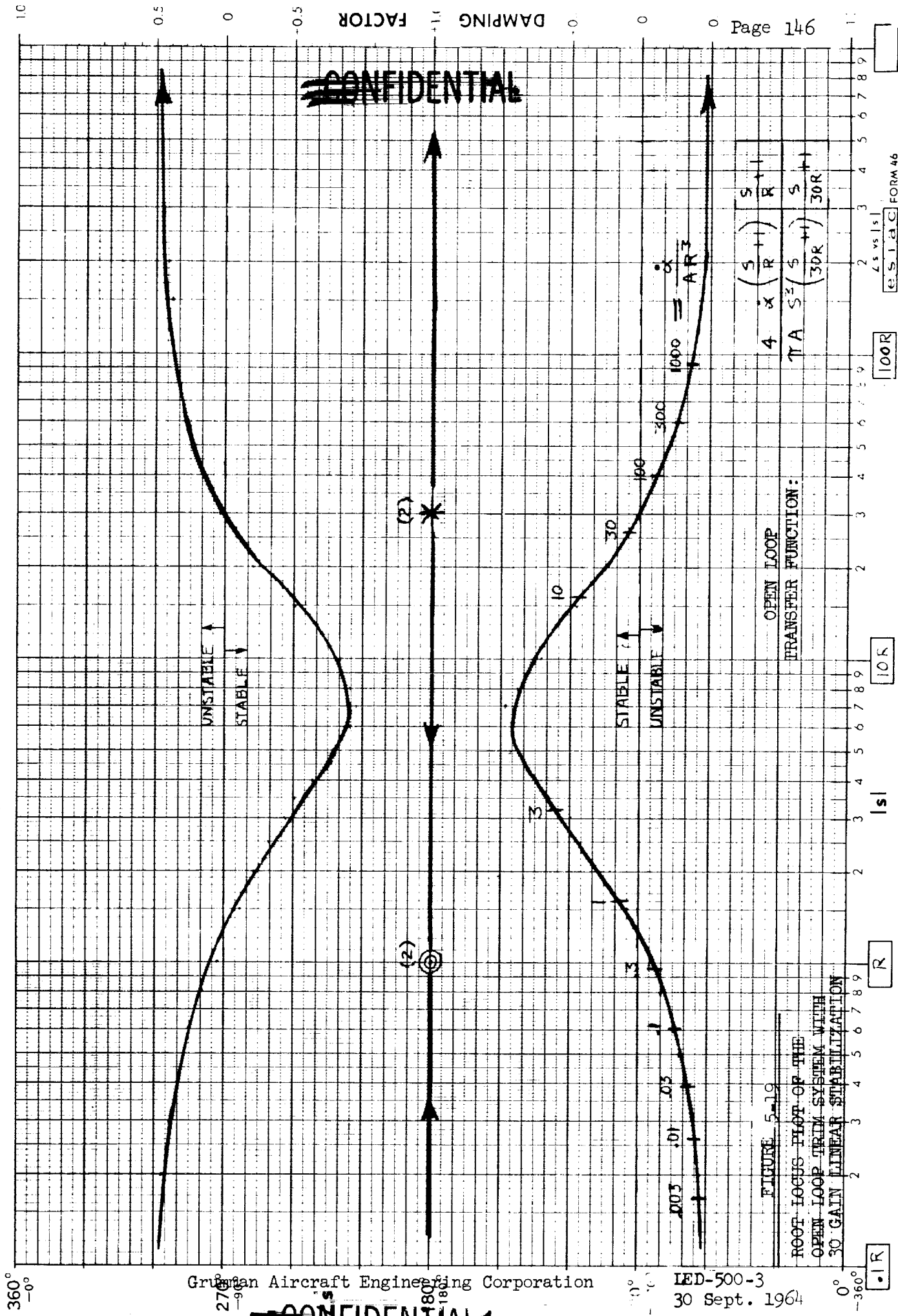
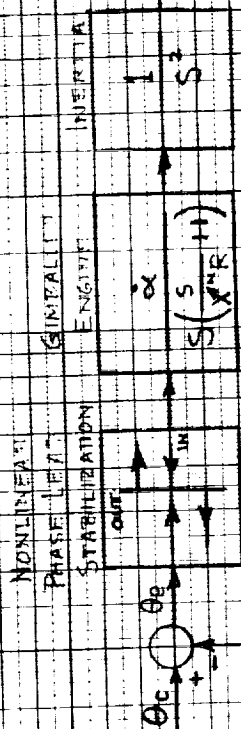


FIGURE 5-13  
ROOT LOCUS SKETCH OF THE OPEN  
LOOP TRIM ATTITUDE CONTROL SYSTEM  
WITH LINEAR PHASE LEAD STABILIZATION



360°  
-0°



RATE AND ATTITUDE FEEDBACK

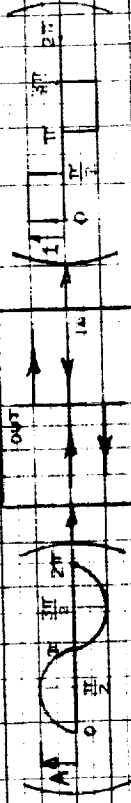
$$\frac{S}{R} + 1$$

PLANAR NORMALIZED GIMBELLED ENGINE TRIM  
ATTITUDE CONTROL SYSTEM WITH NONLINEAR  
PHASE LEAD STABILIZATION (A)

DESCRIPTION FUNCTION

$$(A \sin \omega t) \rightarrow \frac{2\sqrt{2}}{\pi A} \rho^{1/4} e^{j\phi} \rightarrow \left( \frac{2\sqrt{2}}{\pi} \sin(\omega t + \phi) \right)$$

ACTUAL FUNCTION



(B)

CONFIDENTIAL

UPPER HALF-PLANE ROOT LOCUS

(D)

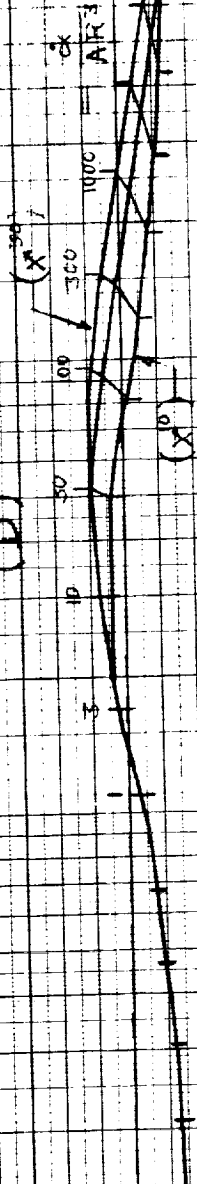


FIGURE 5-20

DESCRIBING FUNCTION ANALYSIS OF THE  
NORMALIZED OPEN LOOP TRIM SYSTEM WITH  
NONLINEAR PHASE LEAD STABILIZATION

OPEN LOOP  
TRANSFER FUNCTION:

$$\frac{2\sqrt{2}}{\pi} \propto \frac{A}{\pi} S^3 \left( \frac{S}{X^N R} + 1 \right) \left( \frac{S}{R} + 1 \right) e^{j45^\circ}$$

$\left\{ \begin{array}{l} X^N = 10 \\ X^N = 20 \\ X^N = 30 \end{array} \right.$

(C)

DAMPING FACTOR

CONFIDENTIAL

0°  
-360°

10 R

100 R

LS vs |s|

FORM 46

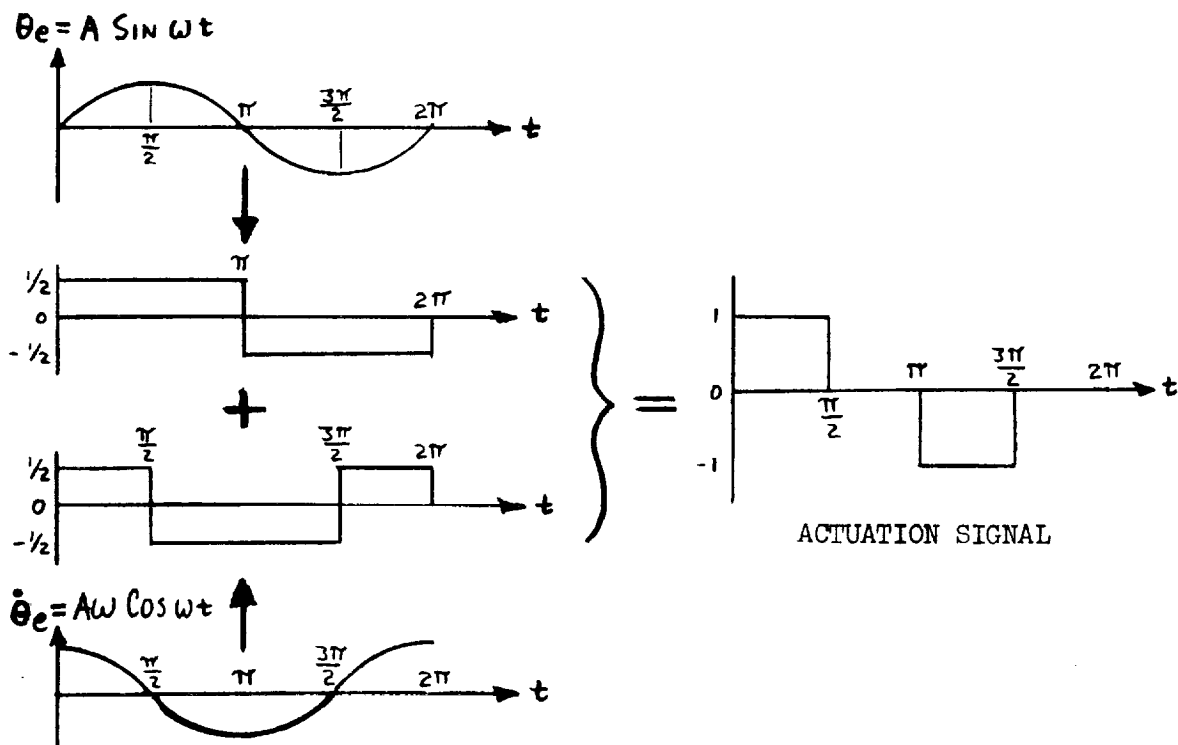


FIGURE 5-21

A CONCEPT BASIS FOR MECHANIZING THE NONLINEAR PHASE-LEAD STABILIZATION

~~CONFIDENTIAL~~

PAGE 149

$$\text{But, } \ddot{\alpha} = \frac{F l \dot{\delta}}{I}$$

$$\text{Thus } \frac{F l \dot{\delta}}{300 I R^3} < A < \frac{F l \dot{\delta}}{3 I R^3} \quad \text{for stability}$$

$$\text{Let, } \dot{\delta} = 0.2 \text{ (}^\circ/\text{sec)}, \quad \frac{1}{R^3} = K_R^3 = (2.0)^3 = 8.0 \text{ (sec}^3\text{)}$$

$$\therefore \frac{1.6 \text{ (}^\circ\text{sec}^2\text{)}}{300} \frac{F l}{I} < A < \frac{1.6 \text{ (}^\circ\text{sec}^2\text{)}}{3} \frac{F l}{I}$$

The associated perturbation period can be determined by:

$$2\pi f = \frac{2\pi}{P} = R W_R = \frac{W_R}{K_R} \quad \therefore P = \frac{2\pi K_R}{W_R}$$

$$\text{If: } K_R = 2.0 \text{ (sec)} \quad \therefore P = \frac{4\pi}{W_R}$$

$$\therefore 0.84 = \frac{4\pi}{15} < P < \frac{4\pi}{1.5} = 8.4 \text{ (sec)}, \quad \text{for stability.}$$

At orbit Insertion, Minimum Thrust:

$$F = 1000 \text{ (lbs)}, \quad l = 2 \text{ (ft)}, \quad I = 20,000 \text{ (lb-ft-sec}^2\text{)}$$

$$\therefore \frac{F l}{I} = \frac{(1000) (2)}{20,000} = 0.1 \left( \frac{1}{\text{sec}^2} \right)$$



$$\therefore 0.00053^\circ < A < 0.053^\circ$$

$$\text{But, } \theta_e = A \sin \frac{2\pi t}{P}$$

$$\therefore 0.00053^\circ \sin \left( \frac{2\pi t}{0.84} \right) < \theta_e < 0.053^\circ \sin \left( \frac{2\pi t}{8.4} \right)$$

At touchdown, Maximum Thrust:

$$F = 10,000 \text{ (lbs)}, \quad \ell = 5 \text{ (ft)}, \quad I = 10,000 \text{ (lb-ft-sec}^2\text{)}$$

$$\therefore \frac{F\ell}{I} = \frac{(10,000)(5)}{(10,000)} = 5.0 \left( \frac{1}{\text{sec}^2} \right)$$

$$\therefore 0.027^\circ \sin \left( \frac{2\pi t}{0.84} \right) < \theta_e < 2.7^\circ \sin \left( \frac{2\pi t}{8.4} \right)$$

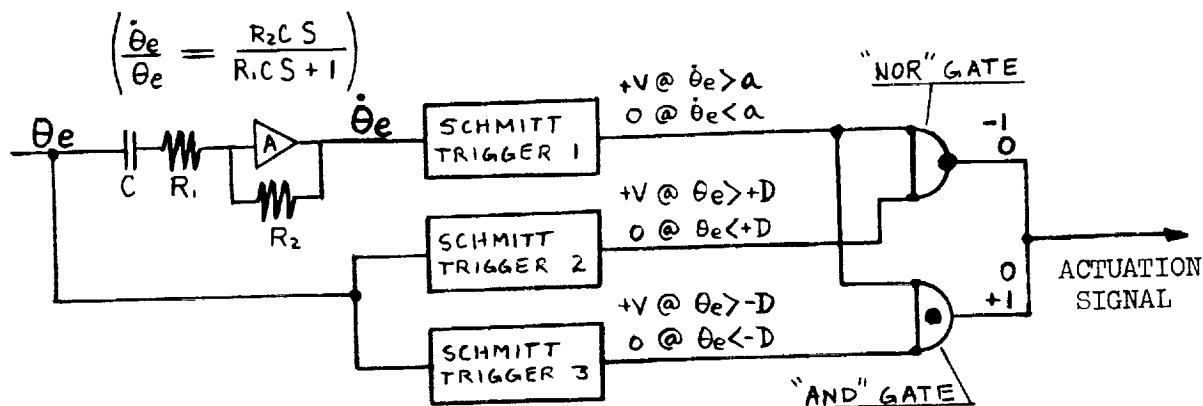
5.6.2.3--Mechanization Concepts for Nonlinear (Relay) Stabilization--While it has been demonstrated that this particular nonlinear phase lead compensation will stabilize the trim system, it must also be shown that a mechanization of this function is feasible and practical. In considering the mechanization aspect, the system illustrated in Figure 5-22 has been employed. Note that use is made of the error signal and its derivative. Ordinarily, derivative networks are not particularly useful because of the high distortion and noise of their outputs. However, there are three reasons to expect no significant performance deterioration from this aspect for this system:

- (a) The mechanization employs only sign information from the derivative network output. Thus, amplitude distortion has little effect on performance.
- (b) Derivative network cutoff frequencies may be as low as 20 radians per second, providing a distinct limit to the noise and distortion output.

Code 26512 Eng-23A

INPUT		OUTPUT
$\theta_e$	$\dot{\theta}_e$	
$>+D$	$>a$	$+1$
$\begin{matrix} \leq +D \\ \geq -D \end{matrix}$	$>a$	$+1$
$<-D$	$>a$	$0$
$>+D$	$<a$	$0$
$\begin{matrix} \leq +D \\ \geq -D \end{matrix}$	$<a$	$-1$
$<-D$	$<a$	$-1$

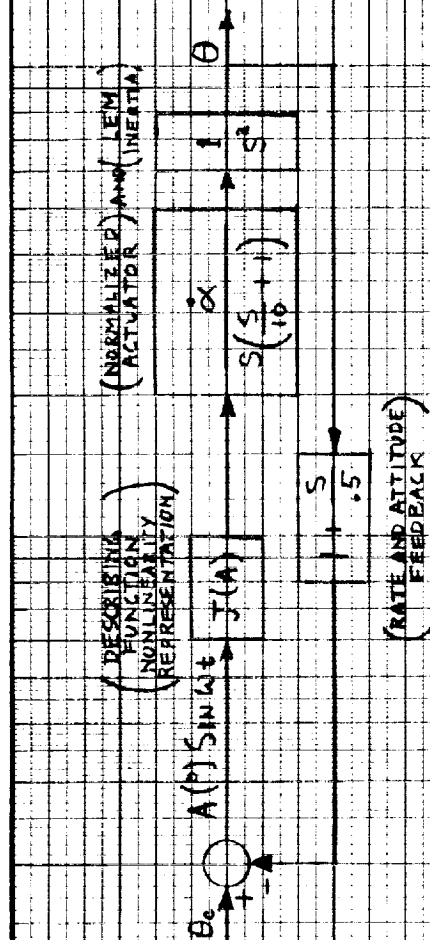
(A)  
STABILIZATION LOGIC  
TRUTH TABLE



(B)  
STABILIZATION MECHANIZATION SCHEMATIC

FIGURE 5-22

STABILIZATION MECHANIZATION

360°  
-0°IF THE ATTITUDE DEADZONE IS  $D(^\circ)$ , THEN:

$$J(A) = \frac{2\sqrt{2} J(1+D/A)}{\pi A} \rho^{j \tan^{-1} \left( \frac{1+D/A}{1-D/A} \right)}$$

$$\text{OR: } J(A) = R e^{j\phi}$$

$$\text{IF: } \frac{D}{A} \geq 1, \quad J(A) = \frac{4}{\pi A} e^{j90^\circ}$$

$$\text{IF: } \frac{D}{A} \ll 1, \quad J(A) = \frac{2\sqrt{2}}{\pi A} e^{j45^\circ}$$

270°  
-90°

Grumman Aircraft Engineering Corporation

Ls

**CONFIDENTIAL**

ROOT LOCUS PLOT WITH A DEADZONE (D) OF 0.10 DEGREES

ONSET INSERTION, MINIMUM THRUST

TOUCHED DOWN, MAXIMUM THRUST

$\frac{1}{A^0} = 0.03$

FIGURE 5-23

TRIM SYSTEM WITH MAXIMUM STABILIZATION

OPEN LOOP  
TRANSFER FUNCTION:

$$\frac{2R \left( \frac{s}{10} + 1 \right) e^{j\phi}}{s^3 \left( \frac{s}{10} + 1 \right)}$$

90°  
-270°

30 Sept. 1964

LED-500-3

30

10.0

1.0

0.1

Ls vs |s|

FORM 46

~~CONFIDENTIAL~~

- (c) The slow response actuator will act as its own low-frequency filter. It will be unable to respond to high-frequency transients and noise signals.

A compensation logic truth table is presented in Figure 5-22A. Large values of D are desirable (as will be discussed in the following section) and finite tolerances on "a" are quite acceptable.

5.6.2.4--Maximum Stabilization--Note that it is not necessary that the trim control system provide attitude convergence to amplitudes very much smaller than 0.1 degrees. Thus, for error signals below 0.1 degrees, the trim system does not require attitude information from the stabilization network. Suppose the Schmitt Trigger Deadzone (D) is not infinitesimal. Then, for perturbation amplitudes below the deadzone level (D), the stabilization system would pass through only error rate ( $\dot{\theta}_e$ ) information. Thus, the stabilization describing function would provide  $90^\circ$  of phase lead at the low amplitudes ( $|\theta_e| < \text{deadzone}$ ), and  $45^\circ$  of lead at the high amplitudes ( $\theta_e > \text{deadzone}$ ).

The describing function of this nonlinearity has been found to be

$$J(A) = \frac{2\sqrt{2}}{\pi A} \sqrt{1+D/A} \left[ \epsilon^{j \tan^{-1} \left( \sqrt{\frac{1+D/A}{1-D/A}} \right)} \right]$$

where: D = deadzone

A = perturbation amplitude

Thus, for A ≤ D

$$J(A) = \frac{4}{\pi A} e^{j90^\circ}$$

And, for A >> D

$$J(A) = \frac{2\sqrt{2}}{\pi A} e^{j45^\circ}$$

The root locus of the trim system with this stabilization network has been presented in Figure 5-23. Note that the minimum stable amplitude for any mission phase is about 0.5 degrees and that the system remains stable at very low perturbation amplitudes.

5.7--Ascent Thrust Vector Control--It has been estimated that the mean torque unbalance on the LEM during powered ascent will be 250 ft-lbs. about the Y and Z axes or 500 ft-lbs. about Y or Z axis. Both these levels are well within the 1100 ft-lbs. control (pure couple) torque capability of a single pair of RCS jets, and therefore additional means of thrust vector control will not be required during powered ascent. However, approximately 170 lbs. of propellant will be required to control these torque unbalances (see section 3.5) and a

~~CONFIDENTIAL~~

control logic which will yield useful  $\Delta V$  from this propellant is desired.

If only those jets which add impulse parallel the main engine are selected (plus-X logic) it will only be necessary to fill the main tanks with the required propellant for  $\Delta V$  minus the amount required for moment unbalance control. The equations which determine the propellant saving are:

$$\Delta V = \underbrace{\left( \frac{F_m}{\dot{m}_1} \right) \log_e \frac{M_o}{M_1}}_{\text{no moment unbalance}} = \underbrace{\left( \frac{F_m + D_1 F_R}{\dot{m}_1 + D_1 \dot{m}_2} \right) \log_e \frac{M_o}{M_2}}_{\text{moment unbalance exists}} \quad (1)$$

$$\text{let } A \equiv \frac{F_m}{\dot{m}_1} \quad B \equiv \frac{F_m + D_1 F_R}{\dot{m}_1 + D_1 \dot{m}_2} \quad (2)$$

$$\text{then } A \log \frac{M_o}{M_1} = B \log \frac{M_o}{M_2} \quad (3)$$

$$\text{and } \log M_2 = \frac{(B-A) \log M_o + A \log M_1}{B} \quad (4)$$

$$\text{and } W_A = W_{RCS} - g_o (M_1 - M_2) \quad (5)$$

Substituting the parameter values tabulated in Table 5-3 which are typical of the LEM vehicle, a propellant saving of 112 lbs. is provided.

However, with this method, only main tank propellant will be consumed for the trajectory impulse when there is no moment unbalance and therefore the main tank contingency propellant allowance will have been depleted by the amount of propellant saved using the plus - X jet select logic during powered ascent. The RCS propellant not used because of the absence of moment unbalance will serve in place of the used main engine contingency propellant.

In the presence of moment unbalance, no main tank contingency propellant will be burned because of the assistance to the main engine of the plus - X RCS thrust. However, in the event of an RCS jet failure, pure couple logic and the main engine contingency propellant will be used (112 lbs.).

Code 26512 Eng-23A

~~CONFIDENTIAL~~

It should be noted that the plus -X logic method of control provides 1100 ft.-lbs. of control moment about a single axis (which is the same as pure couple logic) but only provides 770 ft.lbs. about an axis 45 degrees from the Y and Z axis. For unbalance moments about this axis, only half the control provided with pure couple jet, is available. However, this will be adequate for the currently expected powered ascent moment unbalance. Therefore, it can be concluded that plus -X logic RCS control be used for powered ascent thrust vector control.

TABLE 5-3

A	= 9760 ft/sec
B	= 9684 ft/sec
M <sub>0</sub>	= 240.84 slugs
M <sub>1</sub>	= 121.27 slugs
W <sub>RCS</sub>	= 133 lb. (obtained from reference)
g <sub>0</sub>	= 32 ft/sec <sup>2</sup>

~~CONFIDENTIAL~~

5.8--Conclusions--The recommended torque unbalance trim system for powered descent, and the one incorporated into the control assembly specifications at this time, is the open loop gimballed engine trim system with nonlinear phase lead stabilization.

Linear phase-lead stabilization was rejected because of its inability to provide satisfactory compensation through the descent stage range of inertias and thrust levels. Uncompensated (unstable) trim systems were rejected in favor of the stabilized trim systems. The uncompensated trim systems cause an increased RCS duty factor and propellant expenditure during attitude limit cycles because they induce a de-stabilizing influence on the attitude. It has been estimated (Ref. 32) that an uncompensated trim system would cause the expenditure of an extra 45 to 75 pounds of RCS propellant in addition to increasing the number of operating cycles of the reaction jet thrusters, and would require tight tolerance levels for the actuation signal response.

Closed loop trim systems were rejected because of their inherent dependence on the reliability and accuracy of feedback sensors, and the additional complication of required integral compensation.

Proportional gimballed engine actuators were rejected in favor of on-off irreversible drive actuators, which have superior reliability weight, and power consumption factors. For the same reasons, a fast response gimballed engine LEM attitude control system was rejected in favor of a slow response gimballed engine trim system, and other trim techniques (fuel management, addition RCS jets, etc.) were rejected in favor of the gimballed engine.

Because of the structural geometric constraints on the ascent stage configuration, ascent thrust vector trim techniques of engine gimbaling and fuel management can be readily proven impractical. However, the predicted torque unbalance magnitude during powered ascent is well within the control capability of the RCS jet thrusters. Thus, the existing RCS jets will be employed for powered ascent thrust vector control.

~~CONFIDENTIAL~~

SECTION 6

ATTITUDE CONTROL WITH GUIDANCE FEEDBACK

~~CONFIDENTIAL~~



SYMBOLS USED IN SECTION 6

<u>Symbol</u>	<u>Definition</u>	<u>Units</u>
A	accelerometer constant	ft/sec
B	accelerometer damping coefficient	ft-lb-sec/rad
e	modulator input signal	rad
$\bar{e}$	attitude error plus integral compensation	rad
$f_P$	pulse repetition frequency	pulses/sec
$f_O$	minimum pulse repetition frequency	pulses/sec
F	reaction jet thrust	lb
G	integral compensation gain	sec <sup>-1</sup>
I	vehicle moment of inertia	slug-ft <sup>2</sup>
K	combined reaction jet and modulator gain	ft-lbs/rad
$K_R$	rate gyro gain constant	sec
$K_\Theta$	attitude feedback gain	---
$l$	accelerometer distance to c.g.	ft
L	reaction jet moment arm	ft
m	accelerometer pendulosity	lb-sec <sup>2</sup> /rad
M	vehicle mass	slugs
P	limit cycle period	sec
t	time	sec
$T_{RC}$	reaction jet torque	ft-lb
$T_U$	unbalance torque	ft-lb
$T_w$	pulse width	sec
X,Y,Z	spacecraft axes (See Figure 2-1)	---
$\ddot{Z}$	Z axis acceleration	ft/sec <sup>2</sup>

~~CONFIDENTIAL~~SYMBOLS USED IN SECTION 6 (Continued)

<u>Symbol</u>	<u>Definition</u>	<u>Units</u>
$\alpha$	lead network constant	---
$\alpha_t$	thrust to mass ratio	ft/sec <sup>2</sup>
$\alpha'_t$	earth g's	ft/sec <sup>2</sup>
$\epsilon$	attitude error	rad
$\dot{\epsilon}$	attitude error rate	rad/sec
$\theta$	vehicle attitude	rad
$\theta'$	quantized attitude feedback	rad
$\theta_c$	attitude command	rad
$\dot{\theta}$	vehicle attitude rate	rad/sec
$T$	pendulous accelerometer time constant	sec
$T_1$	lead network time constant	sec
$\Omega$	forward loop deadband	rad

Code 26512 Eng-23-1A

### 6.1 - Introduction

In all previous analyses and discussions the effects of guidance attitude feedback on the attitude control loop were neglected. Some of these control problems are considered herein. They are:

- a) Control of attitude errors generated during powered ascent due to c.g. offset (integral compensation).
- b) Thrust vector control by abort guidance during powered ascent (pendulous accelerometer).
- c) Attitude control by use of a quantized attitude feedback signal (strap down gyro guidance feasibility study).

Each of the above is discussed separately, in detail, in the following:

### 6.2 - Integral Compensation ( $T_1$ Abort Guidance Law)

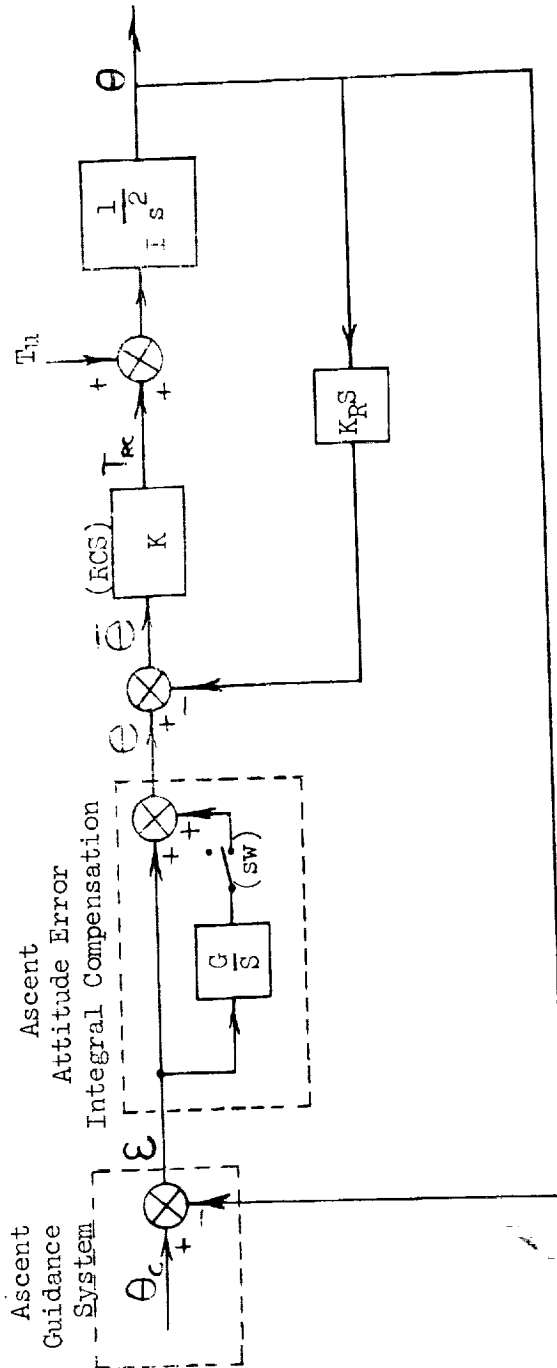
During the powered ascent phase of the LEM mission, the ascent engine thrust axis will remain fixed with respect to the LEM "X" body axis. However, even if the thrust axis is perfectly aligned with the "X" body axis, the probable c.g. offset will produce a substantial thrust-induced torque on the vehicle. The RCS cannot counter-balance this torque without causing small quasi-steady-state LEM attitude errors on the order of a few tenths of a degree. Since this level of attitude error must be reduced, to meet AGS  $T_1$  Compensation Law requirements, integral compensation (16) is required for powered ascent when using the AGS for guidance.

A block diagram of the planar LEM attitude control system is presented in Figure 6-1. Without integral compensation (switch open; Figure 6-1), a steady torque unbalance ( $T_u$ ) will produce a steady state vehicle attitude error ( $\theta_{ss}$ ) given by,

$$\theta_{ss} = \frac{T_u}{K} + \Omega$$

where  $K$  represents the linearized RCS gain and  $\Omega$  represents the deadzone. With integral compensation (switch closed), the steady state attitude error is zero.

While integral compensation will provide the desired attitude error magnitude during the powered ascent phase, it would be desirable to know that this integral compensation does not deteriorate system



Linearized  
Characteristics =  $1 + \frac{KG}{s^3} \left( \frac{K_R s^2}{G} + \frac{s}{G} + 1 \right) \approx 1 + \frac{KG}{s^3} \left( \frac{s}{G} + 1 \right) (K_R s + 1)$  If  $GK_R \ll 1$   
Equation

$$T_{RC} \text{ (Linearized)} = K, \quad K = \frac{(100 \text{ lb}) (11 \text{ ft})}{0.5} = 126,000 \frac{\text{ft-lb}}{\text{rad}}$$

$$G = 0.3 \text{ sec}^{-1}, \quad K_R = 0.3 \text{ sec}, \quad I = 2200 \text{ slug-ft}^2$$

Figure 6-1 Schematic of planar RCS attitude control with attitude error integral compensation

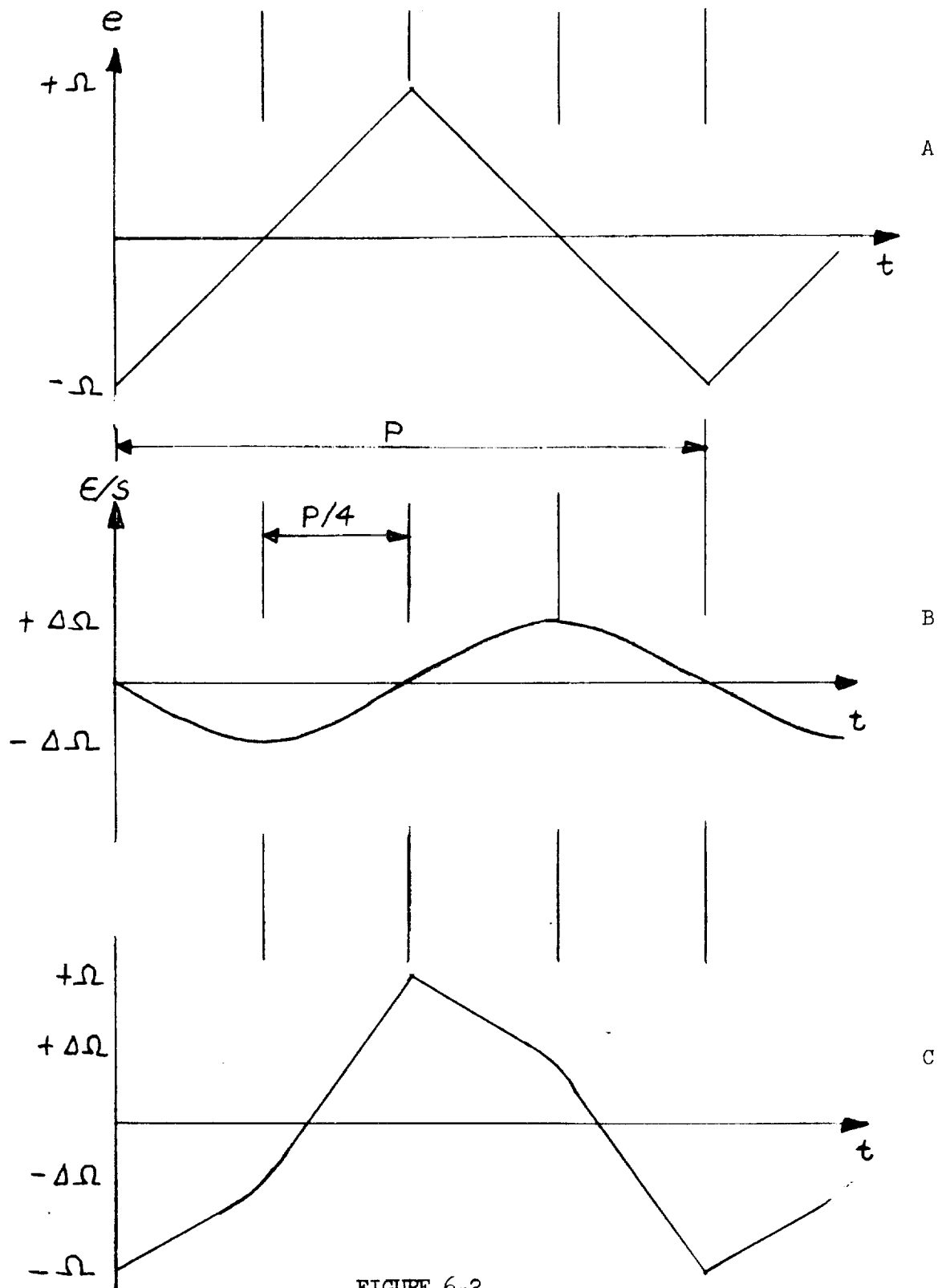


FIGURE 6-2

INTEGRAL COMPENSATION EFFECT ON LIMIT CYCLE ERROR SIGNAL

~~CONFIDENTIAL~~

performance during other phases of operation, thus precluding the necessity of special switching. Therefore, the effect of integral compensation on RCS limit cycle characteristics during the coasting phase was considered.

Figure 6-2A illustrates the LEM attitude error ( $\epsilon$ ) as the RCS constrains the attitude within the error deadzone limits ( $\pm\Omega$ ). The integral compensation will operate on this error signal to produce an output ( $\epsilon/s$ ) as shown in Figure 6-2B. The maximum value of the output ( $\Delta\Omega$ ) of the integral compensation can be calculated:

$$\Delta\Omega = G \int_0^{P/4} \epsilon(t) dt = G \dot{\epsilon} \int_0^{P/4} t dt$$

$$\Delta\Omega = G \dot{\epsilon} \left. \frac{t^2}{2} \right|_0^{P/4} = G \dot{\epsilon} P^2/32$$

$$\text{But } \dot{\epsilon} = 4/p$$

$$\therefore \Delta\Omega = \Omega GP/8$$

Inspection of the input to the RCS, Figure 6-2C, shows that to avoid deteriorating the limit cycle,

$$\frac{\Delta\Omega}{\Omega} \ll 1$$

$$\text{Thus } \frac{GP}{8} \ll 1$$

For the same reasons the maximum absolute rate of change of  $\frac{G\epsilon}{s}$  should be much less than the rate of change of  $\epsilon$ .

$$\text{i.e. } \frac{d}{dt} \left[ G \dot{\epsilon} \frac{t^2}{2} \right] \bigg|_{t=P/4} \ll \frac{E}{P/4}$$

$$\text{Thus } \frac{GP}{4} \ll 1$$

This last criteria, being the more stringent, would control. Therefore, in order to insure no deterioration of the RCS duty cycle by the integral compensation during coasting, the limit cycle period (P) must be

$$P \ll 13.3 \text{ (seconds)}$$

if the integral gain is 0.3.

Code 26512 Eng-23-1A

~~CONFIDENTIAL~~

TABLE 6 - 1SYSTEM CONSTANTS

$$K = 138,000 \text{ ft-lb/rad}$$

$$K_{\theta} = 1$$

<u>Case</u>	<u><math>\alpha_T</math> (ft/sec<sup>2</sup>)</u>	<u><math>I_T</math> (slug-ft<sup>2</sup>)</u>	<u><math>K_r</math> (sec)</u>	<u>X c.g. (in)</u>	<u><math>l</math> (ft)</u>
1) Hohmann orbit	13.7	18,700	0.5	187	-9.25
2) Hover	5.3	10,000	0.5	212	-7.15
3) Liftoff	14.6	2,800	0.2	245	-4.42
4) Burnout	30.0	2,100	0.2	245	-4.42

$$\text{Navigation base } X = 298''$$

$$\therefore l = -X + X_{cg}$$

~~CONFIDENTIAL~~

An integral compensation gain of 0.3 was selected as providing reasonably rapid error compensation without causing unacceptable phase lag. This error reduction time constant of 3.3 seconds will cut attitude error to 40% in 3 seconds, and 5% in 10 seconds.

The ascent coasting phase limit cycle period of rotation for  $\pm 1/10^\circ$  deadzone under consideration is about 3 to 6 seconds, depending upon the axis. When the deadzone is increased to  $\pm 5^\circ$  for minimum propellant consumption, the limit cycle period is measured in minutes. Limit cycle periods are substantially longer during the descent coasting phase, but powered descent phase limit cycle period is only one to three seconds (self stabilized trim system). Therefore, if integral compensation is required to reduce the steady-state attitude errors during the thrusting ascent phase, it must be inoperative during the coasting phases of ascent and descent. It is also desirable to have it inoperative during powered descent since the gimbal trim system will remove any attitude offset during powered descent and since integral compensation is destabilizing.

Therefore, if AGS tolerance limits for vehicle attitude bias errors are smaller than can be achieved with the uncompensated control system, it will be necessary to use integral compensation during ascent thrusting. This compensation network must be switched out for all coasting flight phases and descent thrusting phases.

### 6.3 - Pendulous Accelerometer Study (T<sub>1</sub> Abort Guidance Law)

For accurate control of the LEM trajectory in the abort guidance mode, information as to the relative positions of the controlling thrust vector and the vehicle body axes is required. If the thrust vector is misaligned, extraneous accelerations, which would induce position and velocity errors, will be introduced. A pendulous accelerometer (17) (18) has been considered for use in the Abort Guidance System (AGS) in order to correct for thrust vector misalignment when using the T<sub>1</sub> guidance law.

The method previously considered for correction employed a lateral accelerometer. This method generated a single correcting signal (assuming a constant error), and all errors accruing after this one correction would remain within the system. The pendulous accelerometer has the capability of monitoring both "Z" and "X" acceleration, thus continuously measuring any thrust vector offset angle.

Steady state attitude errors due to the thrust vector not passing through the vehicle C. G. have not been included in this analysis because,

- a) the pendulous accelerometer feedback has no effect upon this steady state angle.

~~CONFIDENTIAL~~



- b) this error will be eliminated through the use of integral compensation as described in section 6.2.

It is also assumed that operation will occur in the linear region of the RCS.

Four distinct phases of the mission have been considered --- Hohmann orbit, hover, liftoff and burnout (the attitude control system is shown with accelerometer dynamics in Figure 6-3). For all four cases, the pendulous accelerometer, which will be mounted on the navigation base, is above the vehicle C.G. This configuration could lead to possible instabilities, and therefore, the values of accelerometer constants which are necessary and sufficient to guarantee stable operation must be determined by analyzing the open loop transfer function.

The open loop transfer function can be shown to be (from Figures 6-3 and 6-4).

$$G H = \frac{K}{Is^2} (K_{\theta} + K_r s) + \frac{(\ddot{Z} + \ell s^2)}{T (\tau s + \ell)} \quad (6-1)$$

where

$K \equiv$  linear PRM gain.

$\tau \equiv$  pendulous accelerometer time constant (17)

$\equiv B/m\ell' \alpha_t'$

$B \equiv$  accelerometer damping coefficient

$m\ell' \equiv$  accelerometer pendulosity

$\alpha_t' \equiv$  earth g's

$\alpha_t \equiv$  thrust to mass ratio -  $T/M$

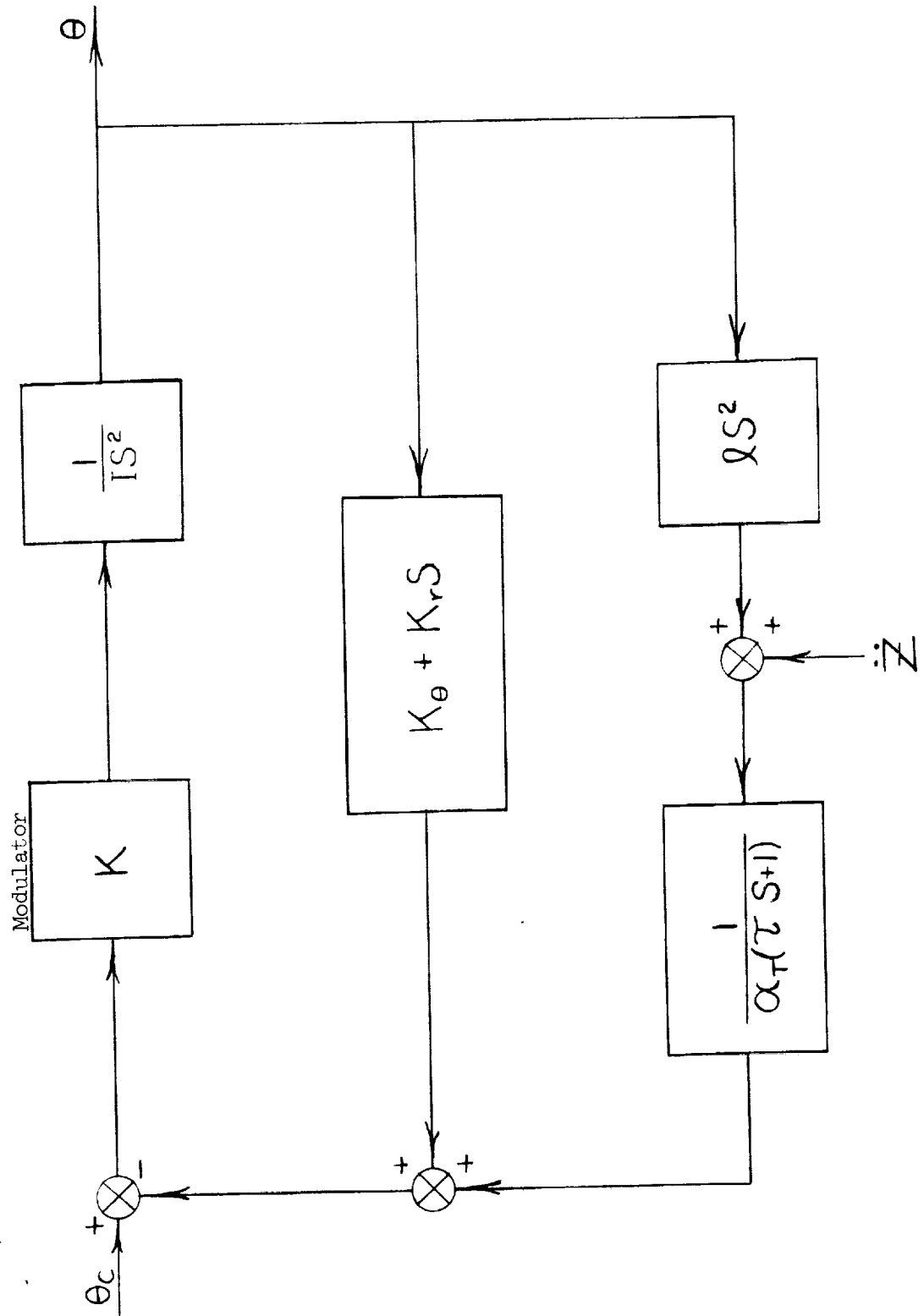
The first order lag representation of the accelerometer is due to the assumption that it will be more than critically damped. Rearranging equation (6-1) we get,

$$GH = \frac{K (\ell + AK_r)}{AI} \frac{s^2 + s \left[ \frac{(AK_{\theta} + K_r T/M)}{\ell + AK_r} \right] + \frac{K_{\theta} T/M}{\ell + AK_r}}{s^2 (s + T/MA)} \quad (6-2)$$

$$\text{where } \alpha_t' = \frac{1}{32.2} \frac{T}{M} \quad (6-3)$$

$$\text{and } A = 32.2 \frac{B}{m\ell'} \quad (6-4)$$

FIGURE 6-3 ATTITUDE CONTROL SYSTEM WITH PENDULOUS ACCELEROMETER



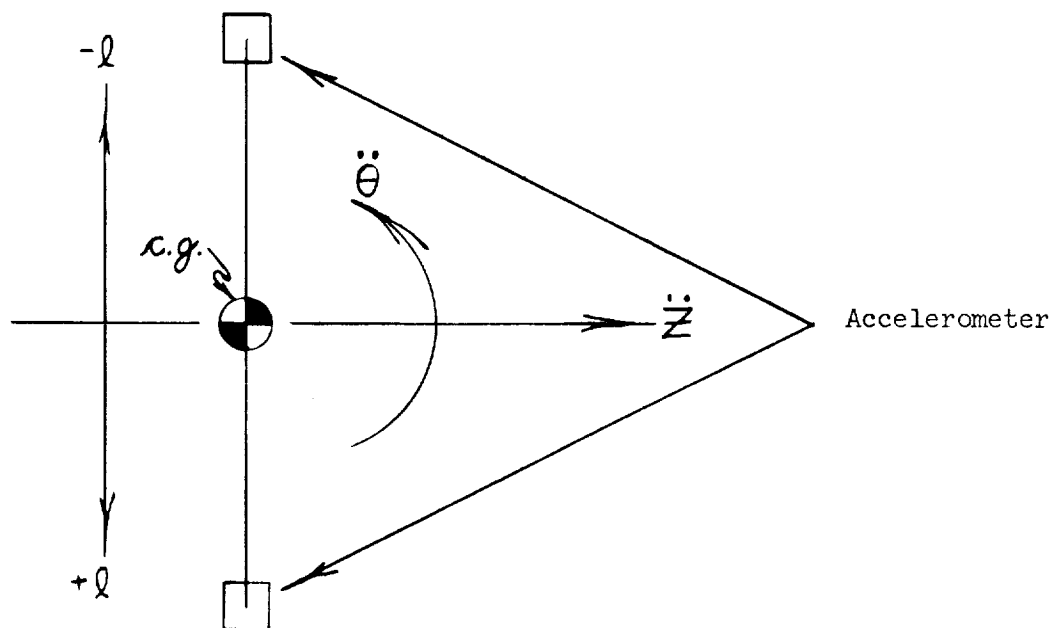


Figure 6-4 Accelerometer locations

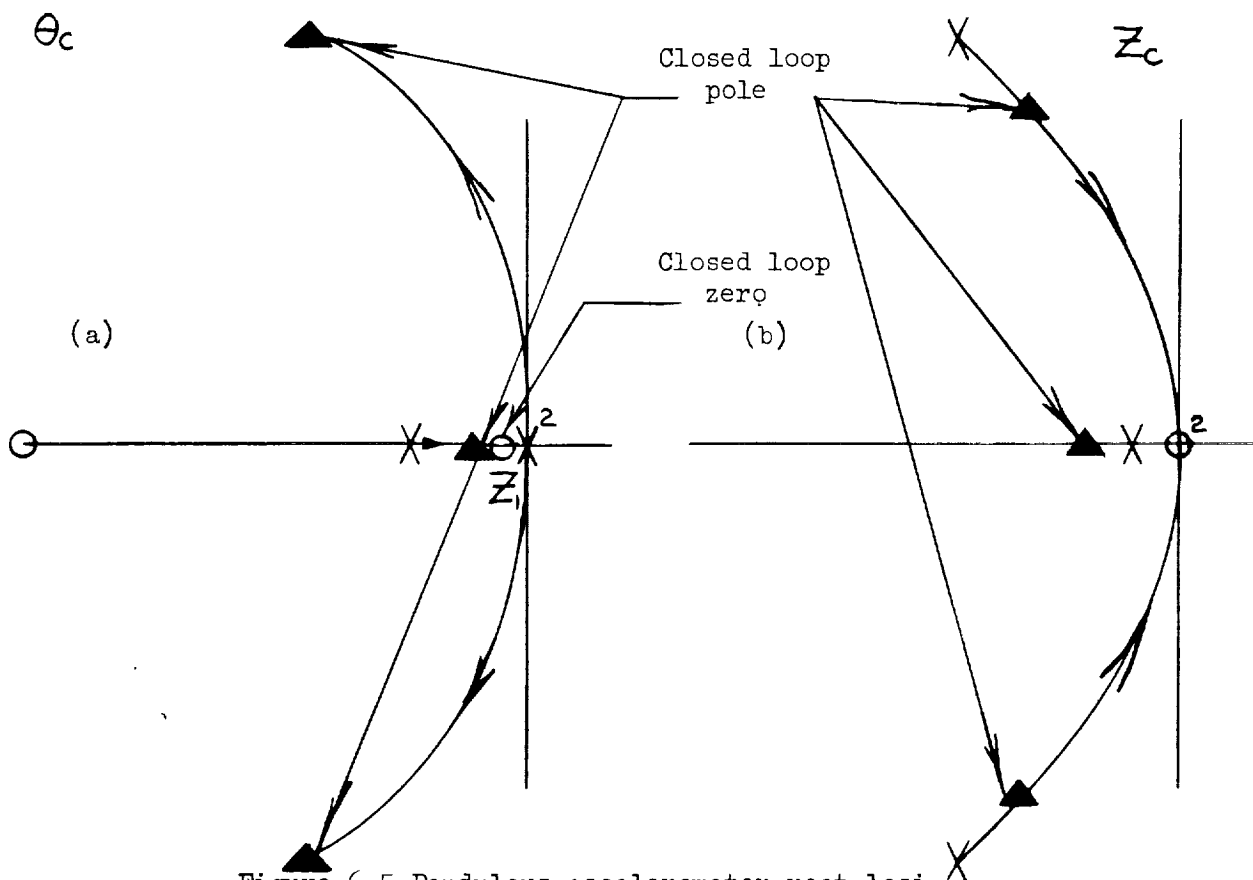


Figure 6-5 Pendulous accelerometer root loci

~~CONFIDENTIAL~~

such that  $\tau$  can be expressed as  $\frac{A}{T/M}$ .

If we define the following quantities

$$Z \equiv l + K_r A$$

$$K^* \equiv KZ/IA$$

$$\omega_1 \equiv \frac{T/M}{A}$$

$$M \equiv (AK_\theta + K_r T/M)/Z$$

$$N \equiv (K_\theta T/M)/Z$$

we can express equation (6-2) as follows,

$$GH = K^* \frac{s^2 + Ms + N}{s^2 (s + \omega_1)} \quad (6-5)$$

The characteristic equation  $(1 + GH)$  of the system can now be determined, and its roots checked to determine system stability. The equation is,

$$s^3 + (K^* + \omega_1)s^2 + K^*Ms + K^*N = 0 \quad (6-6)$$

Necessary conditions for stability require that all the coefficients of the characteristic equation be of the same sign. Since  $l$  is the only quantity that can be negative it can be seen that,

$$K^* + \omega_1 > 0 \quad (6-7)$$

because  $K^*M$  and  $K^*N$  are positive definite. Substituting system parameters, the following restriction on accelerometer constant  $A$  is obtained,

$$A > - \frac{(IT/K M + l)}{K_r} \quad (6-8)$$

Considering the four cases as presented in Table 6-1, the following restrictions are placed on  $A$ .

- a) case 1  $A > 14.8$
- b) case 2  $A > 13.54$
- c) case 3  $A > 20.6$
- d) case 4  $A > 19.8$

To test the sufficiency of the above values, consider the Routh array of the coefficients of the characteristic equation,

$s^3$	1	$K^*M$
$s^2$	$K^* + \omega_1$	$K^*N$
$s^1$	$\frac{(K^* + \omega_1)(K^*M) - K^*N}{K^* + \omega_1}$	0
$s^0$	$K^*N$	

$$\text{We get } (K^* + \omega_1)(K^*M) - K^*N > 0$$

~~CONFIDENTIAL~~

Substituting values for the constants and simplifying we get,

$$(A + K_r T/M) (KZ + IT/M) > K_c IAT/M \quad (6-9)$$

but,  $Z = l + K_r A$  and  $K_\theta = 1$ . Therefore, in order for  $Z > 0$

$$A > l/K_r \quad (6-10)$$

The value of A given by equation 6-8 is less than the value given by equation 6-10. By making 6-10 the governing equation, stable operation is guaranteed because from 6-9 we have,

$$IAT/M + [K_r KZT/M + AKZ + IK_r (T/M)^2] > IAT/M \quad (6-11)$$

is necessary and sufficient. Therefore, the values of A for the four cases considered are,

- a) case 1  $A > 18.5$
- b) case 2  $A > 14.3$
- c) case 3  $A > 22.1$
- d) case 4  $A > 22.1$

A root locus sketch of the system shows the responsiveness of  $\theta$  to a  $\theta$  and  $Z$  input signal. For a  $\theta_c$  command,  $Z_1$  is a closed loop zero (Figure 6-5a). The closed loop pole and zero can be seen (Figure 6-5a) to be almost equal making the residue of this pole approximately zero. The dominant poles are therefore, the complex pair. The accelerometer has, therefore, relatively little effect on the response of  $\theta$  to a  $\theta_c$  input. To see the effect of a  $Z$  command on  $\theta$  we refer to Figure 6-5b. There is no pole in the open loop feedback path to become a zero in the closed loop system. Thus, the real operating point becomes the dominant pole.

A parametric study to show the position of the roots of equation 6-6 as "A" varied was performed. The system time constant was assumed to be entirely due to the real pole, while a damping coefficient was calculated for the complex roots. Figure 6-6 represents a graph of the system time constants and the minimum damping available in any of the four cases as functions of the accelerometer constant A.

The pendulous accelerometer was proposed to provide continuous correction for errors induced due to thrust vector misalignment. A range of accelerometer constants has been determined which will provide adequate system response and also guarantee sufficient damping. An accelerometer constant between 50-150 is recommended for fast system response in high T/M phases (cases 1, 3 & 4) and sufficient damping ( $\zeta > 0.4$ ).

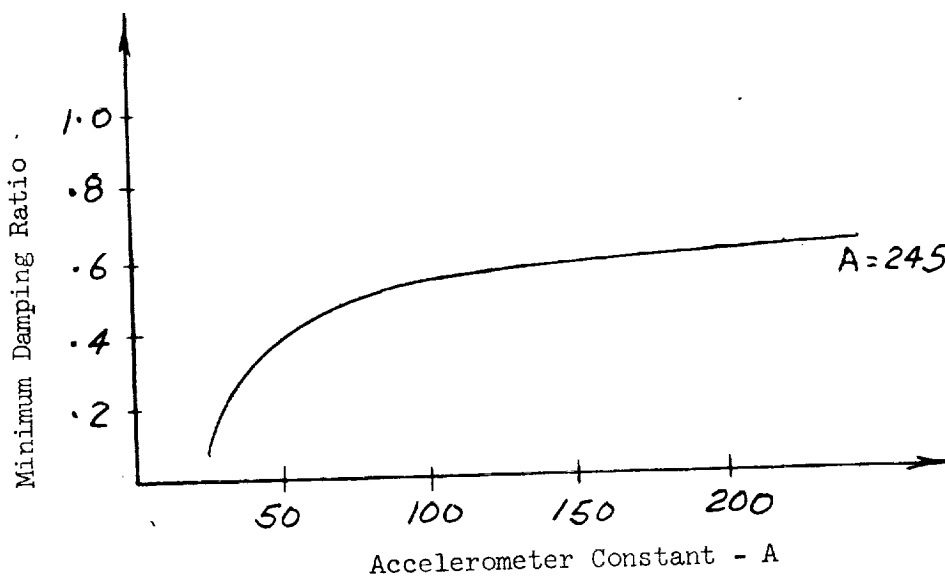
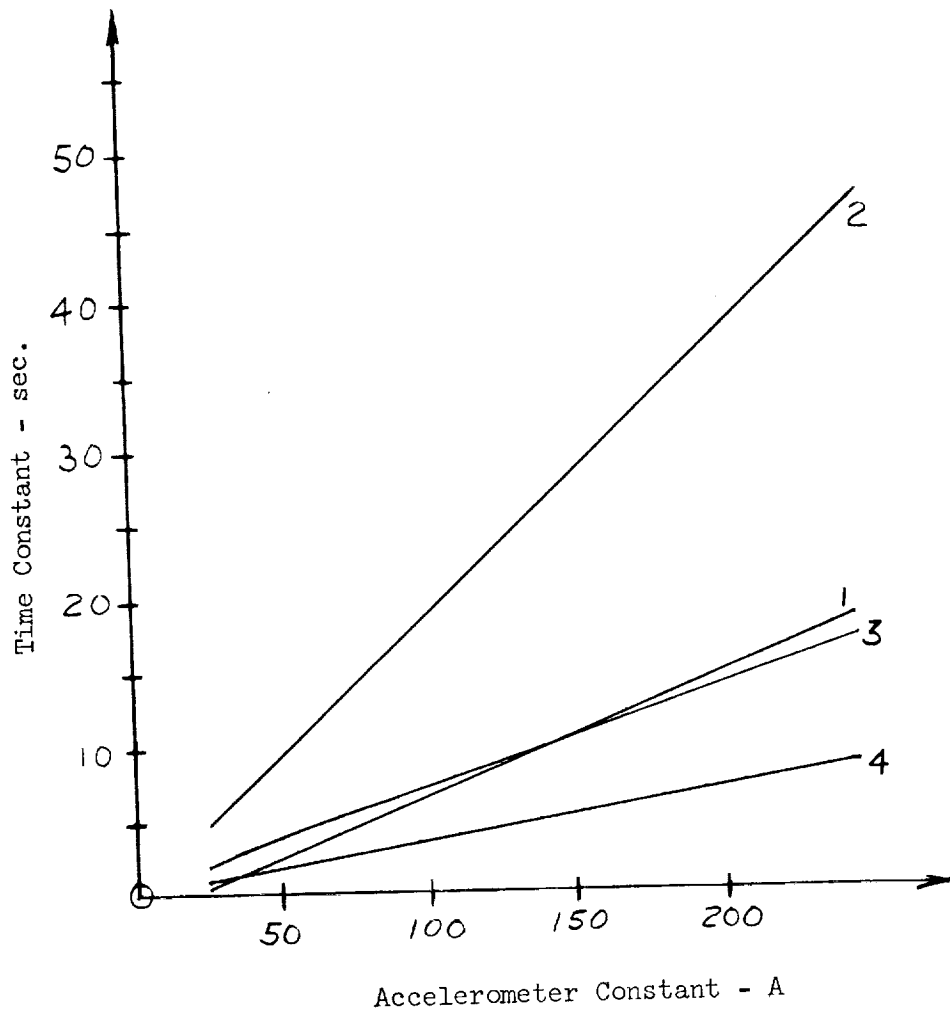


Figure 6-6 Accelerometer constant  $\sqrt{v}$  versus minimum damping ratio and time constant

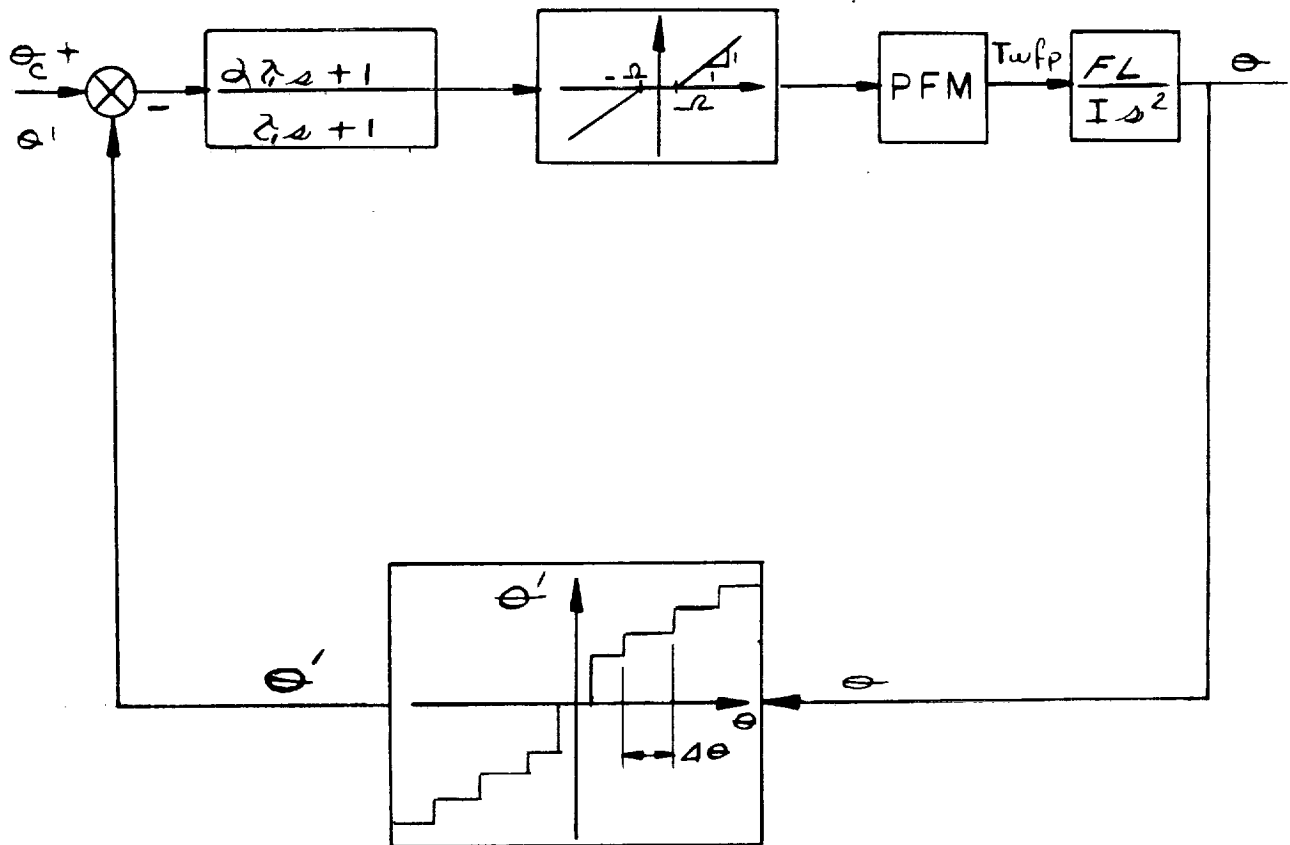


Figure 6-7 Quantized attitude control system

**CONFIDENTIAL**

#### 6.4 - Quantized Attitude Feedback (Strap-down Attitude Reference Feasibility Study)

Substitution of a quantized feedback signal (20) in place of the continuous attitude feedback signal for attitude control (Figure 6-7), in conjunction with a lead network to generate rate information, was studied. The use of quantized attitude information in conjunction with continuous rate feedback was also considered (Figure 6-9).

Three different levels of quantization were considered in this study to represent varying coarseness of attitude information (0.01, 0.03 and 0.08 degrees). The effect that quantization has on transient response and limit cycle operation of the system was investigated by means of an analog simulation. A PFM as shown in Figure 6-8, which yields limit characteristics identical to that of the PRM was used. Different values of  $f_0$  were used to satisfy moment unbalance requirements for various values of inertia, and the effect of  $f_0$  on limit cycle operation was noted.

It would be expected that the effect of quantization on transient response would be dependent upon the ratio of transient size to quantum size. The effect of quantization is expected to be negligible if this ratio is greater than 10. An example is shown in Figure 6-10 in which a 10 mr. transient step response is shown with and without quantization of 0.52 mr. (0.03 deg.). The ratio in this case is approximately 20:1 and the system behaves as predicted. For transients at least this large, it was found for smaller inertias, that for any of the three quantization levels considered, transient responses very similar to the continuous attitude case were produced.

Time histories showing the effects on limit cycle operation of a quantization of 0.03 deg. are shown in Figures 6-11 and 6-12. Both continuous and quantized limit cycle attitudes are plotted in the figures in order that a comparison can be made. It should be noted that the quantized limit cycle frequency and thereby fuel consumption is higher than the continuous system in both cases. Also noted, primarily in the large inertia case ( $I = 10,000$  slug-ft<sup>2</sup>), is that spikes generated by the lead network initiate premature reaction jet firings. The effects of quanta size on limit cycle frequency are summarized in Figure 6-13a.

It was established by an additional case ( $I = 2000$  slug-ft<sup>2</sup> and  $f_0 = 50$  PPS) that large increases in limit cycle frequency are produced by a combination of three effects which are:

- a) quantization of attitude information.
- b) use of lead network to derive rate information from quantized signal.
- c) use of PFM with large  $f_0$ .

If any of the above effects is missing the large limit cycle frequency will be reduced. The effect of  $f_0$  is clearly shown in Figure 6-13a while Figure 6-14 shows an improvement in limit cycle frequency, is obtained by substituting a continuous rate signal (Figure 6-9) with  $K_R = 0.4$  sec. for the lead network. When  $I = 10,000$  slug-ft<sup>2</sup> and  $f_0 = 50$  PPS with continuous rate, a marked decrease in limit cycle frequency to a value below that of  $I = 10,000$  slug-ft<sup>2</sup> and  $f_0 = 6.7$  PPS with rate generated by lead network (Figure 6-13b) is obtained. The use of a PFM with large  $f_0$  is precluded when a PRM is used for attitude control.

**CONFIDENTIAL**



~~CONFIDENTIAL~~

PAGE 174

It is evident from the above that quantization levels of up to 0.08 deg. can be tolerated without substantially affecting transient response for the range of inertias considered and that it is possible to utilize quantization values of at least 0.03 deg. without a great penalty in limit cycle propellant consumption provided that a continuous rate signal is used.

~~CONFIDENTIAL~~

GRUMMAN AIRCRAFT ENGINEERING CORPORATION

REPORT NO. LED-500-3

DATE 30 Sept. 1964

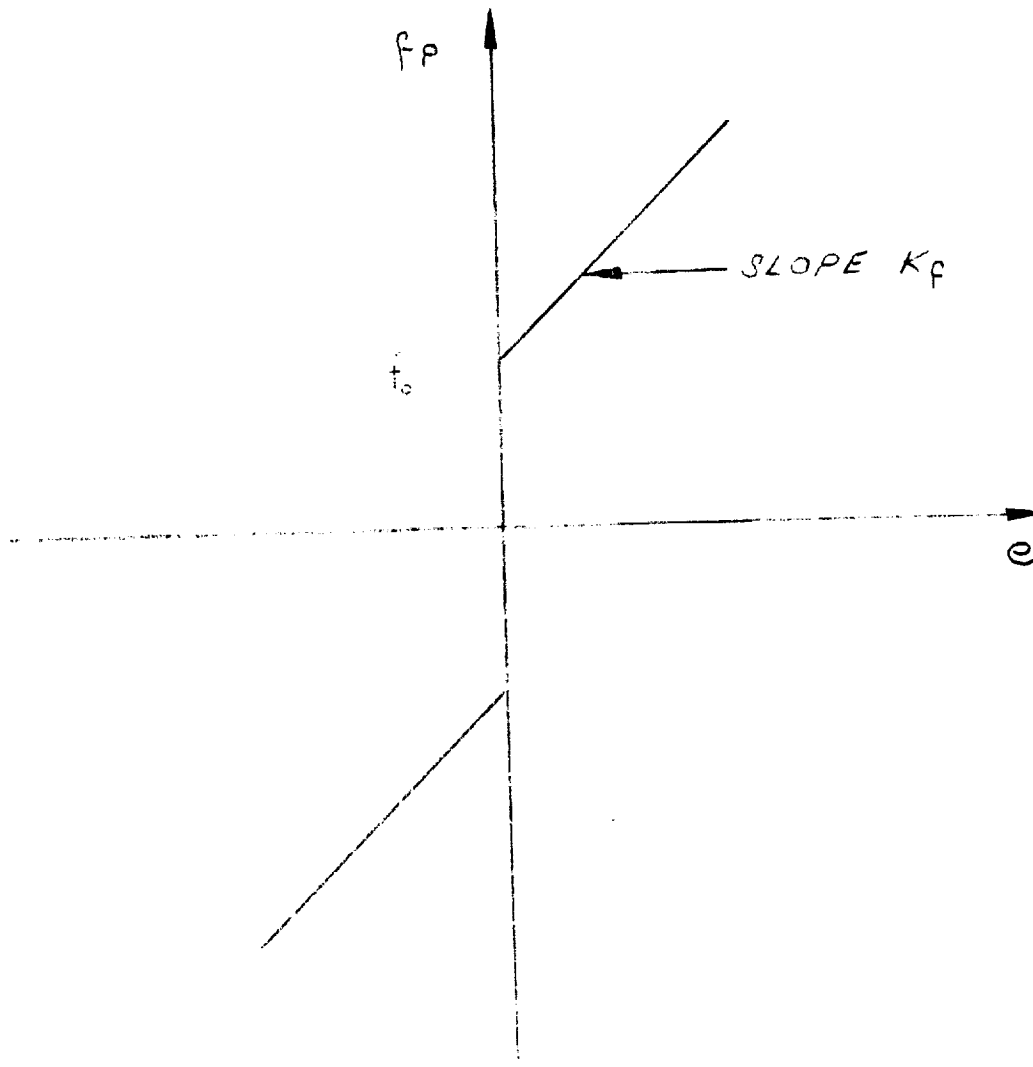


Figure 6-8 IFM characteristics assumed for quantized attitude control system

~~CONFIDENTIAL~~

PAGE 176

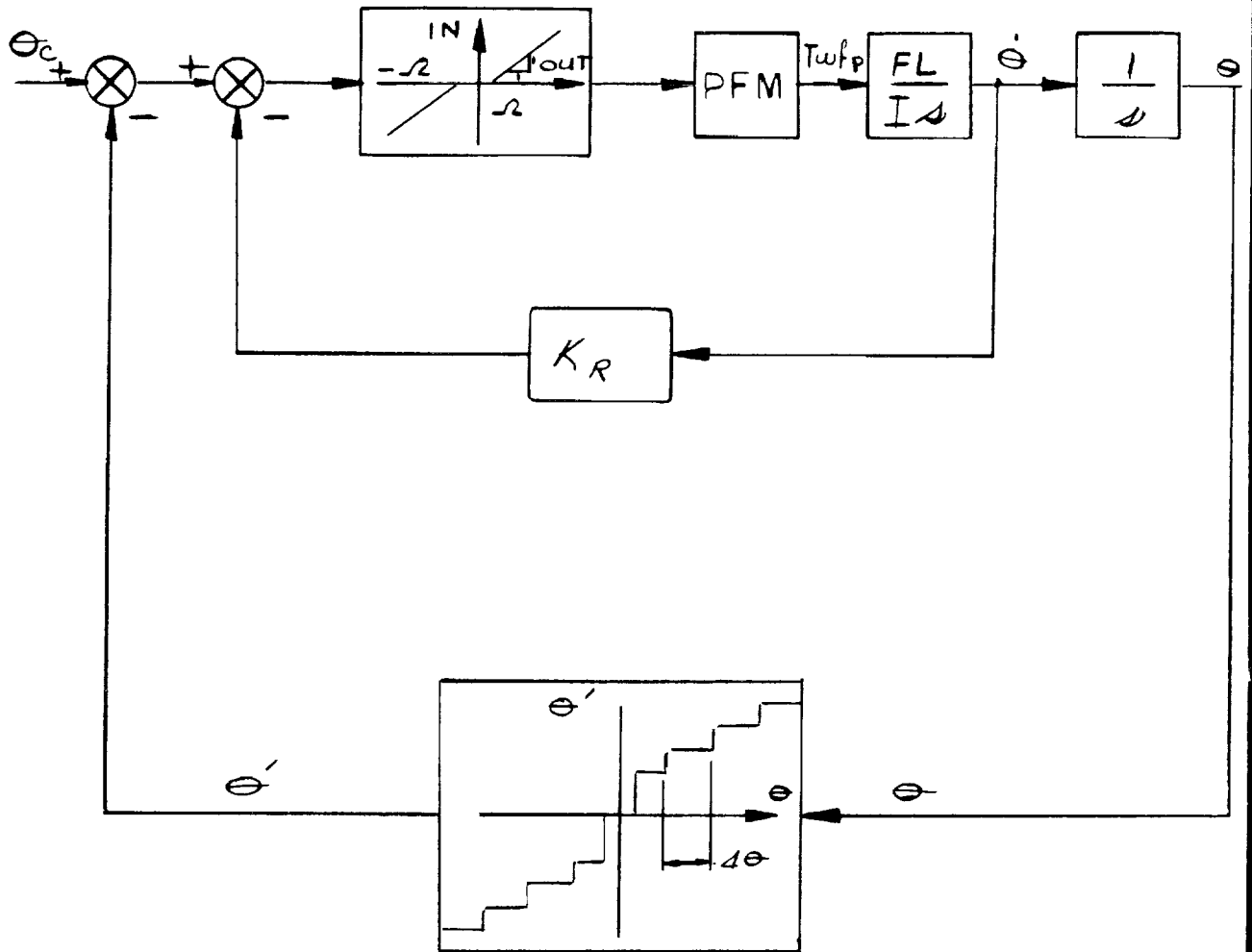
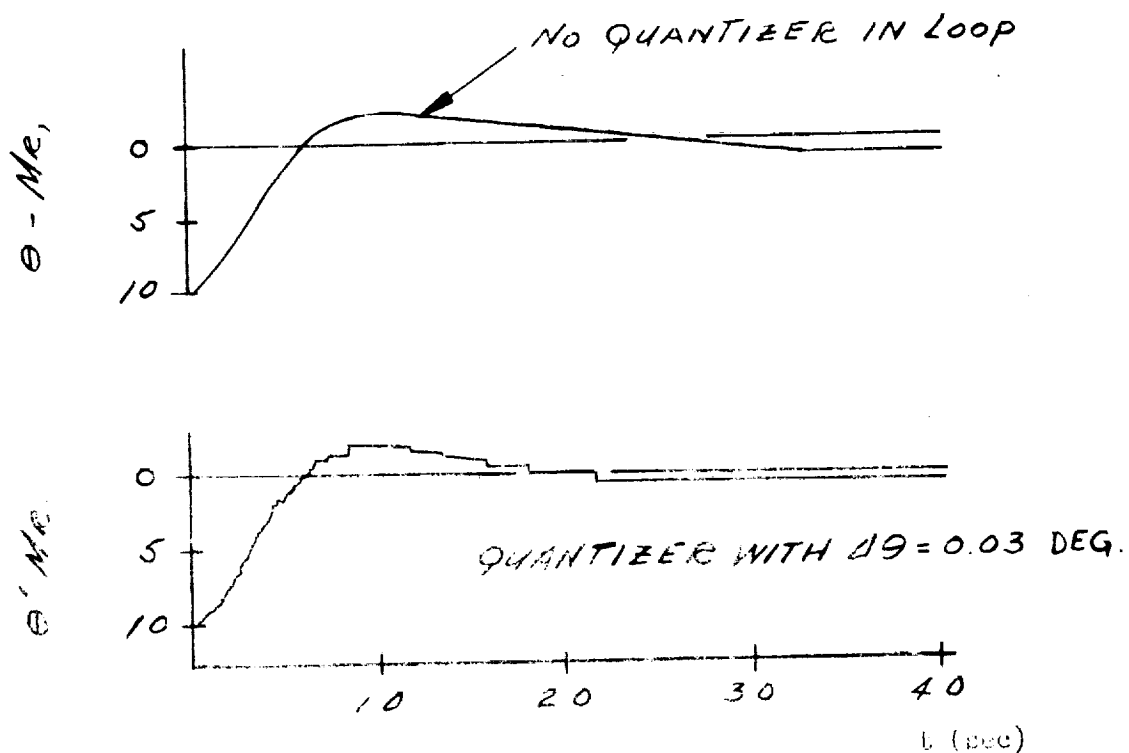


Figure 6-9 - Quantized attitude control system with continuous rate feedback

~~CONFIDENTIAL~~  
GRUMMAN AIRCRAFT ENGINEERING CORPORATION

REPORT IED-500-3  
DATE 30 Sept. 1964

Code 26512 Eng-23A



$I = 10,000 \text{ slug} \cdot \text{ft}^2$   
 $k_F = 11.7 \text{ PPS/mr.}$

Figure 6-10 Comparison of attitude response with quantized and unquantized angle feedback. (Rate generated by lead network)

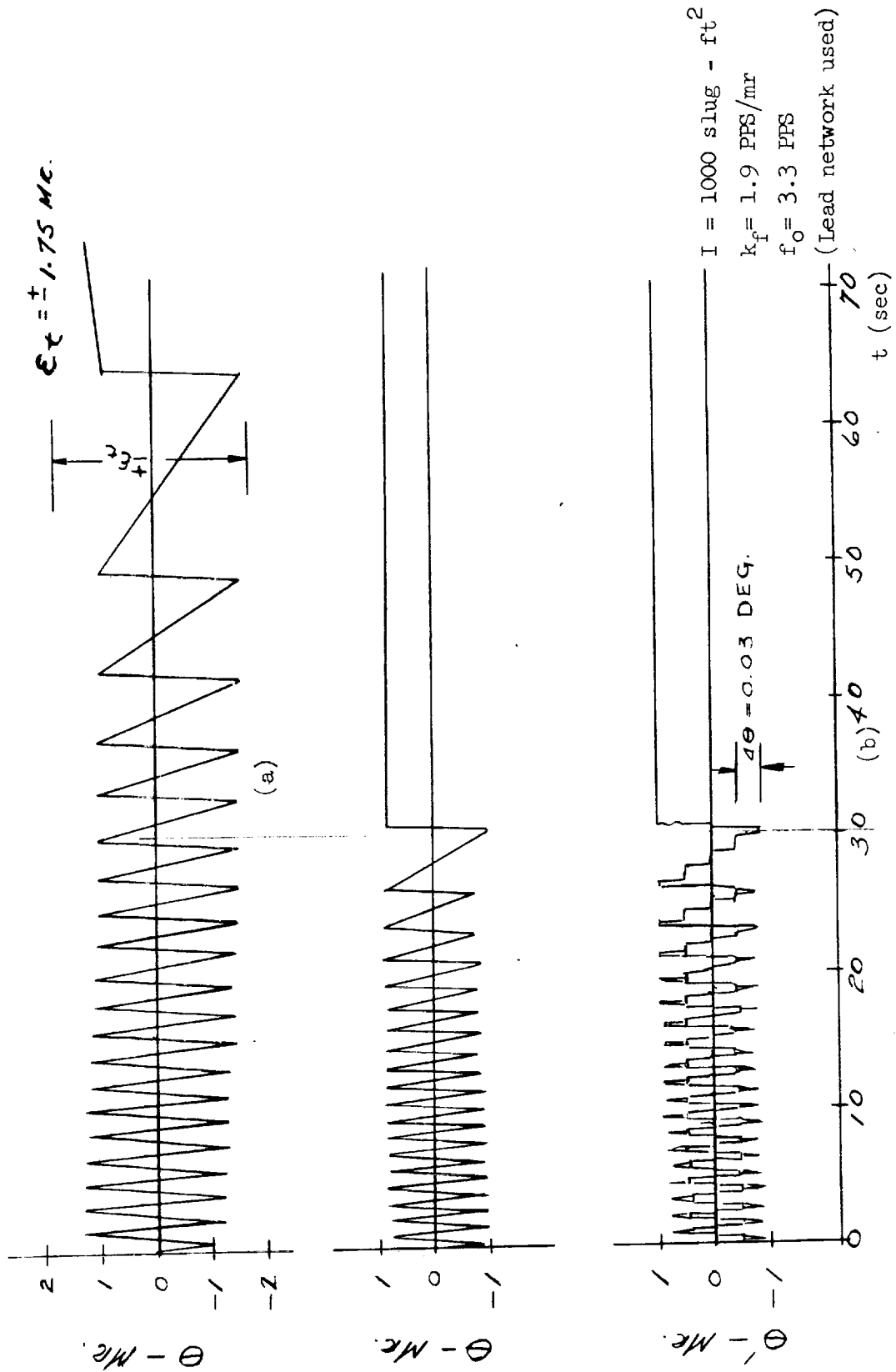


Figure 6-11 Typical limit cycles for continuous (a) and quantized (b) attitude hold mode

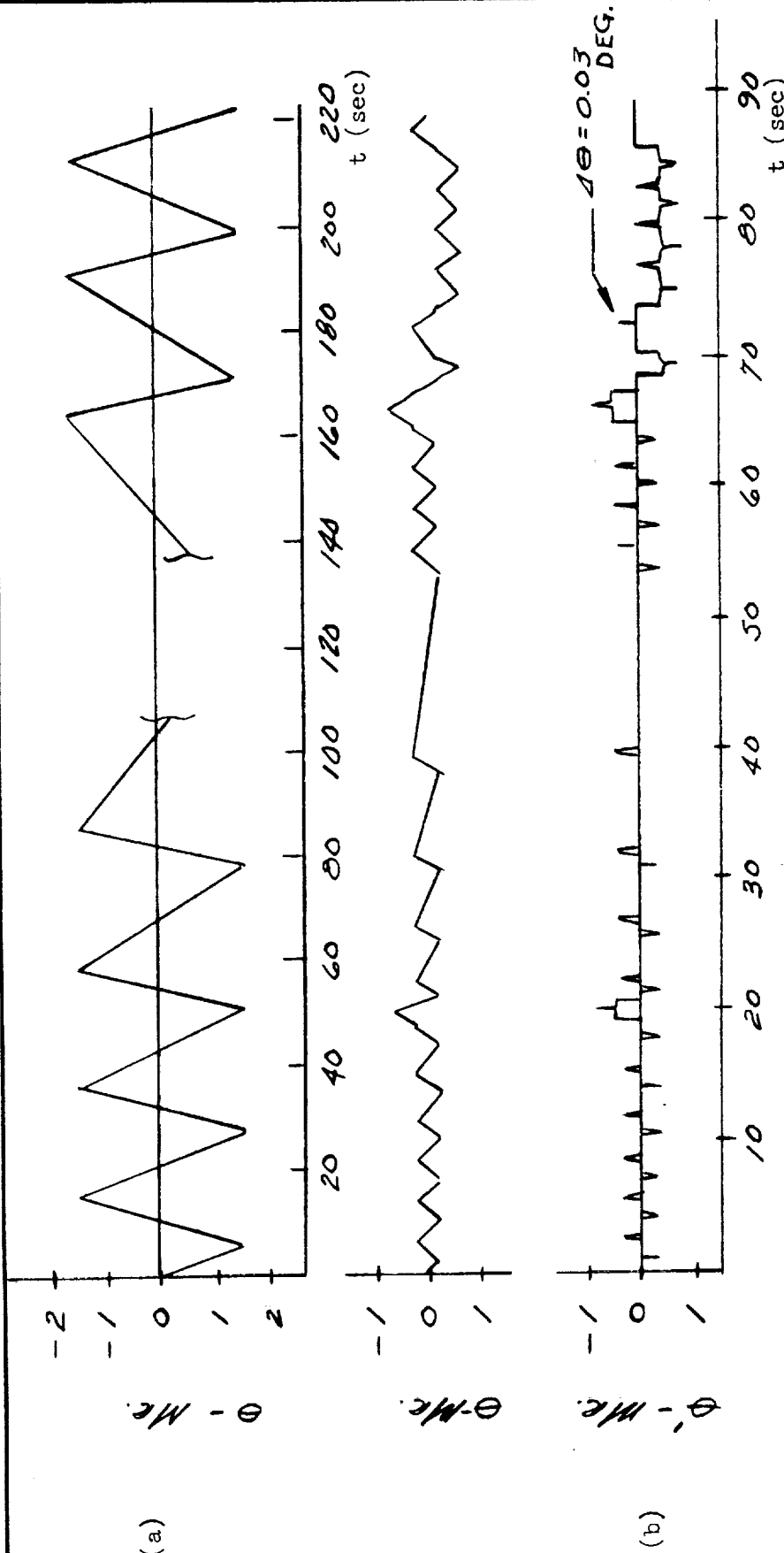
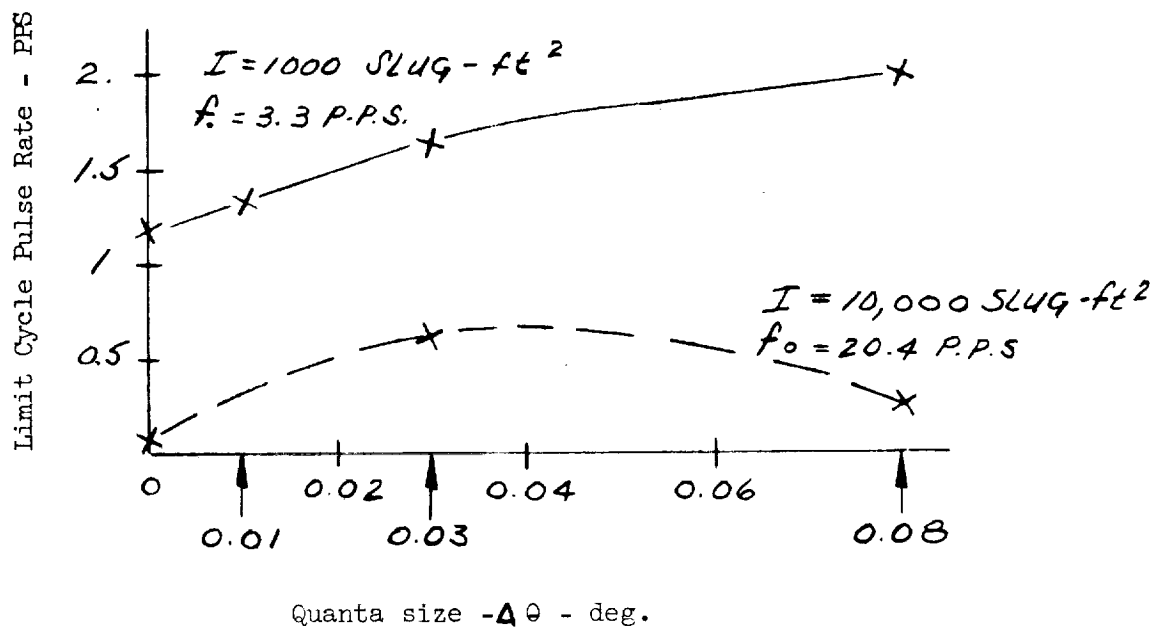
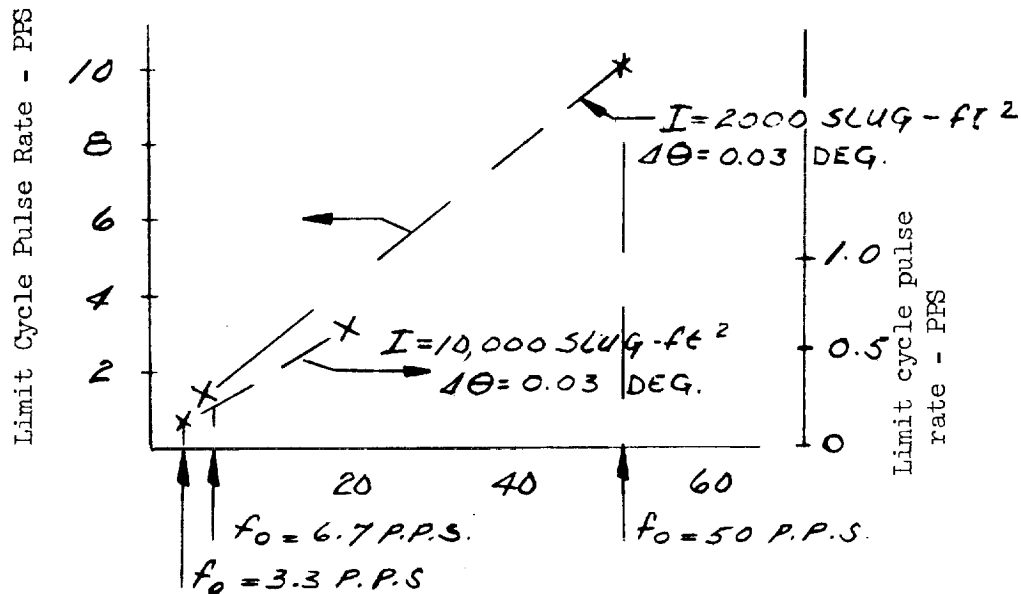


Figure 6-12 Limit cycling for the conditions:  $I = 10,000$  slug-ft<sup>2</sup>,  $k_f = 11.7$  PPS/mr and  $f_o = 20.4$  PPS - (a) continuous angle and (b) quantized angle (rate signal was derived from lead network)



(a)



(b)

Figure 6-13 - Effects of quantization size and minimum frequency on pulse frequency (rate signal derived from lead network)

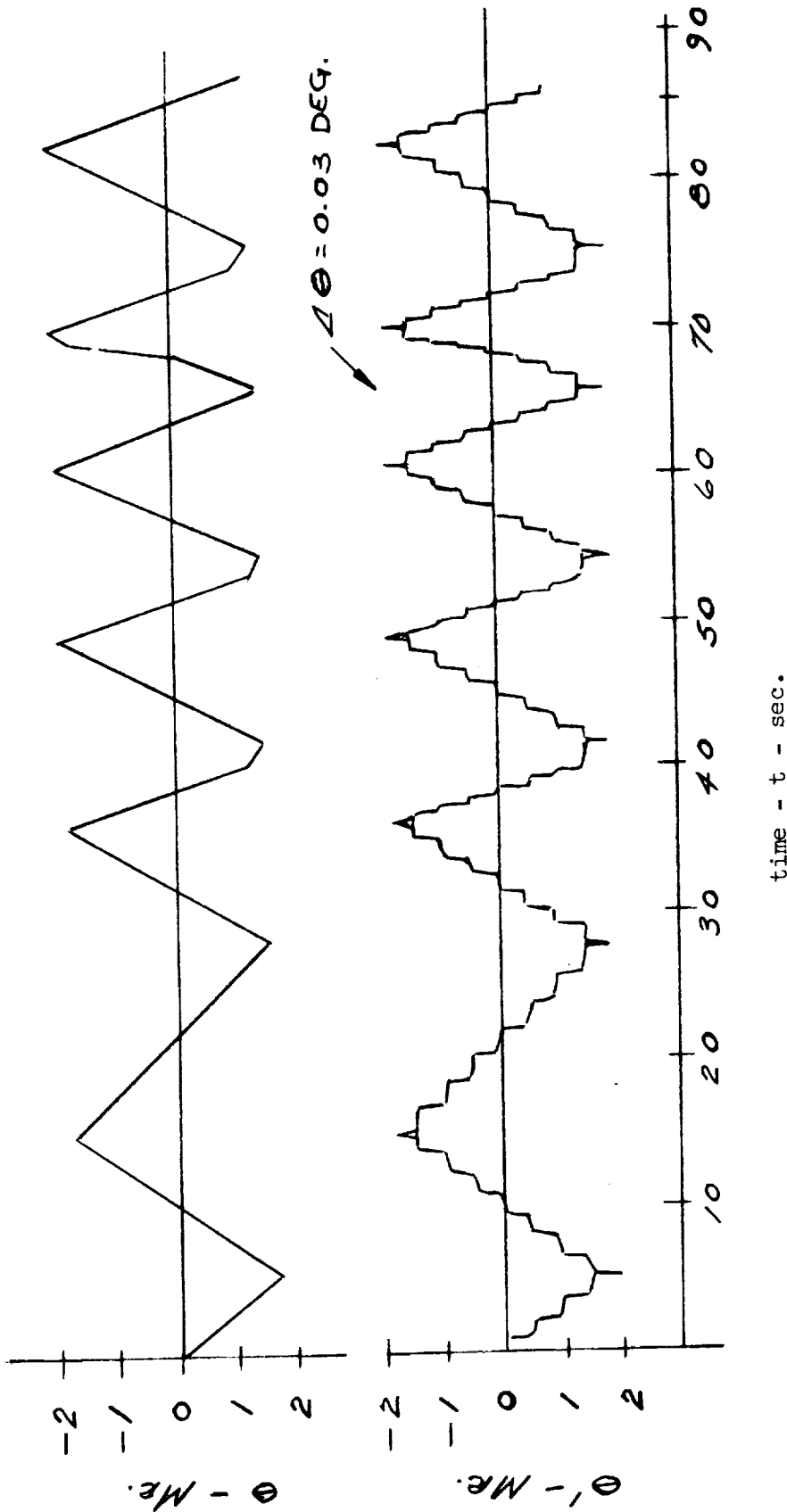


Figure 6-14 Limit cycling using quantized angle with continuous rate -  $I = 10,000 \text{ slug-ft}^2$ ,  $k_f = 11.7 \text{ PPS/mr}$ ,  
 $f_o = 20.4 \text{ PPS}$



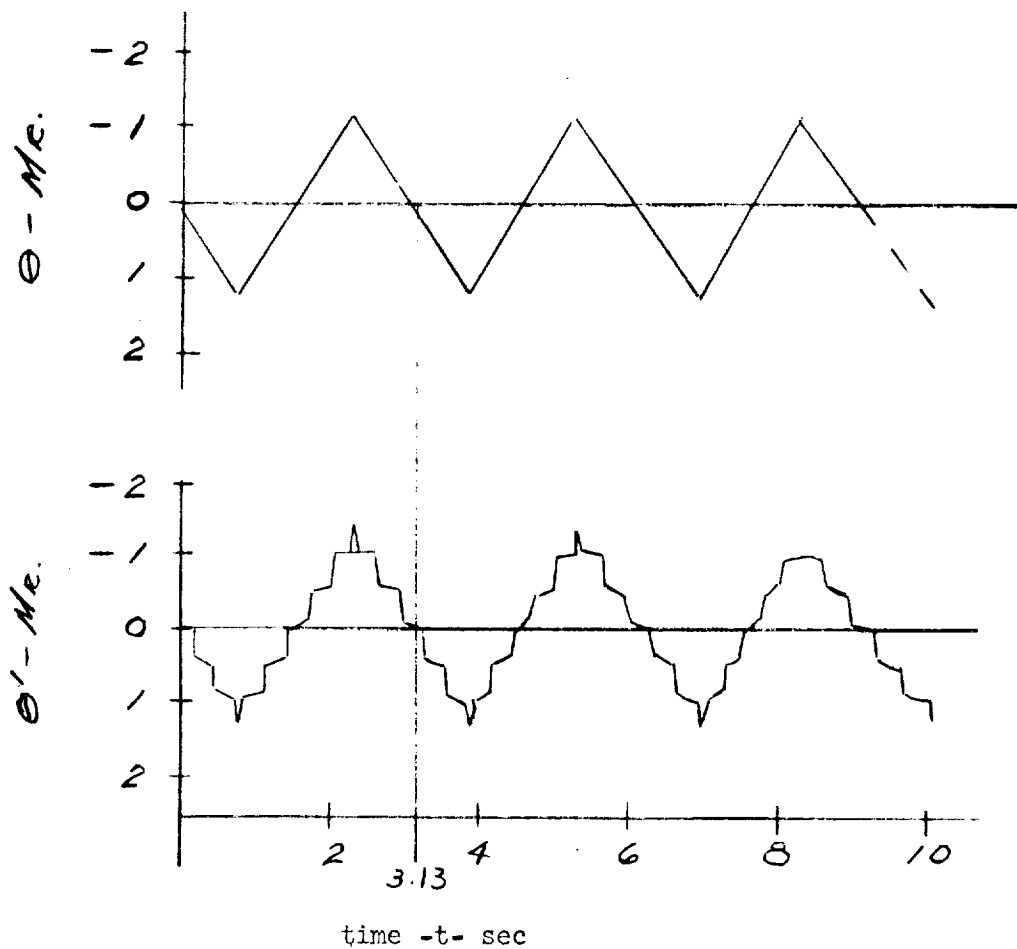


Figure 6-15 Limit cycling using quantized angle with continuous rate --

$$I = 2000 \text{ slug} - \text{ft}^2, f_o = 50 \text{ PPS}, \Delta\theta = 0.03 \text{ deg.}$$

~~CONFIDENTIAL~~

SECTION 7  
PARASITIC MODES ANALYSIS

~~CONFIDENTIAL~~

REPORT LED-500-3  
DATE 30 Sept. 1964

GRUMMAN AIRCRAFT ENGINEERING CORPORATION

~~CONFIDENTIAL~~

## SYMBOLS USED IN SECTION 7

<u>Symbol</u>	<u>Definition</u>	<u>Units</u>
$a$	vertical acceleration	ft/sec <sup>2</sup>
$a_l$	thrust delay	sec
$c_i$	dimensionless ratio	---
$e_i$	input to PRM	rad.
$e_l$	saturation input to PRM	rad.
$F_{iXA}$	force on $i^{\text{th}}$ body in $X_A$ direction	lbs.
$F_{iYA}$	force on $i^{\text{th}}$ body in $Y_A$ direction	lbs.
$h$	distance from bottom of tank to liquid surface	ft.
$h_s$	distance from bottom of tank to pendulum surface	ft.
$h_R$	distance from bottom of tank to rigidly-attached mass	ft.
$I_E$	effective inertia	slug-ft <sup>2</sup>
$I_i$	inertia of body "i" about its cg	slug-ft <sup>2</sup>
$I_R$	inertia ratio	---
$K_{DC}$	open loop gain	rad/sec <sup>2</sup>
$K_E$	effective rate feedback gain	sec
$K_i$	structural spring rate	lbs/ft
$K_M$	PRM linear gain	ft-lbs/rad
$K_O$	operating gain	---
$K_R$	rate feedback gain	sec
$l_1, l_2$	geometric dimensions	ft.
$M_i$	mass of $i^{\text{th}}$ body	slugs
$M_L$	liquid mass	slugs
$M_{LF}$	liquid mass of full tank	slugs
$M_S$	sloshing mass	slugs
$M_R$	rigidly-attached mass	slugs
$N$	describing function gain for PRM	---
$n$	any integer from $-\infty$ to $\infty$	---
$P_{Ri}$	ratio of the distances from $i^{\text{th}}$ open loop pole and zero to $i^{\text{th}}$ closed loop pole	---
$R$	tank radius	inches
$R, R_O$	geometric dimensions	ft.
$T_i$	torque applied to $i^{\text{th}}$ body	ft-lbs
$T_n$	descent engine thrust	ft-lbs
$T_M$	maximum available reaction jet torque	ft-lbs
$T_R$	reaction jet torque as a function of time	ft-lbs

Code 26512 Eng-23-1A

REPORT  
DATELED-506  
30 Sept 1961~~CONFIDENTIAL~~

GRUMMAN AIRCRAFT ENGINEERING CORPORATION

~~CONFIDENTIAL~~SYMBOLS USED IN SECTION 7 (cont.)

<u>Symbol</u>	<u>Definition</u>	<u>Units</u>
$X_{iA}$	position of body "i" measured in $X_A$ direction	ft
$Y_{iA}$	position of body "i" measured in $Y_A$ direction	ft
$X_i, Y_i$	body fixed coordinates to $i^{th}$ body	ft
$X_I, Y_I$	inertial coordinates	ft
$X_R, Y_R$	relative coordinates	ft
$X_{RO}$	static deflection of reaction jet cluster due to descent engine thrust	ft
$\alpha_i$	angle of departure from the $i^{th}$ open loop structural pole	rad
$\beta$	mass ratio	none
$\gamma$	dimensionless ratio	none
$\Delta P_i$	distance between the $i^{th}$ open loop and closed loop structural pole	rad/sec
$\delta$	relative angular displacement of the descent engine	rad
$\zeta_{Ci}$	change in the $i^{th}$ structural damping ratio	none
$\tau$	filter delay	sec
$\tau_P$	position feedback lag	sec
$\tau_Z$	position feedback zero	sec
$\psi$	lem body angular position	rad
$\psi_f$	total feedback signal	rad
$\sigma$	PRM input dead band	rad
$\omega_A$	uncoupled lem body torsional frequency	rad/sec
$\omega_C$	body coupling frequency	rad/sec
$\omega$	uncoupled descent engine torsional frequency	rad/sec
$\omega_L$	uncoupled descent engine lateral frequency	rad/sec
$\omega_{Pi}$	open loop coupled frequency of the $i^{th}$ resonance	rad/sec
$\omega_n$	natural frequency of pendulum	rad/sec
$\omega_{T1}, \omega_{T2}$	thrust coupling frequencies	rad/sec
$\omega_{Zi}$	open loop coupled frequency of the $i^{th}$ anti-resonance	rad/sec

SUBSCRIPTS

0	associated with reaction jet cluster longitudinal dynamics
1	associated with decent engine lateral dynamics
2	associated with decent engine torsional dynamics
A	associated with lem body
B	associated with reaction jet cluster body
C	associated with decent engine body
i	generalized subscript and integer counting variable.

Code 26512 Eng-23A

~~CONFIDENTIAL~~REPORT IED-500-3  
DATE 30 Sept. 1964

GRUMMAN AIRCRAFT ENGINEERING CORPORATION

~~CONFIDENTIAL~~7.1 - Introduction

All preceding analyses neglected the effects of parasitic modes on the attitude control system. In this section effects of propellant sloshing and an elastic airframe are considered, primarily from a stability point of view, and the analytical results are presented. The effect of fuel sloshing and elastic airframe parasitic modes on the control system have been considered separately for this analysis.

7.2 - Propellant Sloshing

7.2.1 - Introduction-- The forces generated by sloshing of the LEM main propellants can have a significant effect on the stability and control of the vehicle. These forces are most readily incorporated into the control system analysis by using mechanical models (19, 22, 23) which produce dynamic effects equivalent to those of the propellants. The model parameters have undergone several refinements before reaching their present stage. Further refinements appear likely because the experimental sloshing tests currently being conducted will probably result in some empirical modifications of the theoretical model parameters. This is particularly true of the descent tank model, since a theoretical hydrodynamic solution is not available for that configuration.

The mechanical models are based on linear hydrodynamic solutions for liquid sloshing in rigid tanks. Such solutions exist for the lateral excitation of spherical tanks (24) and flat-bottomed cylindrical tanks (25). It can be shown that a mechanical model consisting of a rigidly-attached mass and a series of pendulum masses will generate forces which are identical to the sloshing forces predicted by hydrodynamic theory. The rigid mass in the model represents the liquid which moves with the tank and thus does not slosh; the pendulum masses represent the modes of vibration of the sloshing liquid.

Because the liquid has an infinite number of modes of vibration, the model is theoretically required to have an infinite number of pendulum masses to exactly reproduce the sloshing force. However, the masses associated with all but the first mode are relatively small (less than 3% of the first mode mass) and can safely be neglected for most purposes. The model then consists of a rigidly-attached mass and a single pendulum mass.

The mechanical model and its parameters for the spherical ascent tanks are shown in Figure 7-1. The model consists of a pendulum mass,  $M_s$ , supported at a distance  $h_r$  from the bottom of the tank.

The curves of the model parameters were derived from equations for the sloshing force presented in reference 24. The parameters are plotted in terms of the non-dimensional liquid depth ratio  $h/2R$ . All curves of mass parameters have been non-dimensionalized by dividing by  $M_{LF}$ , the mass of the propellant in a full tank. The frequency is given in terms of the parameter  $\omega_n \sqrt{R/a}$ , where  $a$  is the vertical acceleration of the tank (e.g.,  $a = 32.2 \text{ ft/sec}^2$  for a tank on the surface of the earth.)

Code 26512

Eng-23-1A

~~CONFIDENTIAL~~

~~CONFIDENTIAL~~

Due to the fact that the pressures exerted by the liquid in a spherical tank act radially, producing no moment about the center of the tank, the pendulum support and the rigidly-attached mass are both located at the center of the tank for all liquid levels. Any other location for the pendulum support and rigid mass would cause a moment about the center of the tank, and would therefore be inconsistent with the liquid behavior.

The descent tank consists of a short cylindrical section with hemispherical caps. The cylindrical section has a length of  $0.56 R$ . Because no theoretical solution is available for this configuration, it was necessary to fit together the existing solutions for the sphere and the flat-bottomed cylinder to obtain approximate values of the sloshing parameters. The curves of these parameters are given in Figure 7-2.

The sloshing parameter curves for the descent tank are based on a spherical tank when the liquid level is in the lower hemisphere, an "equivalent" flat-bottomed cylindrical tank when the level is in the cylindrical section or in the lower part of the upper hemisphere, and a spherical tank for the nearly full condition. An "equivalent" cylindrical tank is a flat-bottomed cylinder which has the same volume and free liquid surface area as the actual tank. This "equivalent" cylindrical approach has been shown to yield a good approximation to the sloshing behavior in tanks with other than flat bottoms (26). The model parameters for the "equivalent" cylinder were taken from curves given in Reference 27.

A single-axis, planar stability and response study of the LEM ascent and descent stages has been conducted, assuming the models discussed above, for various maneuvers. Two digital computer programs which generate root locus and time response to a unit step input have yielded information about the stability of the control system with propellant sloshing. In addition, limit cycle, moment unbalance, and step command operations have been simulated on the analog computer.

A time history of sloshing mass magnitudes for powered ascent and descent can be seen in Figure 7-3. For the descent stage in the hover phase, the slosh mass peaks up to 23.7% of the total vehicle mass; in the ascent stage the sloshing mass peaks to 22.2% of the total vehicle mass at  $\frac{h}{2R} = 0.5$  (half-full tanks).

The root locus analysis was performed with the linearized control system shown in Figure 7-4. The tank configurations are shown in Figures 7-26 and 7-27.

The modulator was linearized to the extent that it is treated as a pure gain, varied to generate the root locus. The vehicle dynamics consist of the rigid body with two linear pendulums to simulate the propellant sloshing in the fuel and oxidizer tanks. In this planar, single-axis analysis, the vehicle is subject to following degrees of freedom:

- a) one rigid body translation
- b) one rigid body rotation
- c) two sloshing mass oscillations.

The roots of the LEM attitude control system transfer function with sloshing dynamics (obtained by using the root locus program) are submitted to another

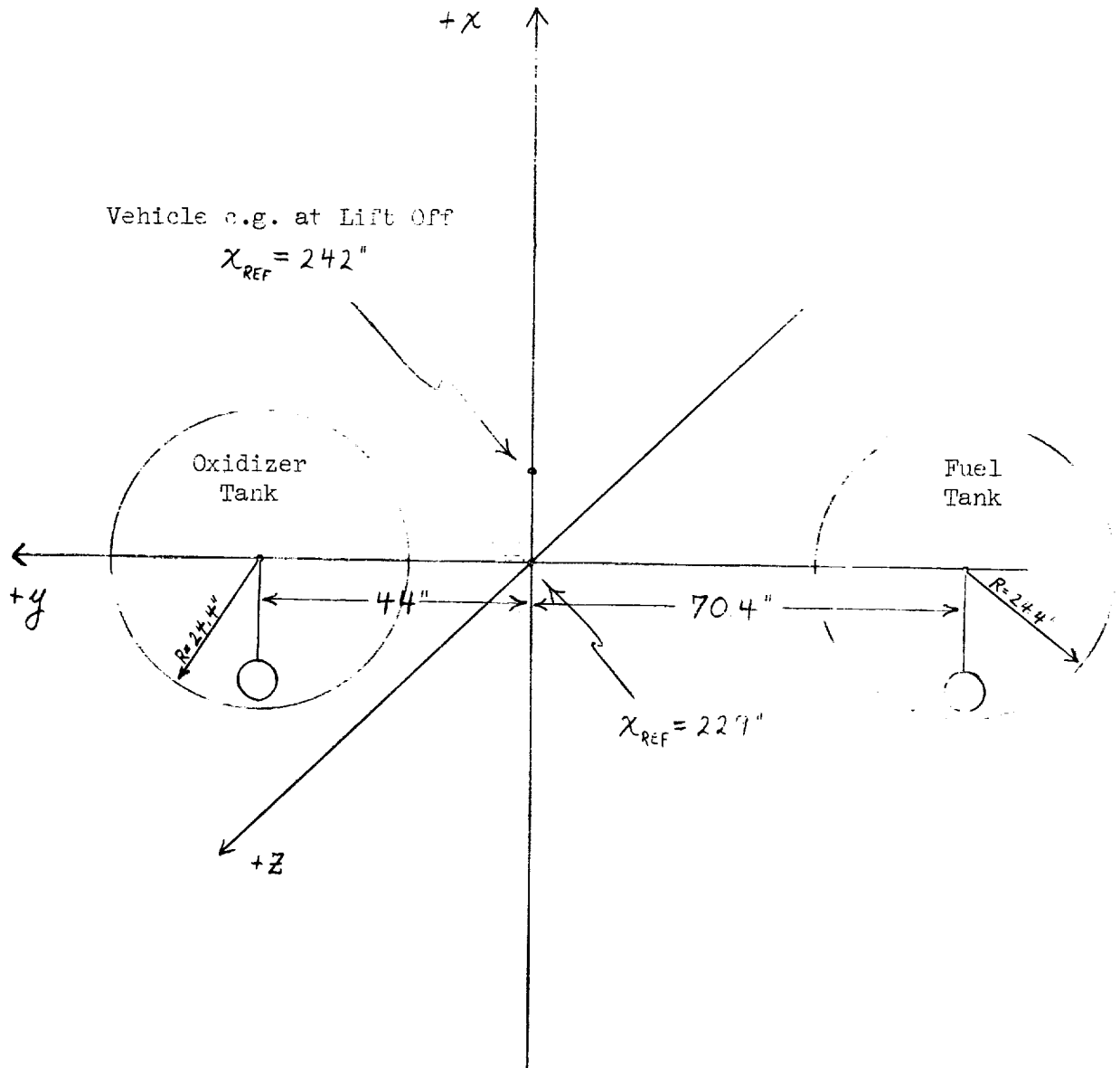
~~CONFIDENTIAL~~

REPORT LED-500-3  
DATE 30 Sept. 1964

~~CONFIDENTIAL~~

Figure 7-26

## ASCENT STAGE PROPELLANT TANK CONFIGURATION



Note: Pendulums represent sloshing propellants in respective tanks.

Code 26512 Eng-23-1A

REPORT LED-500  
DATE 30 Sep 1954

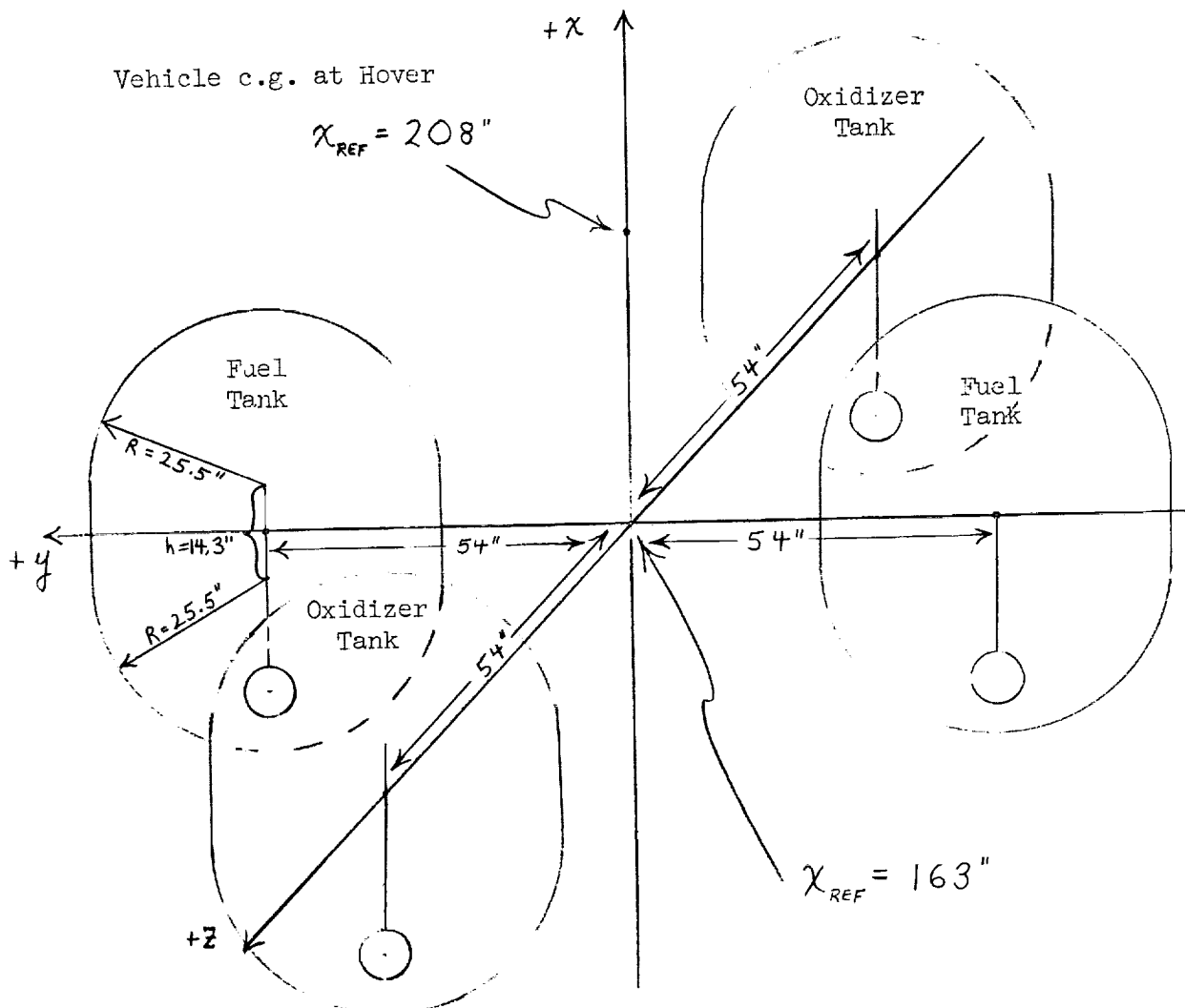
~~CONFIDENTIAL~~

GRUMMAN AIRCRAFT ENGINEERING CORPORATION

~~CONFIDENTIAL~~

Figure 7-27

## DESCENT STAGE PROPELLANT TANK CONFIGURATION



Note: Pendulums represent sloshing propellants in respective tanks.

~~CONFIDENTIAL~~



~~CONFIDENTIAL~~

digital program which computes the vehicle's transient response to a unit step input for various gains.

An analog computer simulation was also used because it simulates the actual vehicle control system better, and the characteristics of the Pulse Ratio Modulator (PRM) can be represented. The PRM is governed by the equations:

$$T_{wmin} = \int_0^{T_w} [1 - x(t)] dt$$

$$T_{wmin} = \int_{T_w}^{T_p} \lambda [x(t)] dt,$$

where  $T_{wmin}$  is the minimum pulse width,  $x(t)$  is the normalized error as a function of time, and  $T_p$  is the pulse period;  $\lambda$  is a parameter which varies the off-time of the pulse period (see section 3).

The control system which was programmed on the analog computer is shown in Figure 7-5.

The rectangular modulator pulses are adjusted by an analog thrust function such that the thrust output behaves as the reaction control jets. Associated with these jets is a nine millisecond delay and a five millisecond decay time constant, which combine to mold the thrust function from the modulator's pulse. An example is shown in Figure 7-6.

In considering an operating gain,  $K_o$ , for digital root locus analysis, it was necessary to assign an effective gain for the modulator. This gain was simply the slope of the angular error (in degrees) versus normalized output for a linear modulator ( $\lambda = 1$ ).

A describing function analysis of the modulator with deadzone and thrust saturation revealed that, for large error signals, the equivalent gain will be much less than the nominal linear gain. Therefore, a gain of  $\frac{1}{2}$  the linear gain  $K_o$  has been marked on the root loci plots to show system roots equivalent to the existence of large error signals.

7.2.2. - Stability Analysis -- The analysis of the LEM control system without the gimbal trim loop, but including the effects of propellant sloshing (equations in Table 7-9), reveals stable operation for most gains (Figures 7-7 and 7-12). For extremely high gains, the rigid body mode of the vehicle is unstable if there is a zero representation of the jet delay (Figures 7-8 and 7-11).

The two sloshing modes (oxidizer and fuel) appear in the root locus on the imaginary axis at a frequency between 2.5 and 4.5 radians/second. The rigid body poles can be seen curving about the rate gyro zero ( $\sigma = -1.25$ ) before they meet and split apart along the negative real axis.

As previously noted, a more significant control system gain is one half the operating gain ( $K_o/2$ ). For this gain, the damping ratios for the rigid body and the predominant sloshing mode are given in the tables 7-1 and 7-2.

~~CONFIDENTIAL~~

~~CONFIDENTIAL~~

TABLE 7-9

Single Axis\*Sloshing Dynamics Equations for LEM Vehicle

Vehicle dynamics:

$$M\ddot{Z} = F_{sz_i}$$

$$I\ddot{\theta} = T_c - F_{sz_i} X_{T_i}$$

Accelerations at pendulum supports:

$$\ddot{Z}_{T_i} = \ddot{Z} - X_{T_i}\ddot{\theta} + Z_{T_i}\dot{\theta}^2$$

Pendulum responses:

$$\ddot{\theta}_{s_i} + 2\zeta_s \omega_{n_i} \dot{\theta}_{s_i} + \omega_{n_i}^2 \theta_{s_i} = - \frac{\omega_{n_i}^2}{a} \ddot{Z}_{T_i}$$

Sloshing forces (due to pendulums):

$$F_{sz_i} = M_{s_i} a \theta_{s_i}$$

\* These equations, which represent the pitch axis, are also valid for the roll and ascent stage yaw axes. The equations describing the descent stage yaw motion, however, do not require a rigid body translational degree of freedom. The effect of gimbaling the descent engine has been neglected throughout. The control system is shown in Figure 7-5.

~~CONFIDENTIAL~~

~~CONFIDENTIAL~~

TABLE 7-9 (CONTINUED)

SYMBOLS USED IN TABLE 7 - 9

$M$	Reduced vehicle mass (slosh masses removed)
$I$	Reduced vehicle inertia (slosh inertia removed)
$Z$	LEM roll body axis
$\ddot{Z}$	Vehicle acceleration in Z-direction
$\dot{\theta}, \ddot{\theta}$	Vehicle rotational velocity and acceleration about pitch axis
$T_c$	Control torque
$F_{szi}$	Sloshing force of the $i^{th}$ tank in the Z-direction
$X_{Ti}$	X-coordinate of the $i^{th}$ tank
$Z_{Ti}$	Z-coordinate of the $i^{th}$ tank
$\ddot{Z}_{Ti}$	Acceleration of $i^{th}$ tank ( $i^{th}$ pendulum support) in Z-direction
$\zeta_s$	Critical damping ratio of sloshing modes
$\theta_{si}, \dot{\theta}_{si}, \ddot{\theta}_{si}$	Angular position, velocity, and acceleration of $i^{th}$ sloshing pendulum
$\omega_{ni}$	Natural sloshing frequency of propellant in $i^{th}$ tank
$a$	LEM inertial acceleration (thrust/vehicle mass)
$M_{si}$	Mass of sloshing propellant in $i^{th}$ tank

~~CONFIDENTIAL~~

~~CONFIDENTIAL~~

TABLE 7-1  
DESCENT YAW AXIS  
DAMPING  
GAIN =  $K_0/2$

$h/2R$ \ MODE	RIGID BODY	SLOSH
1.0	$\zeta = 0.795$	$\zeta = 0.029$
0.5	$\zeta = 1.015$	$\zeta = 0.084$
0.4	$\zeta = 1.195$	$\zeta = 0.053$

TABLE 7-2  
DESCENT ROLL AXIS  
DAMPING  
GAIN =  $K_0/2$

$h/2R$ \ MODE	RIGID BODY	SLOSH
1.0	$\zeta = 0.768$	$\zeta = 0.0042$
0.5	$\zeta = 0.933$	$\zeta = 0.045$
0.4	$\zeta = 1.035$	$\zeta = 0.049$

The spread between the pole and the zero in the sloshing mode for the yaw axis is greater than that of the roll axis (Figures 7-10 and 7-12). However, the sloshing effect is reduced for the yaw axis because more natural damping occurs for this case (Tables 7-1 and 7-2) due to the larger pole-zero spread.

Tables 7-1 and 7-2 show that the vehicle (rigid body) becomes more heavily damped as the inertia (proportional to fluid  $h/2R$ ) decreases. A comparison of the sloshing modes of Figures 7-9 and 7-10 shows that the frequency of the poles and zeroes drops from a range of 4.0-4.6 radians/sec. to 2.7-3.2 radians/sec. This frequency shift is due to the throttling down of the descent engine from 10,500 lbs. thrust to about 4,700 lbs. thrust. Although the lower slosh frequency is closer to that of the LEM control system, the coupling of the sloshing effects with the control system is not noticeably increased and the vehicle stability is unaltered.

It is interesting to note the roll case of Figure 7-11 where the introduction of a small amount of fluid damping completely decouples the sloshing effects from the vehicle control system.

~~CONFIDENTIAL~~

REPORT LED-500-3  
DATE 30 Sept. 1964

~~CONFIDENTIAL~~

Inspection of the LEM ascent stage control system for the roll and yaw axis reveals the same stability as the descent stage (Figures 7-13 and 7-16). A comparison of the sloshing modes of the two axes shows that the slosh coupling effect is much greater for rotation about the yaw axis. Tables of the rigid body and natural slosh damping are given below:

TABLE 7-3  
ASCENT ROLL AXIS  
DAMPING  
GAIN =  $K_o/2$

$h/2R$ \ MODE	RIGID BODY	SLOSH
0.65	$\zeta = 0.964$	$\zeta = 0.0061$
0.35	$\zeta = 1.410$	$\zeta = 0.0038$

TABLE 7-4  
ASCENT YAW AXIS  
DAMPING  
GAIN =  $K_o/2$

$h/2R$ \ MODE	RIGID BODY	SLOSH
0.65	$\zeta = 0.742$	$\zeta = 0.0955$
0.35	$\zeta = 0.960$	$\zeta = 0.0512$

A preliminary analog computer study of the powered-descent phase of the LEM mission reveals stable operation in the limit cycle and in response to various maneuvers. The gimbal trim loop, designed to null out moment unbalances due to thrust misalignment, was not included in the control system for most of this analysis.

After an angular maneuver, the vehicle returns to its normal, stable, single-pulse limit cycle. However, when the gimbal trim servo loop (see Figure 7-5) is inserted into the control system, a high duty factor limit cycle is generated. The gimbal trim system appears to work against the modulator which fires rapidly in opposing blocks of three or four pulses under limit cycle operation.

A proposed solution to this instability is to insert a phase-lead network into the gimbal trim loop such that the gimbal motor is actuated only when an increasing error is sensed (see section 5). This effect will minimize gimbal overshoot and result in more stable operation.

For the ascent stage, the programming of the analog computer is very similar to that of the descent stage. Some parameters must be changed to account for differences in the tank configuration as well as the sloshing and vehicle masses.

~~CONFIDENTIAL~~

~~CONFIDENTIAL~~

This simulation allowed one more degree of freedom than the previous analysis. Instead of only one lateral degree of translation, the vehicle was free to translate in two directions. The two sloshing and the vehicle rotational degrees of freedom remained as before.

The vehicle was found to have a stable, single-pulse, limit cycle to which it returned after various maneuvers. Baffling of the main propellant tanks provided damping which yielded favorable results in fuel consumption and vehicle handling characteristics. Various non-linear effects associated with the pendulum (slosh mode) response were investigated, but were found to have a negligible effect on the gross vehicle properties (attitude and rate).

7.2.3- Transient Response-- Three different fluid levels were investigated for vehicle response to a unit step rotation about the yaw axis, which is the most sensitive to propellant sloshing. For the descent stage, the vehicle response (Figures 7-17, 7-18 and 7-19) shows no appreciable overshoot, partly because the rigid body mode is highly damped (Table 7-1), and also because the slosh and rigid body frequencies are far enough apart that the small slosh residue has very little effect on the vehicle attitude.

Table 7-5 gives the time constant and the rise time for the vehicle at various fluid levels.

TABLE 7-5  
DESCENT YAW AXIS  
TRANSIENT RESPONSE  
GAIN =  $K_0/2$

RESPONSE $h/2R$	TIME CONSTANT (67% of Final Value)	RISE TIME (90% of Final Value)
1.0	1.03 sec	1.48 sec
0.5	0.85 sec	1.70 sec
0.4	0.98 sec	1.63 sec

When  $h/2R = 0.4$  (Figure 7-19), the main engine thrust has been throttled down to less than one half its original value. Because the natural sloshing frequency is proportional to  $\sqrt{a}$  where  $a$  is the local acceleration, it moves closer to the rigid body frequency. However, the increased coupling does not have a significant effect on the vehicle attitude.

For ascent, the vehicle response to an angular unit step input has been inspected for rotation about the yaw axis for two different fluid levels. Because the sloshing frequency is very close to the rigid body natural frequency for a gain of  $K_0/2$ , it can be seen in Figures 7-20 and 7-21 that despite its small residue, the slosh has a significant effect on the vehicle attitude. It is important that sufficient baffle damping be present in the propellant tanks in cases where the slosh mode can be excited by the rigid body frequency.

~~CONFIDENTIAL~~

REPORT IED-500-3  
DATE 30 Sept. 1964

~~CONFIDENTIAL~~

The dominant characteristics for these two cases are given below:

TABLE 7-6  
ASCENT YAW AXIS  
TRANSIENT RESPONSE  
GAIN =  $K_0/2$

RESPONSE $h/2R$	TIME CONSTANT (67% of Final Value)	RISE TIME (90% of Final Value)	OVERSHOOT	RIGID BODY $\omega_n$	SLOSH $\omega_n$
0.65	0.53 sec	0.86 sec	10%	4.21 $\frac{\text{rad}}{\text{sec}}$	3.96 $\frac{\text{rad}}{\text{sec}}$
0.35	0.50 sec	0.91 sec	5.5%	5.22 $\frac{\text{rad}}{\text{sec}}$	3.60 $\frac{\text{rad}}{\text{sec}}$

The relatively large overshoot for  $h/2R = 0.65$  plus the subsequent oscillations, Figure 7-20, are due to the proximity of the slosh and rigid body frequencies. With a small amount of baffle damping in the propellant tanks the sloshing effect would be largely decoupled from the control system, as has been seen for the roll case, Figure 7-11.

7.2.4 - Method of Propellant Damping-- The existence of marginal or unstable sloshing modes in the LEM propellant tanks would impose significant design requirements upon the propulsion tankage and flight control subsystems. The fluid damping which would be provided by bladders if they had been used in the main propellant tanks does not appear adequate to preclude the possibility of marginal sloshing stability (22). The use of anti-slosh baffles permits great flexibility in achieving the desired stability, and is inherently much more reliable than the use of electronic compensation in the control system.

The key parameter in stabilizing the coupled sloshing modes is the damping of the fluid caused by the internal configuration of the propellant tank. The natural damping on the propellant in a smooth-walled spherical tank of LEM diameter is negligible ( $\zeta < 0.005$ ).

To estimate the damping produced by a bladder, a review was made of available test data on bladders in spherical tanks. A considerable quantity of test data has been accumulated by the NASA Lewis Research Center for the damping in spherical tanks with various fluids (water, water-glycerin mixtures, mercury, TBE manometer fluid) with and without diaphragms. Damping tests were conducted on spherical tanks of 32-inch and 20.5-inch diameters with diaphragms of three different thicknesses of butyl rubber and with TBE fluid; and on a 9.5-inch diameter sphere with diaphragms of three different thicknesses using both TBE and mercury as fluids.

The damping ratio for a 48.8-inch sphere with an 0.01-inch diaphragm was extrapolated from the diaphragm test data available using TBE fluids. The effect of viscosity difference between TBE fluid and LEM propellants on damping was then estimated by means of the test data for smooth-walled

Code 26512 Eng-23-1A

~~CONFIDENTIAL~~

~~CONFIDENTIAL~~

spheres with various fluid viscosities. The fundamental trend of fluid damping was checked through a comparison of TBE fluid and mercury for diaphragms in a 9.5-inch sphere. For fluid heights in the range of 0.8 to 0.2 diameter, the damping ratio was calculated as 1% of critical ( $\zeta = 0.01$ ).

The use of ring-type baffles produces a large increase in fluid damping per unit baffle surface area. Reviews of published and unpublished data on baffle damping in spheroids indicate that the circular ring baffle parallel to the fluid surface is very efficient for fluid depths in the region  $0.2 < h/2R < 0.8$ .

7.2.5-Baffle Configuration-- The initial baffle requirements for the main propellant tanks has been determined by Reference 28. Various control system analyses with limited data on baffle performance have generated the following minimum damping requirements in the ascent propellant tanks for various  $h/2R$  fluid levels:

ASCENT TANKS: Two, spherical for  $2R = 48.84$  and a fluid wave amplitude of  $5^\circ$ .

$h/2R$	$\zeta$
0.2 to 0.65	0.05
0.7	0.04

The characteristics of the individual baffles is such that its damping effect peaks up at a fluid level just above the baffle, causing nonlinear damping versus  $h/2R$ . Accordingly, the baffles have been spaced close enough such that for  $0.2 < h/2R < 0.7$ ,  $\zeta \geq 0.03$ .

Four ring baffles of various widths were selected for the ascent tanks. Both three and five-baffle configurations were considered, but were found to be less efficient than the four-baffle configuration.

For the descent stage propellant tanks, the desired damping was also achieved by four baffles:

DESCENT TANKS: Two, short cylindrical section (14.28"), with hemispherical caps, maximum  $h/2R = 1.28$

$h/2R$	$\zeta$
0.25	0.04
0.4 to 0.65	0.05
0.7	0.04
1.0	0.01

for wave amplitudes of  $5^\circ$ .

~~CONFIDENTIAL~~

REPORT LED-500-3  
DATE 30 Sept. 1964



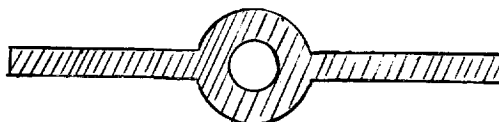
~~CONFIDENTIAL~~

The baffle sizes and their locations are presented below for the ascent and descent tanks:

	<u>Baffle Location</u> (Distance from Bottom of Tank)	<u>Baffle Width</u>
Ascent Tanks	8 - $3/8$ "	1 - $3/4$ "
	14 - $3/8$ "	2"
	21 - $1/2$ "	2 - $1/4$ "
	28 - $3/4$ "	2 - $1/4$ "
Descent Tanks	12 - $3/4$ "	2 - $1/8$ "
	21 - $3/4$ "	3"
	29 - $3/8$ "	3"
	39 - $1/2$ "	2 - $3/8$ "

Baffle configurations and their damping effects are currently being tested on a full-scale slosh rig. It is possible that some empirical refinements will be made on the present descent tank baffle configuration as a result of sloshing tests.

The baffles are constructed of flat ring-shaped aluminum and rest approximately 0.25 inch inside of the tank surface when installed. To increase the torsional rigidity, a tubular inset has been made into the center of the ring baffle, such that a cross-sectional view of the baffle appears:



This construction of the baffle allows greater strength and less weight than one with a rectangular cross-section.

### 7.3-Elastic Airframe

To determine the effects of coupling between the LEM attitude control system and the LEM structural dynamics a stability analysis was performed. The transfer function of the structural dynamics between applied torque, and the LEM angular position was determined for the stability analysis. The coupling between the structural dynamics and the control dynamics was determined by plotting all the open loop poles and zeros in the complex plane. The resulting point on the root locus is determined by use of the maximum describing function gain for the PRM.

~~CONFIDENTIAL~~

~~CONFIDENTIAL~~

The transfer function was determined from the six degree of freedom equations obtained by assuming three degrees of freedom for the LEM body, two degrees of freedom for the descent engine (with respect to the LEM body) and two degrees of freedom for the reaction jet cluster (with respect to the LEM body). The equations determined from Figure 7-22 are:

$$\Sigma F_{AXA} = \bar{M}_A \ddot{X}_{AA} = T_n \quad (1)$$

$$\Sigma F_{AYA} = M_A \ddot{Y}_{AA} = \left[ (K_1 + K_2) Y_R - (K_1 \ell_1 + K_2 \ell_2) \delta \right] \quad (2)$$

$$\Sigma F_{BXA} = M_B \ddot{X}_{BA} = -K_O X_R + T_R/2R_O + K_O X_{RO} \quad (3)$$

$$\Sigma F_{CYA} = M_C \ddot{Y}_{CA} = - \left[ (K_1 + K_2) Y_R - (K_1 \ell_1 + K_2 \ell_2) \delta \right] - T_n \delta \quad (4)$$

$$\begin{aligned} \Sigma T_A = I_A \ddot{\Psi} = & \left[ K_1 (R - \ell_1) + K_2 (R - \ell_2) \right] Y_R - \left[ K_1 \ell_1 (R - \ell_1) + K_2 \ell_2 (R - \ell_2) \right] \delta \\ & + T_n Y_R + 2R_O K_O X_R \end{aligned} \quad (5)$$

$$\Sigma T_C = I_C (\ddot{\Psi} + \ddot{\delta}) = (K_1 \ell_1 + K_2 \ell_2) Y_R - (K_1 \ell_1^2 + K_2 \ell_2^2) \delta \quad (6)$$

$$\ddot{X}_{BA} = \ddot{X}_{AA} + R_O \ddot{\Psi} + \ddot{X}_R \quad (7)$$

$$\ddot{Y}_{CA} = \ddot{Y}_{AA} + R \ddot{\Psi} + \ddot{Y}_R \quad (8)$$

$$X_{RO} = T_n M_B / K_O \bar{M}_A \quad (9)$$

Note:  $\bar{M}_A$  has been used in place of  $M_A + M_C$  above for simplicity, where  $\bar{M}_A \approx M_A$

~~CONFIDENTIAL~~

GRUMMAN AIRCRAFT ENGINEERING CORPORATION

 REPORT LED-500-3  
 DATE 30 Sept. 1964

~~CONFIDENTIAL~~

The structural damping terms were neglected since the change in structural damping ratio is of primary interest.

The transfer function obtained is:

$$\frac{\Psi(s)}{T_R(s)} = \frac{1}{I_E s^2} \frac{\left( \frac{s^2}{\omega_{z_1}^2} + 1 \right) \left( \frac{s^2}{\omega_{z_2}^2} + 1 \right)}{\left( \frac{s^2}{\omega_{p_0}^2} + 1 \right) \left( \frac{s^2}{\omega_{p_1}^2} + 1 \right) \left( \frac{s^2}{\omega_{p_2}^2} + 1 \right)} \quad (10)$$

where

$$\beta = 1 + M_C/M_A \quad (11)$$

$$\omega_L^2 = (K_1 + K_2) / M_C \quad (12)$$

$$\omega_O^2 = (K_1 \ell_1^2 + K_2 \ell_2^2) / I_C \quad (13)$$

$$\omega_A^2 = \left[ K_1 (R - \ell_1)^2 + K_2 (R - \ell_2)^2 \right] / I_A \quad (14)$$

$$\omega_C^4 = \beta K_1 K_2 (\ell_1 - \ell_2)^2 / I_C M_C \quad (15)$$

$$\omega_{T_1}^4 = (K_1 \ell_1 + K_2 \ell_2) T_n / I_C M_C \quad (16)$$

$$\omega_{T_2}^4 = \left\{ (1 + \beta) I_C \left[ K_1 (R - \ell_1) + K_2 (R - \ell_2) \right] + M_C R \left[ K_1 \ell_1 (R - \ell_1) + K_2 \ell_2 (R - \ell_2) \right] \right\} T_n / I_A I_C M_C \quad (17)$$

$$I_R = 1 + I_C / I_A + R^2 M_C / \beta I_A \quad (18)$$

$$\omega_{p_0}^2 = (I_A + 2R^2 M_C) (K_O) / I_A M_B \quad (19)$$

~~CONFIDENTIAL~~

~~CONFIDENTIAL~~

$$I_E = (I_A + 2R_O^2 M_B) (I_R \omega_C^4 + \omega_{T_1}^4 - \omega_{T_2}^4) / (\omega_C^4 + \omega_{T_1}^4) \quad (20)$$

$$\omega_{z_1}^2 = \left[ \omega_\sigma^2 + \beta \omega_L^2 + \sqrt{(\omega_\sigma^2 + \beta \omega_L^2)^2 - 4(\omega_C^4 + \omega_{T_1}^4)} \right] / 2 \quad (21)$$

$$\omega_{z_2}^2 = \left[ \omega_\sigma^2 + \beta \omega_L^2 - \sqrt{(\omega_\sigma^2 + \beta \omega_L^2)^2 - 4(\omega_C^4 + \omega_{T_1}^4)} \right] / 2 \quad (22)$$

$$\omega_{P_1}^2 = \left[ \omega_\sigma^2 + \beta \omega_L^2 + \omega_A^2 + \sqrt{(\omega_\sigma^2 + \beta \omega_L^2 + \omega_A^2)^2 - 4(\omega_C^4 I_R + \omega_{T_1}^4 - \omega_{T_2}^4)} \right] / 2 \quad (23)$$

$$\omega_{P_2}^2 = \left[ \omega_\sigma^2 + \beta \omega_L^2 + \omega_A^2 - \sqrt{(\omega_\sigma^2 + \beta \omega_L^2 + \omega_A^2)^2 - 4(\omega_C^4 I_R + \omega_{T_1}^4 - \omega_{T_2}^4)} \right] / 2 \quad (24)$$

The overall open loop transfer function obtained from control system block diagram (Figure 7-23) is:

$$G(S) = \frac{1}{\tau s + 1} \left( NK_M \right) \frac{1}{I_e s^2} \frac{\left( \frac{s^2}{\omega_{z_1}^2} + 1 \right) \left( \frac{s^2}{\omega_{z_2}^2} + 1 \right)}{\left( \frac{s^2}{\omega_{p_0}^2} + 1 \right) \left( \frac{s^2}{\omega_{p_1}^2} + 1 \right) \left( \frac{s^2}{\omega_{p_2}^2} + 1 \right)} \frac{(\tau_z s + 1)(K_E s + 1)}{\left( \frac{s^2}{\omega_g^2} + \frac{2\xi_g s}{\omega_g} + 1 \right) (\tau_P s + 1)} \quad (25)$$

STRUCTURAL DYNAMICS      FEEDBACK DYNAMICS

FILTER      PRM GAIN      THRUST DELAY

where

$$\tau_z = \tau_P \left\{ \frac{2(K_R + \frac{1}{\tau_P \omega_g^2})}{(K_R + \frac{2\xi_g}{\omega_g}) (1 + \sqrt{1 - \gamma})} \right\} \quad (26)$$

~~CONFIDENTIAL~~

REPORT LED-500-3  
DATE 30 Sept. 1964

GRUMMAN AIRCRAFT ENGINEERING CORPORATION

~~CONFIDENTIAL~~

$$K_E = K_R \frac{\gamma \left( 1 + \frac{2\xi_g}{K_R \omega_g} \right)}{2 \left( 1 - \sqrt{1 - \gamma} \right)} ; \gamma = \frac{4(K_R \tau_p + 1/\omega_g^2)}{K_R^2 + 4K_R \xi_g/\omega_g + 4\xi_g^2/\omega_g^2} \quad (27)$$

If  $\gamma \leq 1$ .

N is the describing function gain plotted in Figure 7-24.

TABLE 7-7

System Parameters

a	=	.01 sec
e <sub>1</sub>	=	.01045 rad
* I <sub>A</sub>	=	6,874 slug ft <sup>2</sup>
I <sub>C</sub>	=	37 slug ft <sup>2</sup>
K <sub>O</sub>	=	35,000 #/ft
K <sub>1</sub>	=	1,200,000 #/ft
K <sub>2</sub>	=	276,000 #/ft
K <sub>R</sub>	=	.8 sec
l <sub>1</sub>	=	1.52 ft
l <sub>2</sub>	=	.29 ft
M <sub>A</sub>	=	326 slugs
M <sub>B</sub>	=	.93 slugs
M <sub>C</sub>	=	11 slugs
R	=	6.3 ft
R <sub>O</sub>	=	5.5 ft
T	=	10,500 #
T <sub>M</sub>	=	1,100 ft-#
τ	=	.02 sec
τ <sub>P</sub>	=	.0238 sec
Ω	=	.00174 rad
ξ <sub>g</sub>	=	.707
ω <sub>g</sub>	=	120 rad/sec

\* LEM Inertia (I<sub>yy</sub> touchdown) minus descent engine and two reaction jet clusters.

~~CONFIDENTIAL~~

TABLE 7-8

Numerical Results

$C_0$	= 1.1032	$\gamma$	= .1162
$C_1$	= 1.1193	$\tau$	= .0254
$C_2$	= .9990	$\omega_A$	= 73.4 rad/sec
$I_E$	= 7349.2 slug-ft <sup>2</sup>	$\omega_C$	= 188 rad/sec
$I_R$	= 1.0656	$\omega_D$	= 276 rad/sec
$K_{DC}$	= 13.40 [1/sec <sup>2</sup> ]	$\omega_L$	= 366 rad/sec
$K_E$	= .7858 sec	$\omega$	= 195 rad/sec
$K_M$	= 126,300 ft#/rad	$\omega_{PO}$	= 462.080 rad/sec
$N$	= .78	$\omega_{P1}$	= 80.943 rad/sec
$X_{RO}$	= .00085 ft	$\omega_{P2}$	= 84 rad/sec
$\alpha_0$	= .82 rad	$\omega_{T1}$	= 43.5 rad/sec
$\alpha_1$	= 3.73 rad	$\omega_{T2}$	= 456.463 rad/sec
$\alpha_2$	= .248 rad	$\omega_{Z1}$	= 79.570 rad/sec
$\beta$	= 1.035	$\omega_{Z2}$	= 79.570 rad/sec

$$\begin{aligned}
 * \xi_{C_0} &= -.001670 \\
 * \xi_{C_1} &= +.000004 \\
 * \xi_{C_2} &= -.001290
 \end{aligned}$$

\* These terms represent the change in structural damping ratio. To determine the closed-loop structural damping ratio add the estimated open loop structural damping ratio to each term. The open loop structural damping ratio should fall in the range of .01 to .02.

It was assumed that the structural poles move only short distances ( $\Delta P_i$ ) and that they move along the departure angle of these poles (Figure 7-25).<sup>1</sup>  $\Delta P_i$  was evaluated by assuming that the distance between the open loop poles and the closed loop structural poles is approximately equal to the distance of the open loop roots to the open loop structural poles, except for open loop roots in the neighborhood of a structural pole. The angle of departure ( $\alpha_i$ ) was evaluated by normal root locus techniques and  $\zeta_i$  was evaluated from the values of  $\Delta P_i$  and  $\alpha_i$ .

The values for  $\zeta$ ,  $\Delta P_i$  and  $\alpha_i$  for the various values of structural resonance (assuming that the order along the "jw" axis of the structural open loop roots are as shown in Figure 7-25) are:

~~CONFIDENTIAL~~

a- Reaction jet cluster longitudinal resonance

$$\alpha_o = \tan^{-1} \tau \omega_{Po} - a \omega_{Po} - \tan^{-1} \left( \frac{\omega_{Po}}{\zeta_g \omega_g} + \frac{\sqrt{1 - \zeta_g^2}}{\zeta_g} \right) - \tan^{-1} \left( \frac{\omega_{Po}}{\zeta_g \omega_g} - \frac{\sqrt{1 - \zeta_g^2}}{\zeta_g} \right) \quad (28)$$

$$\Delta P_o = K_{DC} K_E \omega_g^2 C_o / (2\tau \sqrt{(1/\tau)^2 + \omega_{Po}^2} \sqrt{\omega_{Po}^4 + 2\omega_{Po}^2 \omega_g^2 (2\zeta_g^2 - 1) + \omega_g^4}) \quad (29)$$

$$\zeta_{Co} = -\Delta P_o \cos \alpha_o / (\omega_{Po} + \Delta P_o \sin \alpha_o) \quad (30)$$

where

$$C_o = \frac{(\omega_{Po}^2 - \omega_{z2}^2)(\omega_{z1}^2 - \omega_{Po}^2)(\omega_{P1}^2 \omega_{P2}^2)(\tau_z) \left( \sqrt{\frac{1}{\tau_z^2} + \omega_{Po}^2} \sqrt{\frac{1}{K_E^2} + \omega_{Po}^2} \right)}{\quad} \quad (31)$$

$$(\omega_{Po} - \omega_{P2})^2 (\omega_{P1} - \omega_{Po})^2 (\omega_{z1}^2 \omega_{z2}^2 \tau_P) \sqrt{\frac{1}{\tau_P^2} + \omega_{Po}^2} (\omega_{Po})$$

$$\text{and } K_{DC} = NK_M / I_E \quad (32)$$

b- Descent engine lateral resonance

$$\alpha_1 = \left( -\tan^{-1} \tau \omega_{P1} \right) - a \omega_{P1} - \tan^{-1} \left( \frac{\omega_{P1}}{\zeta_g \omega_g} + \frac{\sqrt{1 - \zeta_g^2}}{\zeta_g} \right) \tan^{-1} \left( \frac{\omega_{P1}}{\zeta_g \omega_g} - \frac{\sqrt{1 - \zeta_g^2}}{\zeta_g} \right) \quad (33)$$

$$\Delta P_1 = \frac{P_{R1} (\omega_{P1} - \omega_{z1})}{\sqrt{1 - P_{R1}^2}} \left[ \frac{P_{R1} \sin \alpha_1}{\sqrt{1 - P_{R1}^2}} + \sqrt{1 + \frac{P_{R1}^2 \sin^2 \alpha_1}{1 - P_{R1}^2}} \right] \quad (34)$$

~~CONFIDENTIAL~~

$$\zeta_{C_1} = \Delta P_1 \cos \alpha_1 / (\omega_{P_1} + \Delta P_1 \sin \alpha_1) \quad (35)$$

where

$$C_1 = \frac{\tau_z \sqrt{\frac{1}{\tau_z^2} + \omega_{P_1}^2} \sqrt{\frac{1}{K_E^2} + \omega_{P_1}^2} (\omega_{P_1}^2 - \omega_{z_2}^2) (\omega_{P_1}^2 \omega_{P_2}^2) (\omega_{P_1} + \omega_{z_1})}{\tau_P \sqrt{\frac{1}{\tau_P^2} + \omega_{P_1}^2} (\omega_{P_1}) (\omega_{P_1}^2 - \omega_{P_2}^2) (\omega_{z_1}^2 \omega_{z_2}^2) (2\omega_{P_1})} \quad (36)$$

$$P_{R_1} = \frac{K_{DC} K_E \omega_{P_0}^2 \omega_g^2 C_1}{\omega_{P_1} (\omega_{P_1}^2 - \omega_{P_0}^2) (\tau) \sqrt{\frac{1}{\tau^2} + \omega_{P_1}^2} \sqrt{\omega_{P_1}^4 + 2\zeta_g^2 \omega_{P_1}^2 (2\zeta_g^2 - 1) + \omega_g^4}} \quad (37)$$

c- Descent engine torsional resonance

$$\alpha_2 = \left( \pi - \tan^{-1} \frac{\omega_{P_2}}{\tau \omega_{P_2}} \right) - a \omega_{P_2} - \tan^{-1} \left( \frac{\omega_{P_2}}{\zeta_g \omega_g} + \frac{\sqrt{1 - \zeta_g^2}}{\zeta_g} \right) - \tan^{-1} \left( \frac{\omega_{P_2}}{\zeta_g \omega_g} - \frac{\sqrt{1 - \zeta_g^2}}{\zeta_g} \right) \quad (38)$$

$$\Delta P_2 = \frac{P_{R_2} (\omega_{P_2} - \omega_{z_2})}{\sqrt{1 - P_{R_2}^2}} \left[ \frac{P_{R_2} \sin \alpha}{\sqrt{1 - P_{R_2}^2}} + \sqrt{1 + \frac{P_{R_2}^2 \sin^2 \alpha}{1 - P_{R_2}^2}} \right] \quad (39)$$

$$\zeta_{C_2} = - \Delta P_2 \cos \alpha_2 / (\omega_{P_2} + \Delta P_2 \sin \alpha_2) \quad (40)$$

where

$$P_{R_2} = \frac{K_{DC} K_E \omega_{P_0}^2 \omega_g^2 C_2}{\omega_{P_2} (\omega_{P_2}^2 - \omega_{P_0}^2) (\tau) \sqrt{\frac{1}{\tau^2} + \omega_{P_2}^2} \sqrt{\omega_{P_2}^4 + 2\omega_g^2 \omega_{P_2}^2 (2\zeta_g^2 - 1) + \omega_g^4}} \quad (41)$$



~~CONFIDENTIAL~~

$$C_2 = \frac{\tau_z \sqrt{\frac{1}{\tau_z^2} + \omega_{p_2}^2} \sqrt{\frac{1}{K_E^2} + \omega_{p_2}^2} (\omega_{z_1}^2 - \omega_{p_2}^2) (\omega_{p_1}^2 \omega_{p_2}^2) (\omega_{p_2} + \omega_{z_2})}{\tau_p \left( \frac{1}{\tau_p^2} + \omega_{p_2}^2 \right) (\omega_{p_2}^2) (\omega_{p_1}^2 - \omega_{p_2}^2) (\omega_{z_1}^2 \omega_{z_2}^2) (2\omega_{p_2})} \quad (42)$$

The coupling between the attitude control system and the LEM structural dynamics does not result in appreciable loss in structural damping. Table 7-8 is a summary of the numerical results obtained when the system preliminary parameters tabulated in Table 7-7 are substituted into the equations obtained by the general analysis presented in this section. If a structural damping ratio of .01 open loop is assumed, the maximum loss in damping would be 16%. Therefore, an adequate stability margin is maintained.

#### 7.4 Conclusion

The analyses presented in this section have shown that the LEM attitude control system is stable for the vehicle and tank configurations considered. It was also concluded that, to improve transient response damping and to reduce RCS propellant consumption, anti-slosh baffles are necessary in both ascent and descent tanks. Initial studies showed that the fluid damping which would be provided by bladders, if they had been used in the main propellant tanks, would not be adequate to preclude the possibility of marginal sloshing stability.

The analysis performed to determine the effect of structural dynamics on the attitude control system showed no appreciable loss in structural damping. In fact, the maximum decrease in structural damping generated would still yield an adequate stability margin.

The analyses presented in this section are of a preliminary nature, containing certain simplifying assumptions. Therefore, more comprehensive analyses will be conducted to determine the stability margins more accurately.

GRAPH METHOD FOR DETERMINING FLIGHT

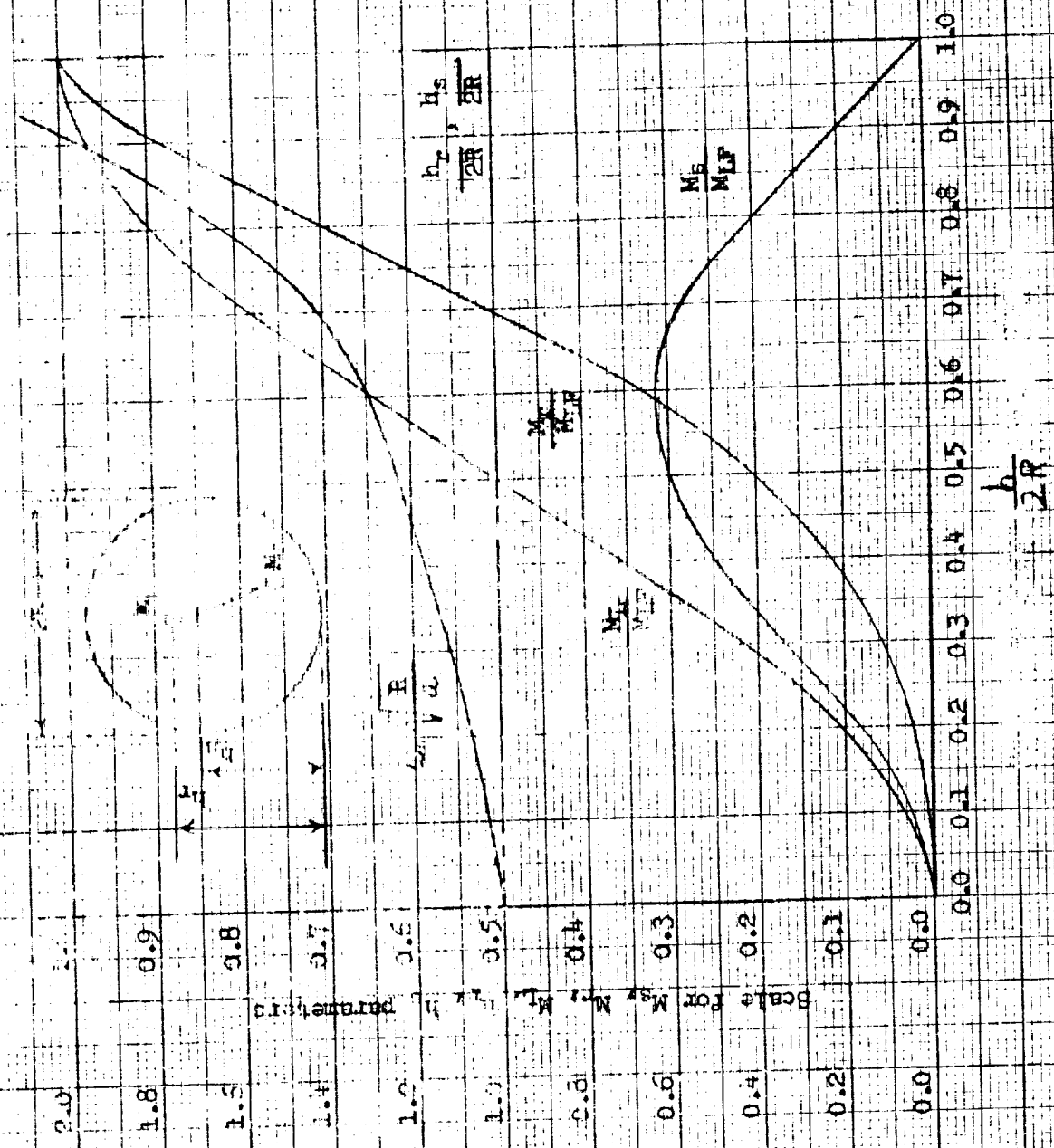
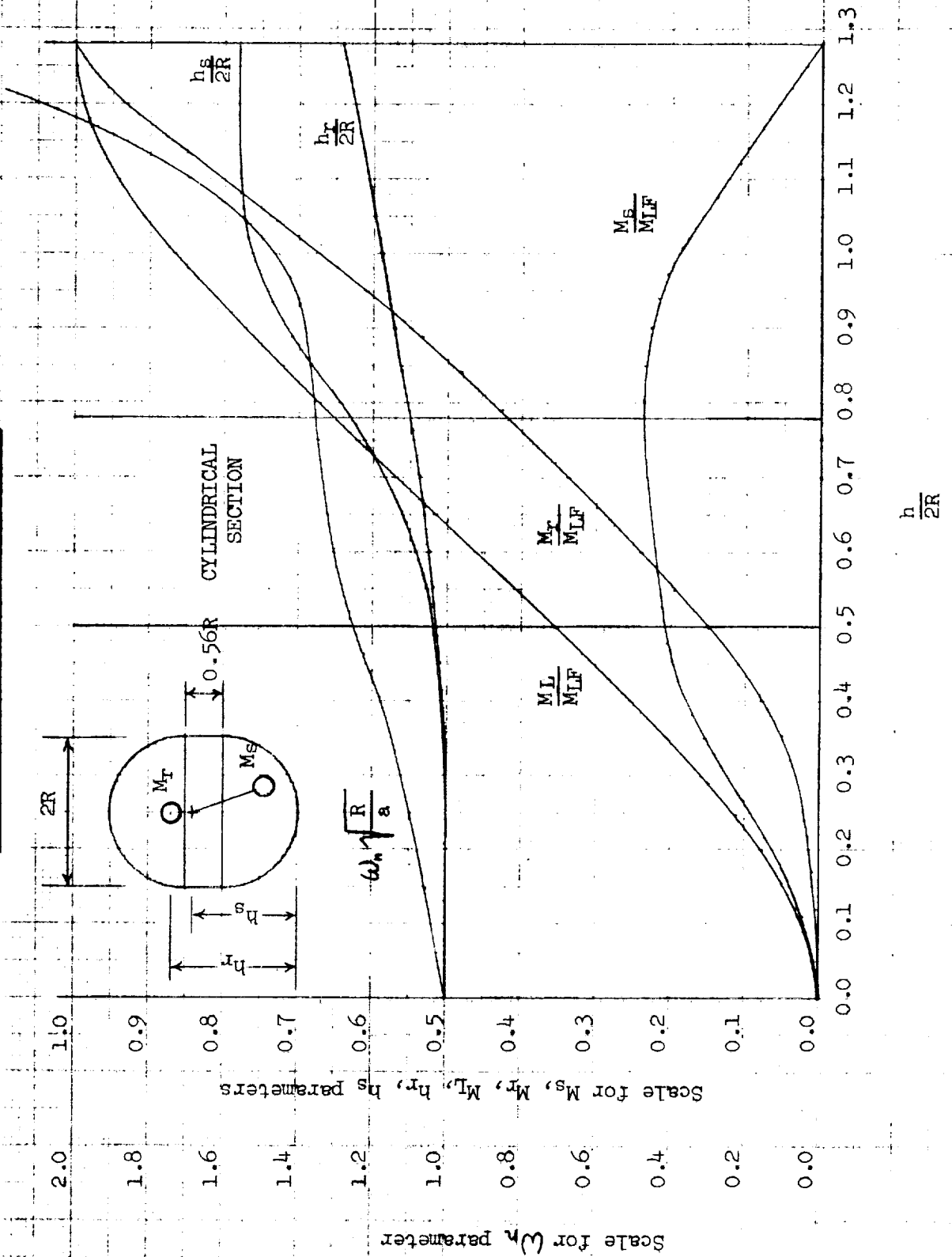
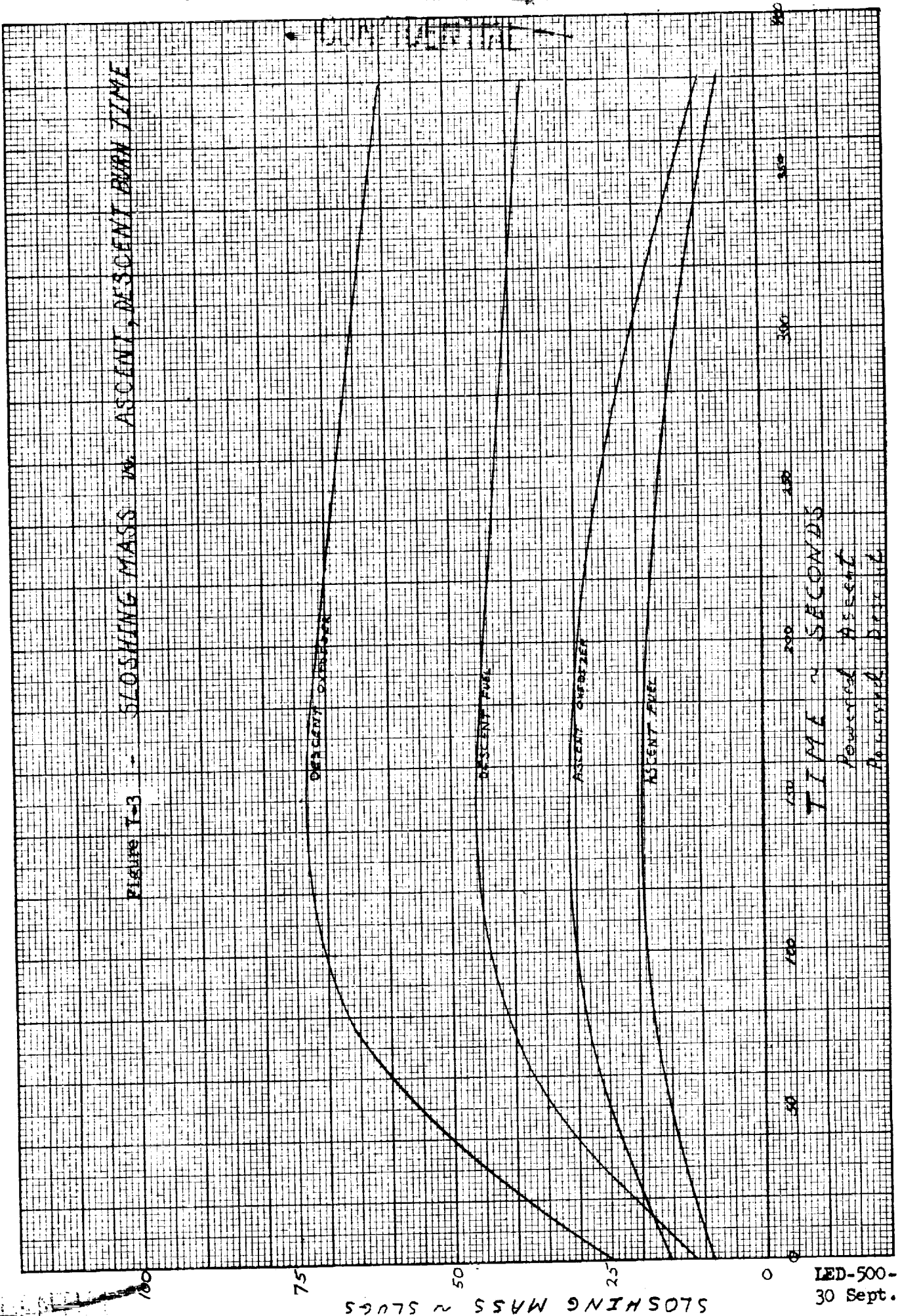


Figure 7-2  
MODEL PARAMETERS FOR DESCENT TANKS



K&E  
KENTLETT & EPPER CO.  
10 X 10 TO THE 1/2 INCH  
MADE IN U.S.A.  
32201-11

Figure T-3 - SLOSHING MASS IN ASCENT, DESCENT BURN TIME



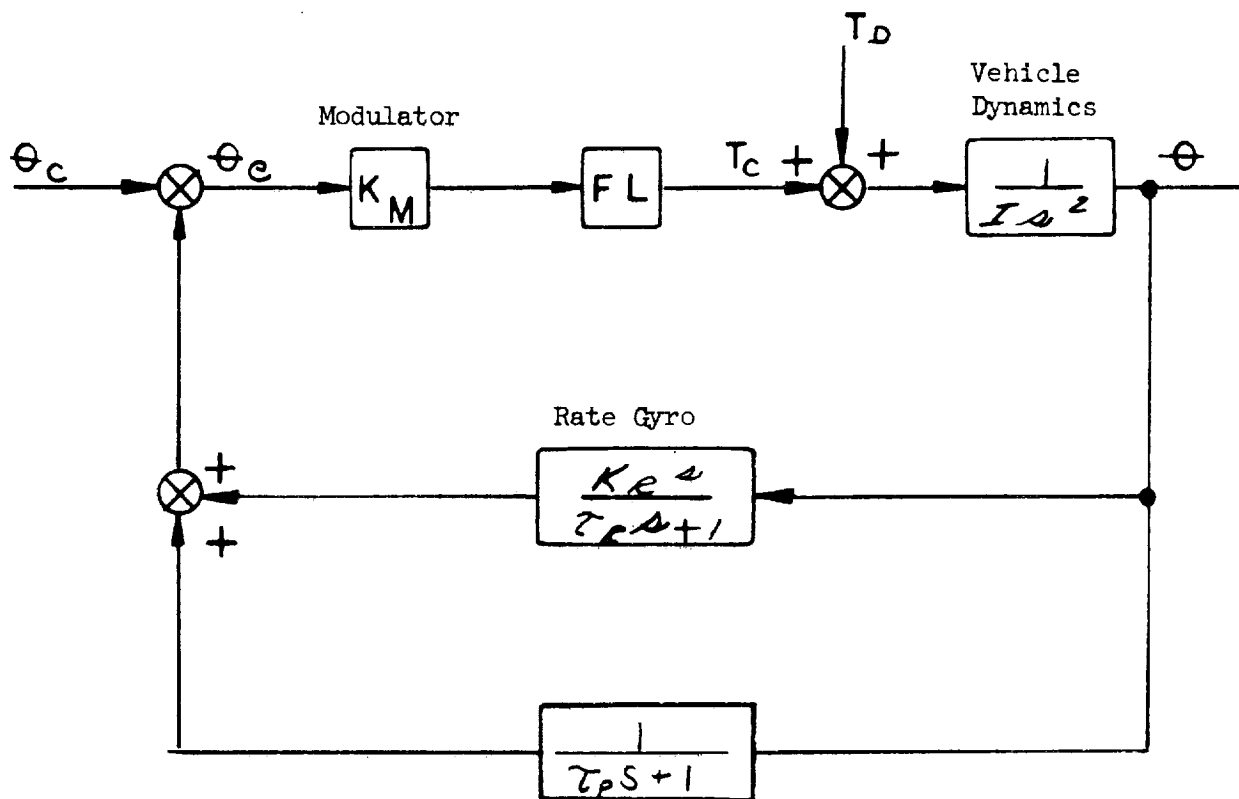


Figure 7-4 - Linearized Control System

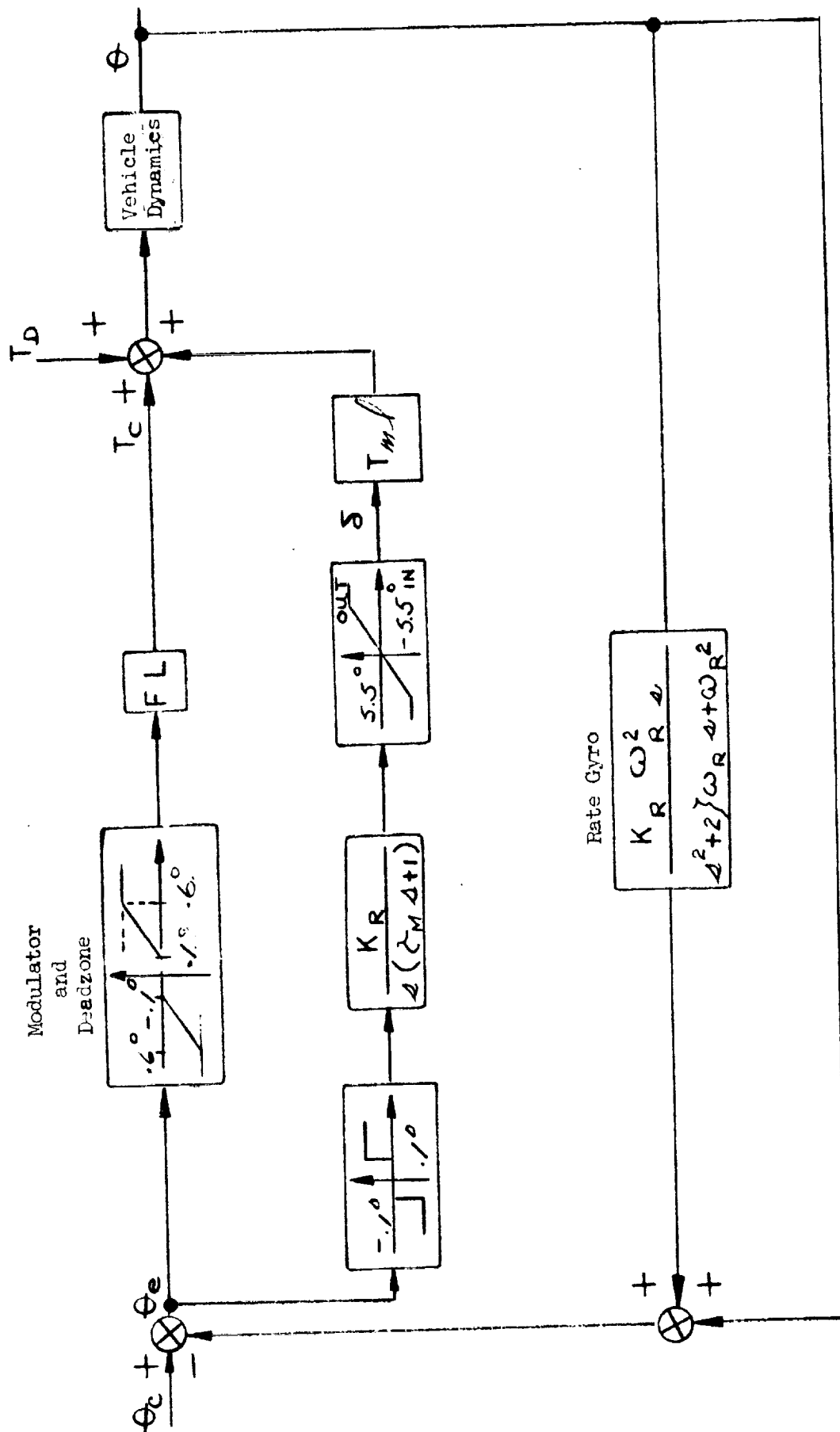


Figure 7-5 - Control System Programmed for Analog Slosh Study

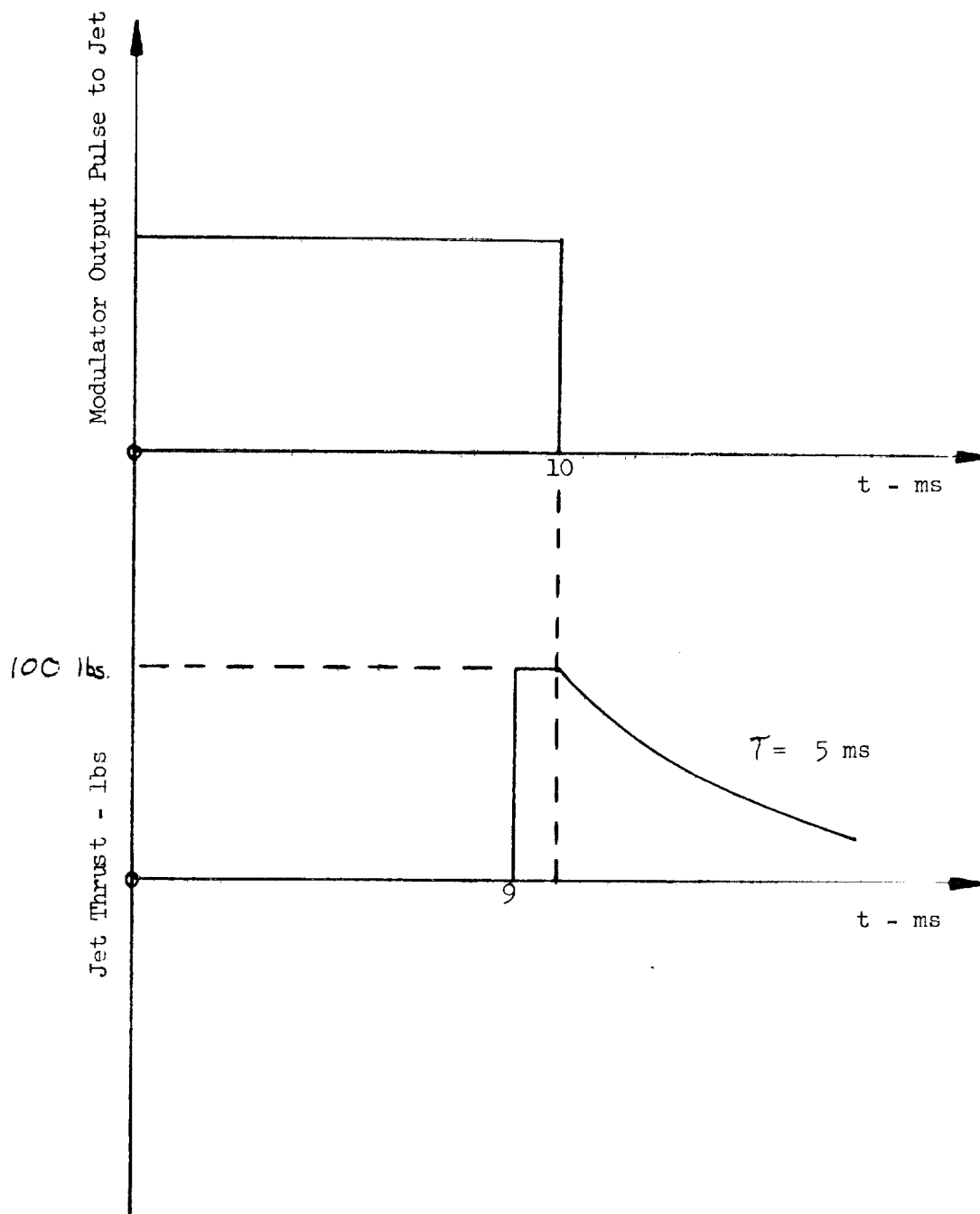


Figure 7-6 - Reaction Jet Thrust Characteristics

Figure 1-7

DESCENT YAW

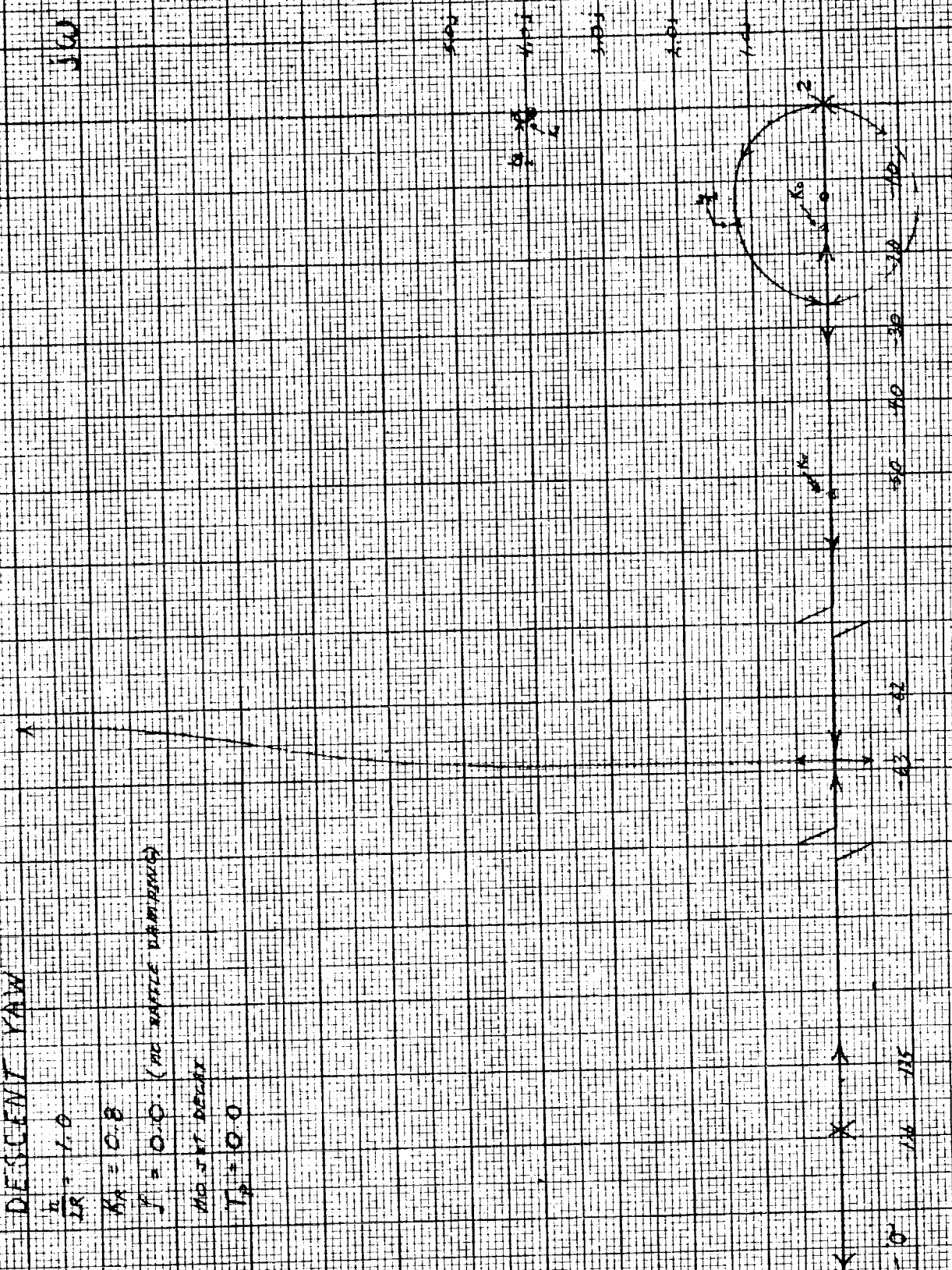
$\frac{h}{LR} = 1.0$

$K_A = 0.8$

$f = 0.0$  (NO BATTLE DAMAGING)

NO 3rd DEGREE

$T_D = 0.0$





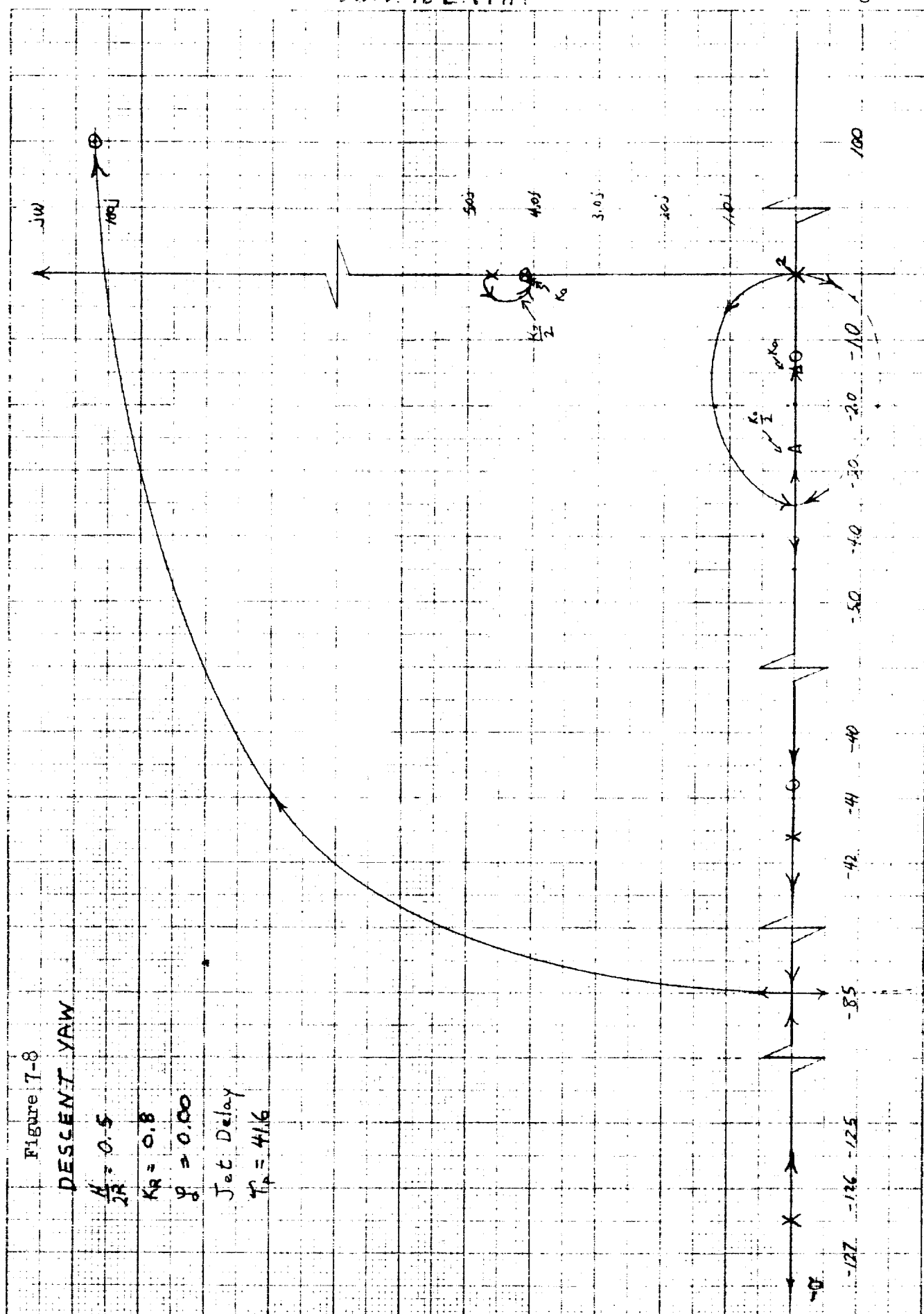


Figure 7-9

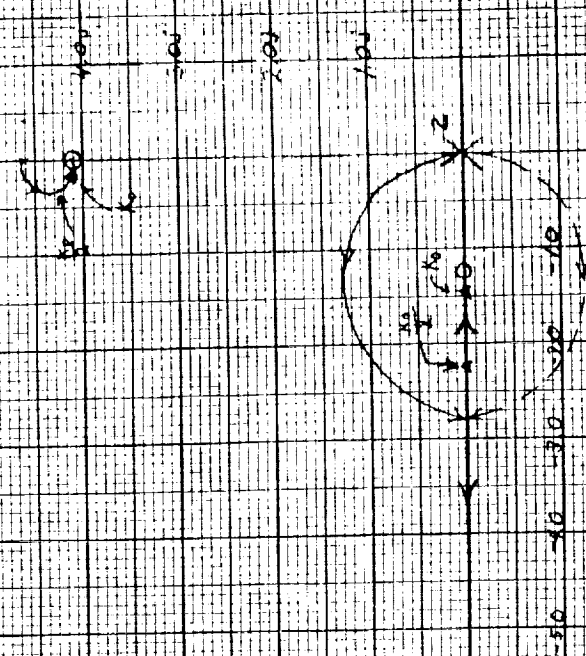
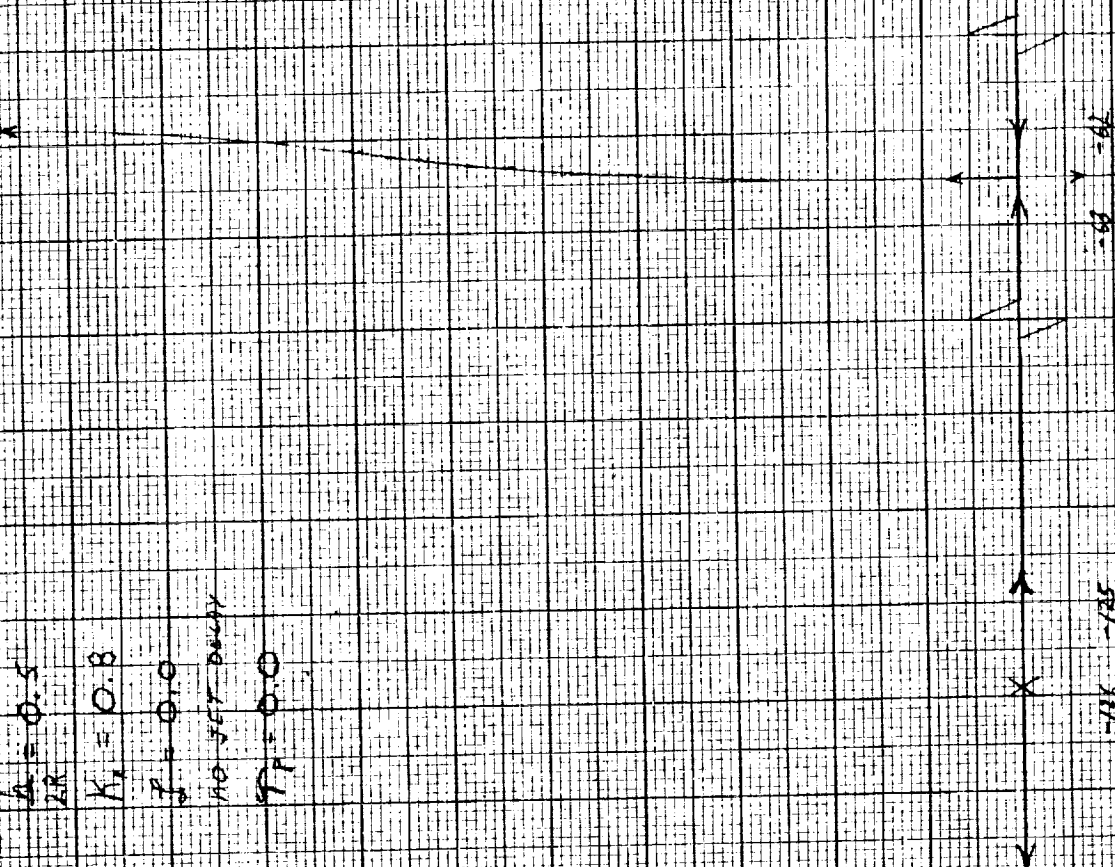
DESCENT YAW

 $K_1 = 0.5$ 

Z.R.

 $K_2 = 0.8$ 
 $f = 0.0$ 

NO SET BACK

 $T_T = 0.0$ 


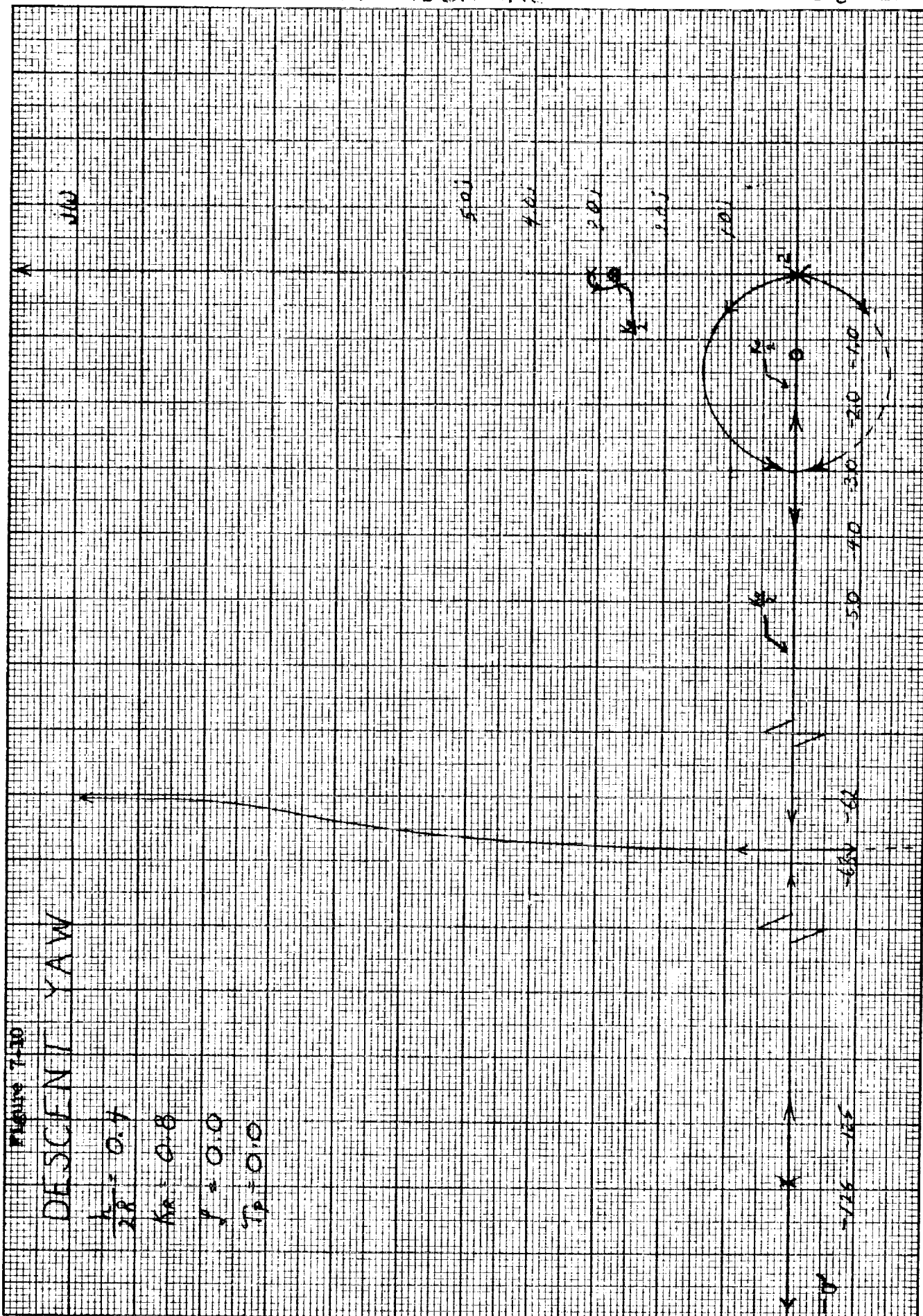


FIGURE 7-12

# DESCENT ROLL

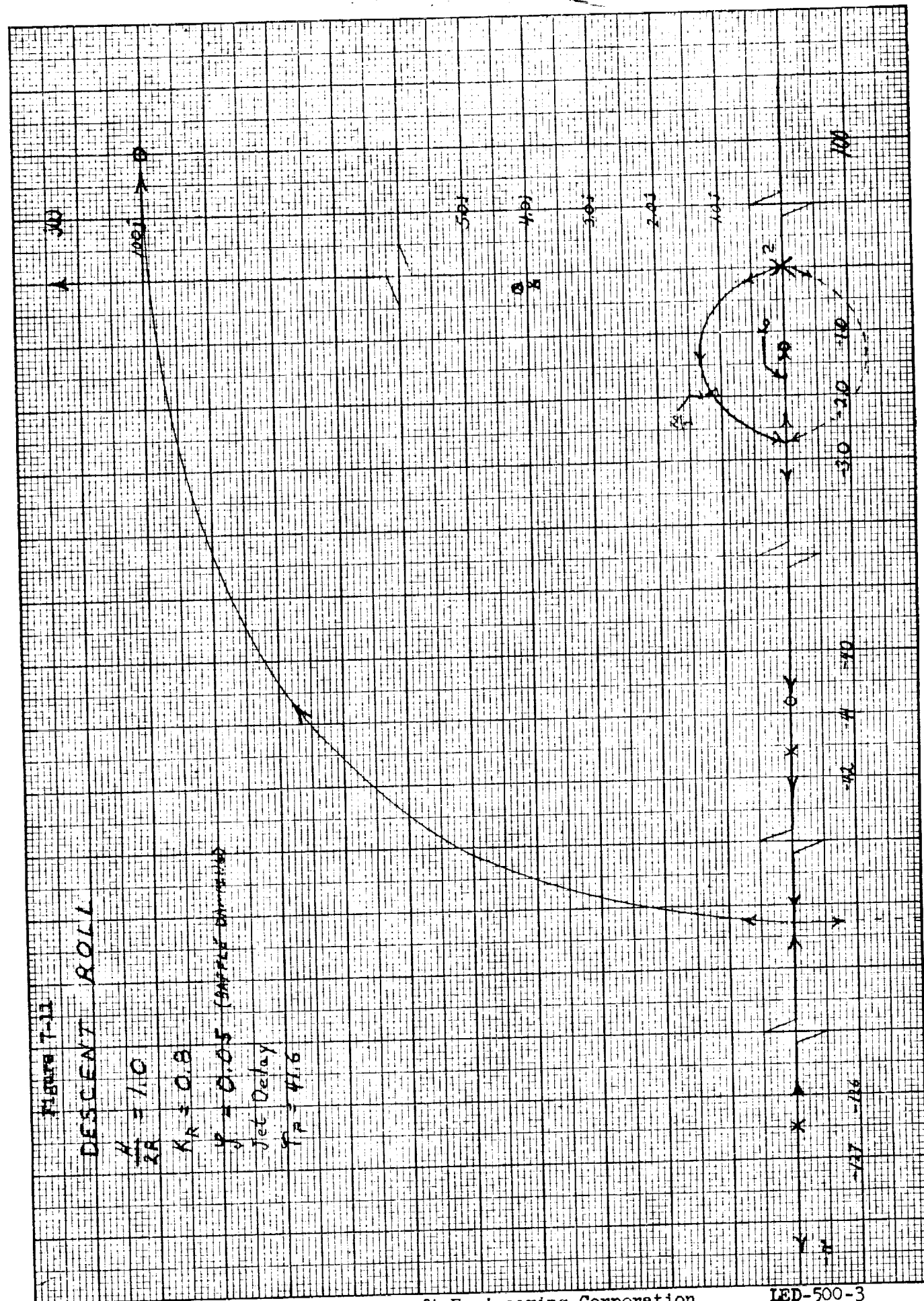
$$\frac{H}{Z_R} = 1.0$$

$$K_R = 0.8$$

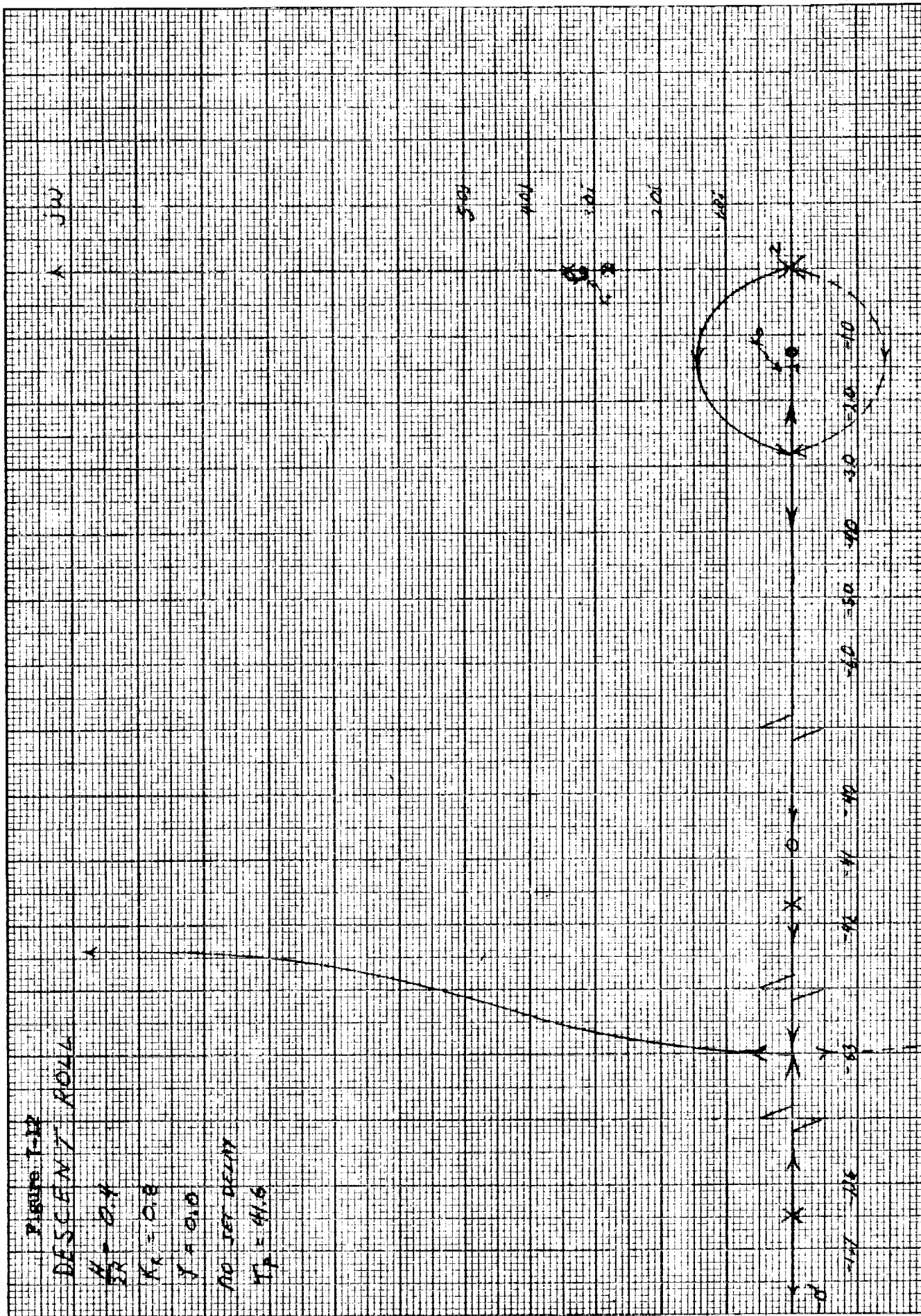
$$\mu = 0.05 \text{ (SAMPLE DAMPED)}$$

Jet Delay

$$\tau_p = 41.6$$







10 X 10 TO THE 1/2 INCH  
3250111

Figure 7-13

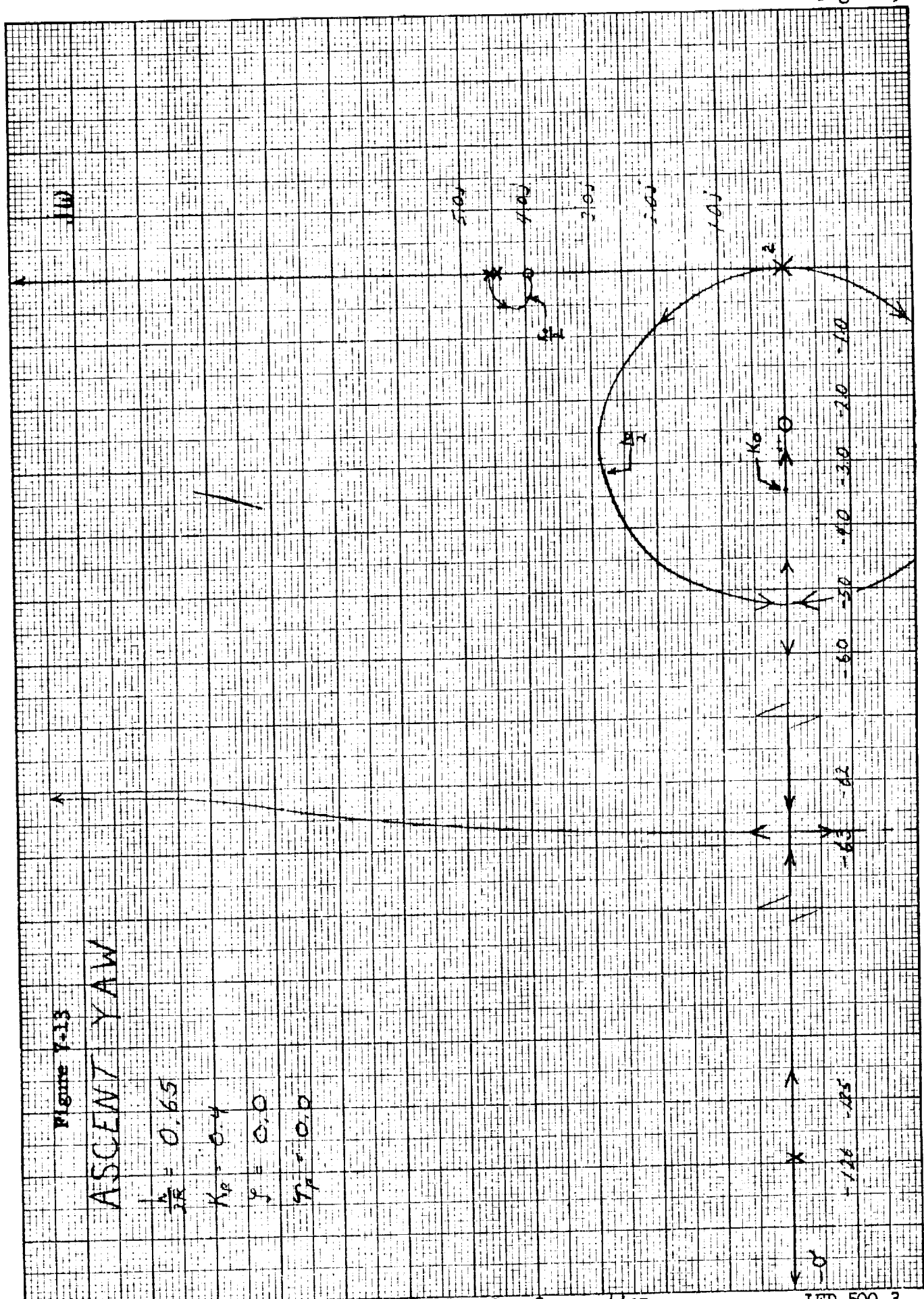
# ASCENT YAW

$$\frac{A}{R} = 0.65$$

$$K_R = 0.4$$

$$\gamma = 0.0$$

$$\eta_T = 0.0$$



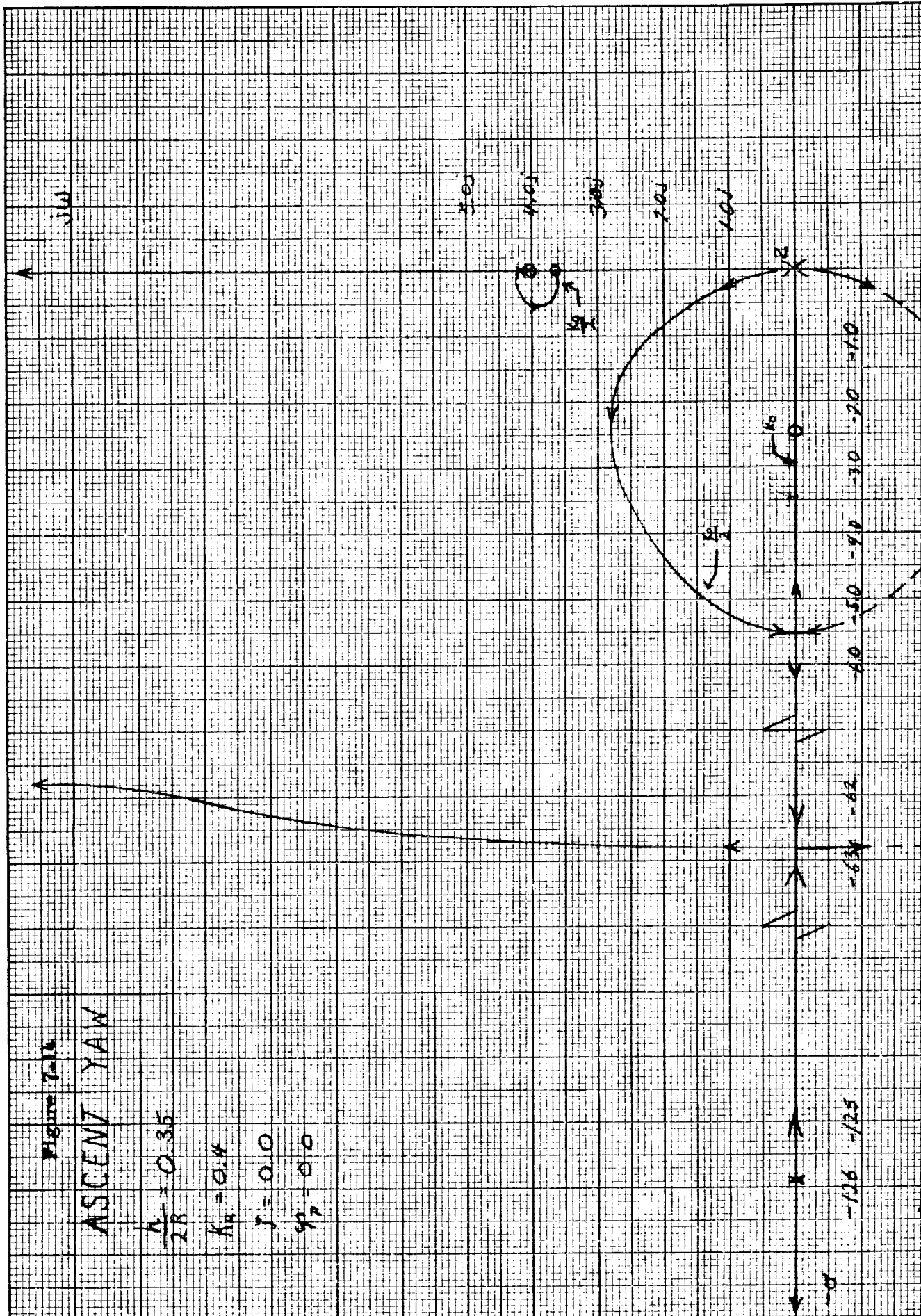
ASCENT YAW

$$\frac{A}{2R} = 0.35$$

$K_p = 0.4$

○ ○ ○ ○ ○

Q  
Q  
H  
A  
E



AT RAVENHILL  
KENNEL & ESSER CO.  
10 X 10 TO THE 1<sup>ST</sup> INCH  
MODEL NO. 3  
3501-11

Figure 7-15

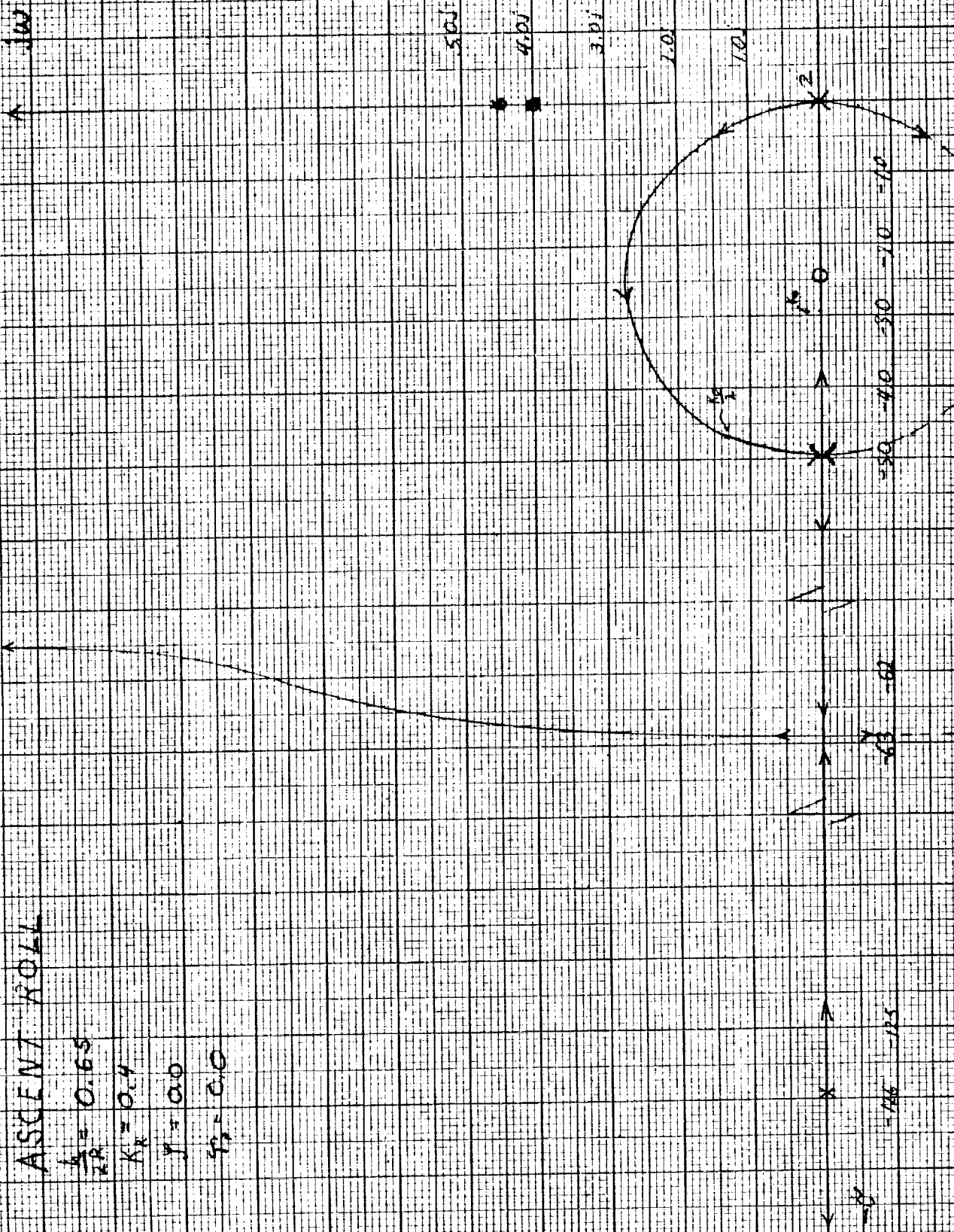
# ASCENT ROLL

$$\frac{b}{2R} = 0.65$$

$$K_R = 0.4$$

$$\gamma = 0.0$$

$$\psi_2 = 0.0$$





K&E  
KENNEL & ESSER CO.  
10 X 10 TO THE 1/2 INCH  
MODEL 7.2 V  
3201-11

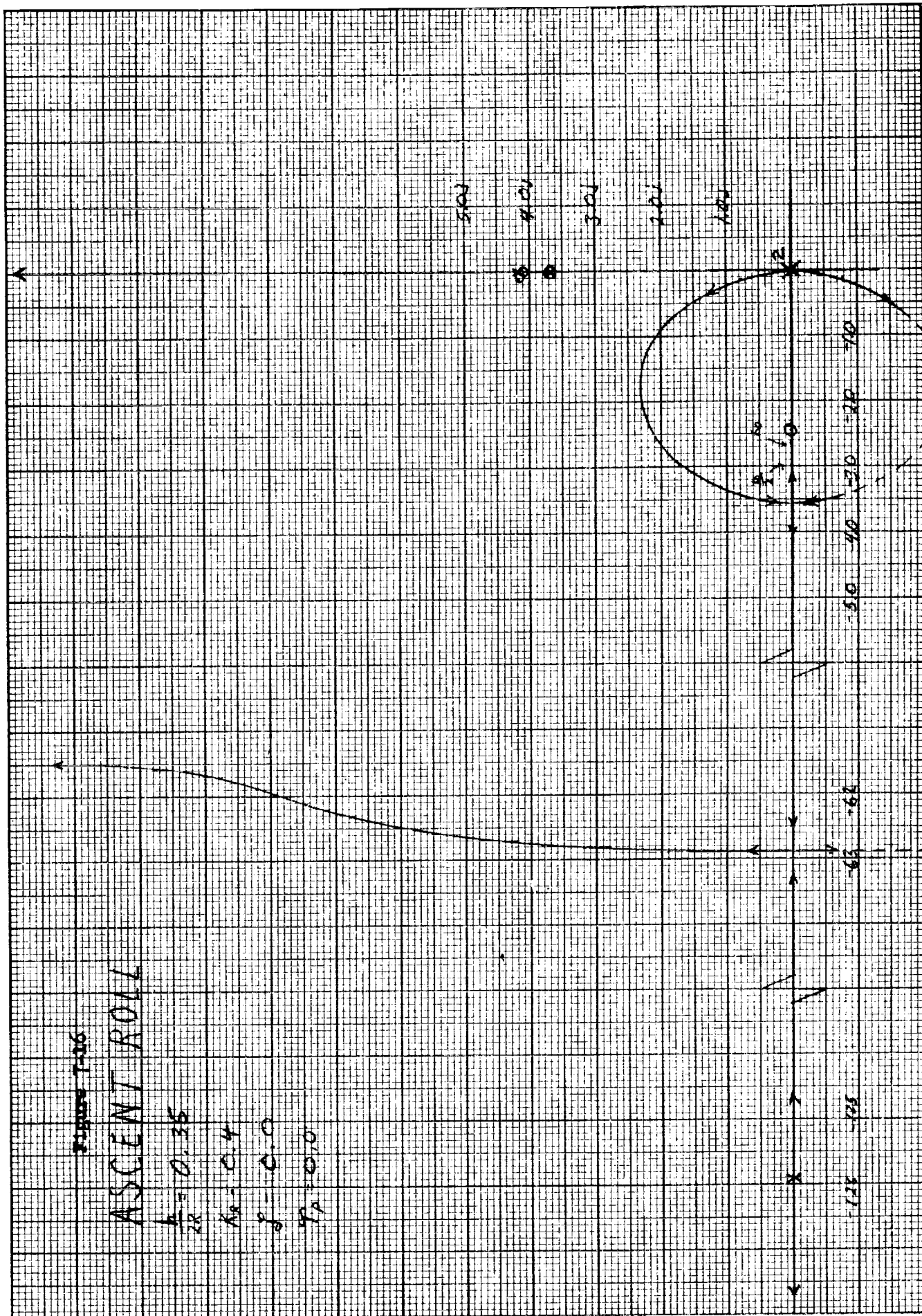


Figure T-217

TRANSIENT RESPONSE  
TO A UNIT STEP INPUT

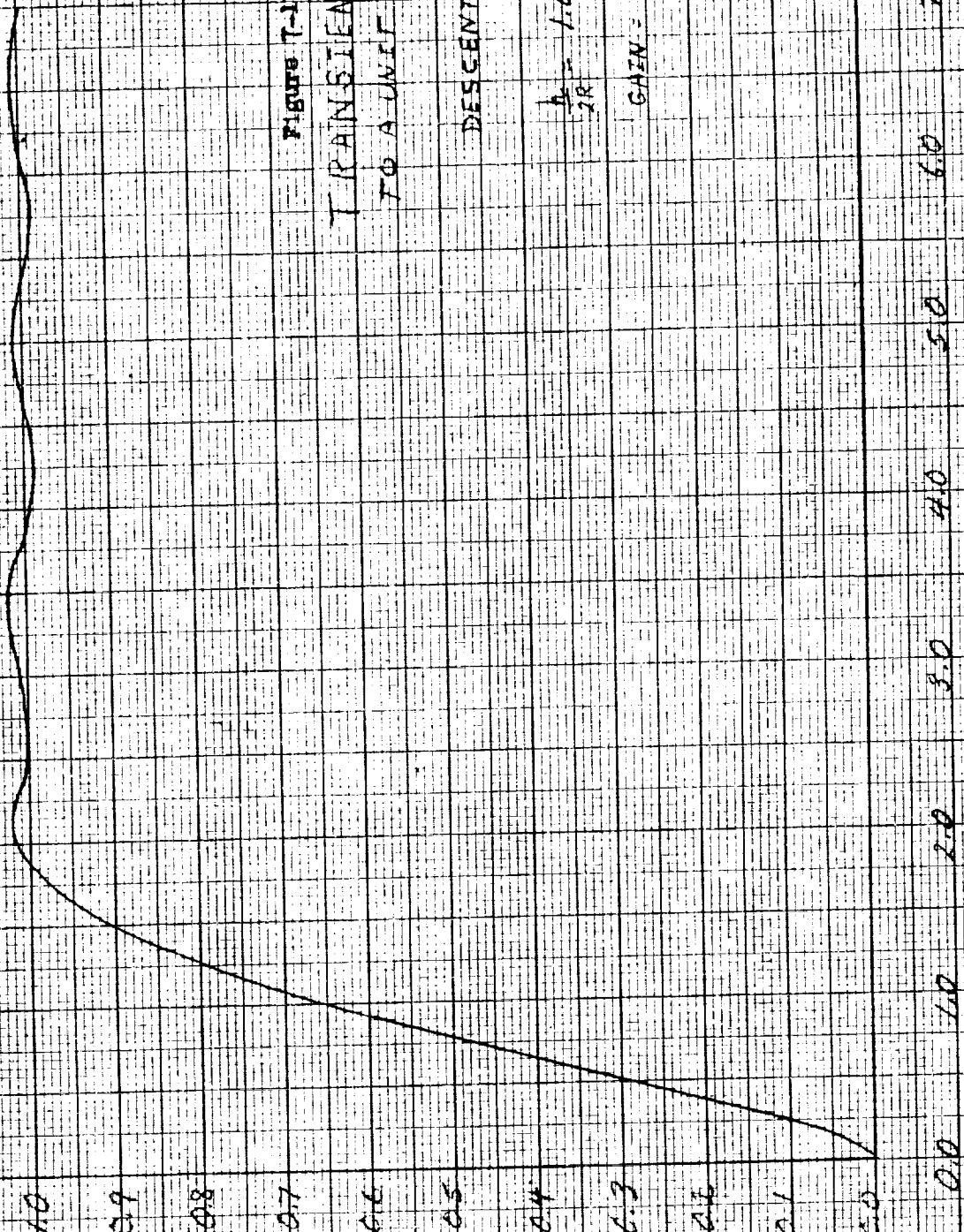
DESCENT YAW

$$\frac{b_0}{2\zeta} = 1.0$$

$$GAIN = K_0/K_1$$

NORMALIZED VEHICLE ATTITUDE

TIME IN SECONDS



K&E KENNEL & ESSER CO.  
10 X 10 TO THE 1/2 INCH  
329L-11

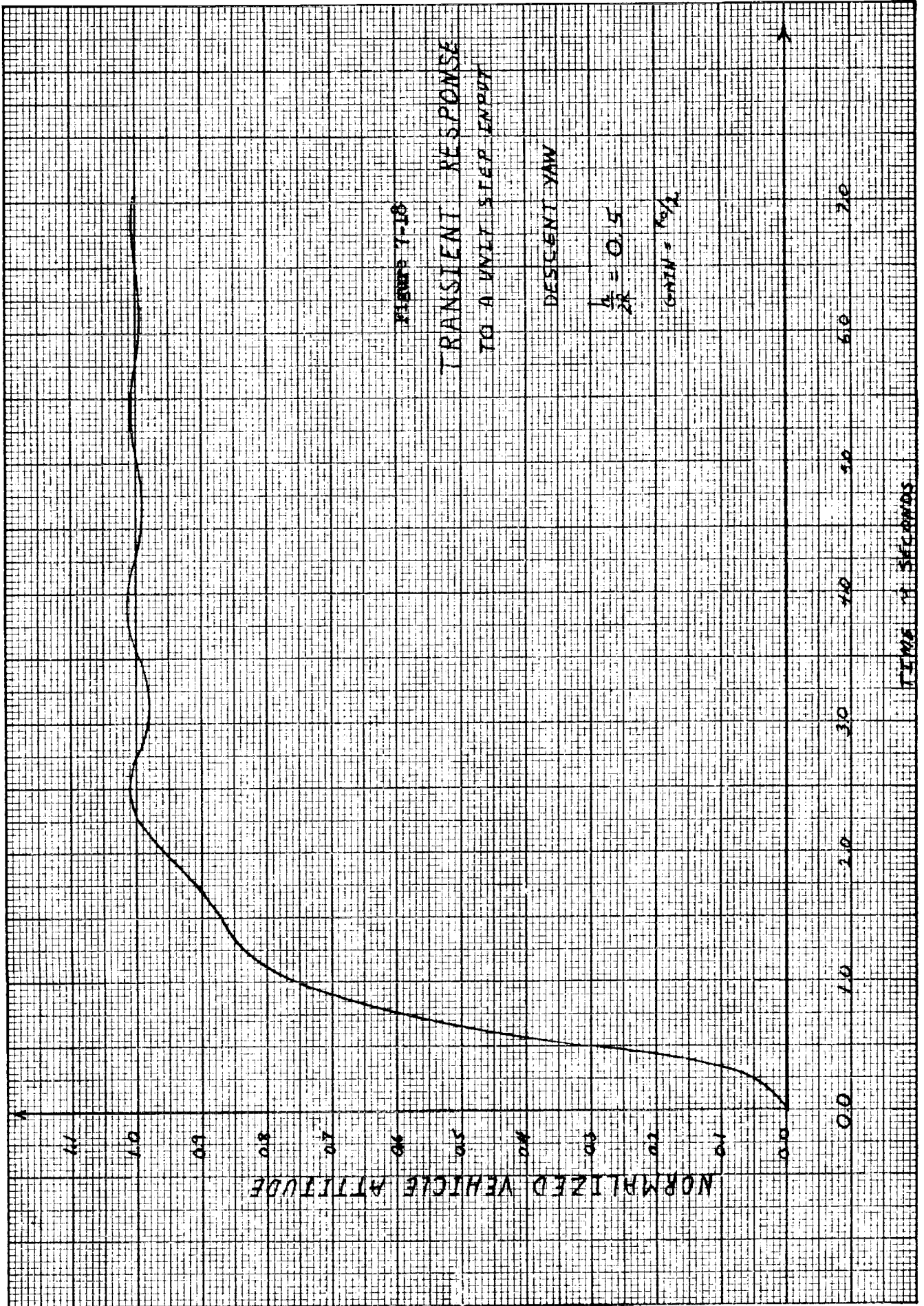


Figure 7-1B

TRANSIENT RESPONSE  
TO A UNIT STEP INPUT

DESCENT YAW

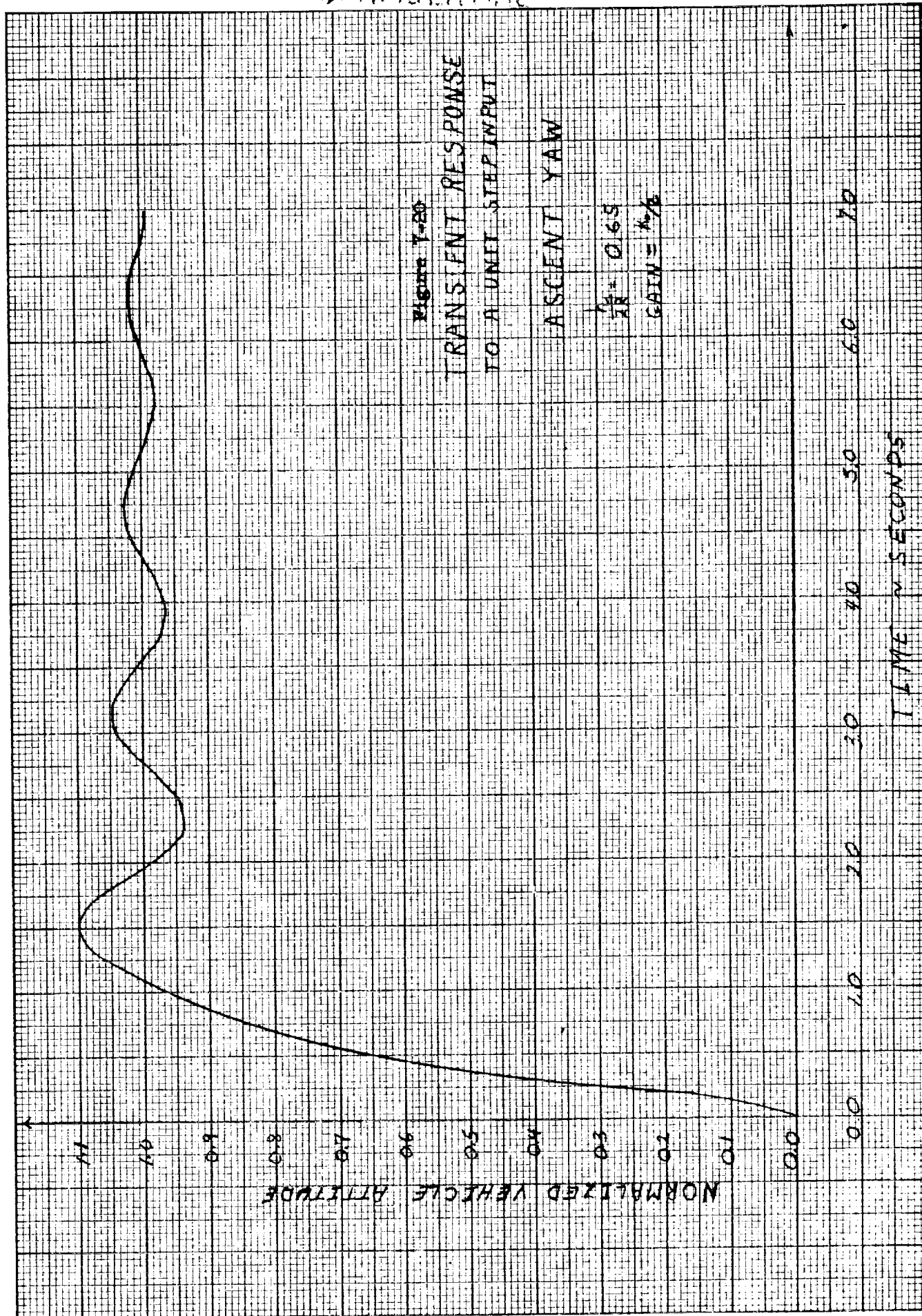
$$\frac{b}{2a} = 0.4$$

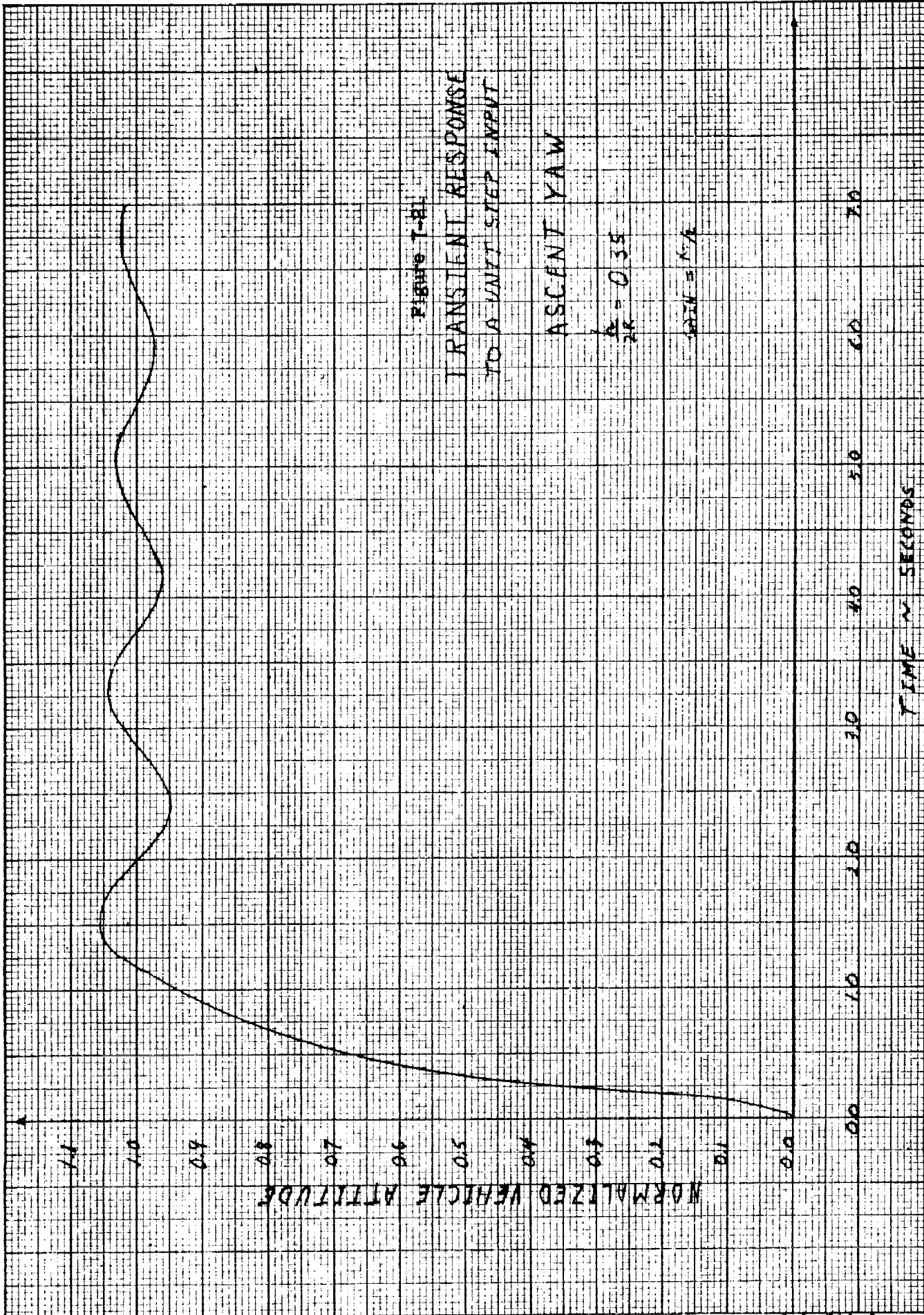
$$GAFN = 16/2$$

NORMALIZED VEHICLE ALTITUDE

TIME - SECONDS







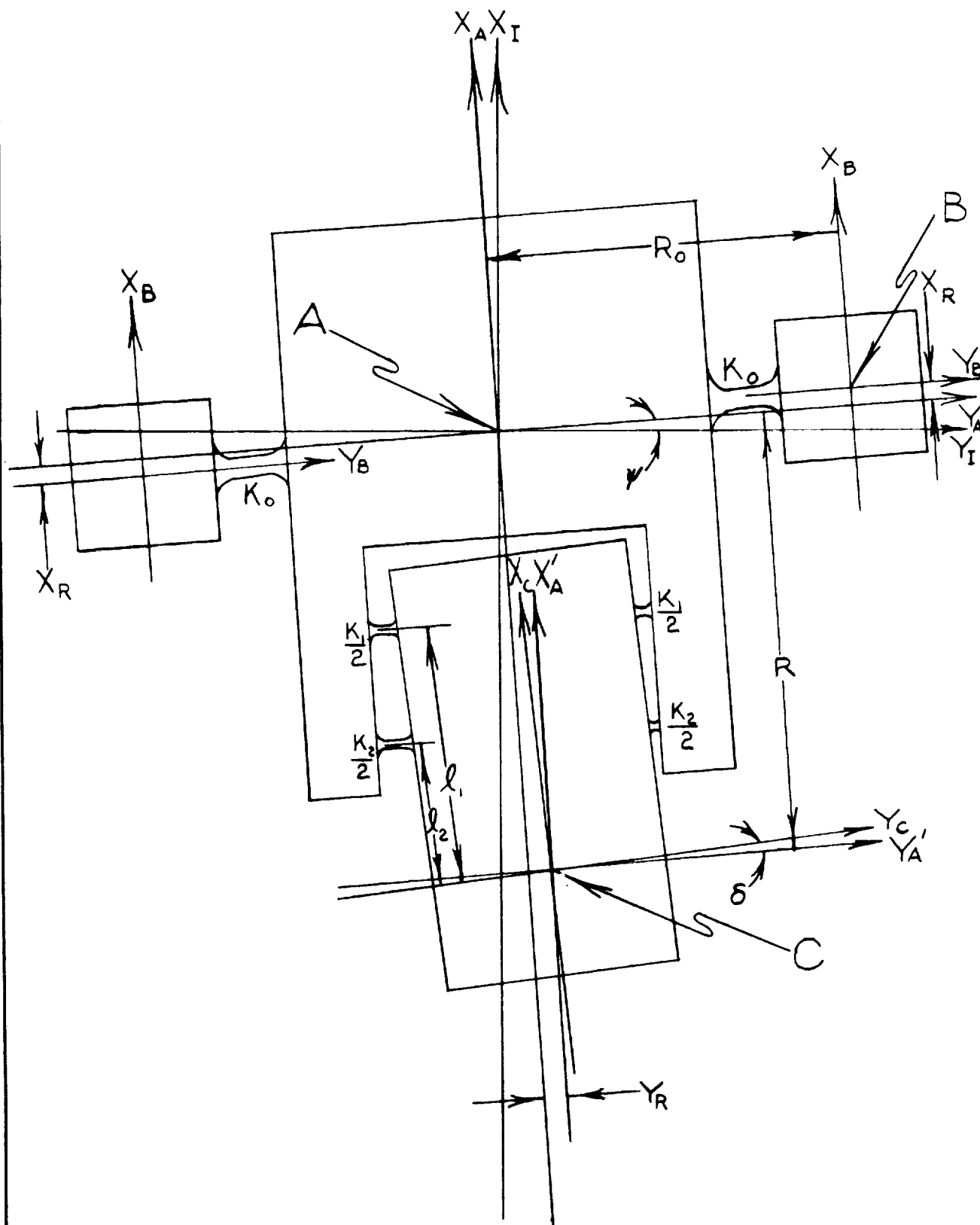


Figure 7-22 - Schematic Model of IEM Structure

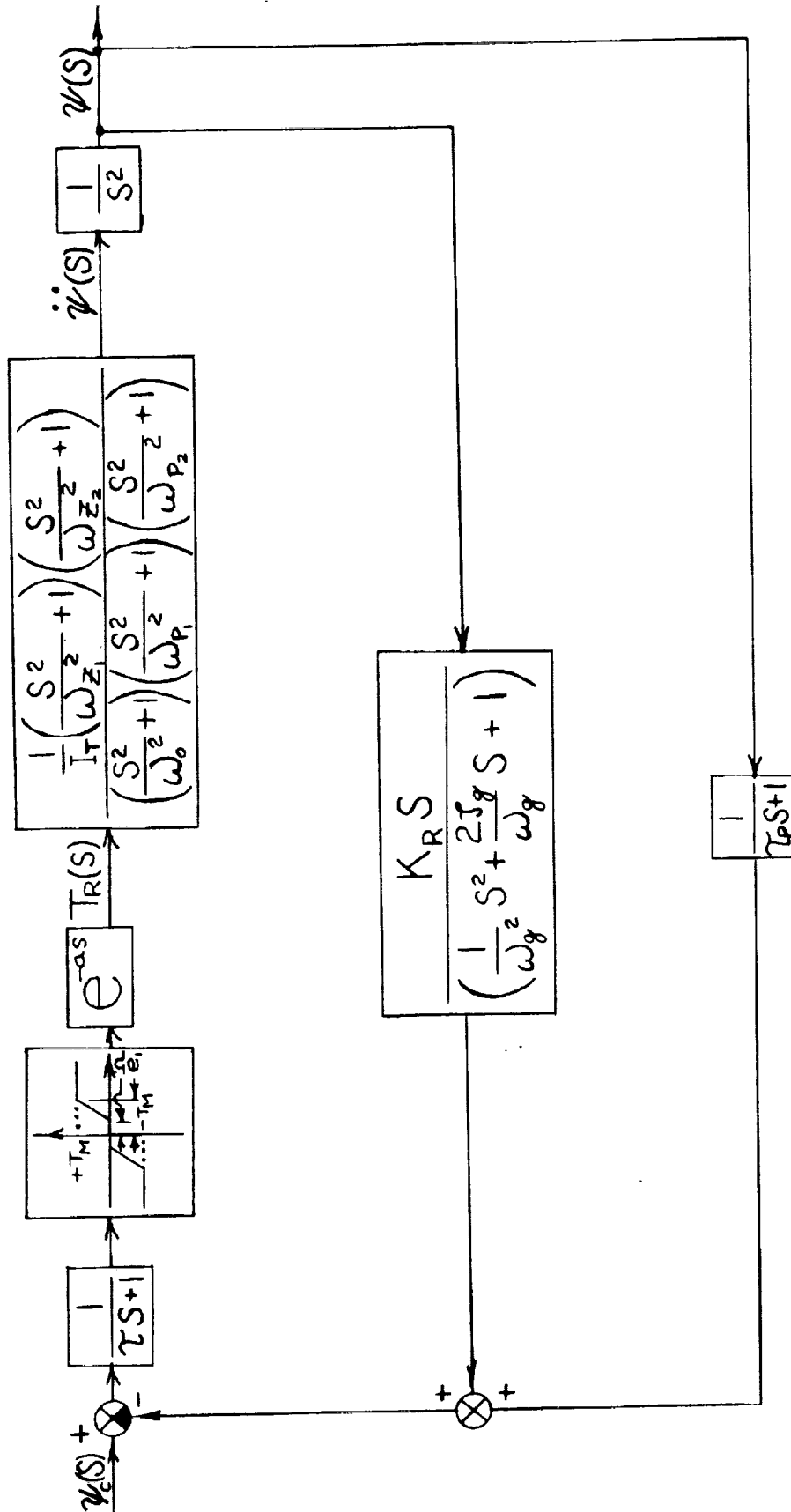
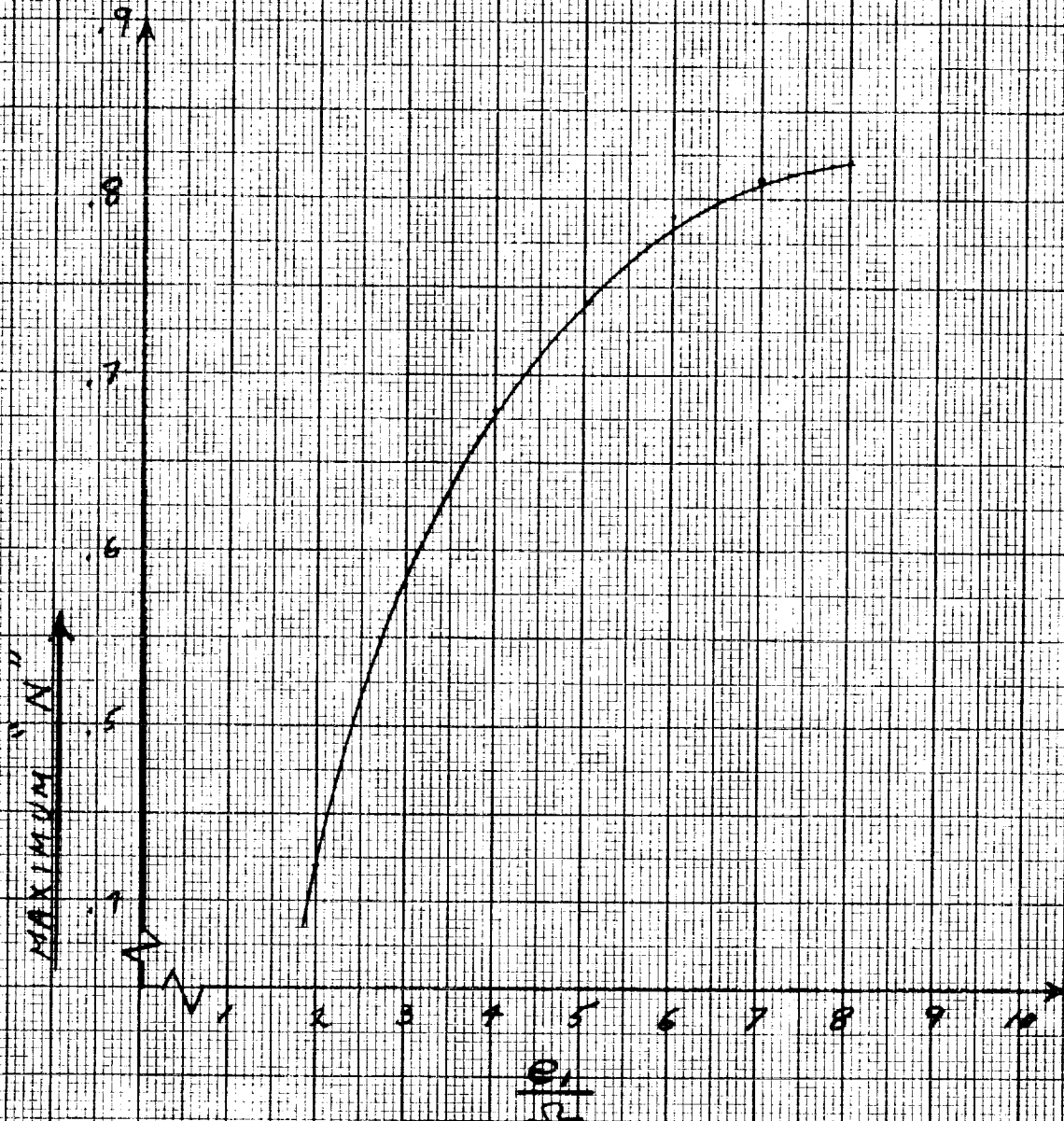


Figure 7-23 - Block Diagram of Attitude Control Loop Including Structural Dynamics



Figure 7-24

MAXIMUM DESCRIBING GAIN RATIO  
VS SATURATION DEAD BAND RATIO



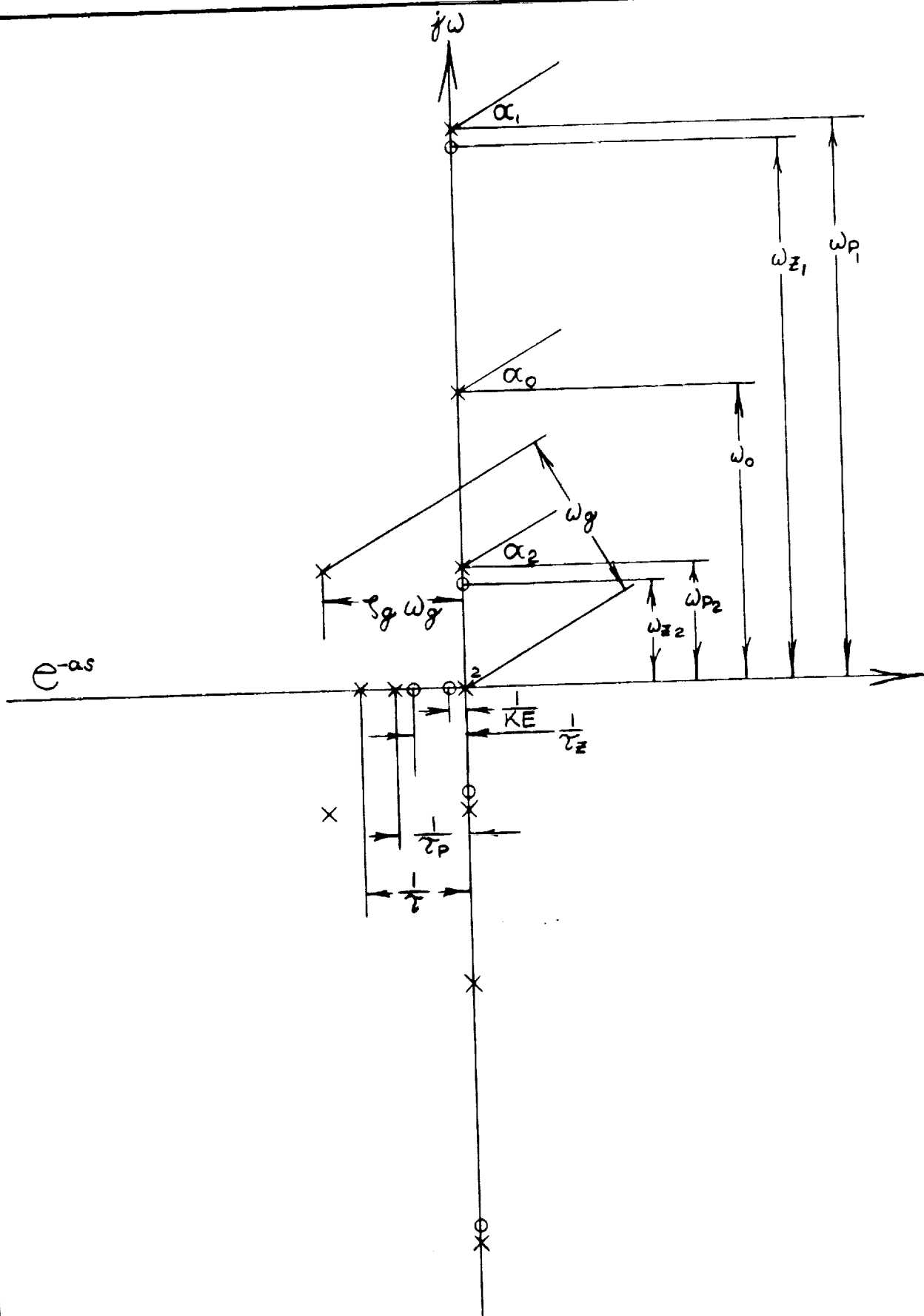


Figure 7-25 - Location of Open Loop Roots in Complex Plane

~~CONFIDENTIAL~~

PAGE 232

SECTION 8  
BIBLIOGRAPHY

Code 26512 Eng-23A

~~CONFIDENTIAL~~

REPORT LED-500-3  
DATE 30 Sept. 1964

GRUMMAN AIRCRAFT ENGINEERING CORPORATION

~~CONFIDENTIAL~~

1. Peters, R., et. al., "Basic LEM Level 2 Functional Diagrams," LDW-540-10000 thru LDW-540-10010, 1 June 1964.
2. Richman, D. and Lipsman, J., "Design Control Specification for the Attitude and Translation Control Assembly," LSP-300-14A, 6 April 1964.
3. Vinke, D. and Lipsman, J., "Design Control Specification for the Descent Engine Control Assembly," LSP-300-13, 5 March 1964.
4. Russell, J. and Lipsman, J., "Design Control Specification for the Rate Gyro Assembly," LSP-300-11, 18 October 1963.
5. Privor, H., "Preliminary Analysis of On-off Attitude Control System for Lunar Excursion Module," GAEC PDM-323A-87, 6 September 1962.
6. Edelmann, R., "Permissible Rate Gyro Deadzone for Various RCS Modulators," LMO-500-82, 12 August 1963.
7. Schaefer, R., "A New Pulse Modulator for Accurate DC Amplification with Linear or Nonlinear Devices," IRE Transactions on Instrumentation, September 1962.
8. Edelmann, R., "Estimated RCS Fuel Required for LEM Attitude Control Excluding Maneuvers During Landing and Docking," LMO-500-78, 1 August 1963.
9. Edelmann, R., "Recommended Reaction Jet Control Modulation Technique for LEM Attitude Control System," LMO-500-39, 24 April 1963.
10. Grossman, R., et. al., "Allocation of Propellants and  $\Delta V$  to Meet the  $\Delta V$  Budget," LED-490-100, 30 April 1964.
11. Fleisig, R., "Minutes of NASA/MS-C-GAEC Meeting on RCS and  $\Delta V$  Budgets on 12 March 1964," LMO-500-167, 25 March 1964.
12. Edelmann, R., "Attitude Control System Deadbands," LMO-500-108, 29 October 1963.
13. Kelly, P., "Attitude Control System for LEM Abort Simulator," LMO-500-79, 2 August 1963.
14. Kelly, P., "Reaction Jet Command Logic for Attitude Control of LEM," LMO-500-20, 29 March 1963.
15. Edelmann, R., et. al., "Estimated RCS Propellant Required for LEM Excluding Maneuvers During Separation, Landing, Rendezvous and Docking - 28,000 lb. and 25,500 lb. Separation Weights," LMO-500-89, 17 September 1963.
16. Dunn, P., "Powered Ascent Attitude Error Integral Compensation," LMO-500-93, 25 September 1963.
17. Hawkins, G., "Pendulum Thrust Misalignment Compensation for Backup Guidance," LMO-500-114, 30 October 1963.
18. Rimer, M., "Stability and Performance Analysis of a Pendulous Accelerometer for Use in the Bugs," LMO-500-124, 27 November 1963.

REPORT LED-500-3  
DATE 30 Sept. 1964

~~CONFIDENTIAL~~

~~CONFIDENTIAL~~

PAGE 234

19. Kelly, P., "Preliminary Investigation of Dynamic Coupling of Propellant Sloshing with the Attitude Control System for LEM Ascent Stage," L500-MO3-12, 8 March 1963.
20. Blanchard, R., "Guidance and Control Dynamics," LTM 7-(B)-7006-1, 10 May 1963.
21. Phagan, R., "Sampled Data Control Analysis Initial Studies," LMO-500-70, 19 July 1963.
22. Pulgrano, L. and Howe, R., "Mechanical Model Representation for the LEM Ascent and Descent Stage Propellants," LMO-500-168, 8 April 1964.
23. Privor, H., "Preliminary Investigation of Dynamic Coupling of Propellant Sloshing with the Attitude Control System for LEM Descent Stage," LMO-500-28, 6 April 1963.
24. Budiansky, B., "Sloshing of Liquids in Circular Canals and Spherical Tanks," Journal of Aerospace Sciences, March 1960.
25. Bauer, H. F., "Fluid Oscillations in the Containers of a Space Vehicle and Their Influence on Stability," NASA TR, to be published.
26. Abramson, H. N. and Ransleben, G., "Some Comparisons of Sloshing Behaviors in Cylindrical Tanks with Flat and Conical Bottoms," ARA Journal, December 1961.
27. Lukens, D., et. al., "Approximate Transfer Functions for Flexible Booster and Autopilot Analysis," WADD TR-61-93, April 1961.
28. Pulgrano, L., "Initial Baffle Requirements for Main Propellant Tanks," LAV-500-33, 12 December 1963.
29. Stack, J., "Preliminary LEM Mass Property History for Control Weight and Current Status," LMO-490-105, 20 March 1964.
30. Satz, H., "Feasibility of Attitude and Moment Unbalance Control Using Positive X-Axis RCS Thrusters During Powered Descent and Powered Ascent," LMO-500-116, 4 November 1963.
31. Dunn, P., "Preliminary Report on the Investigation of the LEM Descent Stage Gimbal Engine - Reaction Jet Attitude Control System," LMO-500-47, 18 May 1963.
32. Dunn, P., "Recommended SCS Response Logic for Operation of the Descent Engine Trim Actuator, and Summary of Analysis of Open-loop Actuator Trim Systems for LEM," LMO-500-177, 30 April 1964.

~~CONFIDENTIAL~~

REPORT LED-500-3  
DATE 30 Sept. 1964

